NATIONAL TECHNICAL UNIVERSITY OF ATHENS

School of Chemical Engineering

Mathematical modeling of thermophysical properties and phase equilibria of pure carbon dioxide and multicomponent mixtures

PhD Thesis

of

Nikolaos I. Diamantonis

Athens, July 2013

Mathematical modeling of thermophysical properties and phase equilibria of pure carbon dioxide and multicomponent mixtures

A dissertation presented

by

Nikolaos I. Diamantonis

to

the School of Chemical Engineering

in partial fulfillment of the requirements for the degree of

Doctor of Philosophy

in

Chemical Engineering

National Technical University of Athens

Athens, Greece

July 2013

Η έγκριση της διδακτορικής διατριβής από την Ανωτάτη Σχολή Χημικών Μηχανικών του Εθνικού Μετσόβιου Πολυτεχνείου δεν υποδηλώνει αποδοχή των απόψεων του συγγραφέα (Ν. 5343/32 Άρθρο 202 § 2).

The approval of this PhD dissertation by the School of Chemical Engineering of the National Technical University of Athens does not imply the acceptance of the author's opinions (Law 5343/32 Article 202 § 2).

Abstract

Mathematical modeling
of thermophysical properties and phase equilibria
of pure carbon dioxide and multicomponent mixtures

PhD Thesis by Nikolaos I. Diamantonis

Supervisor: Professor Ioannis G. Economou

Supervising Committee: Professor Andreas G. Boudouvis
Professor Ioannis G. Economou
Assistant Professor Epaminondas C. Voutsas

Carbon Capture and Sequestration (CCS) is one of the most promising technologies for the reduction of CO_2 in the atmosphere. Flue gas sources such as power plants and other manufacturing processes that depend heavily on fossil fuels, can be equipped with systems that capture the CO_2 from the flue gas stream, and then transport the CO_2-rich stream via pipelines to places where oil reservoirs near depletion, saline aquifers, or other underground cavities, can receive and store it.

The part of CO_2 pipeline transport is often overlooked and simulated with natural gas transport. However, its importance raises the need for multi-disciplinary research on the details involved, that are substantially different than natural gas. In particular, since the CO_2 pipeline networks may run close to populated areas, thorough hazard assessment studies are required both for the regulatory frameworks and the public acceptance campaigns. A hazard assessment study is based on fluid calculations in and out of the pipeline, such as normal flow, and dispersion in the event of a rupture. All these calculations rely heavily on the models used for the prediction of thermophysical properties of the fluids involved, which are mainly CO_2 mixtures with other compounds.

A large number of properties are necessary for the aforementioned calculations, ranging from density and compressibility, to derivative thermodynamic properties such as speed of sound and the Joule-Thomson inversion curve, and even further to transport

properties that include viscosity and self-diffusion coefficient. By employing an accurate, robust, and reliable thermodynamic model that covers the entire table of properties and conditions, improved quality of hazard assessment studies can be ensured.

In this work, several equations of state (EoS) have been assessed for their capabilities of predicting accurately the thermodynamic properties of CO_2 mixtures with other gases. Extensive comparisons with literature experimental data have been performed, showing the similarities of the approaches in relatively simple properties such as density and vapor-liquid equilibria, while pointing out the superiority of higher order EoS (i.e. Perturbed Chain – Statistical Associating Fluid Theory, abbreviated as PC-SAFT) when it comes to more complex properties such as derivative thermodynamic and transport properties. More specifically, the derivative thermodynamic properties were calculated by analytically derived expressions, which means that the computational cost is kept low, while the physical background of each approach is tested. On the other hand, transport properties include the notion of time, thus it is impossible to be calculated by equilibrium thermodynamics EoS that do not take into account time. To overcome this obstacle, several established models of the literature have been combined with the EoS, and re-tuned, in order to extend the properties calculation framework to those properties. Viscosity models both for pure components and mixtures were linked with the EoS, and the use of the meta-heuristic optimization method of Particle Swarm Optimization aided the production of the parameters' tables. Calculations for mixtures of CO_2 were compared with the few experimental data that are available in the literature. Gaps of experimental data were identified, in order to act as a suggestion for future experimental work. The combined approaches and the new optimized parameters constitute integral parts of a broader thermodynamic simulator that was developed in this work.

Several useful conclusions are drawn from this work that can be used further to simulators dedicated to the pipeline transport part of the CCS process. Higher order EoS, such as PC-SAFT and truncated PC – Polar SAFT, can predict more accurately the thermodynamic properties of the systems of interest, while the overhead computational cost is not prohibitive. Especially the derivative thermodynamic properties point out the power of higher order EoS over cubic EoS since the latter usually exhibit

higher deviations compared to experimental data. Transport properties can be very efficiently calculated via the combination of an EoS with a specific property model, given that the parameters have to be re-tuned in order to achieve a good fit for the respective reference systems and states. In this work, several optimization exercises have been performed in order to come up with the parameters' tables for each EoS and every model.

Keywords

Carbon Capture and Sequestration, carbon dioxide, thermodynamic model, equation of state, derivative properties, transport properties

Abstract in Greek

Μαθηματική μοντελοποίηση
των θερμοφυσικών ιδιοτήτων και της ισορροπίας φάσεων
του καθαρού διοξειδίου του άνθρακα και πολυσυστατικών μιγμάτων του

Διδακτορική Διατριβή Νικολάου Ι. Διαμαντώνη
Επιβλέπων: Καθηγητής Ιωάννης Γ. Οικονόμου

Επιβλέπουσα Επιτροπή: Καθηγητής Ανδρέας Γ. Μπουντουβής
Καθηγητής Ιωάννης Γ. Οικονόμου
Επίκουρος Καθηγητής Επαμεινώνδας Χ. Βουτσάς

Η δέσμευση και γεωλογική αποθήκευση του άνθρακα (Carbon Capture and Sequestration) είναι μια πολλά υποσχόμενη τεχνολογία, που στοχεύει στη μείωση της συσσώρευσης του διοξειδίου του άνθρακα (CO_2) στην ατμόσφαιρα. Πηγές αερίων ρύπων, όπως εργοστάσια παραγωγής ενέργειας, και άλλες μονάδες παραγωγής που αντλούν την απαιτούμενη ενέργεια από την καύση ορυκτών πόρων, μπορούν να εξοπλιστούν με κατάλληλα συστήματα τα οποία θα δεσμεύουν το CO_2 από το ρεύμα καυσαερίων, και στη συνέχεια θα το μεταφέρουν μέσω δικτύου αγωγών σε τοποθεσίες όπου υπάρχουν υπόγειες κοιλότητες που μπορούν να χρησιμοποιηθούν ως χώροι αποθήκευσης και απομόνωσης του CO_2.

Το κομμάτι της μεταφοράς του CO_2 μέσω δικτύου αγωγών, συχνά θεωρείται συναφές αντικείμενο με την μεταφορά φυσικού αερίου, κάτι που όμως δεν ισχύει απόλυτα. Εντούτοις, η σημαντικότητά του αναδεικνύει την ανάγκη για διεπιστημονική έρευνα πάνω στις λεπτομέρειες, οι οποίες διαφέρουν ουσιαστικά από εκείνες των αγωγών φυσικού αερίου. Συγκεκριμένα, οι αγωγοί που μεταφέρουν CO_2, ενδέχεται να διέρχονται σε μικρές αποστάσεις από κατοικημένες περιοχές, γεγονός που επιβάλλει την κατάρτιση διεξοδικών μελετών διακινδύνευσης, οι οποίες είναι ουσιαστικό κομμάτι της συμμόρφωσης με το νομικό πλαίσιο, και των εκστρατειών για την κοινωνική αποδοχή της συγκεκριμένης τεχνολογίας. Οι μελέτες αυτές βασίζονται κυρίως σε ρευστομηχανικούς υπολογισμούς εντός και εκτός των αγωγών, συμπεριλαμβάνοντας

συνθήκες κανονικής ροής, καθώς και φαινόμενα διασποράς που εμφανίζονται κατά την ρήξη ή αστοχία του αγωγού. Απαραίτητα δεδομένα για αυτούς τους υπολογισμούς αποτελούν οι θερμοφυσικές ιδιότητες των ρευστών που εμφανίζονται στη διεργασία, τα οποία είναι κυρίως καθαρό CO_2 και πολυσυστατικά μίγματά του με άλλα αέρια.

Ένας σημαντικός αριθμός ιδιοτήτων απαιτούνται για τους προαναφερθέντες υπολογισμούς, καλύπτοντας ένα μεγάλο εύρος από την πυκνότητα, και τις παράγωγες θερμοδυναμικές ιδιότητες, όπως η ταχύτητα του ήχου και η καμπύλη αναστροφής Joule-Thomson, έως τις ιδιότητες μεταφοράς στις οποίες συγκαταλέγονται το ιξώδες και συντελεστής διάχυσης. Εφαρμόζοντας ένα ακριβές και αξιόπιστο θερμοδυναμικό μοντέλο, το οποίο μπορεί να καλύψει όλο το εύρος ιδιοτήτων και συνθηκών που απαιτούνται, μπορεί να εξασφαλισθεί καλύτερη ποιότητα και ακρίβεια για τις μελέτες διακινδύνευσης.

Στην παρούσα εργασία, ένα πλήθος καταστατικών εξισώσεων (ΚΕ) αξιολογήθηκαν διεξοδικά ως προς τις δυνατότητές τους για την πρόβλεψη ιδιοτήτων του καθαρού CO_2, αλλά κυρίως πολυσυστατικών μιγμάτων του με άλλα αέρια. Πειραματικά δεδομένα από τη βιβλιογραφία χρησιμοποιήθηκαν ώστε να γίνουν οι απαραίτητες συγκρίσεις, αναδεικνύοντας ομοιότητες των μεθόδων όταν αυτές εφαρμόζονται για σχετικά απλές ιδιότητες όπως η πυκνότητα και η ισορροπία φάσεων ατμού – υγρού, ενώ οι ΚΕ ανώτερης τάξης, όπως για παράδειγμα η PC-SAFT, αποδείχθηκαν πολύ πιο ακριβείς για τους υπολογισμούς παράγωγων θερμοδυναμικών ιδιοτήτων και ιδιοτήτων μεταφοράς. Συγκεκριμένα, οι παράγωγες θερμοδυναμικές ιδιότητες υπολογίζονται από αναλυτικές εξισώσεις, κάτι που σημαίνει ότι το υπολογιστικό κόστος δεν αυξάνεται δραματικά, ενώ παράλληλα το φυσικό περιεχόμενο των ΚΕ δοκιμάζεται. Στον αντίποδα, οι ιδιότητες μεταφοράς περιέχουν ως μεταβλητή το χρόνο, κάτι που καθιστά αδύνατο τον υπολογισμό τους από ΚΕ προερχόμενες από τη θερμοδυναμική ισορροπίας. Η δυσκολία αυτή μπορεί να αντιμετωπισθεί μέσω της επέκτασης των ΚΕ με τη βοήθεια ειδικών μαθηματικών μοντέλων, τα οποία όταν συνδυασθούν και παραμετροποιηθούν εκ νέου, δίνουν τη δυνατότητα υπολογισμού ιδιοτήτων μεταφοράς. Τα μοντέλα για τον υπολογισμό του ιξώδους καθαρών συστατικών αλλά και μιγμάτων, συνδέθηκαν με τις υπό μελέτη ΚΕ, ενώ η χρήση ενός μετα-ευρετικού αλγορίθμου βελτιστοποίησης οδήγησε στην κατάρτιση πινάκων παραμέτρων για κάθε συστατικό και κάθε ΚΕ που μελετήθηκε.

Υπολογισμοί ιξώδους μιγμάτων συγκρίθηκαν με τα ομολογουμένως λιγοστά πειραματικά δεδομένα της βιβλιογραφίας, δίνοντας σχετικά χαμηλά σφάλματα. Παράλληλα, τα κενά πειραματικών δεδομένων προσδιορίστηκαν, με σκοπό να λειτουργήσει ως πρόταση για μελλοντική έρευνα. Οι συνδυασμένες μέθοδοι αυτές, και οι νέες παράμετροι αποτελούν τμήματα ενός μεγαλύτερου θερμοδυναμικού προσομοιωτή που αναπτύχθηκε κατά τη διάρκεια αυτής της εργασίας.

Πολλά χρήσιμα συμπεράσματα βγήκαν από αυτή τη δουλειά, τα οποία μπορούν να αξιοποιηθούν περαιτέρω στην ανάπτυξη προσομοιωτών που αφορούν αποκλειστικά την μεταφορά CO_2 μέσω δικτύων αγωγών. Οι ΚΕ ανώτερης τάξης, όπως η PC-SAFT και η tPC-PSAFT, μπορούν να προβλέψουν τις θερμοδυναμικές ιδιότητες των μελετώμενων συστημάτων με μεγαλύτερη ακρίβεια, ενώ το επιπρόσθετο υπολογιστικό κόστος δεν κυμαίνεται σε απαγορευτικά επίπεδα. Ειδικά οι υπολογισμοί για τις παράγωγες θερμοδυναμικές ιδιότητες τονίζουν την υπεροχή των ΚΕ ανώτερης τάξης απέναντι στις ευρέως διαδεδομένες κυβικές ΚΕ, αφού οι τελευταίες συνήθως εμφανίζουν αρκετά μεγαλύτερα σφάλματα.

Οι ιδιότητες μεταφοράς μπορούν να υπολογισθούν αποτελεσματικά μέσω του συνδυασμού των ΚΕ με εξειδικευμένα μοντέλα, με βασική προϋπόθεση ότι οι παράμετροι πρέπει να επαναπροσδιορισθούν έτσι ώστε το μοντέλο να είναι ρυθμισμένο για την εκάστοτε ΚΕ. Τμήμα της παρούσας εργασίας είναι αφιερωμένο στη βελτιστοποίηση παραμέτρων για τα διαφορετικά μοντέλα, καθώς και τα συστατικά που μελετώνται.

Λέξεις κλειδιά

Δέσμευση και αποθήκευση άνθρακα, διοξείδιο του άνθρακα, θερμοδυναμικά μοντέλα, καταστατικές εξισώσεις, παράγωγες θερμοδυναμικές ιδιότητες, ιδιότητες μεταφοράς

Αφιερωμένο με πολλή αγάπη στους γονείς μου Γιάννη και Αναστασία και στον αδελφό μου Αλέξανδρο

Thermodynamics is a funny subject. The first time you go through it, you don't understand it at all. The second time you go through it, you think you understand it, except for one or two small points. The third time you go through it, you know you don't understand it, but by that time you are so used to it, so it doesn't bother you anymore.

Arnold Johannes Wilhelm Sommerfeld (1868 – 1951)

Acknowledgments

Even though the PhD journey is a long and mainly lonely road, there are certain people that walked with me during longer or shorter periods, having definitely a positive impact on my work and everyday life. To those people I would like to dedicate this part of my thesis.

I am sincerely and heartily grateful to my supervisor, Professor Ioannis Economou. He has always been there for me, encouraging me continuously and giving invaluable advice on my work. His vast experience on the topics I studied has been a great motivation and led to increasing my levels of confidence in my work and my passion to learn more. Also, I would like to especially thank him for giving me the opportunity of spending 28 months in Abu Dhabi, as a visiting PhD student in the Petroleum Institute. We had a very good time there, both in and out of the university, and I would like to thank Prof. Economou and his family, for their support while in Abu Dhabi.

Special thanks I would like to address to my supervising committee members, Prof. Andreas Boudouvis, and Assist. Prof. Epaminondas Voutsas, for their support and the very constructive discussions we had. Although we were not collaborating on a daily basis, they were always interested in my progress and willing to spend quality time together.

Furthermore, I am deeply indebted to my senior colleagues and co-authors from NCSR "Demokritos", Dr. Dimitrios Tsangaris and Dr. Georgios Boulougouris, with whom we worked closely to carry out the CO2PipeHaz project. Their experience and insight have been extremely valuable in all the stages of the project.

I would also like to thank my colleagues and friends from the Molecular Thermodynamics and Modeling of Materials Laboratory in NCSR "Demokritos", which is directed by Prof. Economou.

During my stay in Abu Dhabi, I was fortunate to work together with professors and researchers from The Petroleum Institute, and engineers and executives from the Abu Dhabi Company for On-shore Oil Operations (ADCO), from whom I acquired a

substantial amount of knowledge, on a wide range of topics. I would like to offer my special thanks to them for their support and trust; Dr. Shahin Negahban, Dr. Hisham Sadaawi, Prof. Cor Peters, Dr. Francisco Vargas, Dr. Vasileios Michalis, Mohamad El Kadi, and Mohamed Sherief.

I also wish to thank Prof. Ilja Siepmann and Angel Cortés from the University of Minnesota, for the excellent ongoing collaboration on a very interesting research topic. Our discussions with Prof. Siepmann have always been spurring new questions and further thought, and working together with Angel has been a real pleasure.

I would like to express my gratitude for the financial support from the 7th European Commission Framework Program for Research and Technological Development for the project "Quantitative failure consequence hazard assessment for next generation CO_2 pipelines" (Project No.: 241346), and Abu Dhabi Company for On-shore Oil Operations (ADCO) for the project "Thermodynamic Model Development for the ADCO CO_2 EOR".

At this point I wish to thank my friends, who are "the family one chooses". Marios, Vasilis, Thanasis and Yiannis, Mayte, Christine and Joelle, Nuno, Sameer, Richard, Khalfan, Mohamed Ali and Taha, Andrew and Themie, Kyriakos, Alexandros, Panagiotis, Andreas and Prodromos, are definitely people with whom I share many happy moments and they have supported me a lot, each of them in their own way. Thank you for just being there for me.

It would have been impossible for me to contemplate this road, without the love and support of my parents, Yiannis and Anastasia, who continuously strived to give me all the prerequisites and the mindset to walk along the path of studying. They have been always patient during my absence and two warm hugs during my presence. A special thought is devoted to my brother, Alexandros, who has been always supportive, especially during the small hours.

Ευχαριστώ Thank you شكرا

Nikolaos Diamantonis

Athens, July 2013

Table of Contents

List of Tables

List of Figures

List of Abbreviations

AAD	Average Absolute Deviation
BWR	Benedict – Webb – Rubin
CCS	Carbon Capture & Sequestration
CPA	Cubic Plus Association
EOR	Enhanced Oil Recovery
EoS	Equation of State
FT	Friction Theory
GERG	Groupe Européen de Recherches Gazières
GHG	Greenhouse Gas
HV	Huron-Vidal mixing rules
IPCC	Intergovernmental Panel on Climate Change
LJ	Lennard – Jones
MSA	Mean Spherical Approximation
NIST	National Institute of Standards and Technology
PC-SAFT	Perturbed Chain – SAFT
PR	Peng – Robinson
PR/G	Peng – Robinson / Gasem
PSO	Particle Swarm Optimization
PT	Patel – Teja
PVTx(y)	Pressure – Volume – Temperature – Compositions
REFPROP	Reference Fluid Thermodynamic and Transport Properties

RK	Redlich – Kwong
SAFT	Statistical Associating Fluid Theory
SLE	Solid – Liquid Equilibria
SRK	Soave – Redlich – Kwong
SRK-HV	SRK with Huron-Vidal mixing rules
SRK-VdW	SRK with van der Waals mixing rules
SVE	Solid – Vapor Equilibria
tPC-PSAFT	truncated Perturbed Chain – Polar SAFT
VLE	Vapor – Liquid Equilibria
3P1T	3-parameter cubic EoS with 1 Parameter Temperature-dependent

List of Symbols

Latin Letters

A	Parameter for PR EoS
a	Parameter for PR EoS
A^{res}	Residual Helmholtz free energy
a^{res}	Residual Helmholtz free energy per mole
a_i	Constant coefficients for zero-density limit viscosity calculation according to Vesovic et al.
$a_{th.exp.}$	Thermal expansion coefficient
B	Parameter for PR EoS
B_{IC}	Isothermal compressibility coefficient
b	Parameter for PR EoS
b_i	Coefficients for excess viscosity calculation according to Vesovic et al.
c	Parameter for volume translation method
C_v	Isochoric heat capacity
C_p	Isobaric heat capacity
d	Effective diameter for diffusivity calculations
d_{ij}	Constant coefficients for excess viscosity calculation according to Vesovic et al.
D_0	Self-diffusion coefficient of a hard-sphere fluid according to kinetic theory
$D_{0,chain}$	Low density limit of the self-diffusion coefficient of a chain fluid
$D_{dense,chain}$	Correction term for the calculation of self-diffusion coefficient for dense chain fluids
D_E	Self-diffusion coefficient of a hard-sphere fluid according to Enskog theory
$\frac{e}{k}$	SAFT dispersion energy parameter by Chen and Kreglewski

f_i^j	Fugacity of component i in phase j
$f(\rho)$	Empirical factor for the calculation of self-diffusion coefficient (Yu and Gao)
$F(N_{spheres}, \rho)$	Empirical factor for the calculation of self-diffusion coefficient (Yu and Gao)
F_c	Empirical factor
$F_R(N_{spheres}, \rho, T)$	Empirical factor for the calculation of self-diffusion coefficient (Reis et al.)
$g(\rho)$	Radial distribution function
G	Gibbs free energy
G_η^*	Reduced effective cross-section
H	Enthalpy
JT	Joule-Thomson coefficient
K_i	Equilibrium ratio of vapour over liquid composition of component i , K-factor
K_T	Isothermal bulk modulus
k_{ij}	Binary interaction parameter
k_T	Isothermal compressibility coefficient
m	Number of segments in the chain molecule
MW	Molecular weight
N	Number of molecules
$N_{spheres}$	Number of hard spheres in a chain
$N_{spheres,i}$	Number of spheres of component i
$N^*_{spheres,mix}$	Reduced number of spheres of the mixture
P	Pressure
P_c	Critical pressure
P_{att}	Attractive term of pressure
P_{rep}	Repulsive term of pressure
Q	Quadrupole moment
R	Universal gas constant

$R(\rho)$	Empirical factor for the calculation of self-diffusion coefficient (Reis et al.)
S	Entropy
T	Temperature
T^*	Dimensionless temperature
T_c	Critical temperature
T_r	Reduced temperature (w.r.t. T_c)
T^{red}	Reduced temperature (w.r.t. $\frac{\varepsilon}{k}$)
U	Internal energy
v	Molar volume
v_c	Critical volume
w	Speed of sound
x_i	Mole fraction of component i
Z	Compressibility factor
z_i	Feed composition of component i

Greek Letters

$\alpha(T)$	Temperature dependent function for the attractive term of PR
α_v	Thermal expansion coefficient
β	Phase split
$\Delta\eta$	Excess viscosity
$\Delta\eta_c$	Critical viscosity
ΔH_{vap}	Heat of vaporization
$\varepsilon^{A_iB_i}$	Association energy
$\frac{\varepsilon}{k}$	Energy scaling parameter
ε_{ij}	Energy of dispersion interactions between segments
η	Total dynamic viscosity

η_0	Viscosity at the dilute gas limit
$\eta_{p.f.}$	Packing fraction
κ	Function of acentric factor
$\kappa^{A_iB_i}$	Volume of association interactions
$\kappa_{alc/wat}$	Association factor used only for alcohols and water
κ_{att}	Temperature dependent coefficient for the attractive term of viscosity according to Friction Theory
κ_{rep}	Temperature dependent coefficient for the repulsive term of viscosity according to Friction Theory
$\kappa_{rep-rep}$	Second order temperature dependent coefficient for the repulsive term of viscosity according to Friction Theory
μ	Dipole moment
μ_i^j	Chemical potential of component *i* in phase *j*
μ_{JT}	Joule-Thomson coefficient
μ_r	Dimensionless dipole moment
ρ	Density
σ_{ij}	Chain segment diameter
σ_p	Effective polar segment diameter
ω	Acentric factor
ω_{sound}	Speed of sound
$\Omega^*(T^*)$	Collision integral

Subscripts

i	Integer enumerator
j	Integer enumerator
mix	Mixture

Superscripts

res	Residual
ideal	Ideal
ref	Reference
hs	Hard spheres
chain	Chain
disp	Dispersion
assoc	Association
polar	Polar interactions
ind	Induced polar interactions
nc	Number of components

1. Introduction

1.1. Motivation

The continuous increase of global energy needs leads to the increase of fossil fuel consumption. Fossil fuels are currently the predominant source of energy, because of a number of factors, ranging from the level of maturity of new technologies, to the social acceptance of novel technologies. The inevitable result of fossil fuels consumption is the accumulation of greenhouse gases in the atmosphere, leading to environmental problems and global climate change. The most important greenhouse gas, in terms of quantity and impact, is carbon dioxide (CO_2). Research effort is directed worldwide to the development of techniques in order to minimize the accumulation of CO_2 in the atmosphere. One of the most popular techniques is the Carbon Capture and Storage (or Carbon Capture and Sequestration), abbreviated as CCS, which is defined as the process of capturing the CO_2 from the emissions of a large point source (power plant, cement plant, etc.), transporting it to the site where the storage will happen, and then depositing it to a geological formation, or subsea at a high depth. This action should ensure that the CO_2 will not escape to the atmosphere.

The process consists of three main parts: capture, transport, and storage. Transport of CO_2 takes place either in long networks of pipelines, or with the use of ships, where the distance is a deterrent to the use of pipelines. Usually, the part of pipeline transport is overlooked, even though it is of equal importance to the other two. Due to the extensive research on the pipeline transport of natural gas, the resulting practices are often extrapolated to the pipeline transport of CO_2, which is not always a wise approach, since the CO_2 pipelines may be crossing in close proximity to densely populated areas. Thus, a more thorough investigation regarding the hazard assessment of the pipelines should be performed before the actual commissioning of such projects. The most economical state for the transport of CO_2 is that of supercritical. It is well known from the literature that supercritical CO_2 is one of the most powerful solvents, so a

pipeline carrying supercritical CO_2 might suffer from sealing and corrosion problems. The hazards are not limited in the pipeline, but they are also related to the environment, in the unfortunate event of a rupture.

A transportation infrastructure that carries CO_2 in large enough quantities to make a significant contribution to climate change mitigation will require a large network of pipelines spanning over hundreds of kilometers. Given that the most economical means of transporting CO_2 is in the supercritical state due to its low viscosity and high density, a typical 100 km, 0.8 m diameter CO_2 pipeline under such conditions would contain approximately 9000 tonnes of inventory. In the event of pipeline failure, for example a full bore rupture, a significant proportion of the inventory would be discharged in the first few minutes. At a concentration of 10%, an exposed individual would lapse into unconsciousness in 1 min. Furthermore, if the concentration is 20% or more, the gas is instantaneously fatal [1]. Since CO_2 is heavier than air, it can be accumulated in depressions in the land, in basements and in other low-lying areas such as valleys near the pipeline route, presents a significant hazard if leaks continue undetected. [2]

Hydrocarbons will eventually ignite or explode in such areas if, and when, conditions are "right", but CO_2 can remain undetected for a very long time. Also, CO_2 will be mixed with potentially toxic substances whose natural dispersion might be impeded by the dense CO_2 vapor layer close to the ground, further increasing hazards. In 1986 a cloud of naturally-occurring CO_2 spontaneously released from Lake Nyos in Cameroon killed 1,800 people in nearby villages [3].

There are several other hazards associated with the accidental release of CO_2. It can act as an ignition source for nearby combustible materials due to friction induced static discharge. In 1953, such an incident resulted in 29 fatalities [4]. CO_2 also reacts with water to form carbonic acid leading to the corrosion of carbon steel pipelines [5]. Supercritical CO_2, widely considered to be the most economical state for pipeline transportation is a powerful solvent giving possible toxic contamination and sealing problems. Its release may lead to low temperatures resulting in brittle fracture of surrounding equipment [5]. High velocity solid CO_2 discharge may pose the risk of

erosion impact (supercritical CO_2 with solid CO_2 pellets is used commercially as a cutting media). [6]

It is obvious that the thermodynamic modeling of CO_2-containing systems is of key significance to CCS, since a large number of properties are required by pipeline outflow simulators and dispersion models, which in turns are necessary for a holistic approach of the hazard assessment studies for CCS processes.

1.2. Objectives

The main objectives of this dissertation have been the following:

- Development of an extended framework for the calculation of phase equilibria and thermodynamic properties of system containing CO_2,
- Assessment of several Equations of State (EoS) on their capabilities of representing thermodynamic properties of varying complexity,
- Extension of certain EoS in order to predict transport properties of CO_2 mixtures,
- Investigation of multi-component mixtures' behaviour in the presence of CO_2,
- Assessment of parameters and optimization of them, in order to provide accurate thermodynamic representation of the mixtures of interest, at the studied conditions range,
- Integration of the thermodynamic properties simulator with simulators for pipeline outflow and dispersion, in order to investigate the impact of several thermodynamic models on the final results.

1.3. Structure of Thesis

In this section, the way the thesis is structured will be described, in order to present briefly the topics discussed here, as well as guide the reader through it.

The motivation and the objectives are presented in this brief Chapter 1, in order to set the boundaries of the area studied in this work. The following two chapters are dedicated to the theoretical background of the work. The results and discussion are presented in Chapters 4, 5, 6, and 7. Finally, the thesis closes with the conclusions and proposals for future work.

More specifically, Chapter 2 provides an extensive literature review of the models used for the prediction of several thermophysical properties, mainly of mixtures containing CO_2.

In Chapter 3, the models used in this work are presented in detail, giving their mathematical formalism, as well as the methods and the algorithms employed for the calculations. The EoS SAFT, PC-SAFT, tPC-PSAFT, Peng-Robinson, the equations for the thermodynamic derivative properties, as well as models for viscosity, diffusion coefficient, and thermal conductivity are given. The phase equilibria calculations, and some auxiliary methods used (such as Particle Swarm Optimization) are explained.

The thermodynamic derivative properties of pure CO_2 and its mixtures with other gases are investigated in Chapter 4. Speed of sound and Joule-Thomson coefficient are the highlights of thermodynamic derivative properties that are significant to process design applications.

Chapter 5 contains the work on phase equilibria calculations for several mixtures that contain CO_2. The effect of other gases (CH_4, O_2, N_2, Ar, H_2S, SO_2) is investigated thoroughly, since these gases are often found in a CO_2 pipeline. A special section is dedicated to the CO_2-H_2O mixture because of its great scientific and industrial significance. This mixture is formed as soon as the injected CO_2 comes in contact with the formation water in the underground reservoir, as well as it is the main mixture formed in the case of underwater storage of CO_2. Also, corrosion issues are closely related to the behavior of this system. Extensions to a multicomponent synthetic oil, as well as phase equilibria calculations, where one phase is solid, are also presented in the last sections of Chapter 4, in an effort to cover conditions below the triple point of CO_2.

Another important group of properties that can be of cornerstone importance to process design are viscosity, thermal conductivity, and diffusion coefficient. Results for these properties are discussed in Chapter 6.

Chapter 7 discusses a multi-disciplinary work that shows how thermodynamic models can be linked to outflow and dispersion simulators, and the effect they can have on the final outcome.

The conclusions from this work are collectively presented in Chapter 8, while Chapter 9 contains suggestions and thoughts for future work in this area.

2. Literature Review

2.1. General Information on CCS

The increasing population on earth creates a growing need for energy, which primarily comes from fossil fuels. The combustion of such fuels imposes a strong perturbation on carbon cycle, causing the accumulation of greenhouse gases (GHGs) in the atmosphere. As a consequence, there is a growing concern over the impact that this accumulation can have on the global climate change.

The greatest contribution to GHG emissions is made by carbon dioxide (CO_2) [7]. The global CO_2 emissions, measured in billion tons, were 22.7 in 1990, 25.4 in 2000, and 33.0 in 2010 [8], while generally CO_2 contributes on average 80 % of the GHGs [9, 10].

Controlling the emissions of greenhouse gases (GHGs) in the atmosphere poses major technological and scientific challenges. CO_2 is the leading greenhouse gas in terms of volume and plays a significant role in climate change. As the world energy demand steadily increases and burning of fossil fuels, a key mechanism of CO_2 emission, remains high, CCS technologies become vital in reducing emissions of GHGs [7, 11-13].

The mitigation of CO_2 has been the center of scientific and technological attention for many years. The early stages of the efforts have been documented by Steinberg [14]. In the proceedings of the 1st International Conference on Carbon Dioxide Removal [15], the scientific community was encouraged to focus its attention on the problem.

Hence, the academic and industrial community directed their efforts into developing technologies for the reduction of the CO_2 emissions in the atmosphere. According to the IPCC's (Intergovernmental Panel on Climate Change) report [7], there are five technological options for reducing the emissions or the accumulation of CO_2 in the atmosphere: switching to low-carbon energy sources, expanding forests, energy

efficiency, solar radiation management, and carbon dioxide removal. One very promising technology, as it is shown by the extent of the projects realized worldwide, is CCS, which falls in the category of carbon dioxide removal. In Europe, there are two already operating large scale CCS projects, the Sleipner CO_2 injection [16] and the Snøhvit CO_2 injection [17], while the European Union currently supports six CCS projects through its Zero Emissions Platform [18].

CCS consists of three stages that the CO_2-containing stream has to go through: capture, transport, and storage. Each part has a dedicated set of methods that spur individual research activities on the details and the challenges identified in them. Overview of the CCS process, for all its three stages, are given in recent reviews [11, 19-28] which cover techno-economic aspects.

Although CCS has been studied thoroughly, there are still unresolved issues. For example, the cost of investment, the impact on the environment, the energy cost of capture and storage and the hazards associated with accidental release cannot be managed satisfactorily and further work in research and engineering is needed. Several studies have been reported on the life cycle analysis of a CCS process associated with different types of CO_2 emitters [29-33].

From a technological aspect, a very important element of CCS technology is related to the transportation of CO_2-rich flue gas from the capture unit to the storage field. For this purpose pipelines are mainly used [34-36], which run for several hundreds of kilometers with the possibility of crossing in close proximity to inhabited areas. A thorough risk assessment study is always needed for this part, in order to estimate the effect of a potential fracture on the pipeline and of course lead the design to avoid such incidents.

A propagating fracture will result in the loss of a considerable part of the pipeline, and hence is undesirable. Propagating fractures can be of two types: brittle or ductile. Brittle propagating fractures are prevented by ensuring that the pipeline steel is operating on the safe regime according to its specifications. Ductile propagating fractures are prevented by specifying a minimum toughness to ensure that a ductile fracture will arrest;

or, in the case that the required toughness is too high, by using mechanical crack arrestors. However, brittle fracture propagation is not an issue in modern pipeline steel, while a ductile fracture will not propagate if there is not sufficient amount of energy in the system to overcome the resistance to propagation. [37]

CO_2 pipelines are mostly susceptible to propagating ductile fractures because the CO_2 is usually transported in the supercritical dense phase. At high pressures, supercritical CO_2 behaves as a liquid, and has a liquid-like density, but it yields a very large volume of gas when its pressure is lowered, because of its very high vapor pressure. [37, 38]

The design of CO_2 transport pipelines relies heavily on the accurate knowledge of the thermodynamic properties of the fluid. From volumetric to derivative properties, they are all important for the optimum design. The most efficient way of transporting CO_2 is in the supercritical state [35], although other researchers [36] claim that the transport could be done in the sub-cooled liquid state. Hence, a wide range of conditions should be covered, from supercritical conditions to ambient temperature and pressure [39], as well as different compositions of the mixture, so as to study the effect of impurities [40]. Although the stream often consists of almost pure CO_2 (composition >90%) [35], other gases may be found, such as SO_2, NO_x, H_2S, H_2, CO, CH_4, N_2, Ar and O_2, depending on the type of the plant and the capture process [7].

2.2. Thermodynamic Models and CCS

In order to cover these needs in the framework of an engineering project, the available experimental data solely are not enough. In addition, some of the mixtures such as $CO_2 - SO_2$ are very corrosive and, due to this fact, the experimental data available are very limited [41-43]. EoS are appealing alternative tools to predict the properties in the desired conditions – compositions set.

The most widely used thermodynamic models for process design are based on EoS. More specifically, cubic EoS rooted to van der Waals theory are highly preferred

due to their simplicity, ease of implementation, and limited computing requirements. In this respect, the Redlich-Kwong (RK) EoS [44] has been one of the first approaches for real fluids, while the Peng-Robinson (PR) [45] and the Soave-Redlich-Kwong (SRK) [46] are the most popular ones. In parallel, there are many semi-empirical higher order EoS developed for specific components or systems as, for example, the EoS by Span and Wagner [47]. Such EoS are usually accurate for the components and conditions developed but are difficult to generalize for multi-component mixtures. In recent years, higher order EoS rooted to statistical mechanics have gained significant interest by the engineering community. The most widely used EoS in this category are based on the Statistical Associating Fluid Theory (SAFT) [48, 49] and its variations, most notably the Perturbed Chain-SAFT (PC-SAFT) [50]. Thanks to the increased computational power at relatively low price, SAFT and PC-SAFT are now available in commercial process simulators. A number of reviews [51, 52] concerning these models are available in the literature.

For CCS applications, important thermodynamic properties include vapor pressure, density and various second order thermodynamic properties such as heat capacities, speed of sound, Joule-Thomson coefficients and isothermal compressibility. The calculation of these properties is a great challenge for all kinds of EoS. It is believed though, that EoS with molecular background, such as SAFT-family EoS, may have better performance in this type of calculations because they include all the important molecular contributions [53, 54].

SAFT-based EoS for CCS applications have attracted some attention but have not been studied and developed enough, even though they have been shown to be very accurate for complex CO_2 mixtures, such as with amines and ionic liquids [55-60]. Thus, it is of high value to assess the accuracy of SAFT versus cubic EoS and improve its performance as we aim towards a single EoS that can be used in the entire CCS process, namely, capture, transport and sequestration.

One of the integral parts of the design in all three stages of CCS is the thermodynamic model used. The systems to be studied may contain a wide range of

components, including pure CO_2, and mixtures with other gases, amines, ionic liquids, water, and brines. The significance of implementing a reliable and accurate thermodynamic model for each stage of the CCS process lies on the calculation of the energy penalty [19, 61], as well as the operating conditions of the equipment, and the selection of material in order to avoid corrosion issues [62]. Although the focus of this work is mainly on pipeline CO_2 transport, some information will be given for the other two parts later, for the sake of completeness.

2.3. Phase Equilibria and Volumetric Properties

As far as phase equilibria modeling of systems related to CCS technologies is concerned, several approaches have been reported in the literature that vary with respect to components, methods and conditions investigated.

Nakamura et al. [63] identified the growing significance of mixtures of CO_2 with other gases for energy related processes, and they pointed out the little attention that these systems had received by then. Their work focused on the development of a perturbed-hard-sphere EoS which was similar to the one given by Carnahan and Starling [64] applied to fourteen pure polar and non-polar components, and several of their mixtures. Five parameters for each of the pure components were given, as well as two binary interaction parameters for every binary mixture. Nevertheless, the authors stated that due to the lack of experimental data for the mixtures studied, the parameters are reasonable estimates in most of the cases. CO_2 mixtures had a central role in their study: The examined thirteen CO_2 binary mixtures (with H_2, Ar, N_2, CO, CH_4, C_2H_4, C_2H_6, C_3H_6, C_3H_8, H_2O, NH_3, H_2S, SO_2), while for nine of them (CO_2 with H_2, Ar, N_2, CH_4, C_2H_4, C_2H_6, C_3H_8, H_2O, H_2S) experimental data were available.

The properties that were calculated in that work were density, enthalpy, entropy, and fugacity coefficients, with very little comparison to experimental data, due to the absence of the latter. However, compressibility factor calculations were presented to be in fair agreement with available data.

McCoy and Rubin [65] developed an engineering economic model of CO_2 pipeline transport, and they identified the significance of the impurities effect on property estimation. Their approach to thermodynamics was based on the use of the standard Peng-Robinson EoS [45] with parameters and mixing rules taken from the established database of Reid et al. [66]. They pointed out the non-linear behavior of CO_2 compressibility, especially in the range of pressures common for pipeline transport. Moreover, they illustrated the effect that impurities, such as H_2S, can have on the compressibility.

Frey et al. [67] applied a density and temperature dependent volume translation function on SRK EoS (abbreviated as DMT), in order to estimate phase equilibria and density of mixtures, including the $CO_2 - H_2O$ and $CO_2 - CH_4$ mixtures, which are of immediate interest to the CO_2 transport for CCS processes. They argued that the use of a single binary interaction parameter does not overcome the obstacle of accurate simultaneous description of dew and bubble point pressures and liquid phase compositions at high pressures. Comparing the translated and the original EoS only for the phase equilibria predictions, no significant differences were found, while the greatest influence was claimed to be rooted only to the selection of mixing rules. On the other hand, the molar volumes of the mixtures were predicted more accurately by the DMT.

Carroll [68] used the PR and SRK EoS to study the vapor-liquid equilibria (VLE) behavior of CO_2 mixtures with CH_4 and H_2S, proving that these tools are quite accurate for the prediction of the complex phase equilibria exhibited by these systems. Azeotropy was also included in their study.

Li et al. [69] published a very thorough review of experimental data and theories available for the modeling of PVTxy properties of CO_2 mixtures that are of interest to the whole process of CO_2 capture, transport, and storage. They listed cubic EoS as the first category of theories used in the literature, including PR, Patel – Teja (PT), SRK, and some of their variants with respect to the mixing rules. Several works on EoS that take into account association interactions such as SAFT, and Cubic Plus Association (CPA), were also reported. Moreover, predictive EoS, and EoS that promise high accuracy on

the cost of a large database for parameter fitting, such as the Benedict – Webb – Rubin (BWR) equation and Groupe Européen de Recherches Gazières (GERG) equation, were also included. As a conclusion, it was stated that none of the evaluated EoS could predict equally accurately both VLE and volume for CCS applications. As a bottom line, they suggested that a reference EoS exclusively for CCS has to be developed in the future.

Li and Yan [13] published a study on the comparative performance of five cubic EoS, namely PR, PT, RK, SRK and 3P1T [70], for predicting VLE of CO_2 and binary CO_2-mixtures containing CH_4, H_2S, SO_2, Ar, N_2 and O_2. For every binary mixture, the binary interaction parameter (k_{ij}) was taken as temperature and composition independent. After fitting this parameter for every mixture and for every EoS, it was obvious that the value of k_{ij} was extremely important for the accuracy, especially of the saturated vapor composition. In conclusion, SRK was suggested for the modeling of pure CO_2 VLE, and PR, PT, and 3P1T were recommended for particular binary mixtures.

Later on, Li and Yan [40] assessed the ability of seven cubic EoS (PR, PT, RK, SRK, modified PR, modified SRK, and improved SRK) for predicting the volumes of binary CO_2 mixtures containing CH_4, H_2S, SO_2, Ar and N_2. The binary interaction parameters were different from their previous work [13]; in this case it was adjusted to experimental data for gas and liquid volumes respectively. PR and PT EoS were claimed to be the most accurate in general, while modified PR was recommended only for the case of CO_2 – H_2S liquid volume, and improved SRK for the CO_2 – SO_2 gas volume.

Austegard et al. [71] evaluated the performance of the models SRK with van der Waals mixing rules (SRK-VdW), SRK with Huron Vidal mixing rules (SRK-HV), and the CPA EoS for the prediction of the mutual solubilities of H_2O, CO_2 and CH_4. New model parameters were refitted for the SRK-HV and the CPA EoS. It was concluded that the SRK-HV EoS is the preferred model for these systems, when applied to conditions used for the fitting process. However, its higher accuracy comes at the cost of two temperature dependent variables for each binary system, comparing to CPA that uses only one such parameter. In addition, CPA is substantially more computationally demanding because of the iterative process in solving the associating term. The SRK-HV

model was later used by Munkejord et al. [72] in order to perform fluid dynamics calculations of pipeline depressurization of a CO_2 – CH_4 mixture. They found that the HV mixing rules do not really affect the result since none of the components is polar, and that a volume shift fitted to experimental data is needed for overcoming the pitfalls of the cubic EoS in the liquid regime.

2.4. Derivative Thermodynamic Properties

From a scientific standpoint, it is agreed that the prediction of derivative thermodynamic properties is one of the most demanding tests for an EoS [53, 73]. The majority of literature publications related to SAFT and its variations refer to phase equilibria calculations of pure fluids and mixtures while very few studies have been published on derivative properties calculation. The derivative properties can be calculated by analytical expressions directly derived from the mathematical formalism of the SAFT EoS, without the need for numerical solvers. Deviations from experimental data should be attributed to the model inefficiency and parameters' calculation which is usually based on fitting VLE data [53, 74].

Previous work on using SAFT-family EoS for the calculation of derivative properties has been done by several research groups, for a variety of families of compounds using different approaches. For example, second order properties for n-alkanes were calculated by Lafitte et al. [75] using various versions of SAFT, while Llovell et al. [76-78] used the soft-SAFT EoS to calculate derivative properties for some selected mixtures of n-alkanes.

Experimental data for derivative properties of CO_2 mixtures with gases of interest to CCS are really scarce. In terms of importance, knowledge of the speed of sound is highly needed for a range of applications. It can be used for the prediction of wave propagation in a pipeline, leakage tests, monitoring compositional changes, as well as 4D seismic studies [79-86].

Alsiyabi et al. [87] reported experimental measurements of speed of sound and isothermal compressibility of systems containing CO_2 and impurities, reaching up to a quaternary system. The effect of impurities such as N_2, CH_4, CO, O_2, Ar, and H_2 on these properties was studied. In the same work, a thermodynamic model based on PR EoS, with the use of Mathias-Copeman [88] temperature dependent function, and a modified volume correction fitted on pure CO_2, was also reported. The model was shown to be in excellent agreement with the experimental isothermal compressibility and density data from Span and Wagner [47]. Unfortunately, the model was not tested against speed of sound measurements.

However, derivative properties of mixtures of CO_2 with higher hydrocarbons have been reported due to the interest in the field of supercritical fluids. A relevant work is that of Polikhronidi et al. [89] which contains experimental data for the isochoric heat capacity of the CO_2 – n-decane mixture.

2.5. Transport Properties

A procedure based on corresponding states was developed by Hanley [90] for the prediction of viscosity and thermal conductivity of both pure fluids and mixtures. The inclusion of a new term derived from the modified Enskog theory was the key to correct the relatively high errors that were observed at high densities. The CO_2 – N_2 mixture was one of the mixtures examined, while the deviations between experiments and calculations were within the experimental uncertainty. Noteworthy is the fact that this method does not need transport properties data of the fluid; hence, it can be characterized as predictive.

Vesovic and coworkers published a series of papers [91-93] on the formulation of a new model for viscosity, targeted especially to high density fluid mixtures. The rigid sphere theory is the basis of their approach, suitably modified to self-consistently account for the real gas behavior. Comparing their method with earlier methods, the range of applicability is extended, leading to more accurate predictions of viscosity even at higher

values of pressure. The CO_2 – CH_4 mixture was described by their theory within 5 % deviation from experiments.

Vesovic and Wakeham [92] extended their viscosity model to gas mixtures at high density conditions. According to the method, each pure component was modeled with a pseudoradial distribution function, which is fitted to viscosity experimental data. This expression is a smooth function of density, and it exhibits good performance at the limits of both low and high densities. The power of the method was demonstrated with the modeling of the viscosity of the CO_2 – CH_4 mixture. The pressures that the calculations took place are up to 70 MPa, and in this range, the viscosity of the mixture changes by approximately one order of magnitude. The accuracy reported was quite satisfactory, given that the maximum error is 5 %. Since it is a model based on density, it can be very well used in combination with any EoS, in a manner that the predicted density of the EoS will be the input for the viscosity calculation via the Vesovic and Wakeham [92] method.

In their monograph on transport properties of CO_2 [93], it is reported that their model can be used adequately for engineering applications, but there is room for improvement in terms of the scientific basis of the model. They also expressed the hope for more measurements of transport properties on pure CO_2 and CO_2 – containing mixtures.

Viscosity, thermal conductivity, along with density and heat capacity, were studied by Homer and Kayar [94] in a report that describes the development of a software for the calculation of these properties, according to equations and correlations from the literature [66]. CO_2 is included in the study, but it is not the main component of importance. The modifications reported in that document refer mainly to He and H_2, in order to achieve better agreement at low pressures.

Fenghour et al. [95] revisited the problem of pure CO_2 viscosity modeling, by proposing a method that consists of three distinct terms to account for three different regimes. Thus, the zero-density limit is modeled by the same expression as in [93], the excess viscosity is described by a polyonymic expression of temperature and density, and

the critical contribution is considered negligible because it becomes slightly important only within 1 % of the critical temperature. By using a database of experimental data, only five parameters are fitted for the excess viscosity. The viscosity of the liquid phase, at temperature lower than 260 K and pressure lower than 250 MPa is predicted with deviation with 2 %.

Classical mechanics and its definition for friction were reclaimed by Quiñones-Cisneros et al. [96], and combined with the Van der Waals theory of fluids, produced a new theory for viscosity prediction. The Friction Theory (FT) consists of a dilute gas term, and a friction term which is a function of the attractive and repulsive terms of pressure. The latter can be calculated by any EoS, regardless of its complexity. In the same work, parameterization and assessment of the model for cubic EoS was presented.

Papari [97], in an effort to model the viscosity of CO_2 in the framework of Chapman-Enskog method, stated that due to the internal structure of CO_2, the collision integrals become too complicated. In order to increase accuracy with avoiding overhead complexity, an iterative inversion method was combined with the corresponding states correlation of viscosity. This way, an effective spherical pair potential energy for CO_2 was generated, and it was used to predict low density transport properties. Applying the same approach, Haghighi et al. [98, 99] calculated the viscosity and the diffusion coefficient of some binary mixtures, including $CO_2 - SF_6$ and $CO_2 - CF_4$.

Wilke [100] reported an equation for the calculation of gas mixtures' viscosity, which is based on the kinetic theory of gases, and uses the pure component viscosities and molecular weights. The developed expression was applied for a number of binary and multicomponent mixtures, some of them with CO_2. The data were predicted with sufficient accuracy.

The $CO_2 - N_2$ mixture in particular was studied by Kestin and Leidenfrost [101] experimentally, for the temperature of 20 ^{o}C and pressures up to 22 atm, and Wilke's equation [100] was used to model the data. Experimental data showed a positive deviation from a linear interpolation between the two pure component viscosities while the model predicted a negative deviation. The authors attributed the failure of the model

to the polar nature of CO_2. This conclusion was further analyzed later on by Kestin et al. [102]. Careful experimental work reduced the uncertainty in the determination of composition, which in turns led to very good agreement between data and theory. In their latter work, Kestin et al. [102] used the Chapman-Enskog theory, to model the experimental data.

Another work to support the statement that Wilke's equation can perform well for CO_2 mixtures, is that of Gururaja et al. [103], in which viscosity was measured for the mixtures $CO_2 - O_2$ and $CO_2 - N_2$, and the data were modeled with the use of the equations developed by Wilke [100] and Saxena and Gambhir [104]. For the CO_2 - containing mixtures, it was concluded that Wilke's method performs slightly better than the Saxena and Gambhir model.

Kestin et al. [105] developed an extended corresponding states approach, in order to correlate, among other properties, the viscosity and the diffusion coefficient of monoatomic gases and their binary mixtures. Phase equilibrium was also taken into account. Their approach was to replace the corresponding integrals of the Chapman-Enskog theory with universal functions, which in turn are based on the two-parameter pair potential, assumed to be the same for all the monoatomic gases. Further on, they applied this theory to mixtures that contain CO_2, and they concluded that despite the inclusion of more complex molecules, the accuracy of their theory is not compromised [106].

Nonpolar fluid mixtures and their viscosity prediction was the focal point of the work by Ely and Hanley [107], based on the previous work of Hanley [90]. Methane was selected as the reference fluid, and a 32 terms BWR-type equation was refitted to accommodate the need to cover a wider temperature range. The viscosity of both pure fluids and their mixtures was predicted very accurately, with deviations lower than 10 %. A model analogous to the previously mentioned, was presented later on [108] for predicting the thermal conductivity of pure fluids and mixtures. Critical constants, molecular weight, Pitzer's acentric factor, and the ideal heat capacity are the parameters needed by the model. CO_2 was one of the pure components that were studied, but there

was no reference to mixtures of it. The authors concluded that the model is sufficiently accurate for a wide range of hydrocarbons, exhibiting an average deviation from experimental data of less than 7 %.

2.6. CO_2 Capture

CO_2 capture is quite challenging to be modeled thermodynamically, because it contains a number of highly unlike species. CO_2, amines, ionic liquids, and water create systems with many different types of intermolecular interactions. Since the focus of this work is on the transport part of CCS, a short overview of models for CO_2 capture is given.

A number of methods rely on the thorough study of the chemical reactions between amines and CO_2 [109, 110], which leads to expressions for the equilibrium constant, and by applying Henry's law and certain assumptions, to explicit equations of the CO_2 partial pressure over the alkanolamine solutions. Parameters fitted to experimental data provide a good correlation of them.

Models based on activity coefficient have also been developed through explicit account of the Coulombic interactions. Such an example is the electrolyte – NRTL model [111-115]. In addition, UNIQUAC was used to model CO_2 with aqueous amine solutions at a wide range of conditions [116].

EoS with explicit account of Coulombic interactions between ionic species have also been developed with good accuracy. Several such EoS have been assessed, including the electrolyte-Cubic-Two-State (e-CTS) [117], CPA [118], PC-SAFT [119, 120], and SAFT-Variable Range (SAFT-VR) [121].

2.7. CO_2 Transport Considerations

It has been suggested that the operation pressure of CO_2 pipelines should be above 8.6 MPa, which ensures that CO_2 will always be in a single phase over a range of

temperatures that may be encountered in the pipeline [122]. The range of temperatures is generally defined by the temperature of the surrounding soil. For example, in northern latitudes, the soil temperature varies from a few degrees below freezing in winter, to 6 – 8 ^{o}C in summer, while in tropical locations the soil temperature may reach up to 20 ^{o}C [123]. One more design constraint is the construction material of the pipeline. In-depth analysis of the allowable operating conditions for several materials is given by Mohitpour et al. [39]. The design capacity of the CO_2 pipeline depends on the thermodynamic properties of the transported mixture, which are dictated by the previously mentioned factors.

In a recent comprehensive work, Aursand et al. [124] summarized the methods used for the fluid flow modeling of CO_2 pipelines. A section was devoted to the role of thermophysical models where it was claimed that the existing models for other systems of industrial interest (such as oil – gas – H_2O mixtures) cannot be used straightforwardly to CO_2 applications.

The thermodynamic models that are examined in the following sections refer to EoS rooted in theoretical considerations that are applicable to a wide range of fluids. However, there are some really outstanding reference EoS, such as GERG [125, 126] and REFPROP [127], that are component specific and give very high quality results for pure CO_2 and mixtures.

2.8. Thermodynamics of CO_2 Storage

The most widely accepted approaches to sequester CO_2 are the following two: either in the beds of deep oceans [128], or in oil reservoirs where the injected CO_2 can act as enhancer for the recovery of oil (enhanced oil recovery – EOR) in the case of a not depleted well [129]. All these processes have a common point that is the continuous appearance of mixtures of CO_2 with other components, such as hydrocarbons, gases, or H_2O [7, 35]. H_2O – CO_2 mixture is also important for CO_2 transport via pipelines, since the flue gas that is transported is not totally dry after the separation processes [130-132].

In addition, in the event of a pipeline rupture, CO_2 immediately mixes with the humidity of the atmosphere. One of the most notable design considerations is that CO_2 is an acid gas and in the presence of H_2O may react to form carbonic acid. The corrosion that stems from the formation of carbonic acid is the main challenge for processes that involve CO_2, something that in oil and gas industry is referred to as "sweet gas" corrosion [4]. Also, the formation of hydrates is potent, under certain conditions [133].

With respect to the geological storage of CO_2, the most common systems are the CO_2 – H_2O and the CO_2 – H_2O – NaCl mixtures. A significant amount of work has been done on the thermodynamic modeling of these two systems.

The CPA EoS coupled with two methods for estimation of the cross-association parameters was used by Tsivintzelis et al. [134] in an effort to model the VLE of the CO_2 – H_2O mixture. According to the first method, the energy of association is calculated by the arithmetic mean, while the geometric mean is applied for the volume of association. The second method makes use of experimental data available in the literature. The cross-association between CO_2 and H_2O was concluded to be of crucial role, but self-association of CO_2 should be omitted. Also, a non-zero binary interaction parameter was required due to the high non-ideality of the system.

Pappa et al. [135] used three different forms of PR EoS to model the CO_2 – H_2O mixture. Two of these forms employed different sets of mixing rules (van der Waals one-fluid and universal mixing rules), while the third one took into account the association interactions, so the model was essentially the CPA-PR EoS. In this case, association was taken into account both for CO_2 and H_2O with the assumption of four sites for both molecules. This modeling scheme for CO_2 was used by the same group in other studies as well [136, 137]. The solubility of CO_2 in H_2O was calculated with less than 25.5 % error for temperatures lower than 373 K, while for higher temperatures the maximum error observed was 27.8 %. The authors concluded that for temperatures lower than 373 K the three models perform similarly. At higher temperatures, the CPA-PR approach is superior over the other two.

Another school of thought that was applied to these systems lays its foundations on the SAFT and its variations (PC-SAFT, etc.). This type of EoS has been claimed to be suitable to model the CO_2 – H_2O mixture. Ji et al. [138] used an extension of SAFT that accounts for electrolytic interactions, namely the SAFT1-RPM EoS, to model the CO_2 – H_2O mixture and the effect of NaCl on it. CO_2 was modeled as a 3-associating site molecule, while the cross-association energy and volume parameters were fitted to experimental data and shown to be temperature dependent, especially for temperatures lower than 373 K. They concluded that polar interactions are accounted implicitly via the temperature dependency of these parameters.

A PC-SAFT [50] variation that includes a term for explicit account of polar interactions, the tPC-PSAFT, was used by Karakatsani et al. [139] who modeled CO_2 as a quadrupolar fluid with two sites available only for cross-association with H_2O. Four association sites per molecule were assumed for H_2O, on top of the explicit account of its dipolar nature [55]. A linear temperature dependent binary interaction parameter was used. The non-linear pressure change with composition was very accurately reproduced.

Another application of a polar version of PC-SAFT EoS, namely PCP-SAFT, was presented by Tang and Gross [140]. The quadrupole – quadrupole interactions of CO_2 were explicitly accounted for, while H_2O was treated as a strongly associating component without polar interactions. Very good results for temperatures lower than 373 K were reported, with the use of a temperature dependent binary interaction parameter.

A group contribution version of PPC-SAFT was developed and used by Nguyen-Huynh et al. [141] for the CO_2 – H_2O mixture. H_2O was described as an associating dipolar molecule and CO_2 as a cross-associating quadrupolar fluid. Experimental data were used to fit the cross-association energy. The reported errors for the equilibrium composition were relatively higher compared to earlier studies.

Diamantonis and Economou [142] attempted to evaluate thoroughly the accuracy of two PC-SAFT versions, in particular the original PC-SAFT and the tPC-PSAFT for modeling the VLE of H_2O – CO_2 mixture. H_2O was modeled as a 4-associating site component while CO_2 was considered as either non-associating,

associating with different number of sites, or polar component. In all cases, a single temperature independent binary interaction parameter was used, and in some cases the cross-association volume was fitted, leading to marginal improvement. It was concluded that it is quite challenging to model accurately both CO_2-rich and CO_2-lean phases for certain conditions. According to that work, PC-SAFT with explicit account of H_2O – CO_2 cross-association and with one adjustable parameter (k_{ij}) is the recommended model for the reliable correlation of mixture phase equilibria.

A modification of the Lee-Kesler [143] equation was reported by Duan et al. [144], which depends on fifteen parameters for each pure component. PVT data were used for the fitting of those parameters for the pure components CO_2, CH_4, and H_2O. Very good agreement with experimental data was shown, even for conditions that are outside of the range used in the parameter fitting. In a subsequent work, Duan et al. [145] extended their equation to mixtures of the three studied pure components. The binary CO_2 – CH_4 mixture was modeled with three binary interaction parameters which are temperature dependent. Four different expressions were used for the calculations of this temperature dependence. Such an extensive use of multiple binary parameters resulted in a very good agreement with the experimental PVTx data. However, due to the lack of experimental data for the ternary mixture, especially for the conditions range of interest, only a statement on qualitative agreement was made.

Duan and Sun [146] used their previously mentioned EoS [144, 145] in combination with Pitzer's theory on electrolytes [147] in order to develop a solubility model for CO_2 in seawater. For the vapor phase, the fugacity coefficient of the CO_2 – H_2O mixture was assumed to be similar to that of pure CO_2 for the studied temperature range (273 K – 533 K), therefore Duan et al. [145] EoS can be used for its calculation. The liquid phase activity coefficient of CO_2 was calculated by a virial expansion of Gibbs free energy, according to Pitzer [147]. The reported errors were quite low and in most of the cases within the experimental uncertainty of about 7 %. The model performed well for pressures up to 200 MPa and for ionic strength up to 4.3 m (molality).

Another combined method for phase equilibria calculations of systems that contain oil, gas, and water or brine, was developed by Li and Nghiem [148]. According to their work, three phases were identified, namely vapor, liquid, and aqueous one. PR EoS was used for the modeling of the vapor and liquid phases, whereas the solubility of gas in the aqueous phase was represented by Henry's law. The solute molecular diameter was suggested as the parameter that relates the accuracy of the solubility predictions to the concentration of NaCl in the water. In general, the model was more accurate for predicting the solubility of CO_2 in pure water than in brine.

Harvey and Prausnitz [149] identified the inadequacy of activity coefficient models to represent systems that contain ionic effects. Their method lies on superimposing the ionic effects on a non-electrolytic EoS. Osmotic coefficient data were used to obtain the values of an adjustable salt/solvent parameter, which is necessary for the calculation of ion-ion interactions through the Mean Spherical Approximation (MSA). The charging of the ions was described by a modified version of Born's equation. The nonelectrolyte contribution was modeled based on the Helmholtz energy of a mixture of molecules obeying the Lennard-Jones potential. Various mixtures were examined including $CO_2 - H_2O - NaCl$. Model calculations for this mixture were in very good agreement with the experimental data. For all other mixtures, the salt effect on the phase behavior was underpredicted at high pressures and high salt concentrations. The temperature dependence of the salt/water parameters was considered to be the source of the errors at higher temperatures. The parameters for most of the systems were fitted to experimental data at 25 ^{o}C but it is not clear if they can be applied at higher temperatures.

Another attempt to model the thermodynamics of the same ternary mixture by adding an electrostatic contribution term to an EoS was reported by Zuo and Guo [150]. The PT EoS was extended by a Debye-Hückel term to account for the ion-ion interactions. Two parameters were needed for the molecular species, with the exception of water. One binary interaction parameter for every binary system was used that was adjusted to osmotic coefficient data for water-salt pairs, VLE data for gas-water mixtures, and low pressure solubility data for the salt-gas pairs. The ternary mixture was studied

with this method, and the results were in good agreement with the experimental data. When compared to the results of Harvey and Prausnitz [149], no clear conclusion can be made, because of the quite similar performance of the two models. For the other ternary systems that were investigated, the discrepancies at high pressures that were reported by Harvey and Prausnitz [149] are shown to be significantly reduced with the use of Zuo and Guo [150] method.

An unsymmetric model for VLE calculations with application to the solubility of acid gases, CO_2 and H_2S, in solutions of NaCl – H_2O, was reported by Dubessy et al. [151]. Their model follows different principles for every type of interactions. More specifically, the Stryjek-Vera cubic EoS was used for the representation of the vapor phase, while the liquid phase was described by a combination of the Redlich-Kister's regular solution activity coefficient model with Raoult's and Henry's laws. Finally, the salt effect was taken into account by a blend of Pitzer's model for water activity and an extension of Setchenow's law. The authors claimed that the water content in the vapor phase cannot be neglected, and this is the main difference of this model to the one developed by Duan et al. [145]. The mathematical formalism was developed with gradual increase of complexity, covering the cases of no water content in the vapor phase to no constraint for the composition of the vapor phase. The Henry's constants of each of the studied ternary mixtures were calculated by an equation with fifteen adjusted parameters, fitted to experimental data. The authors concluded that the model works very well for pressures lower than 50 MPa, reasoned by the in-built restrictions of the theories used.

Hassanzadeh et al. [152] identified the drawbacks of implementing a model that is based fully on EoS, in a flow simulator, mainly because of its high computational cost. In order to improve this, they reported a method for converting compositional data from EoS to black-oil PVT data, which in turn can be used for the flow simulations of CO_2 storage applications. The thermodynamic model used in that work is a combination of the models reported by Duan and Sun [146] and Spycher et al. [153]. Coupling these models with Hassanzadeh et al. [152] black-oil conversion method was proven to be four

times faster than the conventional ones, whilst accuracy was not sacrificed. Using their algorithm, CO_2–brine density, solubility, and formation volume factor were predicted.

3. Thermodynamic Models and Algorithms

3.1. Cubic Equations of State

EoS provide the mathematical formalism that interrelates temperature (T), pressure (P), volume (v) and composition (x_i) of a fluid. Most of the EoS used in chemical thermodynamics are pressure-explicit equations. Once the EoS is solved for volume (or equivalently for density), all remaining primary and derivative properties can be calculated using simple thermodynamic relations [154]. Cubic EoS are based on the pioneering work of van der Waals that proposed the first EoS applicable both to liquid and gas states. Because of its simplicity, van der Waals EoS can provide only qualitative description of the thermodynamic properties of real fluids. A large number of cubic EoS have been proposed in the last few decades. Several recent reviews provide an overview of them [155, 156]. In this work, some of the most widely used cubic EoS are used to calculate CO_2 mixture properties.

A general formalism of the cubic EoS has been proposed by Daridon et al. [157], according to which:

$$P = \frac{RT}{v-b} - \frac{a \cdot \alpha(T)}{v^2 + u \cdot b \cdot v + w \cdot b^2} \tag{3.1}$$

where R is the gas constant; a and b are component-specific constants for the attractive intermolecular interactions and the hard core volume of the component, respectively, and are calculated as a function of critical temperature, T_c, and pressure, P_c. Furthermore, $\alpha(T)$ is a component-specific function of temperature that was introduced in order to provide a better agreement with experimental data from low temperature up to the critical point. u and w are numerical constants with the following values for each EoS: $u = w = 0$ for van der Waals EoS, $u = 1$ and $w = 0$ for RK and SRK EoS, and $u = 2$ and $w = -1$ for PR EoS.

Significant effort has been devoted in order to develop accurate expressions for $\alpha(T)$ for different types of fluids [155, 156]. In this work, the original expression proposed by Peng and Robinson [45], as well as the expression proposed by Gasem et al. [158] claimed to be an improvement over the original expression, are examined for pure CO_2 phase equilibria. In Table 3–1, the expressions for a, b, and $\alpha(T)$ for the various EoS are presented.

Table 3–1. Expressions for $\boldsymbol{a}$, $\boldsymbol{b}$, and $\boldsymbol{\alpha(T)}$ for the cubic EoS examined in this work (RK, SRK, PR, PR/G).

EoS	$\boldsymbol{a}$	$\boldsymbol{b}$	$\boldsymbol{\alpha(T)}$
RK	$0.42748\frac{R^2(T_c)^{2.5}}{P_c}$	$0.08664\frac{RT_c}{P_c}$	$\frac{1}{T^{0.5}}$
SRK	$0.42748\frac{R^2(T_c)^{2.5}}{P_c}$	$0.08664\frac{RT_c}{P_c}$	$\left[1+(0.480+1.574\omega-0.176\omega^2)\left(1-\sqrt{T_r}\right)\right]^2$
PR	$0.45724\frac{R^2(T_c)^2}{P_c}$	$0.07780\frac{RT_c}{P_c}$	$\left[1+(0.37464+1.54226\omega-0.26992\omega^2)\left(1-\sqrt{T_r}\right)\right]^2$
PR/G	$0.45724\frac{R^2(T_c)^2}{P_c}$	$0.07780\frac{RT_c}{P_c}$	$exp\left[(2+0.836\,T_r)\left(1-T_r^{0.134+0.508\omega-0.0467\omega^2}\right)\right]$

For mixture calculations, the standard one-fluid van der Waals mixing rules were used [159] with a single temperature independent binary interaction parameter, k_{ij}:

$$a\alpha(T)=\sum_{i=1}^{c}\sum_{j=1}^{c}x_i x_j\sqrt{(a\alpha)_i(a\alpha)_j}\left(1-k_{ij}\right) \tag{3.2}$$

$$b=\sum_{i=1}^{c}x_i b_i \tag{3.3}$$

A temperature-independent k_{ij} allows reliable extrapolation of the calculations over a wide temperature range. A more in-detail analysis of the mathematical framework of the Peng - Robinson cubic EoS is given in the Appendix.

3.2. SAFT and PC-SAFT Equations of State

The higher order SAFT EoS [48, 49, 160, 161] and its extension, PC-SAFT EoS, developed by Gross and Sadowski [50, 162] are used in this study. The theoretical foundations of the SAFT models are rooted to the first order perturbation theory of Wertheim (TPT1) [163-166]. In perturbation theory, the potential energy of a relatively complex molecular fluid is described as the sum of the potential energy of a simple reference fluid and a perturbation or correction term. Usually, the first term is known accurately and the challenging part is the description of the perturbation term. If a suitable perturbation term is developed, then all the remaining thermodynamic properties can be calculated using standard thermodynamic expressions. This term is usually a function of temperature, density or pressure, and composition.

In this respect, SAFT and PC-SAFT EoS are written as summations of the residual Helmholtz free energy terms, A^{res}, that occur due to different types of molecular interactions in the system. The residual Helmholtz free energy is equal to the Helmholtz free energy minus the Helmholtz free energy of the ideal gas at the same temperature, T, and density, ρ. Consequently:

$$\begin{aligned}\frac{A^{res}(T,\rho)}{NRT} = \frac{a^{res}(T,\rho)}{RT} &= \frac{a(T,\rho)}{RT} - \frac{a^{ideal}(T,\rho)}{RT} \\ &= \frac{a^{ref}(T,\rho)}{RT} + \frac{a^{disp}(T,\rho)}{RT} \\ &= \frac{a^{hs}(T,\rho)}{RT} + \frac{a^{chain}(T,\rho)}{RT} + \frac{a^{disp}(T,\rho)}{RT} + \frac{a^{assoc}(T,\rho)}{RT}\end{aligned} \tag{3.4}$$

where a is the Helmholtz free energy per mole and the superscripts *res*, *ideal*, *ref*, *hs*, *chain*, *disp*, and *assoc* refer to residual, ideal, reference, hard sphere (monomer reference fluid), chain, dispersion, and association interactions respectively. Details on the individual terms can be found in the literature [49, 50, 160, 167].

The difference between SAFT and PC-SAFT is based on the reference fluid used. Specifically, SAFT uses the hard-sphere reference fluid while PC-SAFT uses the

hard-chain reference fluid to account for the dispersion interactions. As a consequence, the functional forms of the two models are different.

For non-associating components, SAFT and PC-SAFT require three parameters for each pure component, namely:

- The number of segments, m, in the chain molecule,
- The chain segment diameter, σ_i,
- The energy of dispersion interactions between segments, ε_i,

In SAFT, an additional dispersion energy parameter is used, namely $\frac{e}{k}$, originally proposed by Chen and Kreglewski [168] and correlated to Pitzer's acentric factor and the critical temperature of the component. In SAFT, we use a constant $\frac{e}{k}$ = 10 for most of the compounds, except for a few gases.

Two more parameters are added for pure components that exhibit association interactions:

- The association energy between sites of like molecules, $\varepsilon^{A_iB_i}$,
- The volume of association interactions, $\kappa^{A_iB_i}$.

These parameters are fitted to experimental pure component vapor pressure and saturated liquid density data from low temperature up to close to the critical point.

Dispersion interaction parameters are calculated from Lorentz – Berthelot combining rules [50, 160]. For the chain segment diameter:

$$\sigma_{ij} = \frac{1}{2}(\sigma_i + \sigma_j) \tag{3.5}$$

and for the energy of dispersion between segments:

$$\varepsilon_{ij} = \sqrt{\varepsilon_i \varepsilon_j}(1 - k_{ij}) \tag{3.6}$$

Here again, a temperature-independent k_{ij} is used. In this way, head-to-head comparison between the various EoS is possible.

SAFT and PC-SAFT EoS are extended to mixtures by introducing σ_{mix} and ε_{mix} that are evaluated by the following mixing rules [160] derived from van der Waals one-fluid theory:

$$\sigma_{mix}^3 = \frac{\sum_{i=1}^{c}\sum_{j=1}^{c} x_i x_j m_i m_j \sigma_{ij}^3}{(\sum_{i=1}^{c} x_i m_i)^2} \tag{3.7}$$

$$\varepsilon_{mix}\sigma_{mix}^3 = \frac{\sum_{i=1}^{c}\sum_{j=1}^{c} x_i x_j m_i m_j \sigma_{ij}^3 \varepsilon_{ij}}{(\sum_{i=1}^{c} x_i m_i)^2} \tag{3.8}$$

For the association parameters, the cross association energy and volume are calculated according to the combining rules proposed by Gross and Sadowski [162]:

$$\varepsilon^{A_i B_j} = \frac{1}{2}(\varepsilon^{A_i B_i} + \varepsilon^{A_j B_j}) \tag{3.9}$$

$$\kappa^{A_i B_j} = \sqrt{\kappa^{A_i B_i}\kappa^{A_j B_j}}\left(\frac{\sqrt{\sigma_i \sigma_j}}{\frac{1}{2}(\sigma_i + \sigma_j)}\right) \tag{3.10}$$

Two different types of binary and ternary mixtures calculations are feasible with respect to bubble pressure. The first type refers to calculations using $k_{ij} = 0$. These calculations are based entirely on pure component parameters and are referred to as *predictions.* The second type refers to calculations with k_{ij} fitted to experimental binary VLE data. In this case, the deviation between experimental value and calculated value of the equilibrium pressure was minimizes as a result of the fitting procedure. These calculations are referred to as *correlations.* For the case of the ternary mixture, calculations are referred to as *predictions* even though a non-zero k_{ij} value is used, since

this parameter is obtained from the corresponding binary mixtures without any further adjustment.

3.3. The truncated PC – Polar SAFT

The PC-PSAFT EoS is an extension of PC-SAFT to account explicitly for polar interactions, developed by Karakatsani and Economou [167]. The truncated version of PC-PSAFT (tPC-PSAFT) is a relatively simple, yet accurate, engineering model. Both PC-PSAFT and tPC-PSAFT use the formalism of Larsen et al. [169] for dipolar and quadrupolar interactions. The full development can be found in the work of Karakatsani and Economou [167].

For a system that consists of associating chains, tPC-PSAFT can be expressed as:

$$\begin{aligned}\frac{A^{res}(T,\rho)}{NRT} &= \frac{a^{res}(T,\rho)}{RT} = \frac{a(T,\rho)}{RT} - \frac{a^{ideal}(T,\rho)}{RT} \\ &= \frac{a^{ref}(T,\rho)}{RT} + \frac{a^{disp}(T,\rho)}{RT} + \frac{a^{polar}(T,\rho)}{RT} + \frac{a^{ind}(T,\rho)}{RT} \\ &= \frac{a^{hs}(T,\rho)}{RT} + \frac{a^{chain}(T,\rho)}{RT} + \frac{a^{disp}(T,\rho)}{RT} + \frac{a^{assoc}(T,\rho)}{RT} \\ &+ \frac{a^{polar}(T,\rho)}{RT} + \frac{a^{ind}(T,\rho)}{RT}\end{aligned} \tag{3.11}$$

where a is the Helmholtz free energy per mole and the superscripts *res*, *ideal*, *ref*, *hs*, *chain*, *disp*, *assoc*, *polar* and *ind* refer to residual, ideal, reference, hard sphere (monomer reference fluid), chain, dispersion, association, polar and induced polar interactions respectively. Details on the individual terms can be found in the literature [49, 50, 160, 167].

For an associating component, PC-SAFT requires five parameters that are typically fitted to experimental data, in most cases vapor pressure and saturated liquid density from low temperature up to close to the critical point. These parameters were mentioned in the previous part of this work.

For the case of tPC-PSAFT, two additional parameters account for polar interactions:

- The effective polar segment diameter, σ_p, which is fitted to experimental data, and
- The dipole, μ, or quadrupole, Q, moment of the fluid, which are usually measured experimentally.

Furthermore, the SAFT based EoS that were previously mentioned, can be used to produce analytical expressions for the calculation of the following derivative properties:

$$\text{Isothermal compressibility coefficient: } k_T^{-1} = \rho \left(\frac{\partial P}{\partial \rho}\right)_T \tag{3.12}$$

$$\text{Thermal expansion coefficient: } a_{th.exp.} = k_T \left(\frac{\partial P}{\partial T}\right)_v \tag{3.13}$$

$$\text{Isochoric heat capacity: } C_v = -T \left(\frac{\partial^2 a_{th.exp.}}{\partial T^2}\right)_v \tag{3.14}$$

$$\text{Isobaric heat capacity: } C_p = C_v + \frac{T a_{th.exp.}{}^2}{k_T \rho} \tag{3.15}$$

$$\text{Joule-Thomson coefficient: } \mu_{JT} = T \left(\frac{\partial P}{\partial T}\right)_v - \rho \left(\frac{\partial P}{\partial \rho}\right)_T \tag{3.16}$$

$$\text{Speed of sound: } \omega_{sound} = \sqrt{\frac{C_p}{C_v} \left(\frac{\partial P}{\partial \rho}\right)_T} \tag{3.17}$$

3.4. Phase Equilibria Calculations

By definition, in chemical engineering terminology, multiple phases are in equilibrium when they are at the same temperature (thermal equilibrium), pressure (mechanical equilibrium), and the chemical potential (μ_i^j) of each species is the same in all phases (chemical equilibrium). This can be expressed by the following set of equations:

$$T^\alpha = T^\beta = \cdots = T^\pi \tag{3.18}$$

$$P^\alpha = P^\beta = \cdots = P^\pi \tag{3.19}$$

$$\mu_i^\alpha = \mu_i^\beta = \cdots = \mu_i^\pi \tag{3.20}$$

where $\alpha, \beta, \ldots, \pi$ are the phases that are in equilibrium, and $i = 1,2, \ldots N$ are the components of the system.

Fugacity, f_i^j, is the quantity that can be used in engineering calculations instead of the chemical potential. Thus, the equivalent equation that defines equilibrium at certain temperature and pressure is:

$$f_i^\alpha = f_i^\beta = \cdots = f_i^\pi \tag{3.21}$$

For both liquid and vapor phases, EoS is used to calculate the fugacity coefficient, φ_i^j, of each component in every phase. Fugacity coefficient is related to fugacity with the following expression:

$$f_i^j = \varphi_i^j x_i^j P \tag{3.22}$$

Thus the concept followed for the solution of VLE is:

$$f_i^l = f_i^v \Rightarrow \varphi_i^l x_i P = \varphi_i^v y_i P \Rightarrow \frac{y_i}{x_i} = \frac{\varphi_i^l}{\varphi_i^v} \Rightarrow K_i = \frac{\varphi_i^l}{\varphi_i^v} \tag{3.23}$$

For simplicity, theory will be given for the case of a system that has two phases, one liquid and one vapor. Depending on the sets of given data and the unknowns, the phase equilibria calculations differ. The main phase equilibria calculations of interest to the industry are:

3.4.a. Bubble Point Pressure Calculation

To illustrate better the calculation, the reader is advised to refer to Figure 3–1 which is a flowchart of the bubble point pressure calculation.

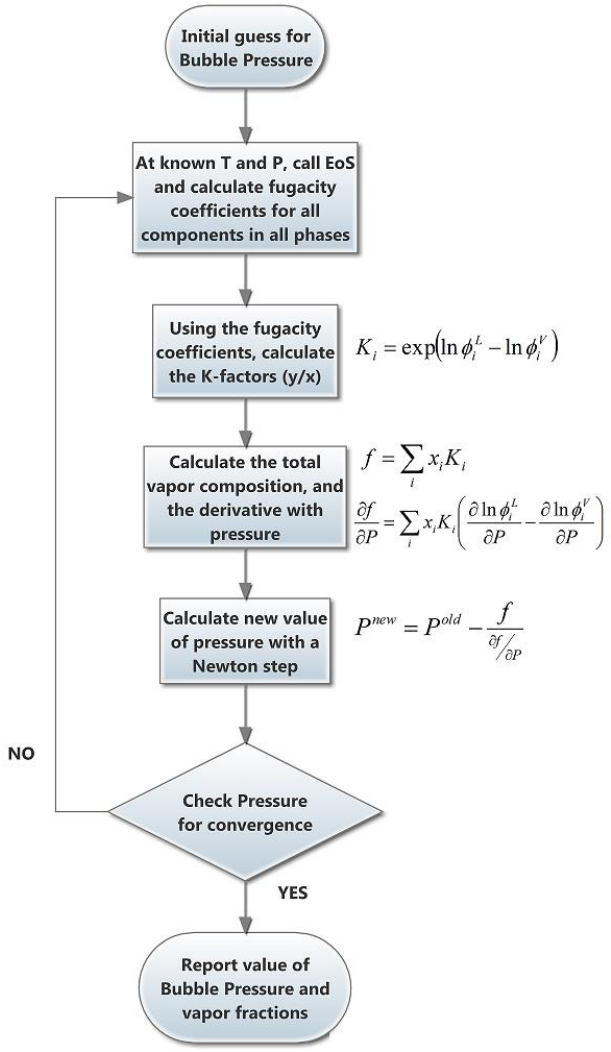

Figure 3–1. Flowchart of Bubble Point Pressure calculation.

In this case, temperature and liquid composition is given, and the target is to calculate the pressure at which equilibrium is achieved (vapor or bubble pressure), and the composition of the vapor phase at these conditions. The pressure is found with an iterative calculation scheme, in which the fugacity coefficients are calculated by any EoS, and the total composition of the vapor phase is checked to be unity.

3.4.b. Isothermal – Isobaric (TP) Flash Calculation

The flash calculation is performed under constant and known conditions of temperature and pressure, with both the liquid and vapor compositions being the unknowns. The flowchart of the TP-flash calculations can be seen in Figure 3–2.

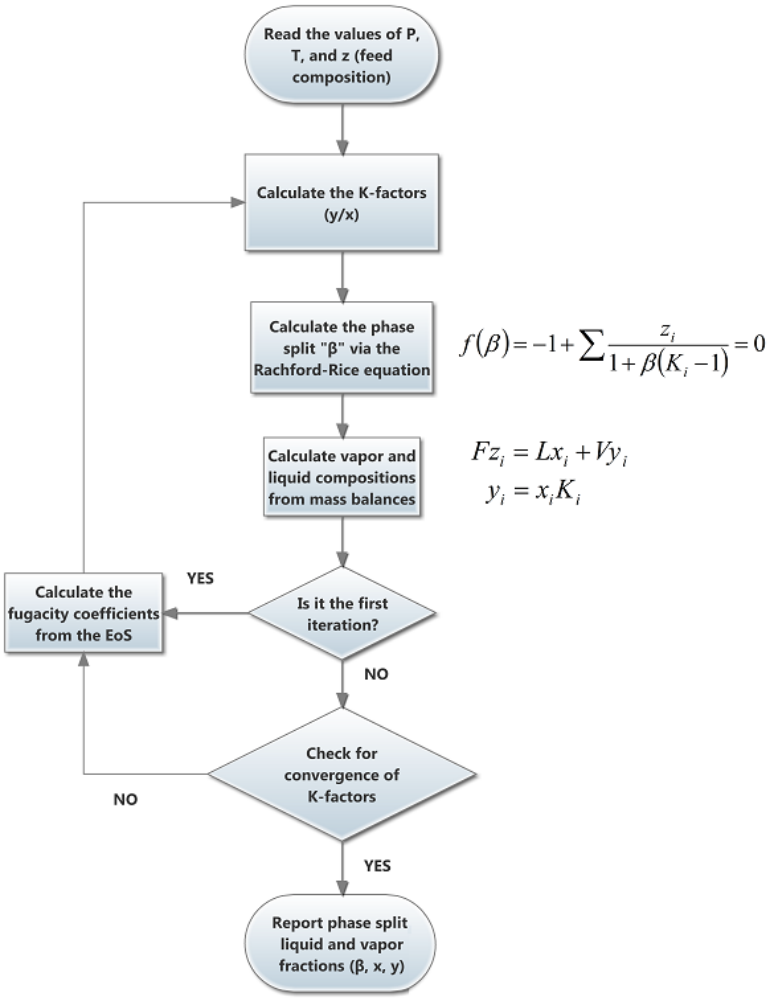

Figure 3–2. Flowchart of TP-flash calculation.

The calculation starts by a guess for the K-factors (ratio of vapor to liquid fractions), then the Rachford-Rice equation (Eq. (3.24)) is solved in order to provide the phase split.

$$f(\beta) = -1 + \sum \frac{z_i}{1 + \beta(K_i - 1)} = 0 \tag{3.24}$$

If it is the first iteration, then an EoS is used to calculate the fugacity coefficients, and from those, the K-factors. The Rachford-Rice is solved again, and the liquid and vapor fractions are calculated one more time. This series of calculations takes place iteratively, until the calculated K-factors converge.

3.4.c. Dew Point Pressure Calculation

This calculation is similar with the bubble point pressure calculation, with the difference that vapor phase composition is given instead of the liquid composition. The flow of the calculations is the same, but now the total composition of the liquid phase is checked to be unity.

3.4.d. Stability Analysis

Equifugacity is only a necessary condition for equilibrium to exist. Except from satisfying this criterion, the system has also to be stable at the conditions (T, P) of the solution. This happens, if and only if, the total Gibbs free energy of the system takes a value that can be considered as a global minimum [170].

When a transfer of δn_i moles of component i from the liquid phase to the vapor takes place, then the Gibbs free energy changes by δG.

$$\delta G = \left(\mu_i^v - \mu_i^l\right)\delta n_i \tag{3.25}$$

Based on this equation, a phase of composition $\boldsymbol{z}$ is considered, and it is assumed that a new phase is formed, which is infinitesimally small, δe, while its composition is $\boldsymbol{w}$. Thus, the change in Gibbs energy can be written as:

$$\delta G = \delta e \sum_{i=1}^{nc} w_i\big(\mu_i(\boldsymbol{w}) - \mu_i(\boldsymbol{z})\big) \tag{3.26}$$

Stability of the phase of composition $\boldsymbol{z}$ is achieved only if δG is non-negative for any positive δe. This is known as the tangent plane condition of Gibbs, and it is expressed as:

$$\sum_{i=1}^{nc} w_i\big(\mu_i(\boldsymbol{w}) - \mu_i(\boldsymbol{z})\big) \geq 0 \tag{3.27}$$

For the TP-flash calculations, a tangent plane stability analysis algorithm is implemented. This algorithm has been developed by Michelsen [171-173], and it is used to verify the stability of a single phase that may occur at specified temperature and pressure.

3.5. Optimization Algorithms

Optimization algorithms are an integral part of any thermodynamic simulator. Very often there is the need for parameters to be regressed to certain experimental data. The simplest case is the binary interaction coefficient, in which the optimized variable is just one, the k_{ij}, and the objective function can be either the minimization of error in saturation pressure, if the data are suitable bubble point calculations, or the minimization of error in K-factors, if the data include vapor fractions and allow flash calculations to be performed. These two cases are the common practices in academia and industry, but it does not restrict the scholar from using any desired objective function, with the subsequent modifications in the method and code.

3.5.a. Secant Method

For the case that there is only one variable with one objective function, the Secant method has been coded and used. The Secant method is a root-finding numerical algorithm and can be described as a finite difference variation of Newton's method. It can be applied on cases that the derivative of the objective function cannot be analytically expressed, without banning the method from use with differentiable objective functions.

If the variable is x, and the objective function that needs to be optimized is $f(x)$, without analytical derivative, then the recurrence relation for each new value of x, will be:

$$x^{(n)} = x^{(n-1)} - f\left(x^{(n-1)}\right)\frac{x^{(n-1)} - x^{(n-2)}}{f(x^{(n-1)}) - f(x^{(n-2)})} \tag{3.28}$$

The method needs two initial values that should preferably be in the close vicinity of the root, so as not to cause any convergence problems.

Practically, Secant may be faster compared to Newton, because it calculates only the function itself, but not the derivative. However, theoretically convergence is achieved sooner with Newton than with Secant.

3.5.b. Particle Swarm Optimization

There are cases that it is necessary to regress more than one variables, with respect to more than one objective functions. As a solution to this problem, a meta-heuristic optimization algorithm was programmed. Particle swarm optimization (PSO) is a population based stochastic optimization technique developed by Kennedy and Eberhart [174] in 1995, inspired by social behavior of fish schooling or bird flocking. The initiation of PSO is done with a group of random particles that get updated in search of the optima. Each iteration creates a new generation of particles that have been updated following two "best" values. The first one is the best value that has been generated so far by that particle (named "pbest"), while the second is the best value by any particle in the swarm, which is considered as a global best (named "gbest"). The velocity that each particle moves with is determined by a function of these two "best" particles.

$$u_i^{(k+1)} = wu_i^{(k)} + c_1 r_1 \left[pb_i^{(k)} - p_i^{(k)} \right] + c_2 r_2 \left[gb_i^{(k)} - p_i^{(k)} \right] \tag{3.29}$$

The method's flowchart can be seen in Figure 3–3.

The index of the particles is represented by i. Hence, $u_i^{(k)}$ is the velocity of particle i at time k and $p_i^{(k)}$ is the position of particle i at time k. The value $pb_i^{(k)}$ is the individual best candidate solution for particle i at time k, and $gb_i^{(k)}$ is the swarm's global

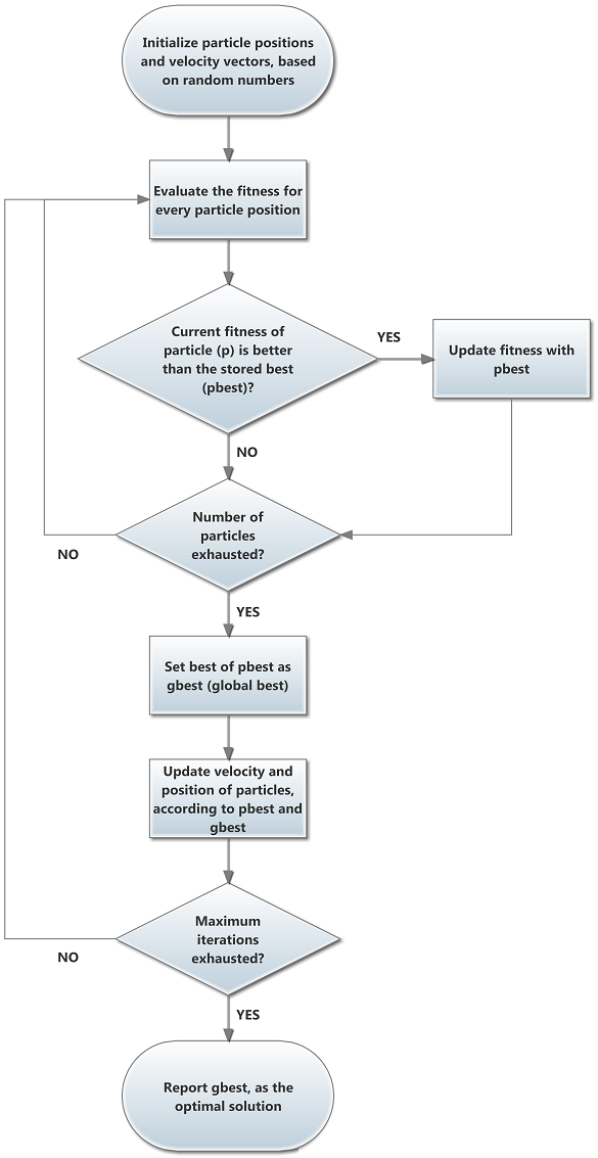

Figure 3–3. Flowchart for Particle Swarm Optimization method.

best candidate solution at time k. The parameters w, c_1, and c_2 ($0 \leq w \leq 1.2$, $0 \leq c_1 \leq 2$, and $0 \leq c_2 \leq 2$) are user-supplied coefficients. The values r_1 and r_2 ($0 \leq r_1 \leq 1$ and $0 \leq r_2 \leq 1$) are random values regenerated for each velocity update.

Each of these three terms plays a different role. Namely, the terms are the inertia, cognitive, and social respectively, and they are responsible of moving the solution more towards the local optimum or more towards the global one.

As soon as the velocity has been determined, the positions of the particles can be updated following the equation:

$$p_i^{(k+1)} = p_i^{(k)} + u_i^{(k+1)} \tag{3.30}$$

3.6. Viscosity Models

3.6.a. Vesovic et al. Model [93]

One of the models for viscosity determination that has been used is the one proposed by Vesovic et al. [93, 95] . This model refers only to the viscosity of pure CO_2 and is based on a set of equations that are dependent on temperature and density.

The formulation of the model consists of three terms, each one describing a different contribution to the final value of the property of viscosity. Thus, the total value of viscosity, η, is calculated by summing the zero-density limit, η_0, the excess viscosity, $\Delta\eta$, and the correction for the critical region, $\Delta\eta_c$.

$$\eta = \eta_0 + \Delta\eta + \Delta\eta_c \tag{3.31}$$

Viscosity at the Zero-Density Limit

The equation that gives the value of this term is:

$$\eta_0(T) = \frac{1.00697T^{1/2}}{G_\eta^*(T^{red})} \tag{3.32}$$

where the temperature must be given in K, while the viscosity is given in μPa·s.

The size $G_\eta^*(T^{red})$ is the reduced effective cross section, given by the empirical equation:

$$lnG_\eta^*(T^{red}) = \sum_{i=0}^{4} a_i (lnT^{red})^i \tag{3.33}$$

In Eq. (3.33) the reduced temperature is given by $T^{red} = \frac{kT}{\varepsilon}$, with $\frac{\varepsilon}{k} = 251.196K$ (energy scaling parameter).

The coefficients $\boldsymbol{a_i}$ take the values that are shown in Table 3–2.

Table 3–2. Values of coefficients $\boldsymbol{a_i}$

i	$\boldsymbol{a_i}$
0	0.235156
1	-0.491266
2	$5.211155 \cdot 10^{-2}$
3	$5.347906 \cdot 10^{-2}$
4	$-1.537102 \cdot 10^{-2}$

Excess Viscosity

The contribution of excess viscosity is calculated from a power series expansion in density. The coefficients that are taking part in Eq. (3.34) depend only on temperature.

$$\Delta\eta(\rho, T) = \sum_{i=1}^{n} b_i(T)\rho^i \tag{3.34}$$

In particular, the coefficients b_i are given from the Eq. (3.35):

$$b_i = \sum_{j=1}^{m} \frac{d_{ij}}{T^{*(j-1)}} \tag{3.35}$$

Density in all equations above should be expressed in units of kg·m^{-3}.

The constants d_{ij} take values after fitting the equations to experimental results of viscosity. For the pure CO_2, the values of coefficients d_{ij} are shown in Table 3–3.

Table 3–3. Values of constant coefficients $\boldsymbol{d_{ij}}$

d_{ij}	**Value**
d_{11}	$0.4071119 \cdot 10^{-2}$
d_{21}	$0.7198037 \cdot 10^{-4}$
d_{64}	$0.2411697 \cdot 10^{-16}$
d_{81}	$0.2971072 \cdot 10^{-22}$
d_{82}	$-0.1627888 \cdot 10^{-22}$

Critical region

Regarding the terms of critical region contributions, it can be neglected due to the fact that the ratio $\frac{\Delta\eta_C(\rho,T)}{\Delta\eta(\rho,T)}$ takes values greater than 0.01 only when the conditions are within 1% of critical temperature, that means less than 5 K range. This is a note that Vesovic et al. do, and they support it with calculations [93].

3.6.b. Friction Theory

The dynamic viscosity of a pure component in the framework of Friction Theory (FT) developed by Quiñones-Cisneros et al. in 2000 [96], is attributed to two terms; the dilute-gas limit and the dense-state correction:

$$\eta = \eta_0 + \Delta\eta \tag{3.36}$$

The viscosity at the dilute gas limit, η_0 , is given by the theory that was developed by Chung et al. [175], according to the following equation:

$$\eta_0 = 40.785 \frac{\sqrt{MW \cdot T}}{v_c^{\frac{2}{3}} \Omega^*(T^*)} F_c \tag{3.37}$$

where:

η_0: dynamic viscosity in μP,

MW: molecular weight (g/mol),

T: temperature in K,

v_c : critical volume in cm^3/mol (tabulated value),

$T^* = 1.2593 \frac{T}{T_c}$: dimensionless temperature,

$\Omega^*(T^*)$: collision integral,

F_c : empirical factor.

The empirical factor F_c for non-polar substances is related to the acentric factor according to the expression:

$$F_c = 1 - 0.2756\omega \tag{3.38}$$

For polar substances, the expression becomes:

$$F_c = 1 - 0.2756\omega + 0.059035\mu_r^4 + \kappa_{alc/wat} \tag{3.39}$$

where, $\kappa_{alc/wat}$ is the association factor that is used only for alcohols and water.

The term μ_r is the dimensionless dipole moment, which is given by the expression:

$$\mu_r = 131.3 \frac{\mu}{(v_c T_c)^{0.5}} \tag{3.40}$$

where, μ is the dipole moment, in Debye.

The Ω^* is the collision integral that was first given by Neufeld et al. [176] as $\Omega^{(2,2)*}$.

$$\Omega^{(2,2)*} = \frac{A}{T^{*B}} + \frac{C}{exp(DT^*)} + \frac{E}{exp(FT^*)} + RT^{*B} sin(ST^{*W} - P) \tag{3.41}$$

Values for the coefficients of this equation can be found in the Table 3–4.

The van der Waals theory of fluids and the friction concepts from classical mechanics are the basis for the dense-state correction, which is given by:

$$\Delta\eta = \kappa_{rep}(T) P_{rep} + \kappa_{att}(T) P_{att} + \kappa_{rep-rep}(T) P_{rep}^2 \tag{3.42}$$

where:

P_{rep} : repulsive term of pressure as given by an EoS

P_{att} : attractive term of pressure as given by an EoS

Table 3–4. Parameters for collision integral equation from Neufeld et al. [176]

Parameter	Value
A	1.16145
B	0.14874
C	0.52487
D	0.77320
E	2.16178
F	2.43787
P	7.27371
R	$-6.4350 \cdot 10^{-4}$
S	18.03230
W	-0.76830

The temperature-dependent coefficients are given by the following equations:

$$\kappa_{rep}(T) = a_1 exp(T_r^{-1} - 1) + a_2\left(exp\left(2(T_r^{-1} - 1)\right) - 1\right) \tag{3.43}$$

$$\kappa_{att}(T) = b_1 exp(T_r^{-1} - 1) + b_2\left(exp\left(2(T_r^{-1} - 1)\right) - 1\right) \tag{3.44}$$

$$\kappa_{rep-rep}(T) = c_2(exp(2T_r^{-1}) - 1) \tag{3.45}$$

Each pure component is characterized by five parameters, namely a_1, a_2, b_1, b_2, c_2 which are fitted to experimental viscosity data. In certain cases, such as n-alkanes, there are linear correlations with the molecular weight that provide values for the parameters for the entire component series.

Mixtures

There are at least two sets of mixing rules [96, 177] proposed for this theory. In this work, the mixing rules proposed by Quiñones-Cisneros et al. were used. More specifically:

$$\eta_{mix} = \eta_{0,mix} + \Delta\eta_{mix} \tag{3.46}$$

$$\eta_{0,mix} = exp\left(\sum_{i=1}^{nc} x_i ln\left(\eta_{0,i}\right)\right) \tag{3.47}$$

where, *nc* is the number of components in the system.

$$\Delta\eta_{mix} = \kappa_{rep,mix} P_{rep,mix} + \kappa_{att,mix} P_{att,mix} + \kappa_{rep-rep,mix} P_{rep,mix}^2 \tag{3.48}$$

$$\kappa_{J,mix} = \sum_{i=1}^{nc} x_i \kappa_{J,i} \tag{3.49}$$

where the index J declares that the equation is applicable for $\kappa_{rep,mix}$, $\kappa_{att,mix}$, and $\kappa_{rep-rep,mix}$.

In this work, PC-SAFT and other equations of state were used to provide $P_{rep,mix}$ and $P_{att,mix}$ to the viscosity model. Also, the hard-sphere term gives the repulsive contribution to the pressure, while the attractive contribution is provided by the dispersion and hard chain terms.

3.7. Diffusion Coefficient

3.7.a. Pure Component Models

Although, for gases at low densities, kinetic theory, in the form of Enskog's solution theory, is sufficiently well understood [178], there is no rigorous extension to higher, liquid like, densities. As a result, semi-empirical modifications have been proposed that take into account the effects of the intermolecular interactions present at higher densities.

According to the original kinetic theory, for a hard sphere fluid characterized by its molecular diameter σ, the low density limit of the self-diffusion coefficient is given as a function of density ρ, temperature T and molecular weight MW, as in Eq. (3.50):

$$D_0 = \frac{3}{8\rho\sigma^2}\left(\frac{kT}{\pi \cdot MW}\right)^{1/2} \tag{3.50}$$

Eq. (3.50) is the result of the kinetic theory for a dilute gas. Enskog's theory on the other hand, provides a correction [178] for the dense hard sphere fluid. It uses the value of the radial distribution function for hard spheres at the contact point (i.e. at distance σ) that is a function of the number density ρ.

$$D_E = \frac{D_0}{g(\sigma)} \tag{3.51}$$

For a hard sphere fluid, the radial distribution function can be approximated and given in an analytical form as the result from the Percus-Yevick integral equation theory [179]. Depending on which closure is used, the compressibility or the pressure, two slightly different formulations for the radial distribution function exist. Interestingly, computer simulations have shown that a combination of the two solutions in the form of the Carnahan-Starling equation [180] can represent the computational experiments with high accuracy at a wide density range.

According to the Carnahan-Starling approach, the radial distribution function at contact $g(\sigma)$ is given in the form of Eq. (3.52):

$$g(\sigma) = \frac{1 - 0.5\eta_{p.f.}}{\left(1 - \eta_{p.f.}\right)^3} \tag{3.52}$$

where, $\eta_{p.f.(1atom)} = \frac{\pi\rho\sigma^3}{6}$ is the so-called packing fraction. For a fluid that consists of a chain of $N_{spheres}$ hard spheres, the packing fraction is $N_{spheres}$ times the packing fraction of the mono-atomic fluid namely, $\eta_{p.f.(chain)} = N_{spheres}\frac{\pi\rho\sigma^3}{6}$.

In 1999, Yu and Gao proposed [181] an equation to calculate the self-diffusion coefficients for polyatomic molecules by taking into account the chain connectivity contribution to diffusion. Based on Yu and Gao, the low density limit of the self-diffusion coefficient, $D_{0,chain}$ is given as

$$D_{0,chain} = \frac{3}{8\rho d^2 {N_{spheres}}^{2/3}}\left(\frac{kT}{\pi \cdot MW}\right)^{0.5} \tag{3.53}$$

where, d is an effective diameter which is a function of the reduced temperature $T^{red} = \frac{T}{\varepsilon/k}$ given by Eq. (3.54):

$$d = 1.1532\sigma\left[1 + \left(\frac{T^{red}}{0.527}\right)^{1/2}\right]^{-1/6} \tag{3.54}$$

The use of an effective diameter that is a function of the reduced temperature introduces a dependency on the strength of the intermolecular dispersion interactions. These are modeled via the interaction parameter ε/k (in K) that is used to model each component. Yu and Gao used the effective diameter in the evaluation of the packing fraction of Eq. (3.52), replacing σ with d.

In analogy to Eq. (3.51), Yu and Gao proposed [181] a correction for denser fluids given by Eq. (3.55) based on molecular simulation computational experiments in hard sphere fluids.

$$D_{dense,chain} = \frac{D_{0,chain}}{\frac{g(\sigma)}{F\left(N_{spheres}, \rho^{red}\right)} + \frac{0.4}{(T^{red})^{3/2}}} \tag{3.55}$$

with:

$$\rho^{red} = \rho N_{spheres} d^3 \tag{3.56}$$

The correction function $F\left(N_{spheres}, \rho^{red}\right)$ depends on the number of chain segments, and the reduced density, and is given from Eq. (3.57) below:

$$\begin{aligned} F\left(N_{spheres}, \rho^{red}\right) &= f(\rho^{red}) \\ &\cdot exp\left[-0.06356\left(N_{spheres} - 1\right)\right. \\ &\left. - 0.05212\left(\frac{N_{spheres} - 1}{N_{spheres}}\right)(\rho^{red}) - 1.9709\left(\frac{N-1}{N}\right)^2(\rho^{red})\right] \end{aligned} \tag{3.57}$$

with

$$f(\rho^{red}) = 1 + 0.94605(\rho^{red})^{1.5} + 1.4022(\rho^{red})^{3} - 5.6898(\rho^{red})^{5} + 2.6626(\rho^{red})^{7} \tag{3.58}$$

Eq. (3.58) is a polynomial correction to high densities, whereas Eq. (3.57) provides a correction term which accounts for chain connectivity obtained from MD simulation data for hard-sphere chains [181].

Following a similar procedure, Reis et al. [182, 183] proposed a correction based on molecular simulation data for Lennard–Jones (LJ) chains, with lengths of 2, 4, 8, and 16 spheres.

According to Reis et al. [182, 183] the self-diffusion coefficient can be expressed in the form of Eq. (3.59):

$$D_{chain,LJ} = \frac{D_{0,chain}}{\frac{g(d)}{R(\rho^{red}, T^{red}) F_R\left(N_{spheres}, \rho^{red}, T^{red}\right)} + \frac{0.4 {N_{spheres}}^2}{(T^{red})^{1.5}}} \tag{3.59}$$

Note that, within the Yu and Gao model, the size of the segments of the molecules is described by the effective diameter of Eq. (3.54), Reis at al. used the temperature independent parameter σ and introduced the effect of the temperature and of the strength of the dispersion interactions characterized by the interaction parameter ε via the introduction of the correction functions $R(\rho^{red}, T^{red})$ and $F_R\left(N_{spheres}, \rho^{red}, T^{red}\right)$ given by Eq. (3.60) and (3.61):

$$R(\rho^{red}, T^{red}) = \left(1 - \frac{\rho^{red}}{1.12(T^{red})^{0.2}}\right)\left[1 + 0.97(\rho^{red})^{0.5} + 5.10(\rho^{red})^{2} + \frac{3.10\rho^{red} - 2.90(\rho^{red})^{0.5}}{(T^{red})^{1.5}}\right] exp\left[-\frac{\rho^{red}}{2T^{red}}\right] \tag{3.60}$$

$$F_R\left(N_{spheres}, \rho^{red}, T^{red}\right) = exp\left[-0.018\left(N_{spheres}-1\right) + \left[-1-1.05\left(T^{red}\right)^{0.5}\right] + 2.09\left(\frac{N_{spheres}-1}{N_{spheres}}\right)\left(\rho^{red}\right)\left[1+\left(\frac{T^{red}}{0.527}\right)^{0.5}\right]^{0.5}\right] \quad (3.61)$$

with

$$\rho^{red} = \rho N_{spheres}\sigma^3 \quad (3.62)$$

The use of Eq. (3.59) instead of Eq. (3.55) has shown [182, 183] to reduce the AAD in the prediction of the self-diffusion coefficient in the model of the previously mentioned LJ chain fluid from 27.8% to 15.3 %.

For pure CO_2 the AAD of both methods are very similar, that is 7.77 % for Eq. (3.55) and 8.01 % for Eq. (3.59). Both methods were implemented successfully in our code and results are presented later.

3.7.b. Extension to Mixtures

Reis et al. [182, 183] proposed an extension of their model to mixtures, using the one fluid theory of van der Waals. According to this theory, the mixture is as a hypothetical fluid with interaction parameters that depend on mixture composition. As a result, Eq. (3.59) can be applied to mixtures using a dimensionless form. In this formulation, reduced density, energy parameter, number of segments and molecular weight (MW) are given in terms of pure component values using Eq. (3.64), (3.65), and (3.66), and the reduced density using Eq. (3.63):

$$\rho_{mix}^{red} = \sum_i \rho_i N_{spheres,i}\sigma_i^3 = \sum_i \rho_i^{red} \quad (3.63)$$

$$\varepsilon^*_{mix} = \sum_i \sum_j x_i x_j \sqrt{\varepsilon_i \varepsilon_j} \tag{3.64}$$

$$N^*_{spheres,mix} = \sum_i \sum_j x_i x_j \left[\frac{N^{1/3}_{spheres,i}\sigma_i + N^{1/3}_{spheres,j}\sigma_j}{(\sigma_i + \sigma_j)} \right]^3 \tag{3.65}$$

$$\frac{1}{MW^*_{1,2}} = \frac{1}{MW_1} + \frac{1}{MW_2} \tag{3.66}$$

In addition to the mixing rules described above, prediction of mutual self-diffusion coefficients requires an expression for the so-called "radial distribution function at contact".

Mansoori et al. (1971) have proposed an expression for this parameter based on the Carnahan–Starling equation for mixtures. According to Mansoori et al. the self-diffusion coefficients at contact for an n-component mixture is given from Eq. (3.67).

$$g(\rho) = \frac{1}{1-\xi_3} + 3\frac{\sigma_1\sigma_2}{(\sigma_1+\sigma_2)}\frac{\xi_2}{(1+\xi_3)^2} + 2\left[\frac{\sigma_1\sigma_2}{(\sigma_1+\sigma_2)}\right]^2 \frac{\xi_2^2}{(1+\xi_3)^2} \tag{3.67}$$

where, ξ_1, ξ_1, ξ_1 are given by Eq. (3.68).

$$\xi_\kappa = \frac{\pi}{6}\rho \sum_{i=1}^{nc} x_i N_i \sigma_i^\kappa \tag{3.68}$$

As a result, the mutual diffusion coefficient in mixtures can be calculated for the low-density limit from Eq. (3.69) and for the dense cases region from Eq. (3.70).

$$D_{0,chain,ij} = \frac{3}{8}\frac{1}{\rho\sigma_{ij}^2 N_{ij}^{2/3}}\left(\frac{kT}{2\pi MW_{ij}}\right)^{1/2} \tag{3.69}$$

$$D_{chain,LJ}(i,j) = \frac{D_{0,chain}(i,j)}{\frac{g(\rho)}{R(\rho^{red},T^{red})F_R(N,\rho^{red},T^{red})} + \frac{0.4N^2}{(T^{red})^2}} \tag{3.70}$$

3.8. Thermal Conductivity

3.8.a. Vesovic et al. Model [93]

In this study, the model for thermal conductivity that Vesovic et al. [93] proposed has been used. This model depends on several coefficients, that are optimized for pure CO_2 and it is based on a set of equations that are dependent on temperature and density only.

The formulation of the model consists of three terms, each one describing a different contribution to the final value of the thermal conductivity.

$$\lambda(\rho,T) = \lambda^o(\rho,T) + \Delta\lambda(\rho,T) + \Delta_c\lambda(\rho,T) \tag{3.71}$$

In all the terms, the convention is that the density is given in kg/m^3, temperature in K, and the results of thermal conductivity are given in units W/m/K.

Density dependence

The term $\Delta\lambda(\rho,T)$ describes the density dependence of thermal conductivity, and is modeled as a simple polynomial of the form:

$$\Delta\lambda(\rho,T) = \sum_{i=1}^{4} d_i\rho^i \tag{3.72}$$

while the coefficient d_i values for pure CO_2 are shown in Table 3–5.

The zero-density limit

Vesovic et al. in their work, they start from an alternative formulation of the kinetic theory of polyatomic gases, proposed by Thijsse et al. [184], and they end up with a set of equations that are suitable for calculations. These equations are presented here:

The thermal conductivity in the zero density limit is calculated from the equation:

$$\lambda^{o}(\rho,T) = \frac{0.475598(T^{1/2})(1+r^{2})}{G_{\lambda}^{*}(T^{red})} \tag{3.73}$$

where:

$$r = \left(\frac{2c_{int}}{5k}\right)^{1/2} \tag{3.74}$$

and:

$$G_{\lambda}^{*} = \sum_{i=0}^{7} b_i / T^{red} \tag{3.75}$$

In Eq. (3.75) the reduced temperature is given by $T^{red} = \frac{T}{\varepsilon/k}$, with $\varepsilon/k = 251.196\,K$ (energy scaling parameter).

The term $\frac{c_{int}}{k}$ is the ideal heat capacity, and especially for pure CO_2, can be written as:

$$\frac{c_{int}}{k} = 1.0 + exp(-183.5/T)\sum_{i=1}^{5} c_i (T/100)^{2-i} \tag{3.76}$$

All the values for the coefficients b_i and c_i are shown in Table 3–5.

Table 3–5. Values of coefficients

i	b_i	c_i	d_i
0	0.4226159	-	-
1	0.6280115	$2.387869 \cdot 10^{-2}$	$2.447164 \cdot 10^{-2}$
2	-0.5387661	4.350794	$8.705605 \cdot 10^{-5}$
3	0.6735941	-10.33404	$-6.547950 \cdot 10^{-8}$
4	0.0	7.981590	$6.594919 \cdot 10^{-11}$
5	0.0	-1.940558	-
6	-0.4362677	-	-
7	0.2255388	-	-

Critical region

It is reported by Vesovic et al. [93] that the critical enhancement of the thermal conductivity is significant along a large range of temperatures and densities in the neighborhood of the critical point. Specifically, the ratio $\frac{\Delta_c \lambda}{\lambda}$ is smaller than 1% only for temperatures and densities that are out of the ranges of 240 K < T < 450 K and 25 kgm^{-3} < ρ < 1000 kgm^{-3} respectively.

Due to the fact that this term has significant effect only in the close vicinity of the critical point, while the calculations in this work span over a much wider range, it will be omitted. This decision is also in agreement with the assumptions regarding the viscosity calculations.

3.8.b. Scalabrin et al. Model [185]

Another approach used to model the thermal conductivity of pure CO_2 has been the "Multiparameter Thermal Conductivity Equation for Carbon Dioxide" proposed by Scalabrin et al. [185].

Scalabrin et al. introduced a multi-parameter equation that was fitted to available experimental data over a wide range of conditions spanning from the triple point of pure CO_2 (T_{tr}=216.592 K, P_{tr}=0.51795 MPa) to 1000 K and pressures up to 200 MPa. The average absolute deviation was below 2 %. The equation is simple even close to the

critical point has low computational cost and is ideal for the use in fluid mechanics simulations.

According to Scalabrin et al., the thermal conductivity is expressed in reduced form λ_r as a function of reduced density and reduced temperature, away from the critical point. In the vicinity of the critical point a correction $\lambda_{r,ce}$ is added to the expression.

Initially, Scalabrin et al. investigated the ability to correlate the available experimental data thermal conductivity using an expression described in Eq. (3.77) using 130 parameters. After elimination of the less sensitive terms, they concluded that the thermal conductivity can be expressed with sufficient accuracy by a much smaller set.

As a result the thermal conductivity is given as the sum of Eq. (3.78), whereas the initial trial function is the Eq. (3.77).

$$\lambda_r(T_r,\rho_r) = \sum_{i=0}^{12}\sum_{j=0}^{10} n_{ij} T_r^{i/2} \rho_r^{j} + \exp(-5\rho_r^2) \sum_{k=0}^{12}\sum_{l=0}^{10} n_{kl} T_r^{k/2} \rho_r^{l} + n_c \lambda_{r,ce}(T_r,\rho_r,\bar{a}) \quad (3.77)$$

$$\lambda_r(T_r,\rho_r) = \sum_{i=0}^{3} n_i T_r^{g_i} \rho_r^{k_i} + \exp(-5\rho_r^2) \sum_{i=4}^{10} n_i T_r^{g_i} \rho_r^{h_i} + n_c \lambda_{r,ce}(T_r,\rho_r,\alpha) \quad (3.78)$$

In total, there are 11 adjustable parameters in Eq. (3.78) that were fitted by Scalabrin et al. over a wide range of conditions.

In this procedure the critical temperature was set to 304.1282 K (resulting to T_r =T/ 304.1282), and the critical density is set to 10.6036 Kmol/m^3 (resulting to ρ_r =ρ/ 10.6036). Additionally, based on the critical pressure and molecular weight used by Scalabrin et al., the thermal conductivity is expressed as

$$\lambda(T,\rho) = \lambda_r(T_r,\rho_r) \cdot \Lambda_c = \lambda_r(T_r,\rho_r) \cdot 4.81384 \quad (3.79)$$

in mW/(m K), where $\lambda_r(T_r,\rho_r)$ is the reduced thermal conductivity value given by Eq. (3.78).

The correction close to the critical point is given in the form of Eq. (3.80) that introduces 12 more adjustable parameters.

$$\lambda_{r,ce}(T_r,\rho_r) = \frac{\rho_r \cdot exp\left[-\frac{\rho_r^{a_1}}{a_1} - \left(a_2(T_r-1)\right)^2 - \left(a_3(\rho_r-1)\right)^2\right]}{\left\{\left[\left[\left(1-\frac{1}{T_r}\right) + a_4((\rho_r-1)^2)^{0.5a_5}\right]^2\right]^{a_6} + [a_7(\rho_r-\alpha)^2]^{a_8}\right\}^{a_9}} \tag{3.80}$$

where α in the denominator of Eq. (3.80) is given by Eq. (3.81).

$$\alpha = 1 - a_{10} arccosh[1 + a_{11}[(1-T_r)^2]^{a_{12}}] \tag{3.81}$$

In Table 3–6,

Table 3–7, and Table 3–8, the values of the parameters used in Eq. (3.78), (3.80), and (3.81) are given.

Table 3–6. Parameter values in Eq. (3.78) for pure CO_2

i	g_i	h_i	n_i
1	0	1.	7.69857587
2	0	5.	0.159885811
3	1.5	1.	1.56918621
4	0	1.	- 6.73400790
5	1	2.	16.3890156
6	1.5	0	3.69415242
7	1.5	5.	22.3205514
8	1.5	9.	66.1420950
9	3.5	0.	- 0.171779133
10	5.5	0.	0.00433043347
			n_c
			0.775547504

Table 3–7. Parameter values in Eq. (3.78) and (3.80) for pure CO_2

i	α_i
1	3.0
2	6.70697
3	0.94604
4	0.3
5	0.3
6	0.39751
7	0.33791
8	0.77963
9	0.79857
10	0.9
11	0.02
12	0.20

Table 3–8. Critical Parameter used in Eq. (3.78), (3.80), and (3.81) for pure CO_2

Tc	304.1282 K
Λc	4.81384
ρc	10.6036 Kmol/m^3

4. Thermodynamic Primary and Derivative Properties of CO_2 and other compounds

4.1. Pure Components

Pure component parameters were fitted to experimental vapor pressure and saturated liquid density data taken from NIST [186]. In Table 4–1 and

Table 4–2, the parameters for SAFT and PC-SAFT are provided together with the percentage average absolute deviation (% AAD) between experimental data and model calculations. H_2S was modeled both as a non-associating and an associating component with one site per molecule, while for H_2O the widely used 4 associating site model was used. The choice of 4C associating scheme over the 2B is supported by the fact that the errors in derivative properties with the 2B were quite higher than those of 4C as it can be seen in Table 4–3 for some representative cases, with the exception of the values for isochoric heat capacity. Very good correlation of the vapor pressure and liquid density was obtained in all cases. Calculation of liquid and vapor phase thermodynamic properties were performed for all components in the temperature range 80 – 695 K and pressures up to 20 MPa, and compared with experimental data.

Table 4–1. SAFT parameters for the components studied in this work and % AAD between experimental data and model correlation for vapor pressure and liquid density in the temperature range indicated. H_2S is modeled both as a non-associating and as a single associating site and H_2O as a 4 associating site component.

Component	m	v^{00} (Å^3)	u/k (K)	e/k (K)	ε^{AB}/k (K)	κ^{AB}	AAD (%)		T (K)
							P^{sat}	ρ^{sat}	
CO_2	2.9271	5.710	136.53	40	-	-	0.92	1.84	225 – 301
CH_4	1.0000	21.566	189.82	0	-	-	0.58	1.82	127 – 191
O_2	1.0000	16.056	154.72	0	-	-	1.58	1.32	90 – 154
N_2	1.0000	19.457	123.53	3	-	-	0.43	0.11	73 – 122
H_2S	2.3482	7.801	207.86	10	-	-	1.80	2.11	188 – 370
H_2S (1)	1.6319	12.325	260.34	10	787.56	0.0049	2.84	3.79	188 – 370
H_2S (3B)	1.9350	10.000	226.38	10	804.1	0.0091	0.69	1.40	284 – 369
H_2O (4C)	2.8530	3.304	167.10	1	1634.70	0.3374	1.09	2.38	275 – 640

Table 4–2. PC-SAFT parameters for the components studied in this work and % AAD between experimental data and model correlation for vapor pressure and liquid density in the temperature range indicated. H_2S is modeled both as a non-associating and as a single associating site and H_2O as a 4 associating site component.

Component	m	σ (Å)	ε/k (K)	ε^{AB}/k (K)	κ^{AB}	AAD (%)		T (K)
						P^{sat}	ρ^{sat}	
CO_2	2.6037	2.555	151.04	-	-	0.49	0.83	217 – 301
CH_4	1.0000	3.704	150.03	-	-	0.33	1.40	127 – 191
O_2	1.1217	3.210	114.96	-	-	0.34	1.80	90 – 154
N_2	1.2053	3.313	90.96	-	-	0.14	1.92	73 – 122
H_2S	1.7163	3.009	224.96	-	-	0.38	1.90	188 – 370
H_2S (1)	1.6592	3.049	228.91	554.68	0.0022	0.22	0.40	188 – 370
H_2S (3B)	1.6295	3.075	230.35	273.55	0.0069	0.16	0.37	188 – 370
H_2O (4C)	3.0094	2.006	173.11	1341.98	0.4257	1.92	0.42	275 – 640

Table 4–3. Comparison of errors (% AAD) in properties of water predicted by PC-SAFT with association schemes 2B and 4C.

	10MPa		25MPa	
	2B	**4C**	**2B**	**4C**
ρ	6.5	2.1	10.1	4.1
k_T^{-1}	15.8	8.8	16.1	12.3
C_v	14.8	17.9	14.9	20.0
C_p	38.3	10.1	17.9	10.0
μ	28.9	25.1	49.7	28.7
ω	45.1	43.9	35.2	34.5

Results for pure CO_2 density at subcritical and supercritical conditions are presented in Figure 4–1. As a first observation, the critical temperature and pressure are clearly overpredicted by both EoS. However, PC-SAFT provides the relatively best prediction with T_c = 309.5 K and P_c = 7.92 MPa, while for SAFT it is: T_c = 315.5 K and P_c = 9.09 MPa. The experimental values are T_c = 304.13 K and P_c = 7.3773 MPa. This is also in agreement with the more accurate prediction of the vapor pressure by PC-SAFT compared to SAFT.

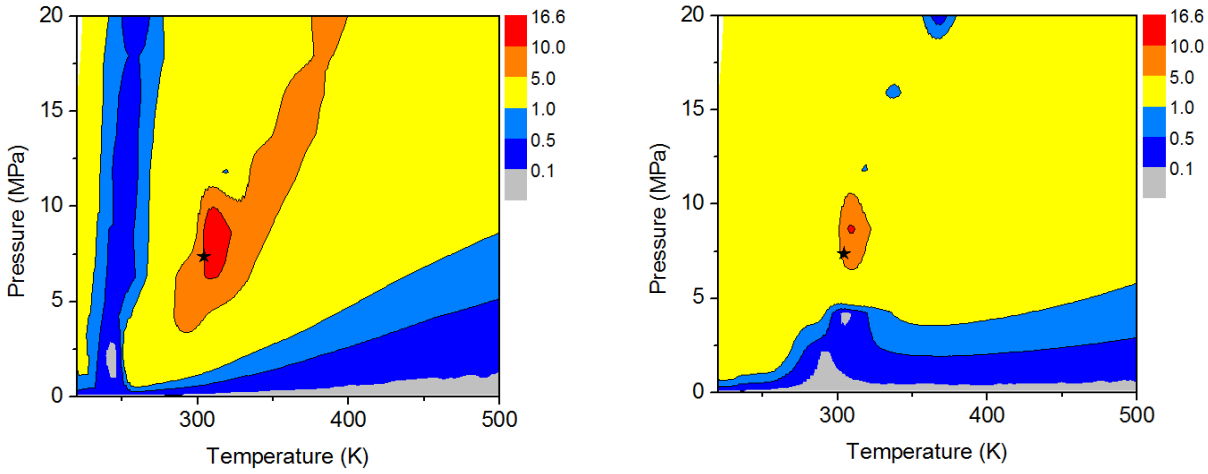

Figure 4–1. Density of pure CO_2 error (% AAD) contour plots over a wide range of conditions [186] for SAFT (a) and PC-SAFT (b). The black symbol shows the estimated critical point.

The increasing inaccuracy in the critical region, due to the fact that both models are mean-field theories that do not account for critical fluctuations, is also the main reason for the high deviations between experimental data and model predictions for the derivative properties, as it will be explained next. Away from the critical region, both at subcritical and supercritical conditions, calculations are in very good agreement with the experimental data.

In Table 4–4, a summary of the % AAD between experimental data and EoS predictions for the various properties of all the components examined is provided. On average, PC-SAFT performs systematically better than SAFT for all the properties, except the Joule-Thomson coefficient. In Figure 4–2 and Figure 4–3, error contours of EoS predictions are shown for the isobaric heat capacity, speed of sound, Joule-Thomson coefficient and isothermal compressibility coefficient of CO_2.

Table 4–4. Summary of % AAD for all the properties calculated from the two EoS.

Component	SAFT AAD (%)						T (K)	P (MPa)
	ρ	k_T^{-1}	C_v	C_p	μ_{J-T}	ω		
CO_2	2.2	5.8	5.9	8.5	16.3	5.1	220 – 500	0 – 20
CH_4	0.1	0.1	0.1	0.3	0.8	0.1	180 – 500	0 – 12
N_2	0.3	0.6	1.0	0.5	4.7	0.7	80 – 500	0 – 12
O_2	0.3	1.0	1.7	1.1	2.7	1.0	80 – 500	0 – 12
H_2S	1.6	6.2	6.1	6.9	18.5	3.7	190 – 510	0 – 20
H_2S (1)	1.2	13.4	4.7	9.1	16.3	8.6	190 – 510	0 – 20
H_2O (4C)	1.8	12.0	13.4	7.3	11.0	8.5	275 – 695	0 – 20
Average	1.0	5.5	4.5	4.4	9.6	3.6		
	PC-SAFT AAD (%)						T (K)	P (MPa)
	ρ	k_T^{-1}	C_v	C_p	μ_{J-T}	ω		
CO_2	1.0	2.0	4.5	3.5	7.8	2.3	220 – 500	0 – 20
CH_4	0.7	1.6	0.8	1.1	5.5	0.7	180 – 500	0 – 12
N_2	0.8	1.2	1.1	0.9	14.3	1.0	80 – 500	0 – 12
O_2	0.6	1.7	1.3	1.3	8.4	1.1	80 – 500	0 – 12
H_2S	0.7	3.9	3.3	4.0	8.3	2.3	190 – 510	0 – 20
H_2S (1)	0.9	4.4	4.4	3.6	11.9	3.1	190 – 510	0 – 20
H_2O (4C)	1.0	9.8	11.6	9.8	12.4	3.1	275 – 695	0 – 20
Average	0.9	3.9	4.0	3.5	10.2	1.9		

The isobaric heat capacity is well described by both equations, but PC-SAFT is giving lower errors. The locus of the extreme values of C_p close to the critical point is well reproduced, but the values that SAFT gives are quite higher than the experimental. The calculation of C_p by the two EoS in this work, can be characterised as successful compared to earlier work with lattice EoS by Lee et al. [187], or with the use of a cubic EoS by Shin et al. [188].

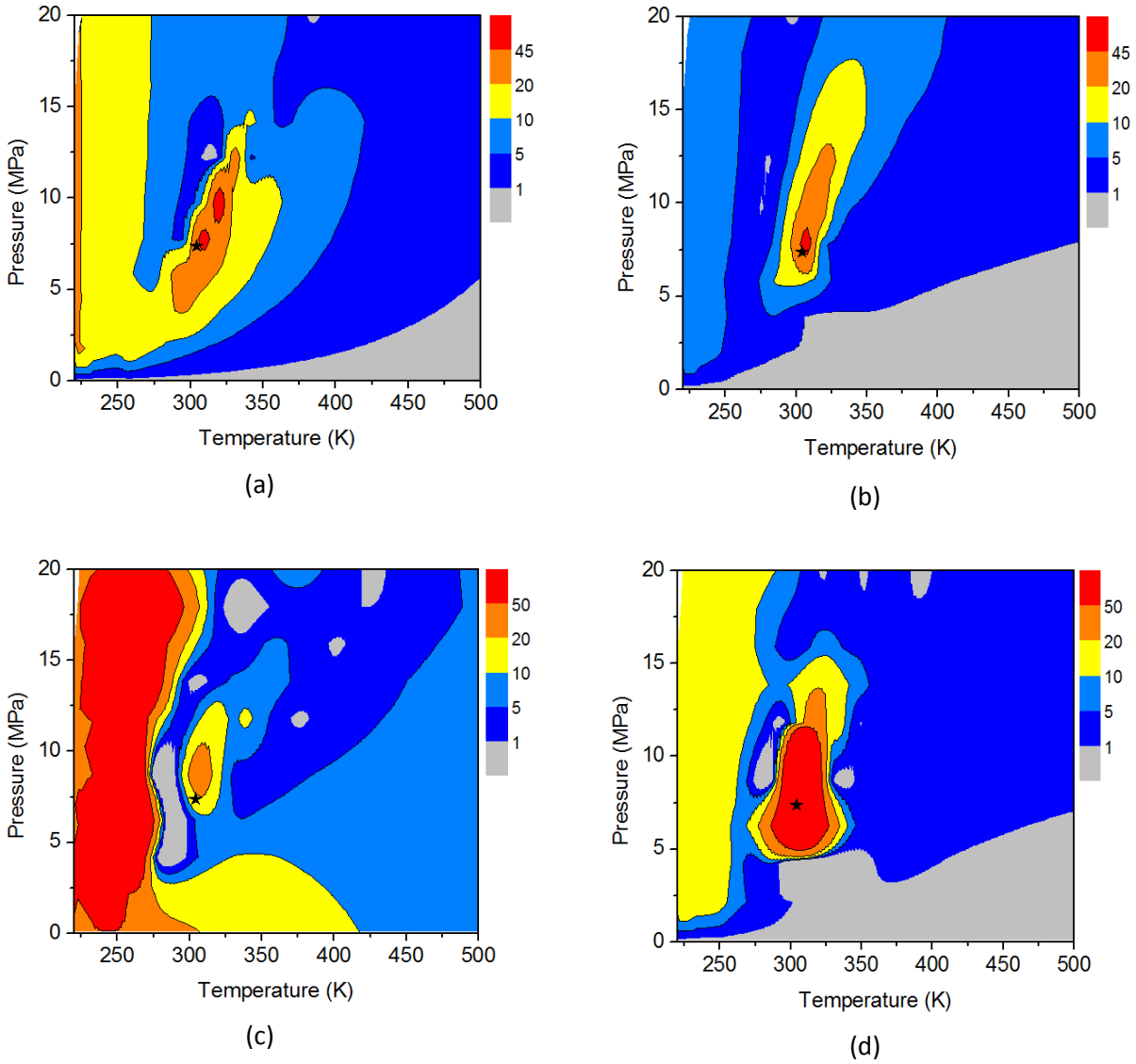

Figure 4–2. Errors in thermodynamic derivative properties of pure CO_2 predicted by SAFT: (a) Isobaric heat capacity, (b) Speed of sound, (c) Joule-Thomson coefficient and (d) Isothermal compressibility coefficient.

However, it is not straightforward to compare the errors given in this work with the errors reported by Llovell et al. [74], and Lafitte et al. [75], because of the different family of components that are studied in these papers. Lafitte et al. had studied n-alkanes from n-C_6 to n-C_{17}.

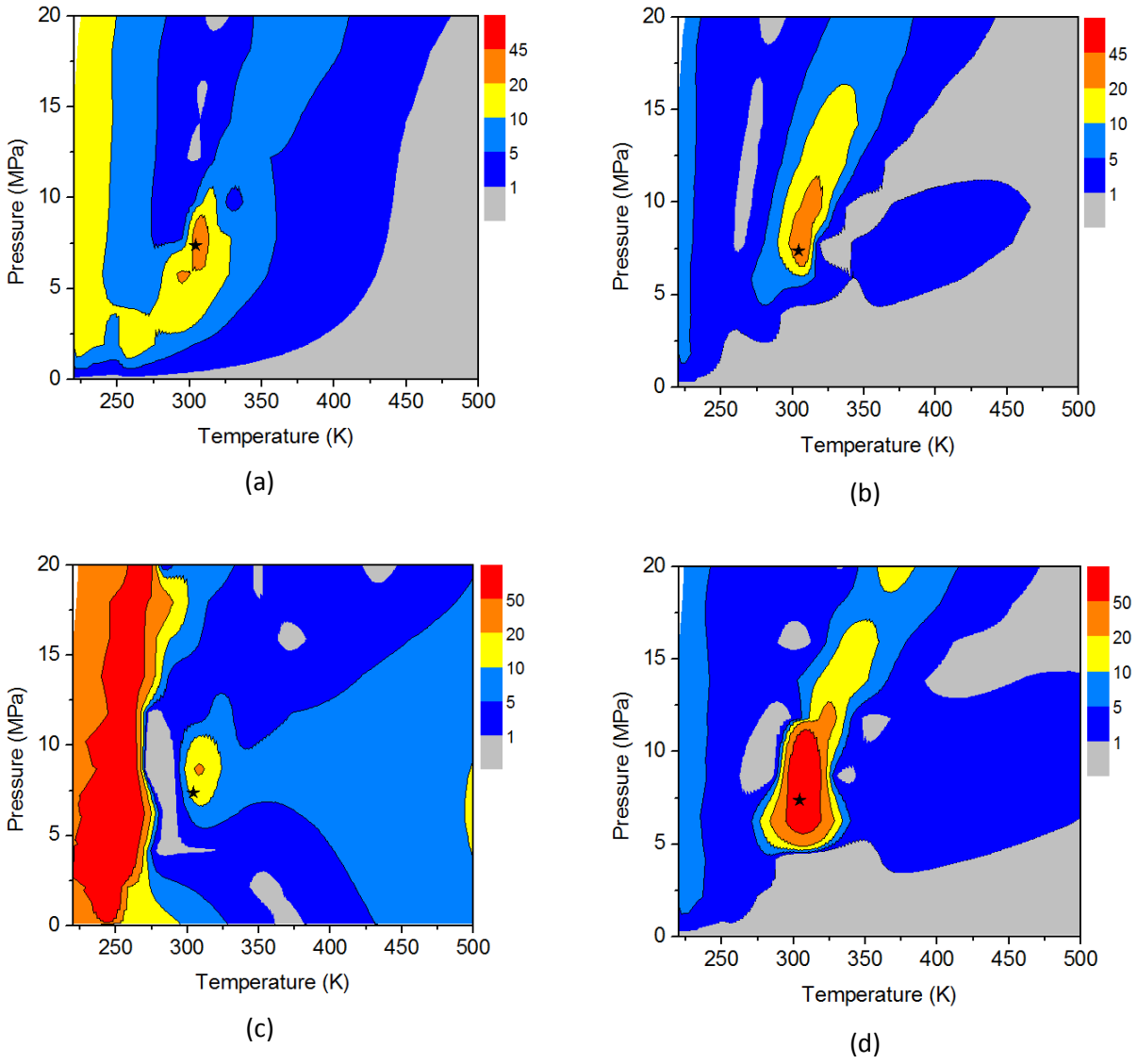

Figure 4–3. Errors in thermodynamic derivative properties of pure CO_2 predicted by PC-SAFT: (a) Isobaric heat capacity, (b) Speed of sound, (c) Joule-Thomson coefficient and (d) Isothermal compressibility coefficient.

The reported errors, regarding the speed of sound for example, range from 10.3 to 16.6 % AAD for PC-SAFT, which is worse than SAFT-VR-SW (4.7-12.2) but better than SAFT-VR-LJC (15.9-23.6). For the components and conditions studied in our work, the respective average errors are in the range (0.1-8.6) for SAFT and (0.7-2.3) for PC-SAFT.

Comparing to the work of Lovell et al. [74] on the calculation of speed of sound of CH_4 in particular, soft-SAFT gives average errors ranging from 1.82 to 3.11 % AAD for supercritical temperatures, while in our work average errors of 0.1% for SAFT and 0.7% for PC-SAFT are reported for the complete range of conditions that was studied.

Calculations for the isochoric heat capacity of CO_2 and the other components from both EoS are within less than 5 % for most gases from experimental data, with an increasing deviation as the critical point is approached. The picture, however, reverts if one focuses on the residual part of the isochoric heat capacity (Figure 4–4 and Table 4–5). Both models are in qualitative agreement with experimental data, only. In the vicinity of the critical point, the deviation increases and experimental data predict an increase in C_v^{res} as a function of temperature while both SAFT and PC-SAFT predict the opposite trend. Such failure has been reported also by Llovell et al. [74, 77] for other fluids with the soft-SAFT EoS.

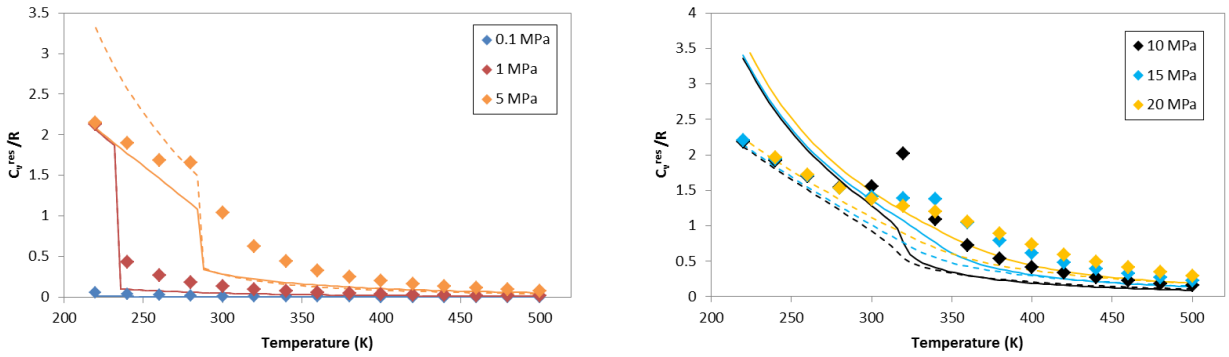

a b

Figure 4–4. Residual isochoric heat capacity of pure CO_2 for (a) subcritical and (b) supercritical regime. Solid lines are SAFT predictions, dashed lines are PC-SAFT predictions and points are experimental data [186].

Table 4–5. Summary of % AAD for C_v^{res} of CO_2 calculated from the two EoS.

	C_v^{res} % AAD	
P (MPa)	SAFT	PC-SAFT
0.1	61.8	50.7
1	60.7	47.0
2	65.8	43.5
5	49.6	38.9
8	46.2	38.7
10	44.5	38.7
12	41.7	37.7
15	38.0	36.2
20	30.8	35.5
Average	48.8	40.8

Calculations for the speed of sound are very accurate for both EoS. PC-SAFT deviates from experimental data at most by 3.1 %, while SAFT performs slightly worse (AAD < 8.6 %), as it can be seen in Table 4–4. From Eq. (3.17), one can see that ω depends on C_p, C_v and $\left(\frac{\partial P}{\partial \rho}\right)_T$. Consequently, one can argue that there is some cancellation of errors in the ratio of the two heat capacities and the error in ω is mainly governed by the error in $\left(\frac{\partial P}{\partial \rho}\right)_T$.

The Joule-Thomson coefficient is the least accurately predicted property from all properties examined here. The overall AAD rises to 9.6 % for SAFT and 10.2 % for PC-SAFT (Table 4–4), something that can be explained based on the fact that the Joule-Thomson coefficient depends on two partial derivatives, as it can be seen in Eq. (3.16), so the error is probably additive. The error is higher close to the points of phase change. At those points, the Joule-Thomson coefficient value changes from negative to very high positive, in a very narrow temperature range. The reason for this inaccuracy may lie in the fact that in those regions there are also abrupt changes in density. This is why, while the pressure increases, the error in Joule-Thomson coefficient decreases, as the density curves become smoother.

The Joule-Thomson inversion curve is an important property for fluids and refers to the conditions where the Joule-Thomson coefficient is zero. The Joule-Thomson inversion curve of CO_2 is presented in Figure 4–5, and it can be seen that the two equations perform reasonably well over the entire temperature examined.

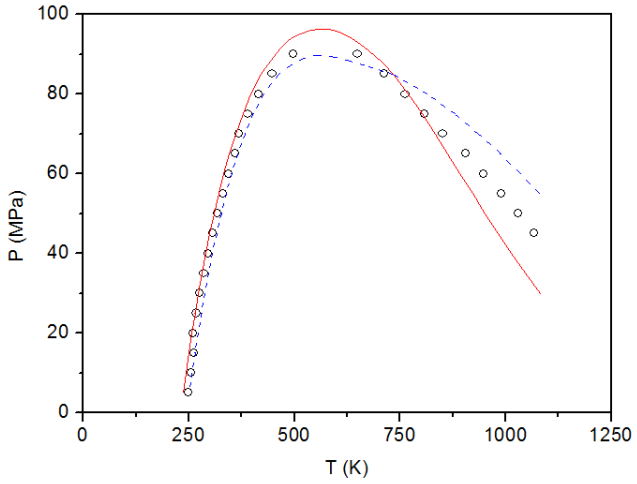

Figure 4–5. Joule-Thomson inversion curve of pure CO_2. Solid lines are SAFT predictions, dashed lines are PC-SAFT predictions and points are experimental data [186].

The last derivative property examined is the isothermal compressibility coefficient k_T^{-1}. Here also, the agreement of the predictions with the experimental data is very good away from the critical point and coexistence curve, because again, the fluctuations of density cause error in the calculation of $\left(\frac{\partial P}{\partial \rho}\right)_T$ which is used for the calculation of k_T^{-1}.

For O_2, N_2 and CH_4, experimental data and model predictions for representative properties are presented in Figure 4–6. In general, the accuracy of the model follows the pattern observed for CO_2, so it decreases close to the critical point and the coexistence curve. The property least accurately predicted is again the Joule-Thomson coefficient. Overall, the properties of three non-polar molecules O_2, N_2 and CH_4 can be modeled by SAFT and PC-SAFT with high accuracy, as seen in Figure 4–6.

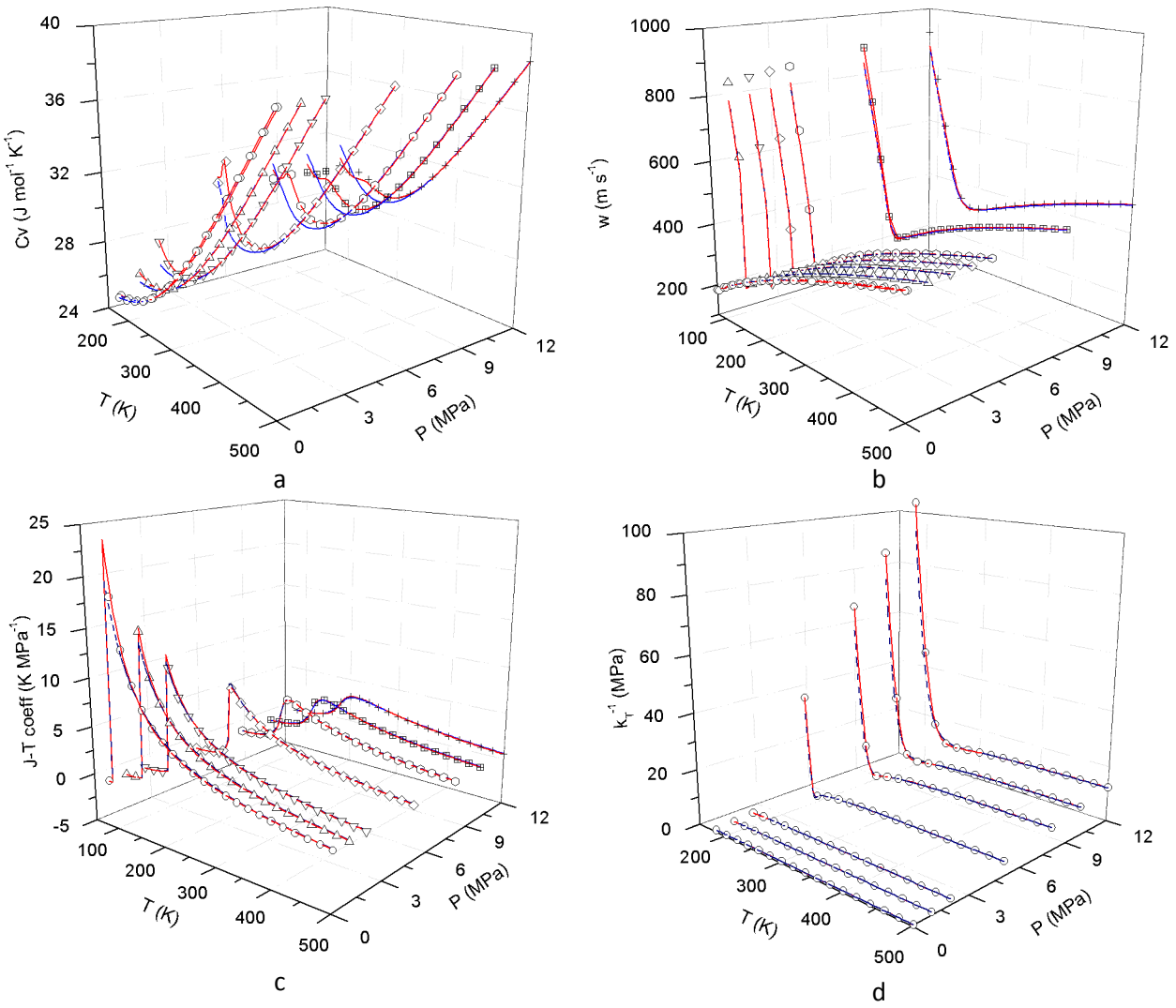

Figure 4–6. (a) Isochoric heat capacity of pure CH_4, (b) Speed of sound of N_2, (c) Joule-Thomson coefficient of O_2, and (d) isothermal compressibility coefficient of CH_4. Solid lines are SAFT predictions, dashed lines are PC-SAFT predictions and points are experimental data [186].

The last part of the analysis refers to explicit account for hydrogen bonding in H_2S and H_2O. Experimental literature data [189] indicate that H_2S form dimers through hydrogen bonding. A 1-site associating model is suitable in this case. Consequently, H_2S was modeled both as an associating ($H_2S(1)$) and a non-associating component (H_2S), and the relevant parameters are presented in Table 4–1 and Table 4–2. The associating model improves only the correlation of saturated liquid density with PC-SAFT while higher deviations are observed for the vapor pressure (both models) and saturated liquid

density correlation with SAFT. Similarly, explicit account of association results in marginal improvement of the correlation of H_2S derivative properties, only. An indicative graph in Figure 4–7 compares the total isobaric heat capacity of pure H_2S calculated only with the associating model against the experimental data.

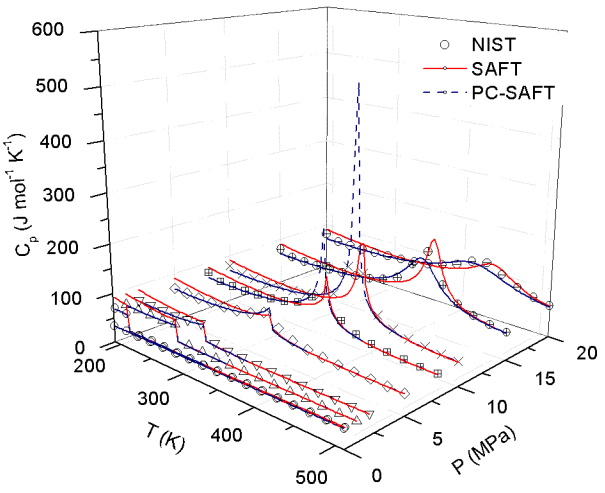

Figure 4–7. Isobaric heat capacity of H_2S. Solid lines are SAFT predictions, dashed lines are PC-SAFT predictions and points are experimental data [186].

Finally, H_2O phase equilibrium properties are correlated accurately with both equations (Table 4–1 and Table 4–2) while derivative properties are predicted with a reasonable accuracy compared to experimental data (Table 4–3). For almost all derivative properties, the highest % AAD between experimental data and model predictions corresponds to H_2O. It should be emphasized here that several other parameter sets provided good correlation of the phase equilibrium, but failed to predict accurately the derivative properties. Consequently, prediction of the latter can be used as an additional test for pure component parameters.

In Figure 4–8, the isobaric heat capacity of H_2O is presented. Clearly, the 4-site PC-SAFT model results in much more accurate prediction compared to the 4-site SAFT model for the liquid phase properties. However, higher deviations are observed for the vapor phase heat capacity, so that the overall errors from the two models are comparable, as shown in Table 4–4.

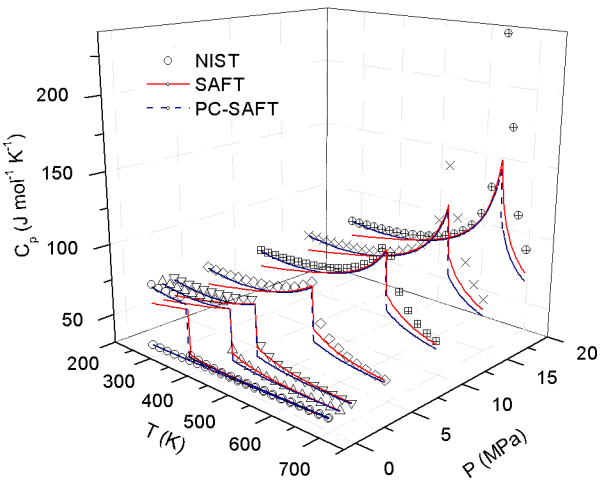

Figure 4–8. Isobaric heat capacity of H_2O. Solid lines are SAFT predictions, dashed lines are PC-SAFT predictions and points are experimental data [186].

4.2. Mixture Calculations

Representative derivative thermodynamic properties are examined in this section. Specifically, the speed of sound and the Joule-Thomson inversion curve for the CO_2 – CH_4 mixture are presented. Experimental data show that the effect of CH_4 on the derivative properties is substantial. Both properties were calculated analytically in all cases. In Figure 4–9, PC-SAFT is shown to exhibit superior performance over the PR EoS in predicting the speed of sound of the mixture. Although qualitative agreement with the experiments is achieved by both models, the PR EoS substantially underpredicts the experimental values. This can be attributed to the stronger physical basis of PC-SAFT compared to the PR EoS. Results of calculations performed with SAFT EoS were similar to those with PC-SAFT EoS while calculations with other cubic EoS (such as SRK, and RK) were similar to calculations with PR EoS.

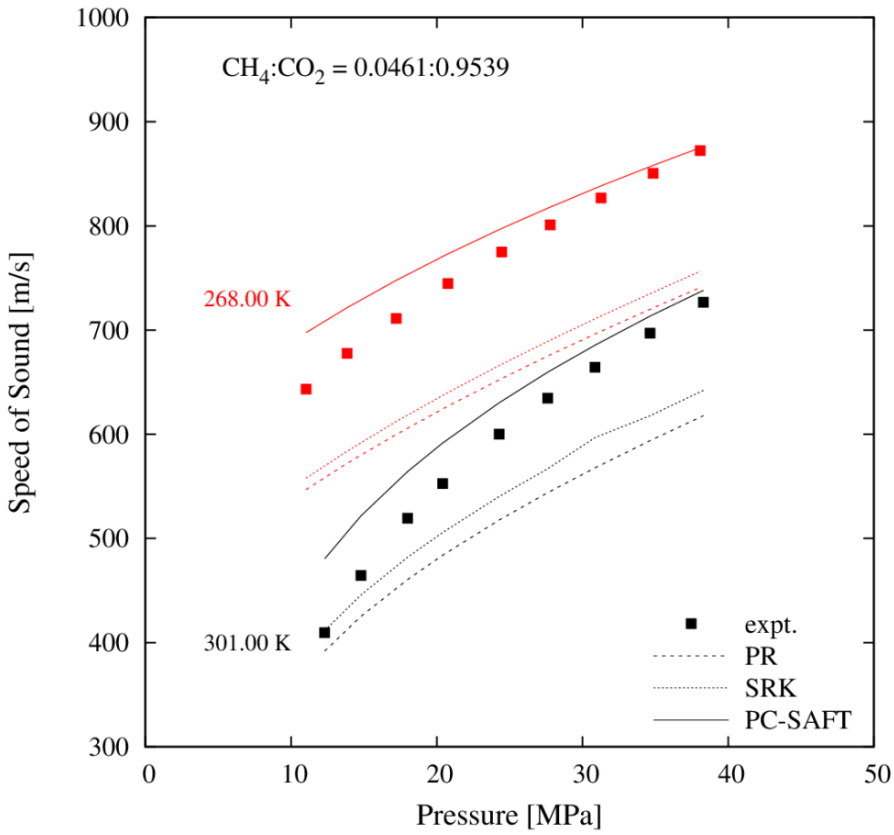

Figure 4–9. Experimental data (points) and predictions from various EoS of the speed of sound for CO_2 – CH_4 mixture.

The Joule-Thomson inversion curve is important for hazard assessment studies of pipeline depressurization, because it dictates whether the outflow stream will follow a cooling or a heating path upon pressure drop. No experimental data for this property are available for CO_2 mixtures. Consequently, calculations are compared against accurate molecular simulation data reported by Vrabec et al. [190]. Figure 4–10 provides comparison between simulation data and predictions from PC-SAFT and PR EoS for the Joule-Thomson inversion curve. Quantitative agreement is obtained between different sets of calculations. Nevertheless, PR significantly overshoots the maxima of the curves for both pure CO_2 and its equimolar mixture with CH_4.

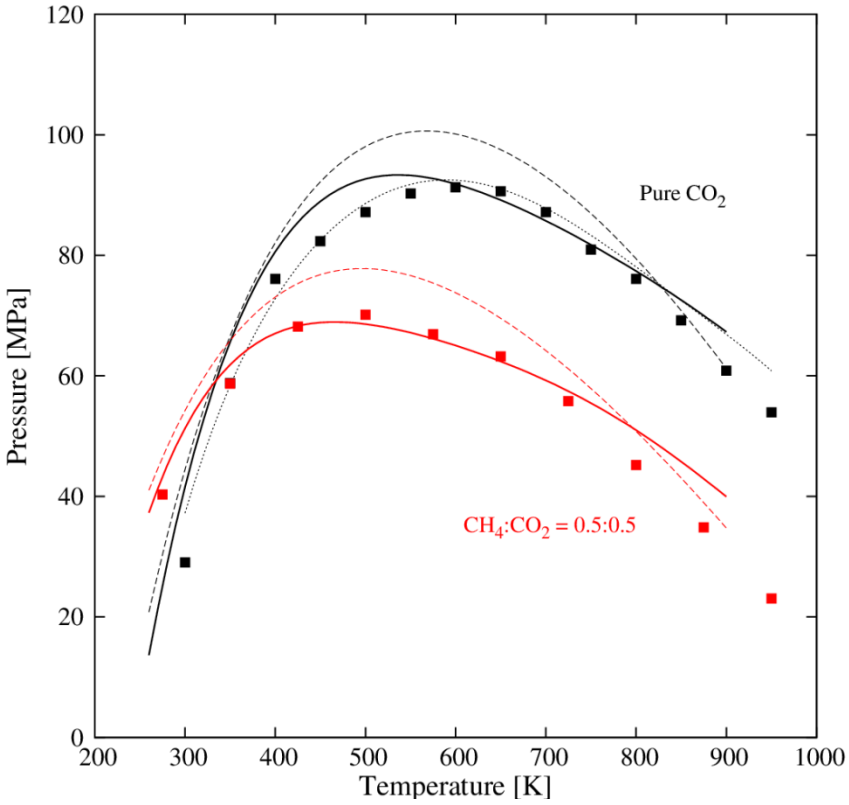

Figure 4–10. Joule-Thomson inversion curve of the CO_2 – CH_4 mixture. PR EoS (dashed lines) and PC-SAFT EoS (solid lines) predictions against molecular simulation data (points) [190], and Span and Wagner EoS [47] for pure CO_2 (dotted black line).

Figure 4–11 is a typical example of the improved capacity of the newly developed SAFT EoS to predict the isothermal compressibility of multi-component systems. Because experimental data for derivative properties of complex mixtures are scarce in the literature, among the available systems, the CO_2-N_2-CH_4-H_2 was selected because it resembles candidate CO_2 pipeline mixtures better. Figure 4–11 compares predictions obtained from two equations of state, the Peng-Robinson (PR) [5] and the newly developed PC-SAFT [6]. PC-SAFT is superior to PR as the % AAD error of 5.3 for PC-SAFT versus 33.2 for PR indicates. It must be emphasized that no data tuning to isothermal compressibility data has been done by any model. The improved capacity of PC-SAFT is attributed more to the fact that the mathematical terms of PC-SAFT resemble physical interactions closer and less to the fact that PC-SAFT has slightly more complex functional form and an extra adjustable parameter.

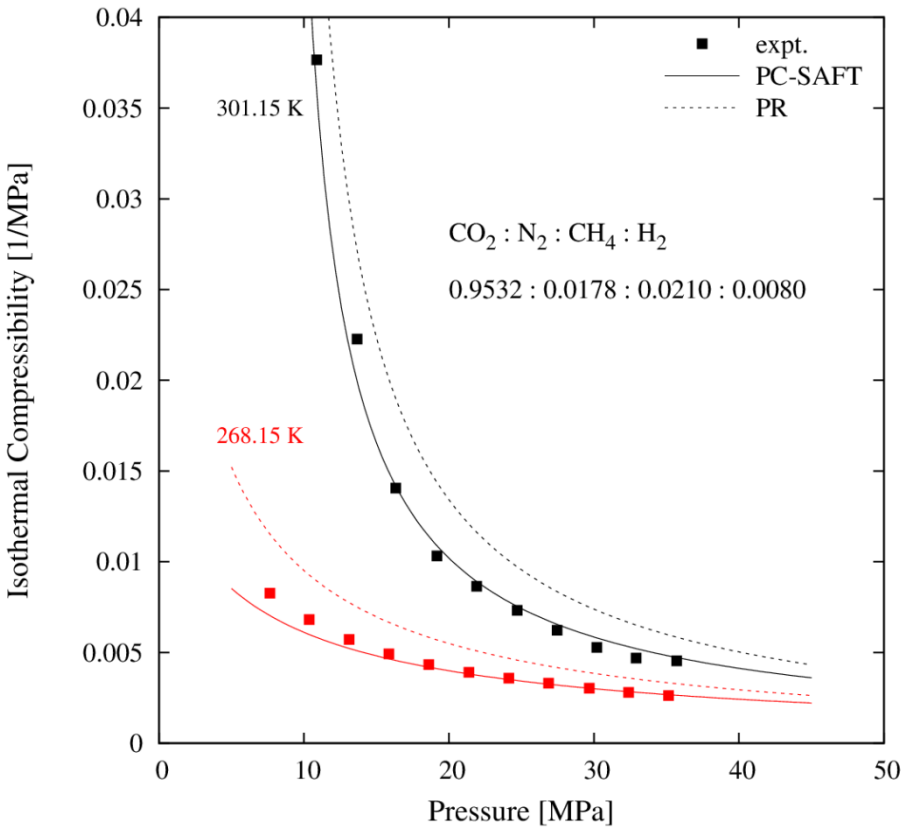

Figure 4–11. Isothermal compressibility of a quaternary CO_2-containing system. Experimental data from [87].

5. Phase Equilibria of CO_2 Mixtures

5.1. CO_2 with Other Gases

Phase equilibria calculations are of utmost importance to applications of CCS. In this work [191], four cubic EoS, namely the RK [44], the SRK [46], the PR [45], and the PR/Gasem [158], together with the SAFT [49, 160], and PC-SAFT [50] are used to model the thermodynamic properties of binary and ternary CO_2 mixtures with other components of relevance to CCS, such as CH_4, N_2, O_2, SO_2, Ar, and H_2S. VLE and density calculations are performed, and a thorough comparison among the various EoS is reported. Considering the fact that it is highly unlikely that the flue stream will occur as pure CO_2, the knowledge of the effect of these impurities on the phase behavior of the stream is of major importance. A temperature independent binary interaction parameter is fitted to literature experimental data for every binary mixture.

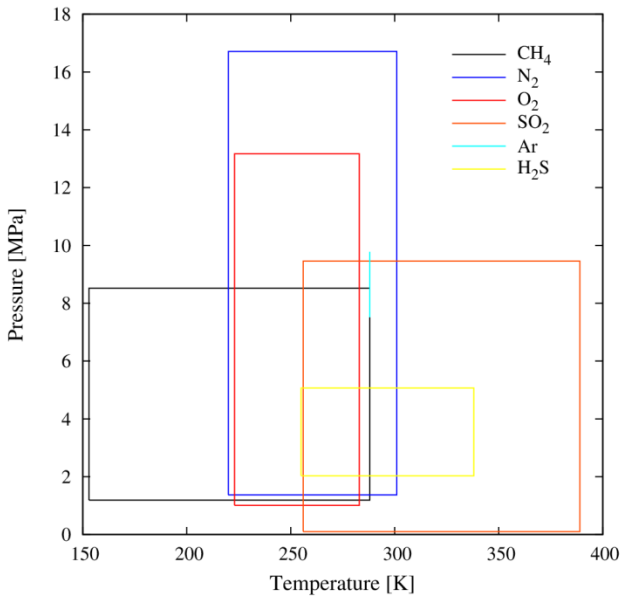

Figure 5–1. Range of conditions that was used in the binary interaction parameter fitting for PR and PC-SAFT EoS by [191].

The mixtures for which experimental data were used for the fitting process, and the conditions covered are shown in Table 5–1 and summarized schematically in Figure 5–1. The binary parameters for the PR and PC-SAFT EoS are presented in Table 5–3.

Table 5–1. Experimental VLE and density data from literature that were used in this study.

System	Temperature (K)	Pressure (MPa)	Reference
CO_2-CH_4	311 - 511	1.4 - 6.9	Reamer et al. [192]
CO_2-CH_4	167 - 301	2.0 - 7.4	Donnelly and Katz [193]
CO_2-CH_4	230 - 250	0.9 - 8.5	Davalos et al. [194]
CO_2-CH_4	89 - 208	0.5 - 6.3	Mraw et al. [195]
CO_2-CH_4	205 - 320	0.2 - 48.0	Esper et al. [196]
CO_2-CH_4	253 - 288	6.2 - 8.5	Arai and Saito [197]
CO_2-N_2	223 - 273	0.7 - 16.9	Dorau et al. [198]
CO_2-N_2	209 - 320	0.1 - 48.0	Esper et al. [196]
CO_2-N_2	253 - 288	3.5 - 14.1	Arai and Saito [197]
CO_2-N_2	220 - 270	1.8 - 14.0	Brown et al. [199]
CO_2-N_2	230 - 250	6.2 - 10.3	Al-Sahhaf [200]
CO_2-N_2	220 - 240	0.6 - 16.7	Al-Sahhaf et al. [201]
CO_2-N_2	273 - 293	4.5 - 12.0	Yorizane et al. [202]
CO_2-N_2	288 - 301	5.1 - 10.3	Krichevskii et al. [203]
CO_2-O_2	223 - 283	1.0 - 13.2	Frendeslund and Sather [204]
CO_2-SO_2	291 - 416	2.7 - 10.5	Caubet [42]
CO_2-SO_2	256 - 308	0.1 - 3.1	Blumcke [205]
CO_2-SO_2	263 - 233	0.1 - 9.0	Lachet et al. [41]
CO_2-Ar	288.15	5.7 - 9.8	Sarashina et al. [206]
CO_2-H_2S	273 - 370	1.0 - 8.0	Bierlein and Kay [207]
O_2-N_2	77 - 125	0.1 - 3.0	Dodge and Dunbar [208]
CO_2-O_2-N_2	273	5.2 - 10.6	Muirbrook and Prausnitz [209]

Critical parameters are necessary for calculations with cubic EoS, thus Table 5–2 provides the critical temperature, T_c, critical pressure, P_c, and acentric factor, ω, values for the various components.

In a similar manner, SAFT and PC-SAFT need their own set of parameters, as it was explained in the section 3.2. For the calculations presented in this work, the Table 4–1 and Table 4–2 provide the parameter values for the two EoS respectively.

The phase envelopes of CO_2 binary mixtures with 5 % mole fraction of different gases were calculated with PR and PC-SAFT. No binary interaction parameters were used at this point. Calculations are illustrated in Figure 5–2, showing that the two models agree well with each other. Clearly, Ar, N_2, CH_4, and O_2 shift both the bubble and dew point curves to pressures higher than the VLE curve of pure CO_2, so that higher energy consumption is needed for the compression of the stream to the dense phase (liquid or supercritical). Another important observation is that the dew point curves of the mixtures almost overlap each other, leading to the conclusion that their effect on the vapor phase is weaker than on the liquid phase. In the vapor phase, the presence of 5% of a given impurity does not have a significant impact on the intermolecular forces among the CO_2 molecules, whereas in the liquid phase, as the density becomes higher, the intermolecular interactions due to the molecules of the impurity are not negligible.

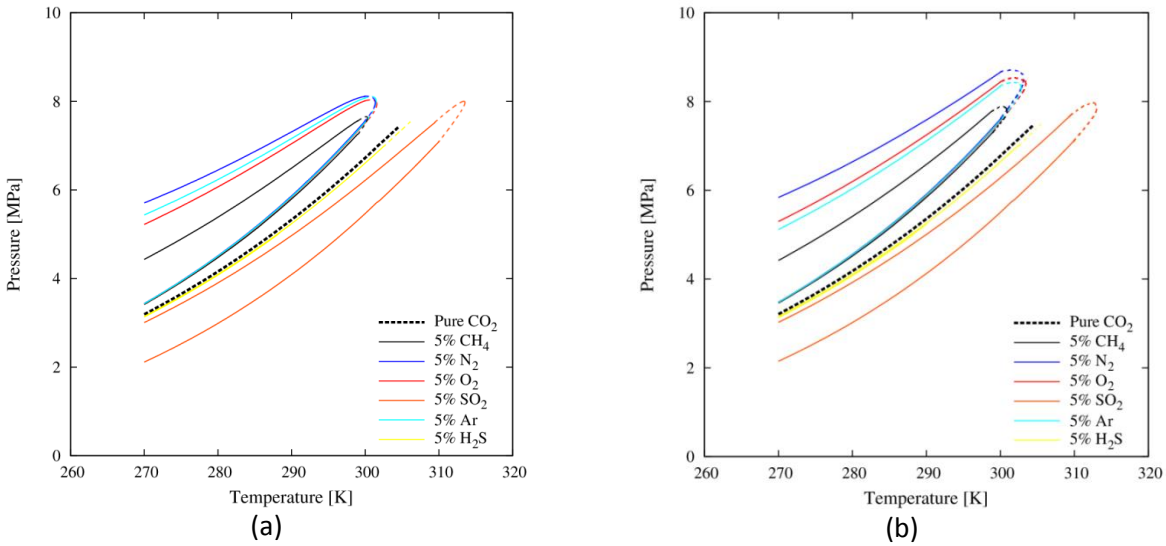

Figure 5–2. Phase envelopes for binary systems of CO_2 with 5 % (mole) of impurities, modeled with PR (a) and PC-SAFT (b).

At the molecular level, this can be explained by the fact that the CO_2-rich environment of the dense liquid phase interacts differently with each of these molecules. It seems that the interactions are driven by the relative volatility, and not by the size differences, since CH_4 is lighter than N_2, yet its bubble point curve lies closer to the pure CO_2 saturation curve than N_2.

Table 5–2. Critical properties of pure components studied in this work [210].

Component	MW (g/mol)	T_c (K)	P_c (MPa)	V_c (cm^3/mol)	ω	μ (D)	κ
CH_4	16.043	190.60	4.610	98.6	0.0115	0.0	0.000
H_2O	18.015	647.30	22.120	55.9	0.3440	0.0	0.000
H_2O	18.015	647.30	22.120	55.9	0.3440	*1.8*	*0.076*
N_2	28.014	126.20	3.397	89.5	0.0358	0.0	0.000
O_2	31.999	154.58	5.043	73.5	0.0220	0.0	0.000
H_2S	34.082	373.30	8.970	87.7	0.0810	0.0	0.000
H_2S	34.082	373.30	8.970	87.7	0.0810	*0.9*	*0.000*
Ar	39.948	150.86	4.86	74.6	0.2510	0.0	0.000
CO_2	44.010	304.35	7.340	91.9	0.2236	0.0	0.000
SO_2	64.065	430.80	7.88	122.0	0.0220	0.0	0.000

The only component that lowers the saturation pressure and shifts the envelope lower than the pure CO_2 curve is the SO_2. This might be happening because the critical temperature of SO_2 is much higher than that of CO_2 (430.80 K and 304.12 K, respectively). Interestingly enough, the addition of H_2S to CO_2 has practically no effect on the phase behavior. The bubble and dew curves of the binary mixture almost overlap, leaving a very narrow two phase region, and the whole envelope is attached on the pure CO_2 saturation curve.

Comparing the performance of PR and PC-SAFT EoS for the prediction of the phase envelopes in Figure 5–2, the only significant deviation is that the bubble point curves of CO_2 – O_2 and CO_2 – Ar have opposite relative position when the two EoS are used. PC-SAFT predicts CO_2 – O_2 at higher pressures than CO_2 – Ar, while the opposite happens with PR. However, the differences are very small. Alfradique and Castier [211] constructed the P-T envelopes of synthetic natural gases containing CO_2 and assessed the predictive capability of PR and PC-SAFT EoS for these mixtures. They concluded that the two EoS result in practically similar calculations, in agreement with our current investigation.

Experimental VLE data for six binary CO_2 mixtures over a broad temperature and pressure range were modeled using cubic EoS, SAFT, and PC-SAFT. The binary mixture of O_2 – N_2 was also modeled because it is needed for the extension of the model

to ternary mixtures. In Table 5–3, the percentage average absolute deviation (% AAD) between experiments and model calculations for each binary mixture, together with the optimum k_{ij} value are shown. PC-SAFT predictions are the most accurate for four mixtures and on the average for all seven mixtures (with % AAD = 11.16). SRK and the two PR models are slightly less accurate overall, while SAFT and RK are the least accurate of the models when no binary parameter is used.

The use of a k_{ij} parameter improves correlation of the data for all EoS. In this case, SRK is on the average the most accurate EoS, with % AAD = 2.95, while the two PR models, SAFT, and PC-SAFT are slightly less accurate. Again, RK is the least accurate with a % AAD = 5.47. However, with the use of k_{ij} in RK improves performance dramatically. The only exception is for the case of CO_2 – SO_2. Here though, RK fails to correlate accurately the vapor pressure of SO_2 and, consequently, it provides inaccurate prediction / correlation of the entire binary mixture phase diagram. Due to its lower accuracy in predicting the vapor pressure of pure CO_2 compared to the other EoS examined in this work, RK will always result in higher errors in the limit of almost pure CO_2, irrespective of the values of the k_{ij} parameter used. Similarly, for the same EoS the use of k_{ij} that improves the correlation of the bubble point curve does not seem to provide an improved description of the dew point curve.

In this work, H_2S was modeled in SAFT and PC-SAFT both as a non-associating and as an associating component with 3-sites per molecule. This is based on indications that H_2S might be forming dimers in the vapor phase due to hydrogen bonding [212]. Calculations for the CO_2 – H_2S mixture using SAFT reveal that when H_2S is treated as an associating component, predictions and correlations are much more accurate compared to calculations where H_2S is a non-associating component. For the case of PC-SAFT, new parameters are reported here for H_2S which is treated as a 3-site associating component. The new parameters (Table 4–1 and Table 4–2) result in accurate correlation of pure H_2S vapor pressure (0.16% AAD) and saturated liquid density (0.37% AAD). However, CO_2 – H_2S mixture predictions and correlations are less accurate compared to calculations where H_2S is modeled as a non-associating component.

Representative results for the CO_2 – CH_4 mixture are shown in Figure 5–4. All models correlate very accurately the experimental data, over the entire pressure range, including the critical region. In Figure 5–5, the K-factors of the two components are plotted for two isotherms. Using a non-zero k_{ij} value, correlation of the CH_4 K-factor improves significantly. In Figure 5–6 through Figure 5–10, experimental data and calculations from the different models are shown for the other binary mixtures. For several of the mixtures examined, experimental data extend to the supercritical region of one of the components. For the case of CO_2 – N_2 (Figure 5–6) and CO_2 – O_2 (Figure 5–7), all EoS become less accurate in the near-critical region.

For five of the binary mixtures examined, experimental liquid density data are available in the literature. The predictability of the different EoS was also evaluated and the results are summarized in Table 5–4. Here again, two sets of results are presented, with zero k_{ij} values and with the k_{ij} values of Table 5–3. The two versions of PR provide overall the best agreement with the experimental data for the case of zero k_{ij} values while introduction of a non-zero k_{ij} results in improvement in the accuracy of all EoS except RK.

Ternary and multi-component mixture VLE data are relatively scarce in the literature. However, they provide a very good basis for the evaluation of models toward their application for real process calculations. In this work, experimental VLE data for one ternary mixture, namely CO_2 – O_2 – N_2, were used to assess model performance. In Table 5–5, the results of this work are presented. When all k_{ij} are set equal to zero, PC-SAFT provides the most accurate prediction of the equilibrium pressure while SRK, PR, PR/G and PC-SAFT result in similar performance for the vapor phase composition. PR is the most accurate with respect to saturated density prediction with PR/G and PC-SAFT being close.

Calculations using the k_{ij} values obtained from the corresponding binary VLE data, show substantial model improvement. SRK, PR, PR/G and PC-SAFT accuracies are close to each other for the equilibrium pressure, vapor phase composition and saturated density (except the liquid density prediction from SRK). SAFT is less accurate than PC-SAFT, but more accurate than SRK and PR for the prediction of the vapor

pressure. It does not extend to the prediction of the composition, however. Interestingly enough, the largest improvement when using non-zero k_{ij} is obtained for the O_2 composition, which is the quantity that is prone to the highest error values. In all cases, predictions from RK are systematically less accurate than all the other EoS. Experimental data and EoS calculations with non-zero k_{ij} values for the K-factor ($K_i = y_i/x_i$) are shown in Figure 5–3. Calculations support the findings of Table 5–5, so that RK predictions are the least accurate of all the models examined.

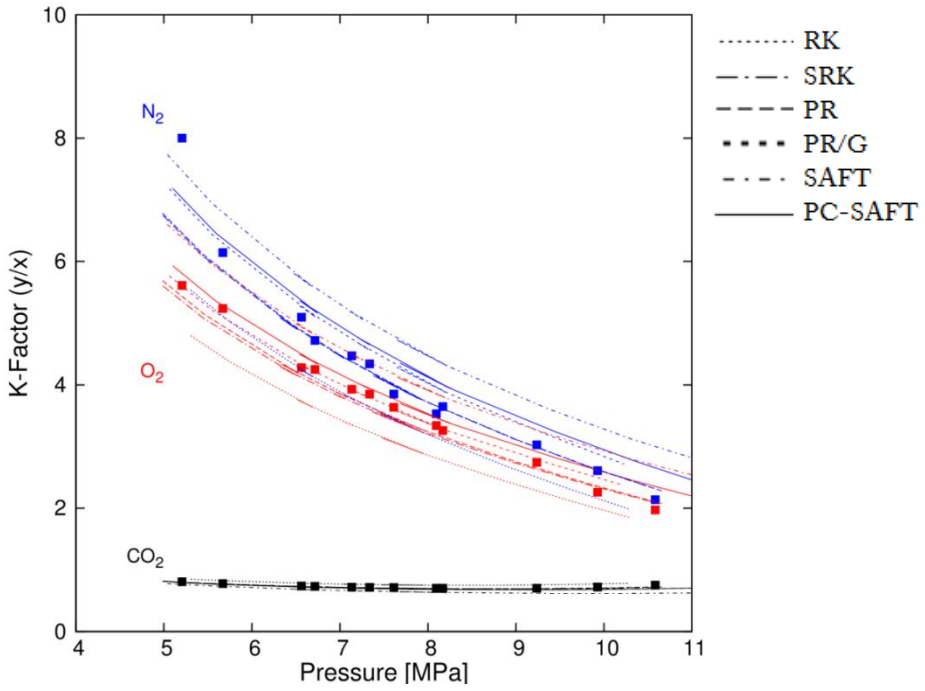

Figure 5–3. K-factors at 273 K for the individual components in the ternary CO_2 – N_2 – O_2 mixture. Experimental data [209] (points) and calculations (correlations).

Table 5–3. % AAD between experimental data and EoS for the mixture bubble pressure and corresponding k_{ij} values. "Pr." refers to calculations with $k_{ij} = 0$ (predictions) while "Cor." refers to calculations with k_{ij} fitted to experimental data (correlations).

			$CO_2 - CH_4$	$CO_2 - N_2$	$CO_2 - O_2$	$CO_2 - SO_2$	CO_2 –Ar	$CO_2 - H_2S$ *		$O_2 - N_2$	Average
RK	Pr.	% AAD	16.54	16.35	26.37	22.50	10.99	8.44		3.02	14.89
	Cor.	% AAD	2.69	2.97	4.12	21.69	1.04	3.06		2.70	5.47
		k_{ij}	0.120	0.082	0.164	0.027	0.205	0.072		0.011	
SRK	Pr.	% AAD	16.73	5.74	22.03	15.27	9.56	13.08		3.13	12.22
	Cor.	% AAD	2.34	3.31	4.78	6.50	2.37	0.86		0.51	2.95
		k_{ij}	0.103	-0.018	0.111	0.051	0.154	0.096		-0.016	
PR	Pr.	% AAD	17.79	4.14	23.20	16.11	9.78	13.38		3.19	12.51
	Cor.	% AAD	2.23	3.73	4.97	6.47	2.32	1.13		0.67	3.07
		k_{ij}	0.100	-0.007	0.111	0.052	0.141	0.098		-0.015	
PR/G	Pr.	% AAD	16.03	4.54	25.89	16.32	11.32	13.30		2.71	12.87
	Cor.	% AAD	2.02	4.68	4.76	7.07	6.55	1.45		0.54	3.87
		k_{ij}	0.100	-0.028	0.108	0.053	0.200	0.101		-0.013	
SAFT	Pr.	% AAD	20.90	6.94	23.89	27.87	6.57	non-assoc.	3B assoc.		
								21.26	15.15	3.08	14.91
	Cor.	% AAD	2.18	2.63	3.47	7.35	4.33	10.92	1.44	1.66	3.29
		k_{ij}	0.100	0.018	0.082	0.076	0.041	0.170	0.082	-0.010	
PC-SAFT	Pr.	% AAD	15.93	6.97	18.50	15.41	4.49	non-assoc.	3B assoc.		
								15.41	24.20	1.42	11.16
	Cor.	% AAD	3.04	6.97	5.07	5.97	2.81	1.34	4.46	0.60	3.69
		k_{ij}	0.061	0	0.049	0.030	0.028	0.067	0.088	-0.005	
Temperature (K)			153 – 288	220 – 301	223 – 283	256 – 389	288	255 – 338		77 – 125	
Pressure (MPa)			1.2 - 8.5	1.4 - 16.7	1.0 - 13.2	0.1 - 9.5	7.5 - 9.8	2.0 - 5.1		0.1 – 3.0	
number of data points			84	77	71	115	4	46		49	

* For CO_2 – H_2S mixture calculations with SAFT and PC-SAFT, H_2S is modeled both as non-associating and associating component. Only the best approach is accounted for in the calculation of the average values, specifically the 3B associating for SAFT and the non-associating for PC-SAFT.

Table 5–4. % AAD between experimental data and EoS calculations for the mixture liquid volume. "Pr." refers to calculations with $k_{ij} = 0$ (predictions) while "Cor." refers to calculations with k_{ij} fitted to experimental VLE data in Table 5–1 (correlations). H_2S is treated as an associating component in SAFT calculations and as a non-associating in PC-SAFT.

		CO_2 - CH_4		CO_2 - N_2		CO_2 - O_2		CO_2 - Ar		CO_2 - H_2S		Average
		k_{ij}	% AAD	k_{ij}	% AAD	k_{ij}	% AAD	k_{ij}	% AAD	k_{ij}	% AAD	
RK	Pr.	0	5.28	0	0.76	0	12.95	0	1.90	0	15.36	7.25
	Cor.	0.120	4.38	0.082	1.64	0.164	12.90	0.205	6.99	0.072	11.47	7.48
SRK	Pr.	0	3.48	0	1.90	0	13.10	0	1.84	0	16.60	7.38
	Cor.	0.103	2. 83	-0.018	1.67	0.111	12.95	0.154	4.42	0.096	10.17	7.30
PR	Pr.	0	6.52	0	1.44	0	1.52	0	4.79	0	11.32	5.12
	Cor.	0.100	5.14	-0.007	1.54	0.111	1.55	0.141	1.83	0.098	7.01	3.41
PR/G	Pr.	0	6.14	0	1.36	0	1.91	0	3.84	0	12.40	5.13
	Cor.	0.100	5.25	-0.028	1.86	0.108	1.92	0.200	2.81	0.101	6.17	3.60
SAFT	Pr.	0	6.50	0	1.82	0	4.79	0	13.42	0	9.95	7.30
	Cor.	0.100	4.49	0.018	1.54	0.082	4.36	0.041	10.15	0.082	8.91	5.89
PC-SAFT	Pr.	0	5.25	0	0.91	0	2.13	0	3.12	0	17.91	5.86
	Cor.	0.061	3.73	-	-	0.049	2.15	0.028	1.94	0.067	3.95	2.54
Temperature (K)		255 – 510		209 - 320		273		288		273 - 363		
Pressure (MPa)		0.1 - 68.9		1.4 - 16.7		4.1 - 11.1		2.4 - 14.5		1.5 - 8.6		
number of data points		778		152		7		76		91		

Table 5–5. % AAD between experimental data and EoS predictions for the equilibrium pressure, vapor phase composition, and saturated densities for the ternary $CO_2 – O_2 – N_2$ mixture, at 273 K and pressure range 5.2 – 10.6 MPa (12 data points used [209]).

			% AAD				
		P^{sat}	Vapor composition			Saturated density	
	k_{ij} (CO_2-O_2 / CO_2-N_2 / O_2-N_2)		CO_2	O_2	N_2	Liquid	Vapor
RK	0 / 0 / 0	11.99	10.36	25.93	16.27	20.01	4.18
	0.164 / 0.082 / 0.011	2.02	6.25	12.17	13.56	19.74	6.70
SRK	0 / 0 / 0	7.40	2.01	13.71	10.69	13.23	5.28
	0.111 / -0.018 / -0.016	2.97	1.29	2.26	4.87	13.23	1.24
PR	0 / 0 / 0	8.07	2.05	14.30	9.65	0.90	1.35
	0.111 / -0.007 / -0.015	2.58	1.04	1.94	4.19	0.92	4.52
PR/G	0 / 0 / 0	7.27	1.80	15.33	9.72	1.22	1.93
	0.108 / -0.028 / -0.013	1.24	1.45	1.75	6.63	1.17	5.46
SAFT	0 / 0 / 0	9.02	5.73	6.70	21.03	3.92	16.23
	0.082 / 0.018 / -0.010	1.90	9.29	16.47	17.45	3.76	5.38
PC-SAFT	0 / 0 / 0	4.17	2.14	9.08	13.29	1.83	1.81
	0.049 / 0 / -0.005	1.84	2.98	3.59	8.25	1.65	4.65

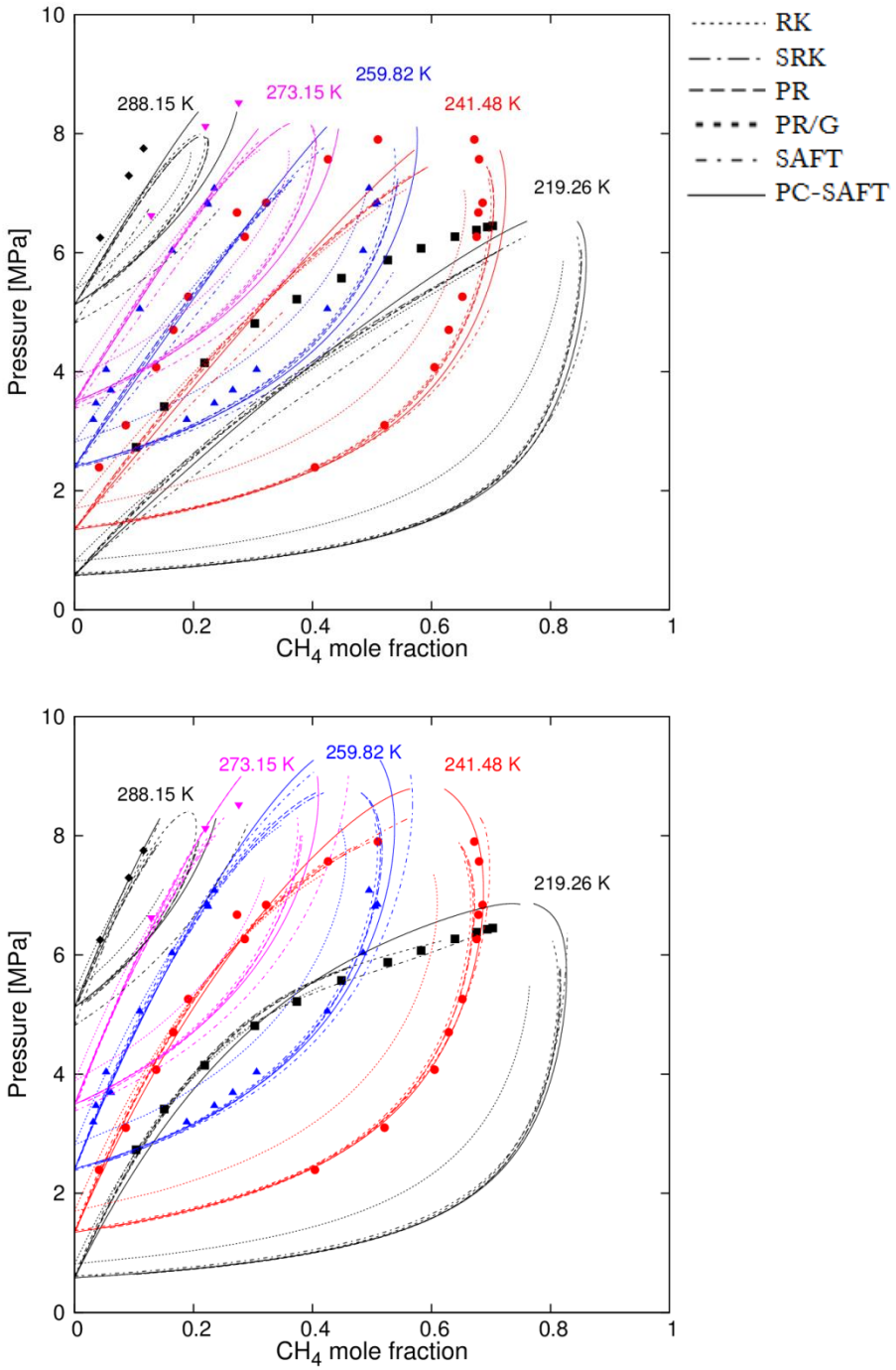

Figure 5–4. Pressure – composition diagram for CO_2 – CH_4 mixture. Experimental data [193, 197] (points) and calculations. Top: predictions ($\boldsymbol{k_{ij} = 0}$), bottom: correlations ($\boldsymbol{k_{ij} \neq 0}$).

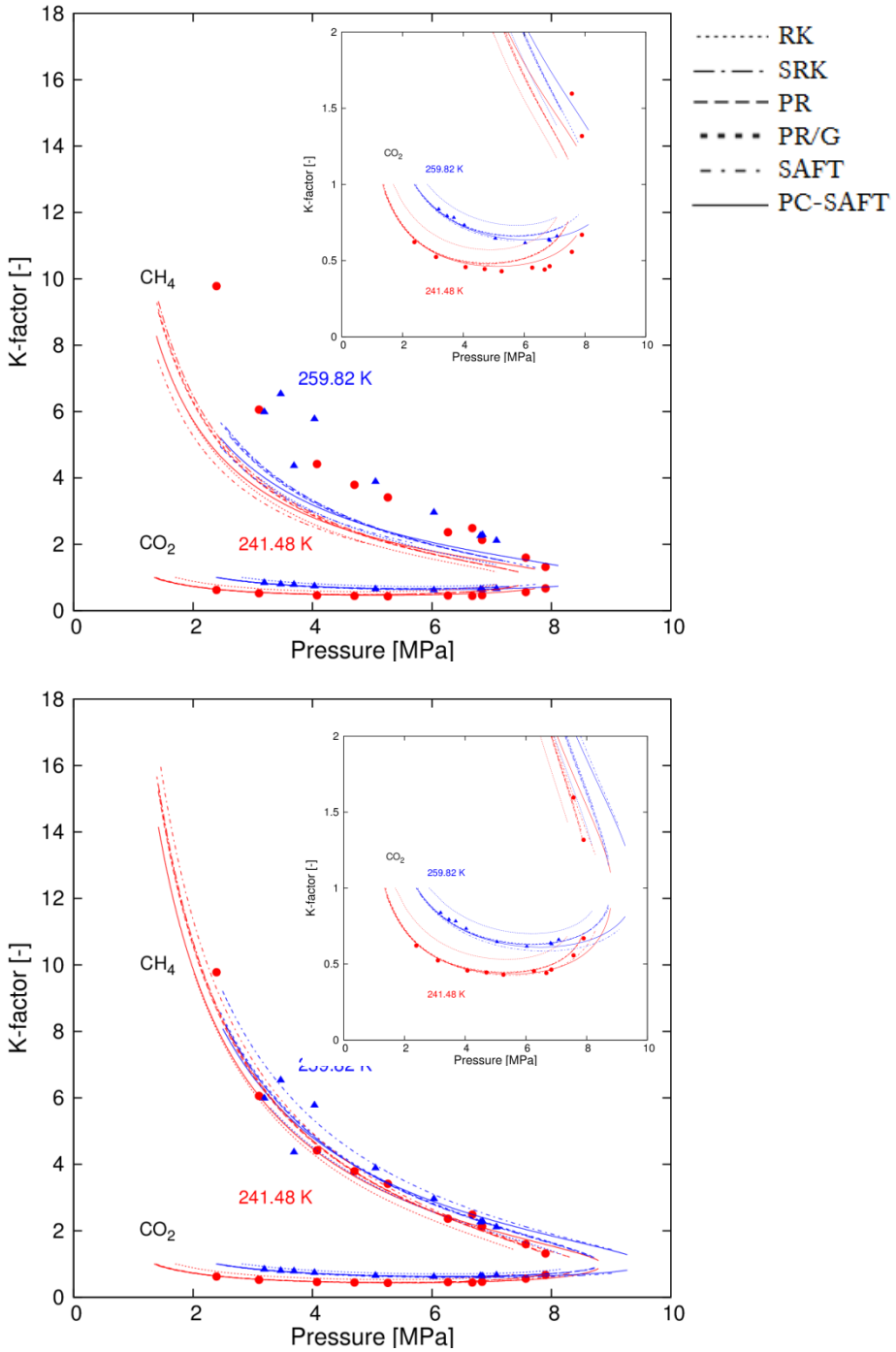

Figure 5–5. K-factor (y/x) – Pressure diagram for CO_2 – CH_4 mixture. Experimental data [193] (points) and calculations. Top: predictions ($\boldsymbol{k_{ij} = 0}$), bottom: correlations ($\boldsymbol{k_{ij} \neq 0}$).

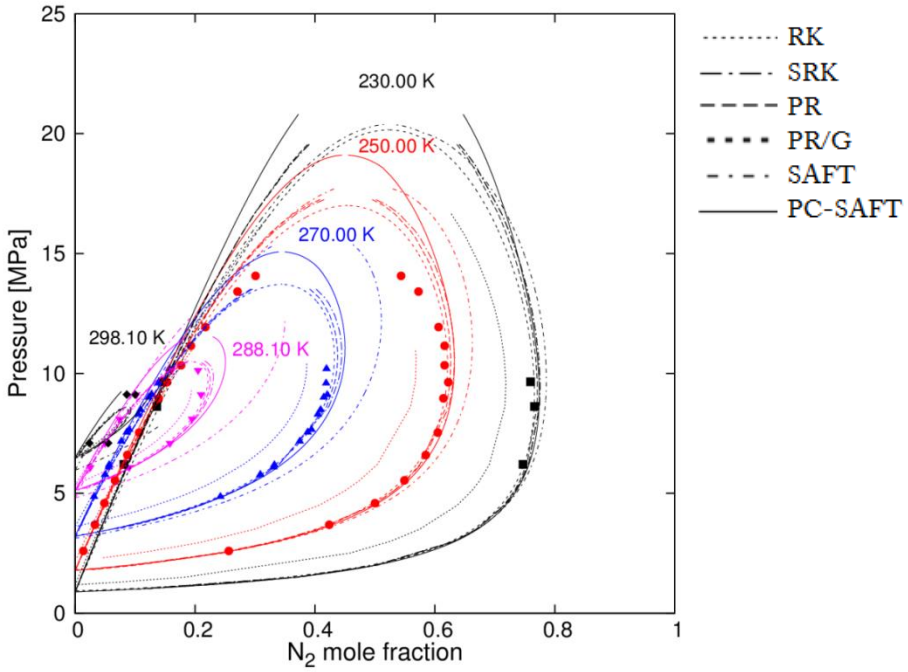

Figure 5–6. Pressure – composition diagram for CO_2 – N_2 mixture. Experimental data [197, 199, 203] (points) and calculations (correlations).

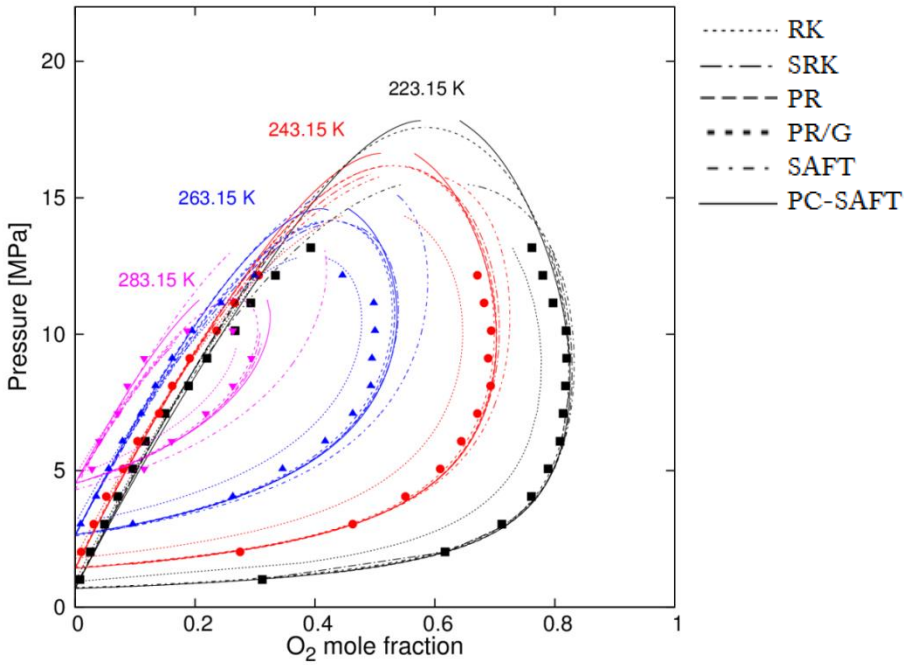

Figure 5–7. Pressure – composition diagram for CO_2 – O_2 mixture. Experimental data [204] (points) and calculations (correlations).

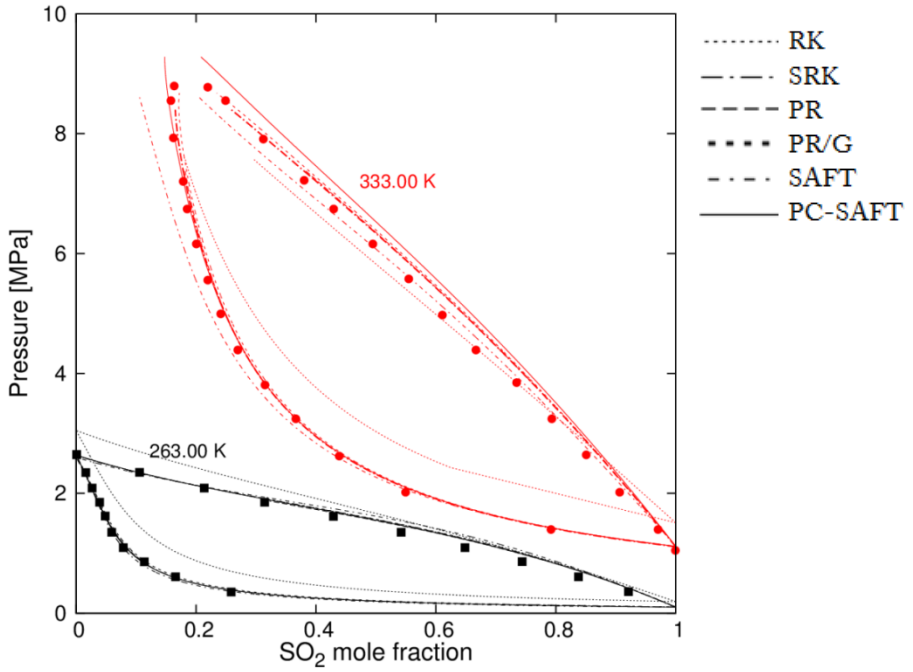

Figure 5–8. Pressure – composition diagram for CO_2 – SO_2 mixture. Experimental data [41] (points) and calculations (correlations).

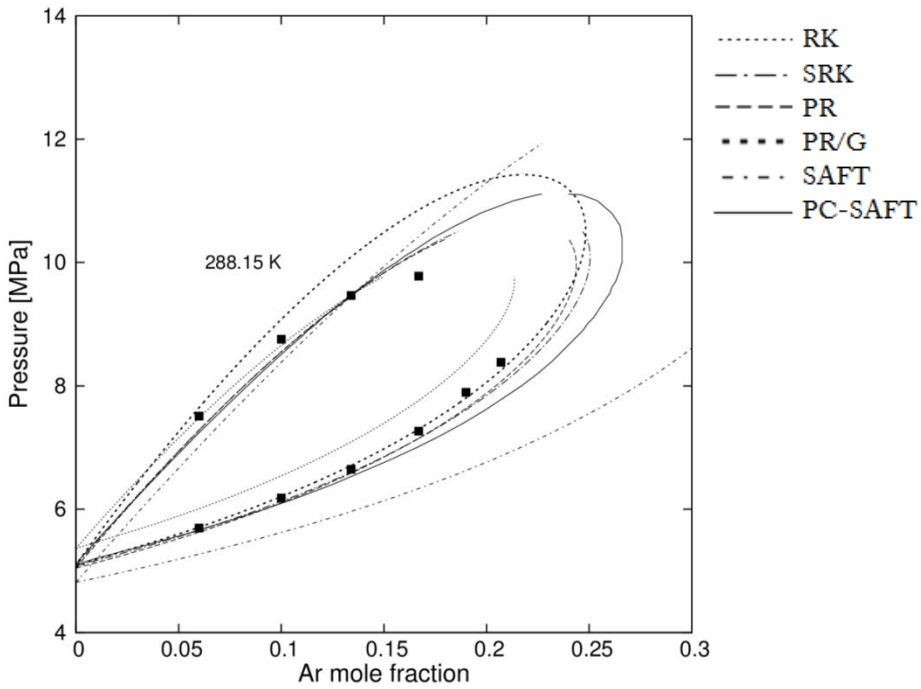

Figure 5–9. Pressure – composition diagram for CO_2 – Ar mixture at 288.15 K. Experimental data [206] (points) and calculations (correlations).

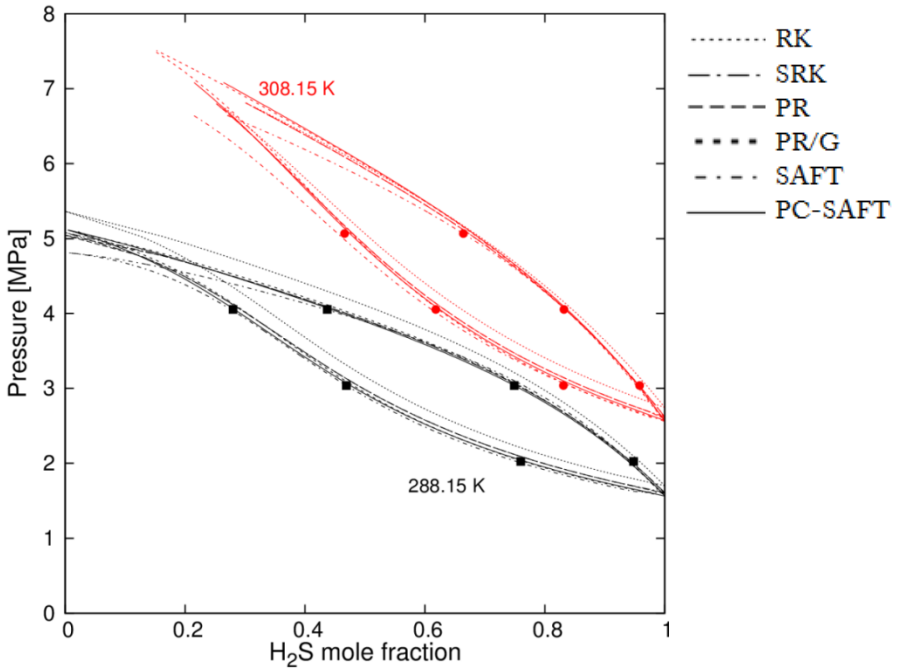

Figure 5–10. Pressure – composition diagram for CO_2 – H_2S mixture. Experimental data [207] (points) and calculations (correlations).

5.2. Water - CO_2 Mixture

As mentioned in the literature review, the mixture of water with CO_2 is of great importance, not only for the storage part of CCS but also for the pipeline transport. Thus, a separate section is dedicated to this system [142].

Due to the fact that CO_2 exhibits quadrupole moment and H_2O exhibits dipole moment, polar interactions were looked into, with the use of tPC-PSAFT, which contains a term that explicitly accounts for the polar interactions. Also, comparison between approaches that take into account polarity and association, individually or in combination, was made and presented in this section.

PC-SAFT and tPC-PSAFT were initially used for pure H_2O and CO_2 to correlate vapor pressure and saturated liquid density data and calculate the model parameters. Different models were tested for the two components. H_2O was modeled as a 4-associating site molecule (4C in the terminology of Huang and Radosz [49]) with two proton donor and two proton acceptor sites per molecule. This is the most commonly

used model for H_2O that has been shown by various researchers [52, 213-217] to provide accurate representation of H_2O and aqueous mixture properties. Model parameters were taken from ref. [218]. In the tPC-PSAFT framework, the dipole – dipole interactions were also taken into account and parameters were taken from [219].

CO_2 was modeled with PC-SAFT as a non-associating component and as an associating component with 2 (2B), 3 (3B) or 4 (4C) sites per molecule. In the tPC-PSAFT framework, CO_2 was modeled as a non-associating component with quadrupole – quadrupole interactions. For the case of non-associating CO_2, model parameters were taken from ref. [218] for PC-SAFT and ref. [219] for tPC-PSAFT while for the three associating models, parameters were fitted to experimental vapor pressure and saturated liquid density data [186]. The objective function for the minimization is:

$$O.F. = min\left[\sum_{i=1}^{N_{data}}\left(\left(\frac{P_i^{EoS}-P_i^{NIST}}{P_i^{NIST}}\right)^2+\left(\frac{\rho_i^{EoS}-\rho_i^{NIST}}{\rho_i^{NIST}}\right)^2\right)\right] \quad (5.1)$$

In Table 5–6, the parameter values for the various models and the accuracy in correlating experimental data are shown. Explicit account of dipole – dipole interactions in H_2O results in decrease of the association energy as one might expect. The accuracy in correlating vapor pressure and liquid density increases. Modeling CO_2 as an associating component results in an improvement in the correlation of the vapor pressure but has almost no effect in the correlation of liquid density. The association energy of CO_2 for all three models is significantly lower than the association energy of H_2O and so association in CO_2 is relatively weak. Explicit account of quadrupolar interactions does not improve the model accuracy in predicting the pure CO_2 vapor pressure and saturated liquid density.

Table 5–6. PC-SAFT and tPC-PSAFT parameters for H_2O and CO_2 fitted to vapor pressure and saturated liquid density and % AAD between experimental data and model correlation. Temperature range: 275 – 640 K for H_2O and 217 – 301 K for CO_2.

Component	m	σ (Å)	ε/k (K)	ε^{AB}/k (K)	κ^{AB}	AAD (%)	
						P^{sat}	ρ^{liq}
PC-SAFT							
H2O (4C)	2.1945	2.229	141.66	1804.17	0.2039	1.98	0.83
CO_2 (inert)	2.6037	2.555	151.04	-	-	0.39	0.88
CO_2 (2B)	2.2414	2.713	159.00	512.88	0.0283	0.15	0.92
CO_2 (3B)	2.3056	2.684	156.83	371.15	0.0277	0.13	1.02
CO_2 (4C)	2.2280	2.731	157.25	307.41	0.0287	0.17	1.18
tPC-PSAFT							
H_2O (4C and dipole[a])	2.8150	2.037	150.71	1575.20	0.3518	0.42	0.49
CO_2 (quadrupole[b])	1.9120	2.854	157.97	-	-	0.82	1.04

[a] For H_2O, μ=1.85D , σ_p=3.093 Å and a=1.49 $Å^3$

[b] For CO_2, Q=4.30D and σ_q=2.974 Å.

Accurate modeling of H_2O – CO_2 phase equilibria is a challenging task. Experimental data and *ab initio* calculations have revealed strong intermolecular interactions between unlike molecules [220-222]. The carbon atom in CO_2 is considered to behave as a Lewis type electron acceptor, while the oxygen atom in H_2O acts as a Lewis type electron donor. In the PC-SAFT and tPC-PSAFT formalisms, such interactions are modeled using a solvating (cross-associating) scheme. In Table 5–7, the various schemes used in this work to model H_2O – CO_2 associating interactions are shown. Furthermore, a temperature independent binary interaction parameter, k_{ij} , was fitted to mixture VLE data in the temperature range 298 – 533 K [223-229].

Regarding the mixing rules applied on the association parameters, two approaches were studied in this work. In the first approach, the cross association energy and volume are calculated according to the combining rules proposed by Gross and Sadowski [162].

In the second approach, the energy of cross-association is calculated from Eq. (3.9), while the volume of cross-association is fitted to mixture VLE experimental data.

In Table 5–7, k_{ij} and $\kappa^{A_iB_j}$ values for the various models are shown.

Table 5–7. Associating models for H_2O and CO_2, binary interaction parameter values and cross-association volumes. In approach 1, the volume of cross association (κ^{AB}) is calculated from Eq. (3.10) while in approach 2 it is fitted to mixture experimental data. Mixture experimental data in the temperature range 298 – 533 K were used to fit $\boldsymbol{k_{ij}}$ and κ^{AB}.

Case #	EoS	H_2O model	CO_2 model	Approach 1 (one fitted parameter)		Approach 2 (two fitted parameters)	
				k_{ij}	κ^{AB}	k_{ij}	κ^{AB}
1	PC-SAFT	4C	Non-associating	-0.0033	-	-	-
2	PC-SAFT	4C	Solvating	0.0376	0.1020*	0.0496	0.1435
3	PC-SAFT	4C	2B	0.0986	0.0749	0.0640	0.0604
4	PC-SAFT	4C	3B	0.1217	0.0741	0.0691	0.0537
5	PC-SAFT	4C	4C	0.1174	0.0754	0.0675	0.0425
6	tPC-PSAFT	4C	Non-associating + quadrupole	-0.0286	-	-	-
7	tPC-PSAFT	4C + dipole	Non-associating + quadrupole	0.0107	-	-	-

* This value was set to $\frac{1}{2} I_{H2O}$.

The objective function used to calculate the binary interaction parameters is:

$$O.F. = min\left[\sum_{i=1}^{N_{data}} \left(\frac{K_i^{EoS} - K_i^{expt,}}{K_i^{expt.}}\right)^2\right] \tag{5.2}$$

where $K_i^{EoS} = \frac{y_i}{x_i}$ is calculated either from PC-SAFT or tPC-PSAFT based on a TP-flash calculation. In Table 5–8, the % AAD in the composition of the liquid and vapor phase from the various models is shown. At the lowest temperature examined (298 K), H_2O – CO_2 exhibit VLE at low pressure, while at pressures higher than 6.4 MPa the system exhibits liquid – liquid equilibria (LLE). In this case, the non-associating model for CO_2 (Case 1) provides accurate correlation of the CO_2 solubility in H_2O (Figure 5–11a) but poor correlation of the H_2O solubility in CO_2 (Figure 5–11b). The accuracy improves significantly when H_2O – CO_2 solvation is taken into account (Case 2). By making $\kappa^{A_iB_j}$ a second fitted parameter in addition to the k_{ij} parameter (Case 2 – Approach 2), the H_2O solubility correlation improves further, but at the expense of CO_2

solubility. Finally, when CO_2 quadrupole – quadrupole interactions are taken into account, model correlation for both phase solubilities significantly deteriorates (Case 6).

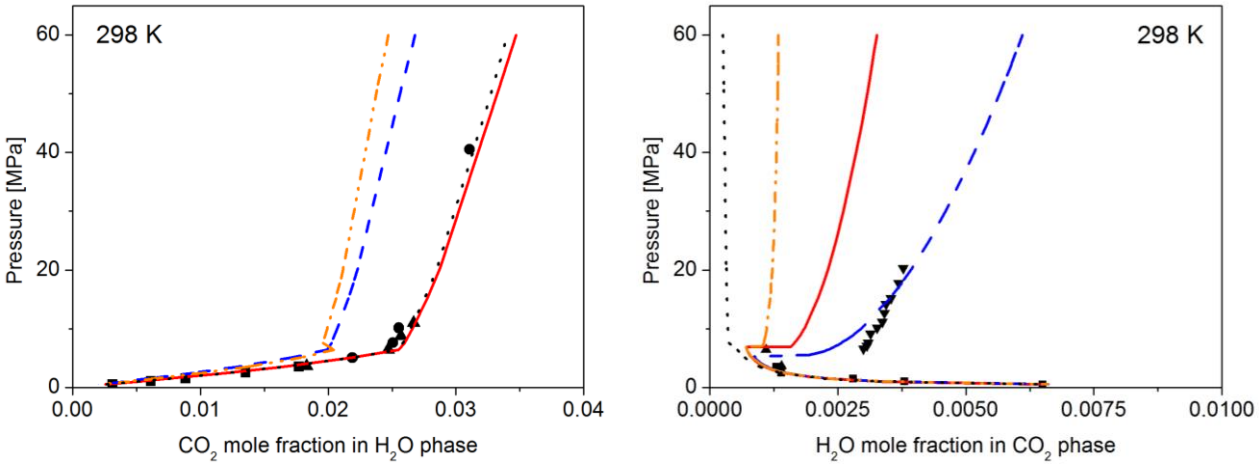

Figure 5–11. Pressure – composition diagrams for the H_2O - CO_2 phase equilibria at 298 K: (a) Aqueous phase and (b) CO_2 phase. Experimental data (■ Valtz [230], ● Wiebe [231], ▲ Nakayama [225], ▼ King [223]), and PC-SAFT model correlation using the different association and polar schemes (· · · · Case 1, —— Case 2 – Approach 1, - - - Case 2 – Approach 2, -·-·- Case 6).

Table 5–8. % AAD in the correlation of the composition of liquid and vapor phases of H_2O – CO_2 mixture in the temperature range 298 – 533 K from the various models.

	%AAD			
Case #	**Approach 1**		**Approach 2**	
	x_{CO2}	y_{H2O}	x_{CO2}	y_{H2O}
1	7.5	37.8	-	-
2	9.7	26.8	10.9	21.6
3	10.3	32.3	9.4	22.0
4	12.0	38.9	10.1	21.7
5	12.7	34.5	10.8	21.7
6	15.0	30.0	-	-
7	17.6	63.2	-	-

In Figure 5–12 and Figure 5–13, the H_2O solubility in CO_2 and CO_2 solubility in H_2O at different temperatures with PC-SAFT (Case 2 – Approach 2) and tPC-PSAFT (Case 6) models are shown. At low temperatures and low pressures, PC-SAFT seems to be more accurate. At temperatures higher than 394 K, calculations from the two models are similar. Calculations from the other models are not presented in detail here, but the overall accuracy of the various approaches can be assessed from Table 5–8. Clearly, explicit account of association and polar interactions in H_2O (Case 7) results in significant reduction of model accuracy.

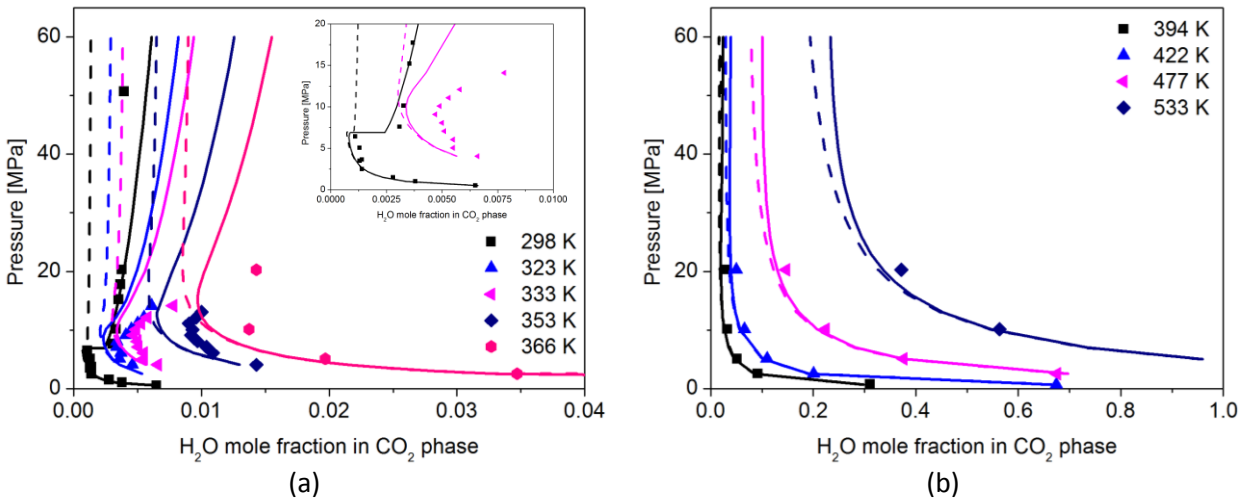

Figure 5–12. Pressure – composition diagrams for the H_2O solubility in CO_2 at different temperatures. Experimental data (points), PC-SAFT correlation (solid lines; Case 2 - Approach 2), tPC-PSAFT correlation (dashed lines; Case 6).

An obvious way to increase correlation accuracy is through the introduction of additional adjustable mixture parameters. Ji et al. [138] used SAFT1-PRM and proposed third order polynomials for k_{ij} , the cross association energy and volume with a total of eleven fitted parameters. Excellent correlation was obtained but with limited predictive capability.

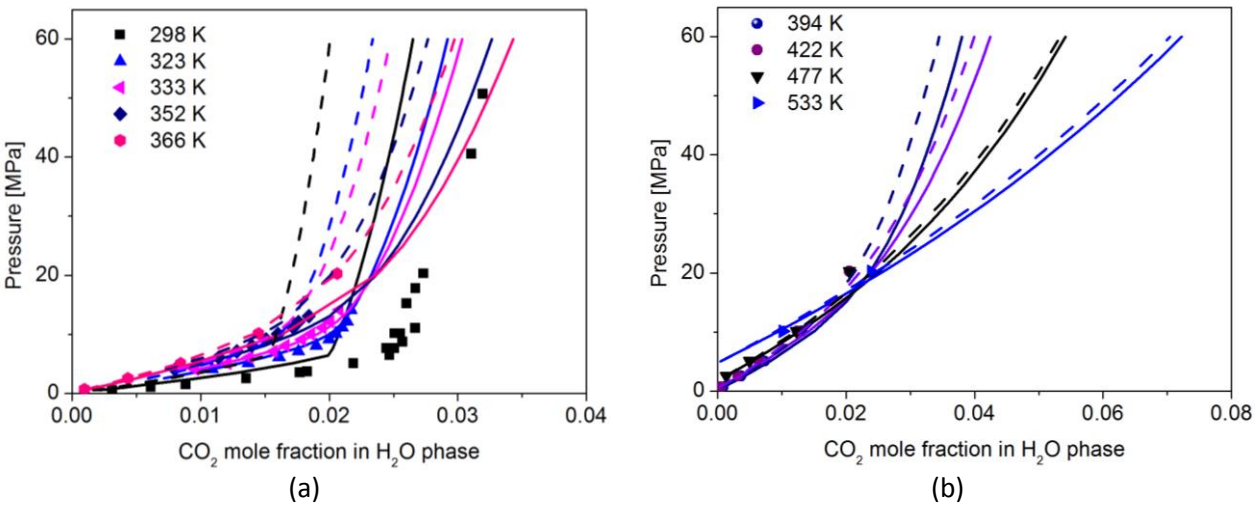

Figure 5–13. Pressure – composition diagrams for the CO_2 solubility in H_2O at different temperatures. Experimental data (points), PC-SAFT correlation (solid lines; Case 2 - Approach 2), tPC-PSAFT correlation (dashed lines; Case 6).

Pappa et al. [135] treated used the CPA-PR model with k_{ij} and the cross association energy as linearly dependent on temperature. Moreover, the sets of parameters that they reported are different for the temperature ranges 278 – 373 K and 373 – 623 K, thus requiring a total of eight parameters to be regressed in order to achieve the final results. Tsivintzelis et al. [134] used CPA with two adjustable parameters, that are k_{ij} and a parameter related to cross association volume. In essence, approach 2 here is equivalent to that approach. Tsivintzelis et al. [134] results are similar to the results presented here. In Table 5–9, a summary of different modeling approaches proposed in the literature are presented for the correlation of H_2O – CO_2 VLE using EoS.

In summary, calculations presented in this work reveal that modeling CO_2 within PC-SAFT as a self-associating component does not improve H_2O – CO_2 VLE and LLE correlation. Instead, by treating CO_2 as a solvating component, the model accuracy is improved. For the case of tPC-PSAFT, modeling of CO_2 as quadrupolar fluid results in good correlation of mixture data but it is still less accurate than PC-SAFT.

Table 5–9. Summary of literature models for H_2O – CO_2 mixture VLE and reported accuracy.

Model	T [K]	No. of adjustable parameters	%AAD x_{CO2}	%AAD y_{H2O}	Reference
SRK with vdW	243-623	2, for solubility of H_2O in CO_2	93	7.3	[71]
SRK with vdW	243-623	3, for solubility of CO_2 in H_2O	3.5	392	[71]
SRK-Huron Vidal	243-623	7	2.6	7.3	[71]
SRK-Huron Vidal	243-623	5	4	7.5	[71]
SRK-Huron Vidal (Pedersen)	243-623	5	11.6	204	[71]
PR-Henry	278-318	7	2.6	11.7	[230]
PR-Huron Vidal	278-318	3 for every isotherm	4.4	6.4	[230]
UMR-PR	278-373	11	5.6	14	[135]
UMR-PR	373-623	11	12.3	14	[135]
PR	278-373	8	6.2	13.9	[135]
PR	373-623	8	10.1	37.4	[135]
CPA-PR	278-373	8	5.9	9.6	[135]
CPA-PR	373-623	8	7.1	10.3	[135]
CPA (CO_2 as 4C with solvation)	243-623	3	11.8	20.6	[71]
CPA (CO_2 as 4C with solvation)	243-623	3	9	16.8	[71]
CPA (CO_2 as 4C with solvation)	243-623	2	21	28.4	[71]
CPA (CO_2 as 4C with solvation)	243-623	1	43	20.9	[71]
CPA (CO_2 as 4C without solvation)	243-623	0 or 1		56	[71]
CPA (CO_2 as 2B)	298-478	2	16.5	11.9	[134]
CPA (CO_2 as 3B)	298-478	2	12.6	14.7	[134]
CPA (CO_2 as 4C)	298-478	2	10.8	15.1	[134]
SAFT-VR	278-318	2	2.2	12	[230]
GC-PPC-SAFT	298-523	2	41.8	50.1	[141]

The optimized models developed here were used to predict the density of H_2O – CO_2 mixture. Experimental data [223, 232] and model predictions from PC-SAFT (Case 2) and tPC-PSAFT (Case 6) at 298.15 K and 332.15 K are presented in Figure 5–14. The % AAD is 0.6 % and 0.8 % for PC-SAFT and tPC-PSAFT, respectively.

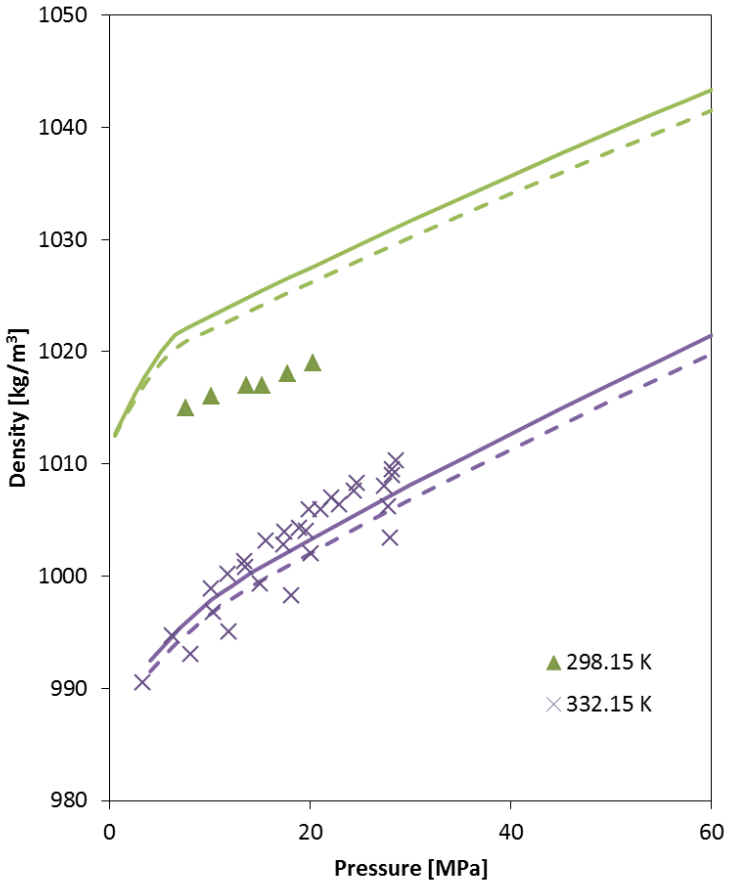

Figure 5–14. Density of CO_2-saturated H_2O at 298.15 and 332.15 K. Experimental data [223, 232], PC-SAFT prediction (solid lines; Case 2 – Approach 2) and tPC-PSAFT prediction (dashed lines; Case 6).

Further investigation on the performance of several models on the prediction of density at high pressure and high temperature, and over a range of compositions, is needed, as it can have a significant effect on the process design. The density of the mixture H_2O-CO_2 was calculated with two different EoS, and the results are shown in Figure 5–15. More specifically, the models employed here, are the PR EoS, as an

ambassador of the cubic EoS used to study the CO_2 containing systems in section 5.1, and PC-SAFT considering CO_2 as a two-site associating molecule and H_2O as a four-site associating molecule, which is the Case 2 according to the convention of this section. It is obvious that PR fails to predict the densities at pressures higher than 39.94 MPa whereas PC-SAFT is capable of capturing the experimental trend over the entire pressure and composition range. The quantitative behavior is very satisfactory, with deviation from experiments equal to 3.85 % AAD for PC-SAFT and 2.73 % AAD for PR. This might not be very clear from Figure 5–15, because at low pressures and high CO_2 concentrations, PR performs slightly better than PC-SAFT, affecting the final result.

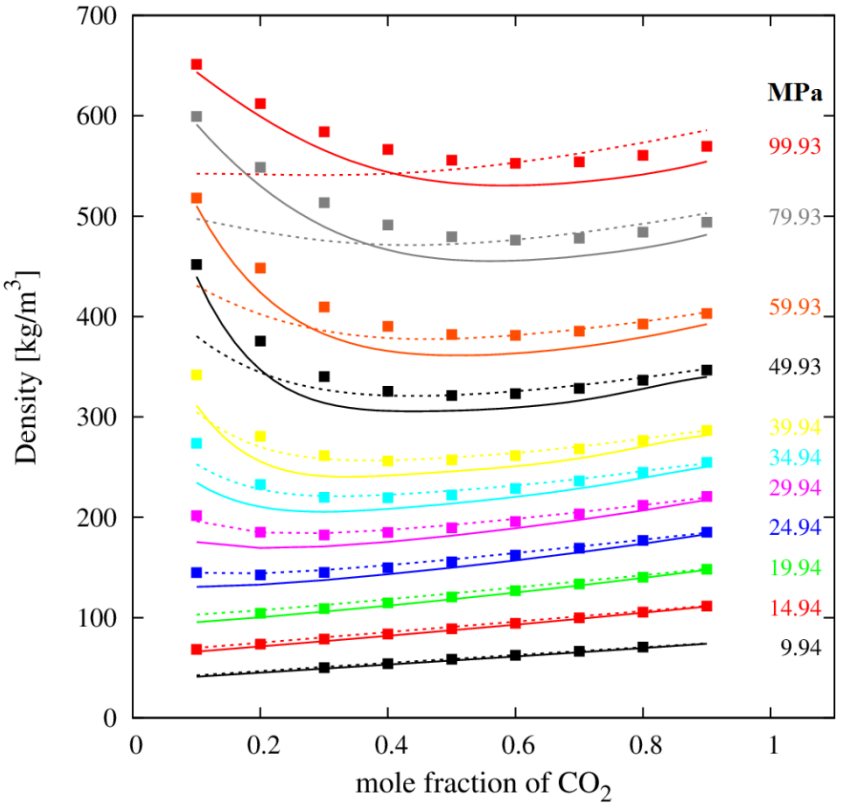

Figure 5–15. Density of CO_2 – H_2O mixture at 673.15 K and high and very high pressures. Predictions from PR (dashed lines), and PC-SAFT (continuous lines). Experimental data (points) from [233].

A similar analysis for this mixture was reported by Duan and Zhang [234], who used molecular dynamics simulations together with a newly developed EoS. The

comparison of their very accurate results with this work is not straightforward, since the number of fitted parameters both for the pure components and the mixture differ significantly.

5.3. Modeling the VLE of a Multicomponent Mixture of Industrial Interest

A more complex 11-component synthetic oil was examined using PR and PC-SAFT EoS. Experimental data vs. predictions from the two models (no binary interaction parameters used) are shown in Figure 5–16 PC-SAFT is more accurate than PR. The latter predicts a critical pressure that seems to be much lower than the projected experimental one.

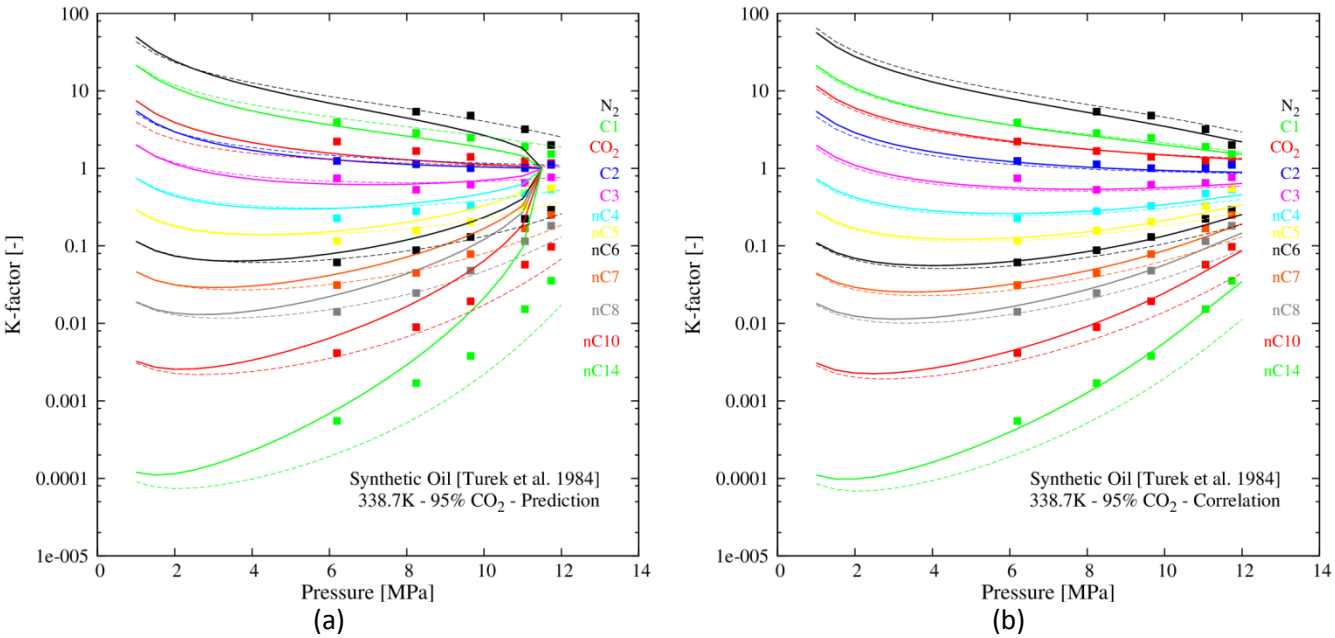

Figure 5–16. Addition of 95 mole % CO_2 to an 11-component synthetic oil. Predictions (a) and correlations (b) of *K-factors* from PR (continuous lines) and PC-SAFT EoS (dashed lines) against experimental data (points).

The K-factors of the light components up to C_3 are underpredicted by PR, while for heavier components, the opposite holds. On the other hand, PC-SAFT behaves

satisfactorily for all components except for CO_2 which is in excess, and n-C_{14} which is the heaviest component.

In order to investigate the effect of binary interaction parameters, a semi-predictive approach was used. Only the interaction parameters of N_2 and CO_2 with the other components were set to an optimal value, instead of fitting all of the 66 binary interaction parameters. Specifically, for the case of PR EoS, the parameters reported by Knapp et al. [235] were used. A large collection of experimental data from the literature was used in order to fit the PC-SAFT interaction parameters for the binary systems of CO_2 with the other components. The values of k_{ij} between N_2 and other components were assumed to be zero, because of the low levels of N_2 in the mixture. In brief, the conditions ranges, the references, and the binary interaction parameter values are reported in Table 5–10. Significant improvement of the results is achieved for PR as it can be seen in Figure 5–16b.

Table 5–10. Optimized binary interaction parameters for CO_2 – n-alkane mixtures, for the PC-SAFT EoS.

Mixture	k_{ij}	Number of Points	T (K)	P (MPa)	References
CO_2 - ethane	0.0959	288	207 – 298	0.3 – 6.6	a, b, c, d, e
CO_2 - propane	0.1084	106	253 – 361	0.3 – 6.7	f, g
CO_2 - n-butane	0.1198	176	278 – 418	0.3 – 8.2	h, i, j
CO_2 - n-pentane	0.1247	172	253 – 463	0.2 – 9.6	k, l, m
CO_2 - n-hexane	0.1312	59	298 – 393	0.4 – 11.6	n, o
CO_2 - n-heptane	0.1353	64	311 – 477	0.2 – 13.3	p
CO_2 - n-octane	0.1418	20	313 – 348	1.5 – 11.4	q
CO_2 - n-decane	0.1399	133	278 – 594	0.3 – 18.8	r, s, t, u

a. [236], b. [237], c. [238], d. [239], e. [240], f. [241], g. [242], h. [243], i. [244], j. [245], k. [246], l. [247], m. [248], n. [249], o. [250], p. [251], q. [252], r. [253], s. [254], t. [255], u. [256]

The PR calculations move much closer to those of PC-SAFT and thus to experimental data, with some deviations only for the heavier components (> nC_6) at high pressures. The K-factor of CO_2 is computed with high accuracy by both models.

5.4. Phase Equilibria Containing Solid CO_2

5.4.a. Solubility of Solid CO_2 in a Liquid Component or Mixture

An algorithm that matches PC-SAFT and a model for solid fugacity was implemented in order to calculate the solubility of solid pure components in liquid mixtures. PC-SAFT was used to calculate the fugacities of the fluid phases while the model for solid fugacity was used for the equi-fugacity condition.

In theory [154], when a pure solid phase is in equilibrium with a liquid phase, the fugacities of the solid and subcooled liquid phases are connected through Eq. (5.3).

$$\ln\frac{f_{i,liq}}{f_{i,solid}}=\frac{\Delta h^{f}}{RT_{t}}\left(\frac{T_{t}}{T}-1\right)-\frac{\Delta C_{p}}{R}\left(\frac{T_{t}}{T}-1\right)+\frac{\Delta C_{p}}{R}\ln\frac{T_{t}}{T}+\frac{\Delta v}{RT}\left(P-P^{sat}\right)+\lambda \qquad (5.3)$$

Δh^{f} : Enthalpy of fusion

ΔC_{p} : Change in isobaric heat capacity from liquid to solid phase

Δv : Change in volume from the liquid to solid phase

λ : Change in Gibbs due to solid-solid phase transition divided by RT

The properties that refer to solid such as Δh^{f}, C_{p}^{solid}, v^{solid} and λ can be retrieved from experiments.

As far as it concerns the terms of Eq. (5.3), the two terms that depend on ΔC_{p} can be neglected due to the fact that they are of approximately equal magnitude.

In this step of the study, another assumption was held that refers to neglecting the Δv related term at low pressures, as well as not taking into account the λ [257]. It should be mentioned that Ting [258] presented results (to which this study is compared) that were produced without the previously mentioned assumptions. To be more illustrative, the equations that are used in each study are:

$$\ln \frac{f_{i,liq}}{f_{i,solid}} = \frac{\Delta h^f}{RT_t}\left(\frac{T_t}{T} - 1\right) \text{ (this study)} \tag{5.4}$$

$$\ln \frac{f_{i,liq}}{f_{i,solid}} = \frac{\Delta h^f}{RT_t}\left(\frac{T_t}{T} - 1\right) + \frac{\Delta v}{RT}\left(P - P^{sat}\right) + \lambda \quad [258] \tag{5.5}$$

Parameters and properties

The next two tables summarize the PC-SAFT parameters and the physical properties used in this work.

Table 5–11. PC-SAFT parameters for components studied for SLE.

	$MW\ [g/mol]$	r_i	$\sigma\ [A]$	$u^0/k\ [K]$	*Ref.*
carbon dioxide	44.01	2.6037	2.5550	151.04	this work
ethane	30.07	1.6068	3.5251	191.37	this work
propane	44.096	2.0020	3.6184	208.11	[50]
n-butane	58.123	2.3316	3.7086	222.88	[50]

Table 5–12. Physical properties for the components that solidify (DIPPR).

	$T_{0i}^f\ [K]$	$\Delta h_{0i}^f\ [J/mol]$	$v_{0i}^{L*}\ [cm^3/mol]$	$v_{0i}^S [cm^3/mol]$	$\Delta Cp_{0i}^{SL*} [J/molK]$
carbon dioxide	216.58	25246	37.347	29.091	20.205

5.4.b. Results

One of the limiting factors for this part of the work is that the data regarding systems where the CO_2 can be found in the solid state are scarce. Thus, in order to validate the model and its implementation, several other systems were used as well.

The results will be presented in groups, depending on whether they contain or not CO_2, while a separate section is dedicated to a ternary system that was modeled for the needs of validation for more complex systems.

Systems that contain CO_2

The implemented solid fugacity model works well with the PC-SAFT EoS, producing results of high accuracy for the solubility of CO_2 in light hydrocarbons in the liquid state. As it can be seen in Figure 5–17, Figure 5–18, and Figure 5–19, the solubility predictions of PC-SAFT are very close to the experimental data. These calculations are predictions, since no work was done to optimize the binary interaction parameters between CO_2 and the solvent. Table 5–13 gives the errors in % AAD, and it is interesting to note that despite the good agreement that is observed visually in the figures, the errors are quite high, a fact that can be attributed to the high discrepancies that occur at low temperatures, where the solubility takes very low values and numerical problems are more apparent. This can be supported illustratively by exhibiting the solubility plots as function of the natural logarithm of the composition. The experimental data form an S-type curve, while the theory is not in agreement with this trend. This might be attributed to the lack of a pressure effect term, which can have significant presence only at high pressures. As it will be shown in results for systems that don't contain CO_2 and are modeled in lower pressures, the discrepancies are not that high (Figure 5–20 and Figure 5–21).

The physical properties that are required by the calculations and have an important effect on the results are the T_{0i}^{f} and Δh_{0i}^{f}, which have been selected on the triple point of CO_2, while the dominant term of the equation is the one that contains the enthalpy of fusion. This has been identified by performing calculations with and without the rest of the terms (pressure effect, heat capacity contribution).

The calculations are not demanding, since the convergence is achieved after 3-14 iterations (depending on the system).

Table 5–13. % AAD error for all the CO_2 containing systems.

System (CO_2 + …)	% AAD
ethane	49.09
propane	46.73
n-butane	48.34

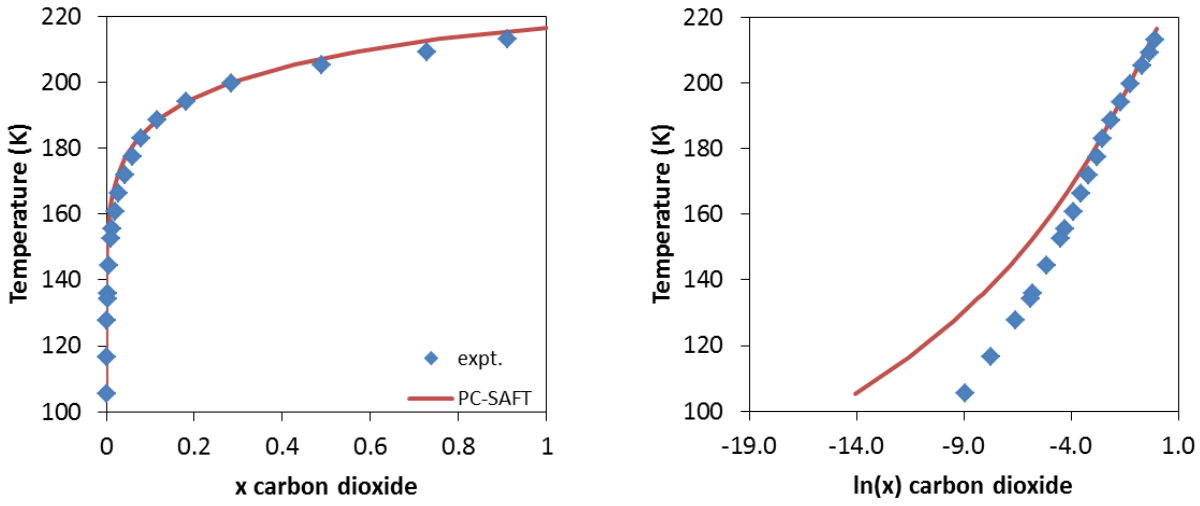

(a) (b)

Figure 5–17. Solid-liquid phase equilibria of the system carbon dioxide in liquid ethane (experimental from Jensen and Kurata [259]).

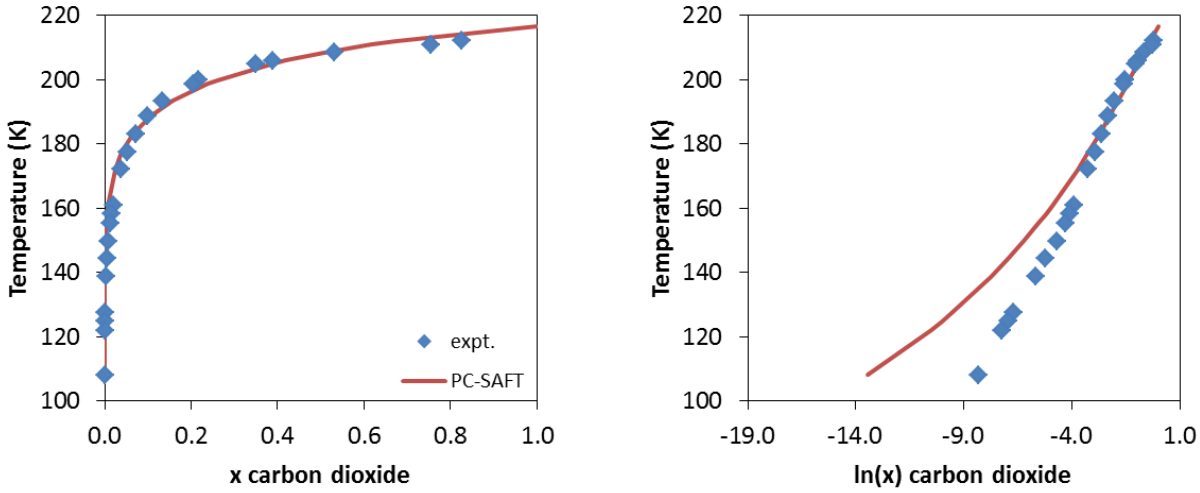

(a) (b)

Figure 5–18. Solid-liquid phase equilibria of the system carbon dioxide in liquid propane (experimental from Jensen and Kurata [259]).

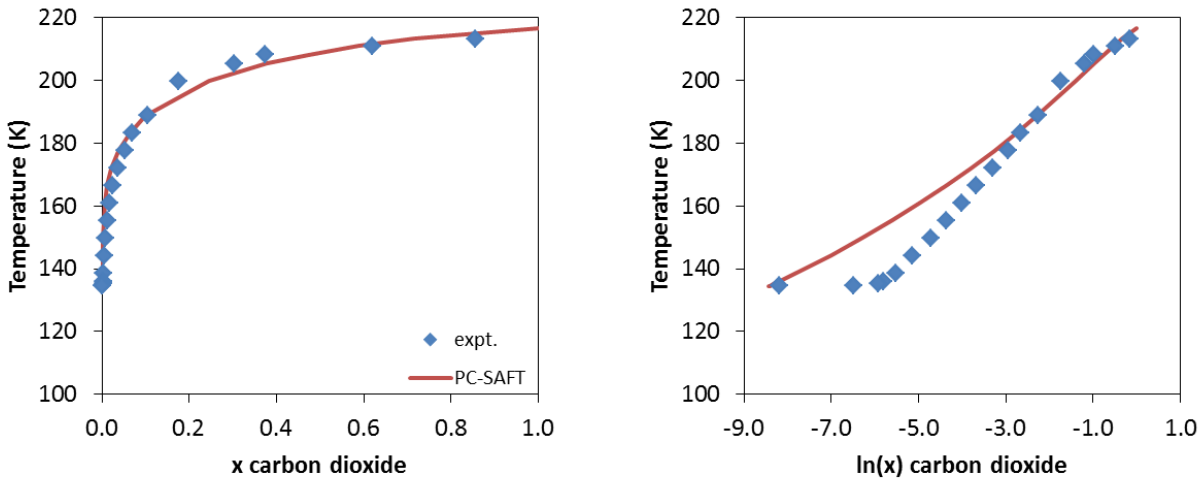

(a) (b)

Figure 5–19. Solid-liquid phase equilibria of the system carbon dioxide in liquid n-butane (experimental from Jensen and Kurata [259]).

Systems without CO_2

Long alkanes, such as n-dodecane and n-hexadecane can be solid at low temperatures, so their binary systems with common solvents such as n-hexane are very good examples for measuring and calculating the solubility of the solid component. Experimental data were used in order to assess the ability of the model to capture this behavior. As it can be seen in Figure 5–20 and Figure 5–21, good agreement between the model and the experimental data is achieved. This is not the case for the system n-dodecane – n-hexane at very low temperatures (< 210 K) which can be attributed to the fact that the parameters of PC-SAFT are not suitable for such low temperatures.

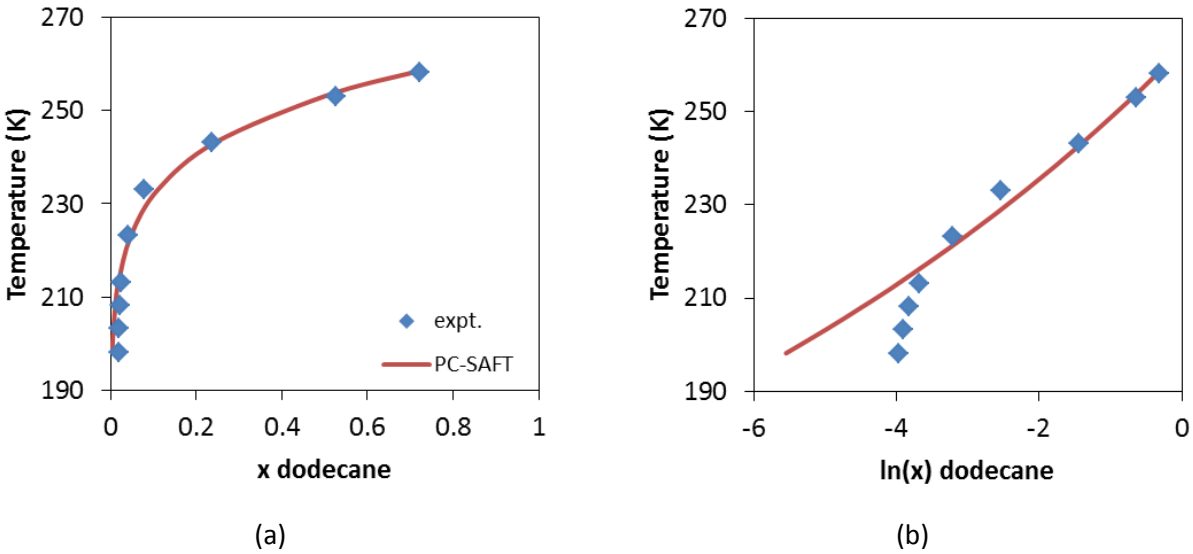

Figure 5–20. Solid-liquid phase equilibria of the system n-dodecane – n-hexane (experimental from Hoerr and Harwood [260]).

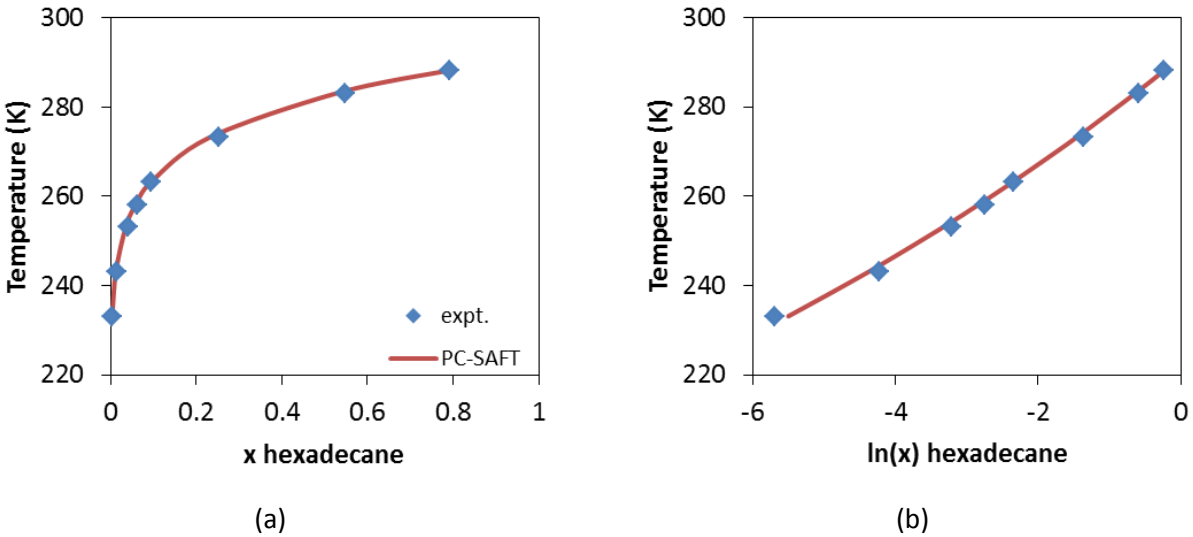

Figure 5–21. Solid-liquid phase equilibria of the system n-hexadecane – n-hexane (experimental from Hoerr and Harwood [260]).

An interesting ternary system

Ever since the implementation of the model was validated for binary systems, the question of what happens with more complex systems arose. The system of methane - n-

decane - phenanthrene was studied experimentally by Jacoby et al. [261], and computationally by Ting [258], so it is a good basis for validation.

The experimental model parameters that were used in the model are presented in Table 5–14.

Table 5–14. Experimental parameters for solid phenanthrene fugacity model

Parameter	Value	Units
Δh^f	16463	J/mol
T_{melt}	372.4	K
λ	217	J/mol
v^{solid}	151.7	cm^3/mol

For the use of PC-SAFT, the parameters were taken from [50] and are shown in Table 5–15.

Table 5–15. Parameters for PC-SAFT equation of state

	MW (g/mol)	m	σ (A)	ε/k (K)
phenanthrene	178.23	3.4890	4.1053	403.06
methane	16.04	1.0000	3.7039	150.03
n-decane	142.29	4.6627	3.8384	243.87

Table 5–16 contains the k_{ij} values that are proposed by Ting and adopted in this study.

Table 5–16. Binary coefficients

Binary	k_{ij}
phenanthrene – methane	0.094
phenanthrene – n-decane	0.015
methane – n-decane	0.012

In Figure 5–22, the plot of the ternary system methane – n-decane – phenanthrene is shown.

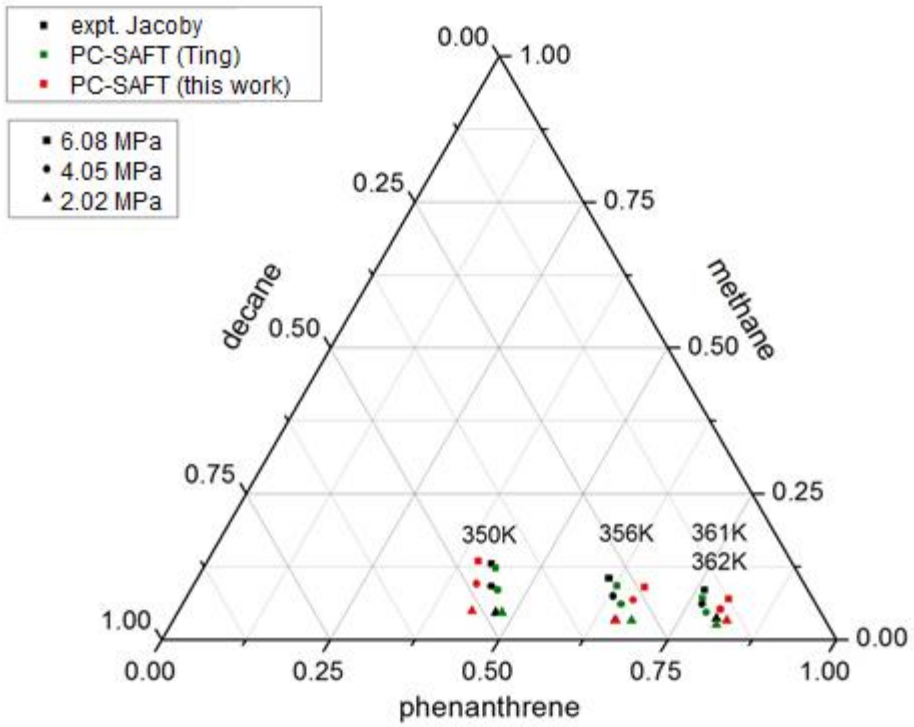

Figure 5–22. Ternary plot for system phenanthrene – methane – n-decane.

Finally, in Table 5–17, the results along with a set of experimental data from Jacoby are presented for the completeness of the assessment. Moreover, the % AAD was calculated so as to provide a measure of accuracy of the calculations. The values of % AAD are contained in as well.

Table 5–17. Experimental values, calculations and % AAD

P [bar]	T [K]	Experimental mole fractions (Jacoby)			PC-SAFT (Ting) mole fractions			PC-SAFT (this work) mole fractions		
		phenanthrene	methane	n-decane	phenanthrene	methane	n-decane	phenanthrene	methane	n-decane
	350	0.424	0.1294	0.4466	0.4336	0.1226	0.4438	0.4024	0.1343	0.4634
60.8	356	0.6105	0.1051	0.2844	0.6295	0.0912	0.2793	0.6709	0.0888	0.2403
	361	0.7622	0.0844	0.1535	0.766	0.0705	0.1635	0.8058	0.0689	0.1253
	350	0.4431	0.0912	0.4657	0.4555	0.0844	0.4601	0.419	0.0952	0.4859
40.5	356	0.6322	0.074	0.2938	0.651	0.0601	0.2889	0.6649	0.0674	0.2677
	361	0.7712	0.0601	0.1687	0.7843	0.0462	0.1695	0.8023	0.0519	0.1458
	350	0.4718	0.0462	0.482	0.4808	0.0469	0.4731	0.435	0.0494	0.5156
20.2	356	0.6559	0.0323	0.3118	0.68	0.0328	0.2877	0.6572	0.0322	0.3107
	362	0.8044	0.0358	0.1598	0.8097	0.0252	0.1651	0.8213	0.0327	0.146
					mole fraction % AAD			**mole fraction % AAD**		
	350				2.26	5.26	0.63	5.1	3.75	3.75
60.8	356				3.11	13.23	1.79	9.89	15.51	15.51
	361				0.5	16.47	6.51	5.73	18.39	18.39
	350				2.8	7.46	1.2	5.44	4.33	4.33
40.5	356				2.97	18.78	1.67	5.17	8.89	8.89
	361				1.7	23.13	0.47	4.03	13.6	13.6
	350				1.91	1.52	1.85	7.8	6.97	6.97
20.2	356				3.67	1.55	7.73	0.19	0.37	0.37
	362				0.66	29.61	3.32	2.1	8.62	8.62
					2.18	**13**	**2.8**	**5.05**	**8.94**	**8.94**

5.4.c. Solid – Vapor Equilibria

Solid-vapor equilibrium (SVE) of pure CO_2 properties is predicted using SAFT and PC-SAFT EoS. However, since these equations have been developed and tuned to fluid phase properties (gas, vapor and liquid) prediction of SVE can be achieved only after model parameters are "retuned". Parameter retuning enables SAFT and PC-SAFT to predict solid properties (i.e. density, enthalpy and fugacity) in place of liquid (i.e. solid density instead of liquid density). When the retuned EoS is used for equilibria calculations, sublimation is obtained. Of course, the "retuned" EoS should not be used at temperatures higher than the triple point.

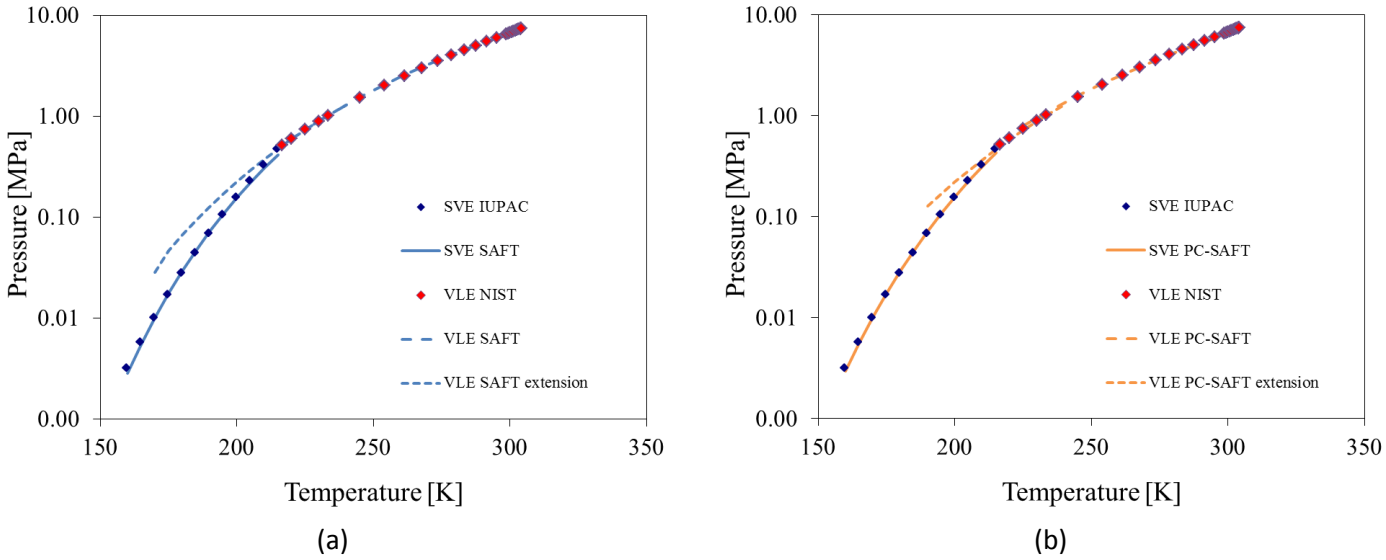

Figure 5–23. CO_2 vapor pressure at temperatures between 160-215 K (SVE) and 215-304 K (VLE), (a) SAFT, (b) PC-SAFT.

The new set of SAFT and PC-SAFT model parameters are calculated by fitting SVE data to IUPAC correlations [262]. Figure 5–23 shows how the original and the modified EoS predict VLE and SVE on a pressure-temperature diagram that extends from the critical point of CO_2 to temperatures well below the triple point. Model predictions and experimental data compare well. The change in slope occurs at the CO_2 triple point. Also, extrapolation to temperatures lower than the triple point is shown for the VLE models. The change in slope shown is achieved by retuning SAFT/PC-SAFT model parameters.

A major disadvantage of the proposed modeling approach is the need to select either the VLE or the SVE parameter set depending on which part of the phase diagram is simulated. As a result, when modeling depressurization along the VLE curve the user of the simulation algorithm must switch model parameter set when the temperature drops below the triple point. The problem becomes more profound, when multi-component SVE is modeled. In this case, the switch between model parameter sets must happen at conditions that depend not only on temperature but also on composition.

Model description and parameter tuning

For modeling pure CO_2, SAFT and PC-SAFT use three adjustable parameters. When modeling VLE, parameter values are obtained by fitting vapor pressure and liquid density experimental data at saturation. In this work, the same equations are used to model solid properties but the parameters are fitted to experimental data of sublimation and solid density. As a result, an engineering model for SVE is obtained.

For tuning model parameters, the temperature range of 160-210 K was considered. The reason for this is that both SAFT and PC-SAFT models were unable to converge at temperatures lower than 120-130 K. Also, the error in sublimation pressure at lower temperatures is relatively high. Furthermore, given that the lowest temperatures observed during rapid pipeline depressurization experiments did not fall below 200 K, model parameter tuning was limited to 160-215 K.

In addition to sublimation data, a data point for the density of solid phase is used during parameter fitting. This is done in order to force regression to reasonable solid density predictions. An unsuccessful attempt was made to include density data points at lower temperatures due to numerical difficulties.

Table 5–18 presents the sublimation data used for the regression of model parameters. An increment of 5 K was selected.

Table 5–18. Data set for SVE calculations

T [K]	P [MPa]	T [K]	P [MPa]
160	0.003137	190	0.068343
165	0.005687	195	0.103968
170	0.009938	200	0.155004
175	0.016796	205	0.226967
180	0.027539	210	0.327075
185	0.043927	215	0.464777

Table 5–19 presents parameter values obtained from tuning the model to the sublimation data of Table 5–18. All parameter sets (SVE and VLE) use values for the parameter m (number of spherical segments) and the parameter v^{00} (characteristic volume of a molecular segment) which are in the same order of magnitude, so as to maintain the physical background. For modeling SVE however, higher m values and lower v^{00} values are used compared to VLE.

Table 5–19. SAFT and PC-SAFT parameters for pure CO_2. SVE and VLE.

CO_2 Parameters	SVE		VLE	
	SAFT	PC-SAFT	SAFT	PC-SAFT
MW (g/mol)	44.0098	44.0100	44.0098	44.0100
m	7.7725	8.2809	2.6830	2.0729
v00 (ml/mol)	1.5129	1.5506	6.3232	2.7852
u0/k (K)	83.08	90.49	143.68	169.21
e/k (K)	40	0	40	0

5.4.d. Solid – Fluid Equilibria Using a Free Energy Solid Model

Introduction

All models in this category use different EoS to account for the fluid and the solid phases. For the fluid phase, classical EoS are used. For the solid phase, the empirical model, recently proposed by Jager and Span [263], based on free energy is used.

Thermodynamic equilibria between phases is established when the pressure, the temperature and the chemical potential of all phases are equal. According to Gibbs phase rule, a two phase pure component system in equilibria has only one degree of freedom and therefore, if the temperature is specified, all remaining properties, including pressure,

are also specified. In a pressure-temperature diagram this fact translates into the well-known VLE curve, the sublimation curve and the solid-liquid melting curve. According to the same rule, for a pure component, three phases will be in equilibria simultaneously only in a single point (no degrees of freedom). This point is the so-called "triple point" named by being the point of three phase coexistence. The triple point location and properties are of great importance to this modeling effort and is used to "anchor" the models as we will explain next.

Every time different thermodynamic models are used to account for different regions of the phase diagram, special consideration must be given to the so-called thermodynamic consistency. Models are thermodynamically consistent if they predict the same value for all thermodynamic properties of overlapping regions (i.e. coexisting curves). In this work, all proposed fluid-solid models are adjusted in a way that all triple point properties are consistent.

Model Description and Parameter Tuning

Thermodynamic Integration

In this formulation, the solid properties are predicted by an empirical equation for the free energy. The chemical potential values needed to calculate fluid-solid coexistence at a given temperature are calculated through thermodynamic integration.

More specifically, the Clausius-Clapeyron equation which provides the means to evaluate the change of the phase equilibrium conditions from one equilibrium point to another is used. The basis behind the Clausius-Clapeyron equation is that at each equilibrium point the Gibbs free energy of each phase in equilibrium is the same and therefore, the differential along the equilibrium phase boundary is zero. Based on this, it can be shown that the derivative of the pressure as a function of temperature along the phase equilibrium curve is given by Eq. (5.6) and it is a function of the enthalpy and volume difference between phases in equilibria.

$$\left.\frac{dP}{dT}\right|_{equl} = \frac{\Delta H}{T\Delta V} \tag{5.6}$$

Free Energy Model

The Gibbs free energy model proposed by Jager and Span [263] is based on Eq. (5.7). The model uses 23 adjustable parameters. Values for these parameters are shown in Table 5–20. In this work, nine of these parameters (g_2-g_{10}, $g_0^a - g_8^a$ and $g_0^\kappa - g_2^\kappa$) are kept to their original values proposed by Jager and Span. The values of these nine parameters have been fitted to experimental data for the solid heat capacity and the thermal equation of state. On the other hand, parameters g_0 and g_1 are retuned for each fluid equation of state used (i.e. SRK, PR,RK). As we will explain next, retuning g_0 and g_1 makes the fluid-solid models thermodynamically consistent.

$$\begin{aligned}\frac{g}{R*\mathrm{T}_0} &= g_0 + g_1\Delta\vartheta + g_2\Delta\vartheta^2 + g_3\left[\ln\left(\frac{\vartheta^2+g_4^2}{1+g_4^2}\right) - \frac{2\vartheta^2}{g_4}\left(\arctan\left(\frac{\vartheta}{g_4}\right) - \arctan\left(\frac{1}{g_4}\right)\right)\right] \\ &+ g_5\left[\ln\left(\frac{\vartheta^2+g_6^2}{1+g_6^2}\right) - \frac{2\vartheta^2}{g_6}\left(\arctan\left(\frac{\vartheta}{g_6}\right) - \arctan\left(\frac{1}{g_6}\right)\right)\right] \\ &+ g_7\Delta\pi\left[e^{f_\alpha(\vartheta)} + K(\vartheta)g_8\right] + g_9K(\vartheta)\left[(\pi+g_{10})^{6/7} - (1+g_{10})^{6/7}\right]\end{aligned} \tag{5.7}$$

where, $\mathrm{T}_0 = 150, \vartheta = \mathrm{T}/\mathrm{T}_0, \Delta\vartheta = \vartheta - 1, \pi = P/101325(Pa), \Delta\pi = \pi - 1,$

$$K(\vartheta) = g_0^k\vartheta^2 + g_1^k\vartheta + g_2^k \text{ , and}$$

$$\begin{aligned}f_\alpha(\vartheta) &= g_0^a\left(\vartheta^2-1\right) + g_1^a\ln\left(\frac{\vartheta^2 - g_2^a\vartheta + g_3^a}{1 - g_2^a + g_3^a}\right) + g_4^a\ln\left(\frac{\vartheta^2 + g_2^a\vartheta + g_3^a}{1 + g_2^a + g_3^a}\right) \\ &+ g_5^a\left[\arctan\left(\frac{\vartheta - g_6^a}{g_7^a}\right) - \arctan\left(\frac{1-g_6^a}{g_7^a}\right)\right] \\ &+ g_8^a\left[\arctan\left(\frac{\vartheta + g_6^a}{g_7^a}\right) - \arctan\left(\frac{1+g_6^a}{g_7^a}\right)\right]\end{aligned} \tag{5.8}$$

Table 5–20. Values of the parameters of Eq. (5.7)

g_0		Adjusted for each EOS. See Table 5–21
g_1		Adjusted for each EOS. See Table 5–21
g_2	-0.0020109135	Ref. [263] (in kJ/mol)
g_3	-0.0027976237	Ref. [263](in kJ/mol)
g_4	0.26427834	Ref. [263]
g_5	0.0038259935	Ref. [263] (in kJ/mol)
g_6	0.00031711996	Ref. [263] (in kJ/mol)
g_7	0.0022087195	Ref. [263]
g_8	-1.1289668	Ref. [263]
g_9	0.0092923982	Ref. [263]
g_{10}	3391.4617	Ref. [263]
g_0^a	0.039993365	Ref. [263]
g_1^a	0.0023945101	Ref. [263]
g_2^a	0.32839467	Ref. [263]
g_3^a	0.057918471	Ref. [263]
g_4^a	0.0023945101	Ref. [263]
g_5^a	-0.0026531689	Ref. [263]
g_6^a	0.16419734	Ref. [263]
g_7^a	0.17594802	Ref. [263]
g_8^a	0.0026531689	Ref. [263]
g_0^k	0.22690751	Ref. [263]
g_1^k	-0.075019750	Ref. [263]
g_2^k	0.26442913	Ref. [263]

Thermodynamic consistency achieved through g_0 and g_1 adjustment

In order to make the solid and fluid models thermodynamically consistent, parameters g_0 and g_1 were adjusted in a way that the Gibbs free energy of all phases (vapor, liquid and solid) is the same at the triple point. This is done by solving the system of Eq. (5.7) and (5.8) with respect to g_0 and g_1. The melting enthalpy at the triple point was set equal to 8.875 kJ/mol as suggested by Jager and Span. Values for the parameters g_0 and g_1 for all solid-fluid models considered in this work are tabulated in Table 5–21.

For all models, the triple temperature was set equal to the experimental value of 216.592 K. The triple pressure was predicted by the models as the "intersection" of the solid-vapor and the vapor-liquid saturation curves.

$$g_{liq}\left(T_{tr},P_{tr}\right)=g_{sol}\left(T_{tr},P_{tr}\right) \tag{5.9}$$

$$s_{sol}\left(T_{tr},P_{tr}\right)=s_{liq}\left(T_{tr},P_{tr}\right)=g_{liq}\left(T_{tr},P_{tr}\right)-\frac{\Delta h^{melt}}{T_{tr}} \tag{5.10}$$

Table 5–21. Values of parameters g_0 and g_1 for the several studied EoS

Fluid Model	Parameter g_0 (kJ/mol)	Parameter g_1 kJ/(K.mol)	Triple Point Predicted by the Fluid-Solid Model	
			T_{tr} (K)	P_{tr} (Pa)
SRK	-0.002960415	0.004191412	216.952	513587.
RK	-0.002075535	0.003282288	216.952	736649.
PR	-0.002924262	0.004082134	216.952	510349.
PRG	-0.002910451	0.004080049	216.952	515269.
S&W	-0.002638575	0.004508873	216.952	517880.

Effect of returning parameter g_0 and g_1 on the solid properties

Parameters g_0 and g_1 were retuned in order to have thermodynamically consistent models. Retuning affects only energy related properties of the solid phase. As shown in Table 5–23 and Table 5–24, only $\frac{\partial g}{\partial T}$ depends on g_0 and g_1. Furthermore, as Table 5–22 shows, the properties affected by $\frac{\partial g}{\partial T}$ are the entropy, the enthalpy, the internal energy and the Helmholtz energy. Consequently, there is no need to check the accuracy of the proposed models as far as solid properties such as cubic expansion coefficient, isothermal compressibility and isochoric heat capacity are concerned. The predictions will remain same with the original predications made by the Jager and Span.

Table 5–22. Relation of thermodynamic Properties to Eq. (5.7) and its partial derivatives

Thermodynamic Property	Relation to g	Thermodynamic Property	Relation to g
Volume	$v = \left.\frac{\partial g}{\partial P}\right\|_T$	Helmholz energy	$f = g - P\left.\frac{\partial g}{\partial P}\right\|_T$
Entropy	$s = -\left.\frac{\partial g}{\partial T}\right\|_P$	heat capacity	$c_p = -\mathrm{T}\left.\frac{\partial^2 g}{\partial T^2}\right\|_P$
Enthalpy	$h = g - T\left.\frac{\partial g}{\partial T}\right\|_P$	Cubic expansion coefficient	$\alpha = \left(\frac{\partial^2 g}{\partial T \partial P}\right) \Big/ \left.\frac{\partial g}{\partial P}\right\|_T$
Internal energy	$u = g - T\left.\frac{\partial g}{\partial T}\right\|_P - P\left.\frac{\partial g}{\partial P}\right\|_T$	Isothermal compressibility	$\kappa = -\left(\frac{\partial^2 g}{\partial P^2}\right) \Big/ \left.\frac{\partial g}{\partial P}\right\|_T$

Table 5–23. Partial derivatives of Eq. (5.7) with respect to temperature and pressure

Gibbs partial derivative	Equation
$\left.\frac{\partial g}{\partial T}\right\|_P$	$R\left\{\begin{array}{l} g_1 + g_2\vartheta - \frac{2g_3}{g_4}\left[\left(\arctan\left(\frac{\vartheta}{g_4}\right) - \arctan\left(\frac{1}{g_4}\right)\right)\right] \\ -\frac{2g_5}{g_6}\left[\left(\arctan\left(\frac{\vartheta}{g_6}\right) - \arctan\left(\frac{1}{g_6}\right)\right)\right] \\ +g_7\Delta\pi\left[e^{f_\alpha(\vartheta)}\frac{\partial f_\alpha(\vartheta)}{\partial\vartheta} + \frac{\partial K(\vartheta)}{\partial\vartheta}g_8\right] + g_9\frac{\partial K(\vartheta)}{\partial\vartheta}\left[(\pi + g_{10})^{\frac{6}{7}} - (1 + g_{10})^{\frac{6}{7}}\right] \end{array}\right\}$
$\left.\frac{\partial g}{\partial P}\right\|_T$	$\frac{RT_0}{P_0}\left\{+g_7\left[e^{f_\alpha(\vartheta)} + K(\vartheta)g_8\right] + g_9K(\vartheta)\frac{6}{7}(\pi + g_{10})^{\frac{-1}{7}}\right\}$
$\frac{\partial^2 g}{\partial T \partial P}$	$\frac{R}{P_0}\left\{+g_7\left[e^{f_\alpha(\vartheta)}\frac{\partial f_\alpha(\vartheta)}{\partial\vartheta} + \frac{\partial K(\vartheta)}{\partial\vartheta}g_8\right] + g_9\frac{\partial K(\vartheta)}{\partial\vartheta}\frac{6}{7}(\pi + g_{10})^{\frac{-1}{7}}\right\}$
$\left.\frac{\partial^2 g}{\partial T^2}\right\|_P$	$R\left\{\begin{array}{l} 2g_2 - \frac{2g_3}{\vartheta^2 + g_4{}^2} - \frac{2g_5}{\vartheta^2 + g_6{}^2} + \\ g_7\Delta\pi\left[e^{f_\alpha(\vartheta)}\frac{\partial^2 f_\alpha(\vartheta)}{\partial\vartheta^2}e^{f_\alpha(\vartheta)}\left(\frac{\partial f_\alpha(\vartheta)}{\partial\vartheta}\right)^2 + \frac{\partial^2 K(\vartheta)}{\partial\vartheta^2}g_8\right] \\ +g_9\frac{\partial^2 K(\vartheta)}{\partial\vartheta^2}\left[(\pi + g_{10})^{\frac{6}{7}} - (1 + g_{10})^{\frac{6}{7}}\right] \end{array}\right\}$
$\left.\frac{\partial^2 g}{\partial P^2}\right\|_T$	$\frac{RT_0}{P_0{}^2}\left\{g_9K(\vartheta)\frac{-6}{7}(\pi + g_{10})^{\frac{-8}{7}}\right\}$

Table 5–24. Partial derivatives of K and fα with respect to temperature and pressure

Derivative of K and f_α	Equation
$\frac{\partial K(\vartheta)}{\partial \vartheta}$	$2g_0^\kappa \vartheta + g_1^\kappa$
$\frac{\partial^2 K(\vartheta)}{\partial \vartheta^2}$	$2g_0^\kappa$
$\frac{\partial f_a(\vartheta)}{\partial \vartheta}$	$2g_0^a\vartheta + g_1^a\left(\frac{2\vartheta - g_2^a}{\vartheta^2 - g_2^a\vartheta + g_3^a}\right) + g_4^a\left(\frac{2\vartheta + g_2^a}{\vartheta^2 + g_2^a\vartheta + g_3^a}\right) + \frac{g_5^a}{g_7^a}\left[\frac{1}{1+\left(\frac{\vartheta - g_6^a}{g_7^a}\right)^2}\right] + \frac{g_8^a}{g_7^a}\left[\frac{1}{1+\left(\frac{\vartheta + g_6^a}{g_7^a}\right)^2}\right]$
$\frac{\partial^2 f_a(\vartheta)}{\partial \vartheta^2}$	$2g_0^a + g_1^a\left(\frac{2\left(\vartheta^2 - g_2^a\vartheta + g_3^a\right) - \left(2\vartheta - g_2^a\right)^2}{\left(\vartheta^2 - g_2^a\vartheta + g_3^a\right)^2}\right) + g_4^a\left(\frac{2\left(\vartheta^2 + g_2^a\vartheta + g_3^a\right) - \left(2\vartheta + g_2^a\right)^2}{\left(\vartheta^2 + g_2^a\vartheta + g_3^a\right)^2}\right) - \frac{g_5^a}{\left(g_7^a\right)^2} 2\frac{\vartheta - g_6^a}{g_7^a}\left[\frac{1}{1+\left(\frac{\vartheta - g_6^a}{g_7^a}\right)^2}\right]^2 - \frac{g_8^a}{\left(g_7^a\right)^2} 2\frac{\vartheta + g_6^a}{g_7^a}\left[\frac{1}{1+\left(\frac{\vartheta + g_6^a}{g_7^a}\right)^2}\right]^2$

Model Validation and Results

The SAFT/PC-SAFT Model

Table 5–25 presents the % AAD for SAFT and PC-SAFT sublimation pressure. It is obvious that PC-SAFT provides a better fit to experimental data. Further analysis of this was provided in the section of the parameter tuning.

Table 5–25. Errors in % AAD for SAFT and PC-SAFT SVE vapor pressure prediction

	SAFT	PC-SAFT
Temperature range [K]	160-215	160-215
% AAD in vapor pressure	5.04	3.47

The Free Energy Based Models

Figure 5–24 compares sublimation pressure predictions using a variety of "mixed" models. The "mixed" models use typical cubic EoS to account for the vapor phase and the Jager and Span free energy model to account for the solid [263]. Table 5–26 presents the % AAD error for the prediction of various physical properties at sublimation. The first column shows sublimation pressure % AAD from the available experimental points (21 points at the temperature range 194-216 K). The remaining columns show the % AAD of various quantities with respect to a "reference model". The reference model uses the GERG EoS (S&W) for the vapor phase and the free energy model of Jager and Span [263] for the solid. The % AAD has been calculated at 220 temperatures between 160 K and the triple point.

The results tabulated in Table 5–26 indicate that, with the exception of SRK, the fluid-solid model consisting of a cubic EoS for the vapor phase and the free energy model for the solid is not very sensitive to the cubic EoS selected assuming that parameters g_0 and g_1 have been retuned.

Table 5–26. Average absolute deviation of different properties at sublimation. Values calculated between 160 K and triple point temperature

EoS model used for vapor phase	Sublimation Pressure from Experimental Data %AAD	Sublimation Pressure %AAD	Vapor Density from S&W equation %AAD	Sublimation Enthalpy %AAD
S&W	0.12	0.0	0.0	0.0
RK	50.67	53.	54.	8.9
SRK	0.54	0.55	1.11	0.31
PR	0.83	0.70	1.10	0.41
PRG	0.55	0.46	0.51	0.50
SAFT	5.78		0.71	4.2
PC-SAFT	3.89		0.52	0.34

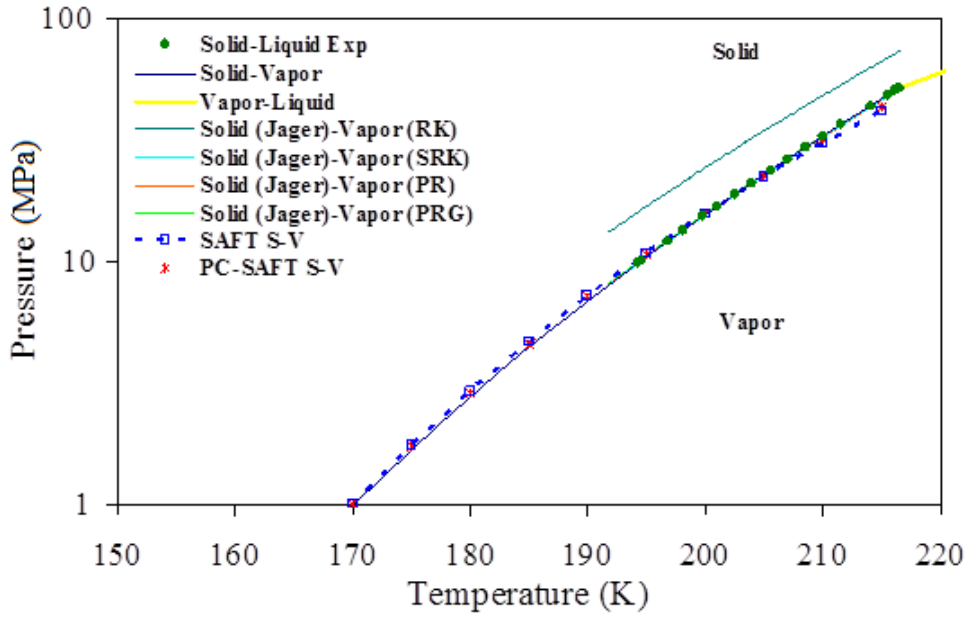

Figure 5–24. Comparison between model predictions and NIST data for the sublimation pressure of pure CO_2. Models are based on different cubic EoS and the free energy of solid CO_2 of Jager and Span.

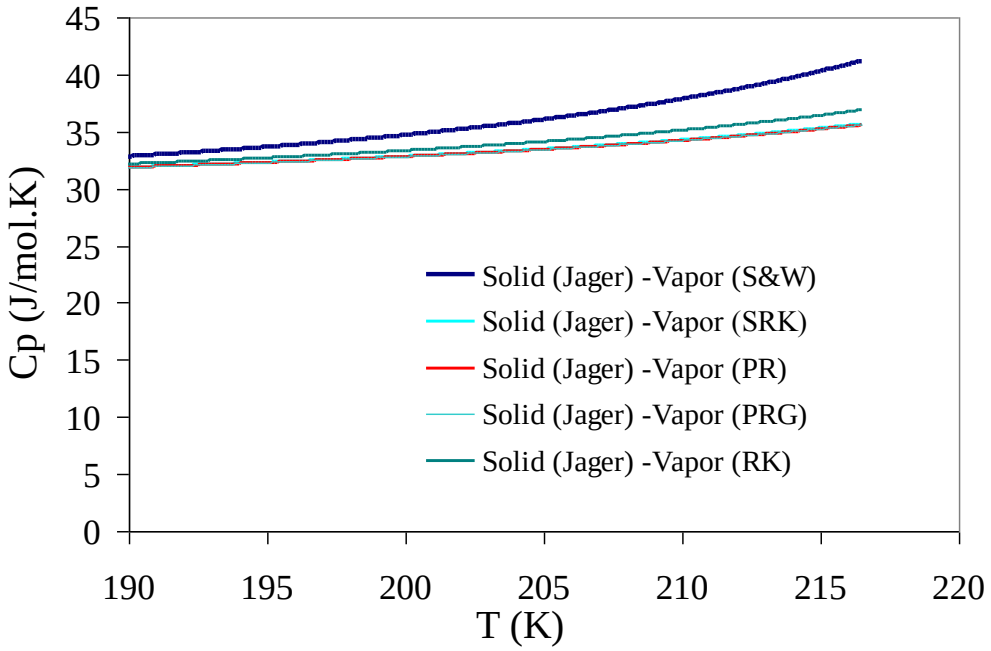

Figure 5–25. Heat capacity of the vapor phase in equilibrium with the solid CO_2.

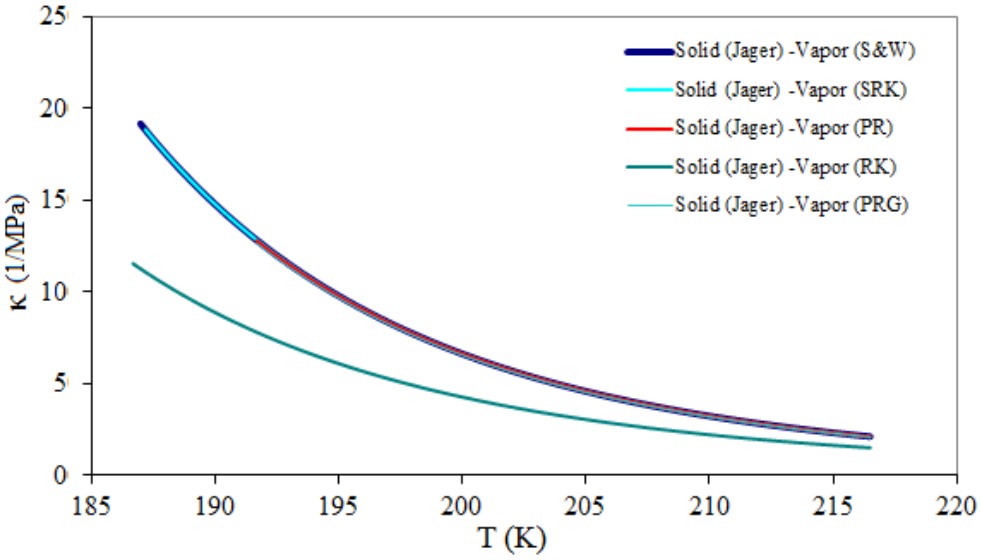

Figure 5–26. Pure CO_2 compressibility of the vapor phase at sublimation

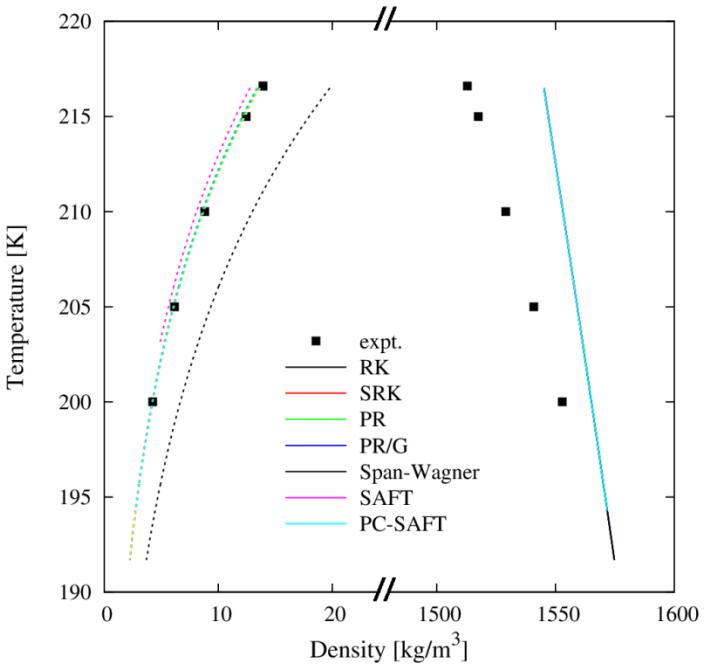

Figure 5–27. Density of the pure CO_2 vapor and solid phases at sublimation. Experimental data from [264].

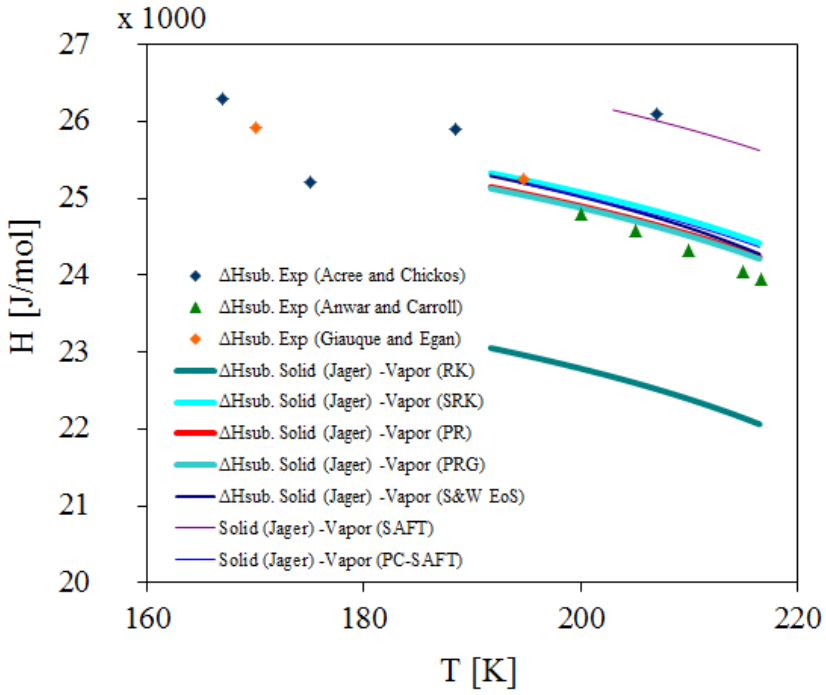

Figure 5–28. Pure CO_2 Enthalpy of sublimation at different temperatures. Experimental data from [264-266]

Figure 5–25 compares how different models predict the heat capacity of vapor phase at sublimation. Some deviations from the GERG model appear at elevated temperatures. Figure 5–26 shows predictions of vapor phase compressibility at sublimation. All equations with the exception of RK behave similarly. The same behavior is seen for the vapor density in Figure 5–27, and for the enthalpy of sublimation in Figure 5–28.

The average error for each model has been calculated and tabulated in Table 5–26. GERG has the lowest error (0.12%). The other models, with the exception of RK, exhibit an error less than 1%. Among those, SRK behaves best.

The most accurate model appears to be the "mixed" model which uses the Free Energy EoS of Jager and Span for the solid phase and the GERG EoS for the vapor. However, comparable results have been obtained with classical cubic EoS for the vapor phase with the exception of RK. This finding is of great importance when the SVE model is embedded in CFD and other outflow simulation environments. When

embedding an EoS, the computational overhead becomes important because EoS calculations are repeatedly requested. As a result, equations such as GERG which are very accurate but mathematically complex, require significant CPU power and cannot be easily embedded. Replacing GERG equation with a cubic one without significant loss of accuracy is a logical alternative.

6. Transport Properties

6.1. Viscosity

6.1.a. Validation

Transport properties, and especially viscosity, are very important for the process design of CCS. As shown in theory section 3.6.b, Friction Theory (FT) is a very powerful and versatile tool to model viscosity based on any EoS.

In order to validate the PC-SAFT based FT viscosity model, model predictions are compared to the published data reported by Tan et al. [177, 267] for the pure n-dodecane and the binary mixture of n-heptane – n-eicosane. The PC-SAFT parameters for these substances are taken from Gross and Sadowski [50] and are presented in Table 6–1. The five FT parameters for each component are taken from Tan et al and are shown in Table 6–2.

Table 6–1. Parameters for PC-SAFT from Gross and Sadowski [50]

	MW $[g/mol]$	m	σ $[A]$	ε/k $[K]$	P^{sat}	ρ^{liq}	T $[K]$
n-heptane	100.203	3.4831	3.8049	238.40	0.34	2.10	182-623
n-dodecane	170.338	5.3060	3.8959	249.21	2.10	0.93	263-658
n-eicosane	282.553	7.9849	3.9869	257.75	7.35	1.13	309-775

Table 6–2. Parameters for PC-SAFT with FT from Tan et al. [267]

	a_1 [μP/bar]	a_2 [μP/bar]	b_1 [μP/bar]	b_2 [μP/bar]	c_2 [μP/bar^2]
n-heptane	-0.87307	-0.57616	-1.04953	-0.16112	$1.9588 \cdot 10^{-4}$
n-dodecane	-2.45459	-1.32203	-2.49950	-0.52644	$3.6395 \cdot 10^{-4}$
n-eicosane	-3.17433	-2.95400	-3.00067	-1.65457	$5.9762 \cdot 10^{-4}$

The errors in % AAD are 10.98 % at P = 10 MPa and 7.96 % at T = 360 K. Notice that the temperature effect is stronger than the pressure effect. Also, as Figure 6–1

shows, the error increases as temperature increases but does not change significantly with pressure.

For pure n-dodecane one isotherm and one isobar were chosen. The results are compared against reference data from NIST [186]; very good agreement is obtained as indicated in Figure 6–1.

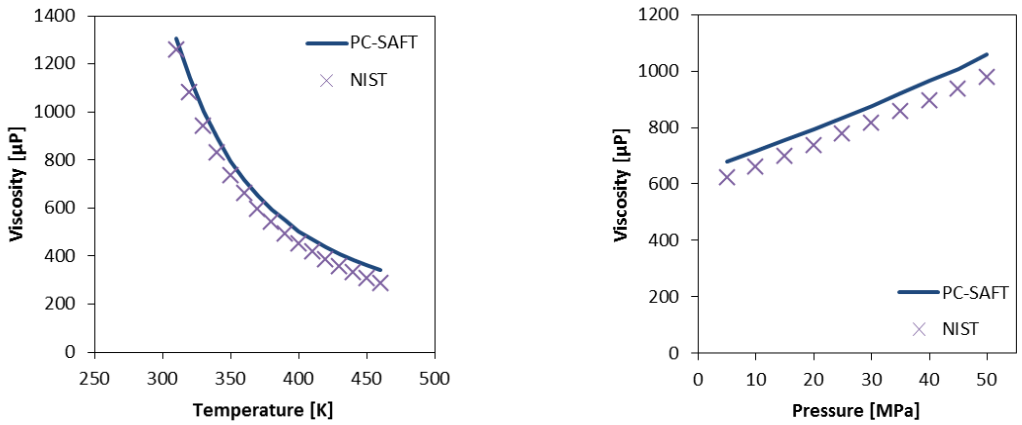

(a) (b)

Figure 6–1. Viscosity of n-dodecane along the isobar of 10 MPa (a) and along the isotherm of 360 K (b).

Figure 6–2 shows the contribution of each term of FT to the total viscosity for the case of n-dodecane.

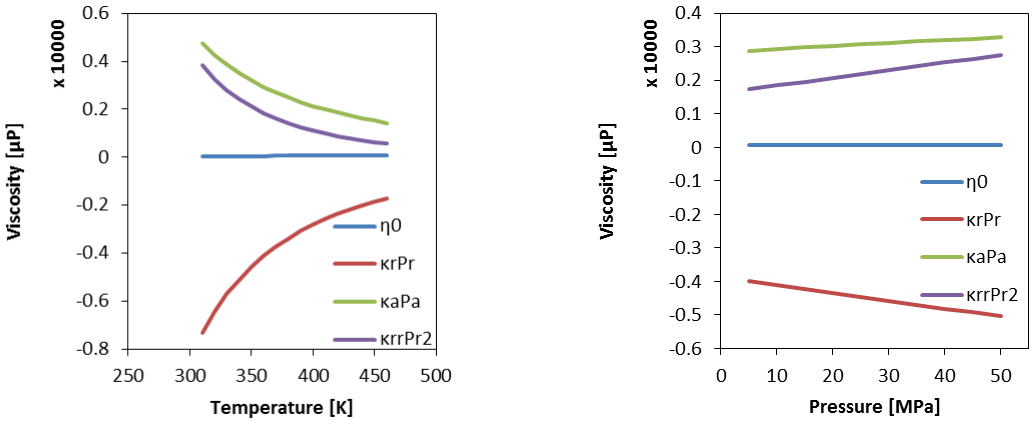

(a) (b)

Figure 6–2. Contribution of FT terms to the total viscosity of n-dodecane along the isobar of 10 MPa (a), and along the isotherm of 360 K (b).

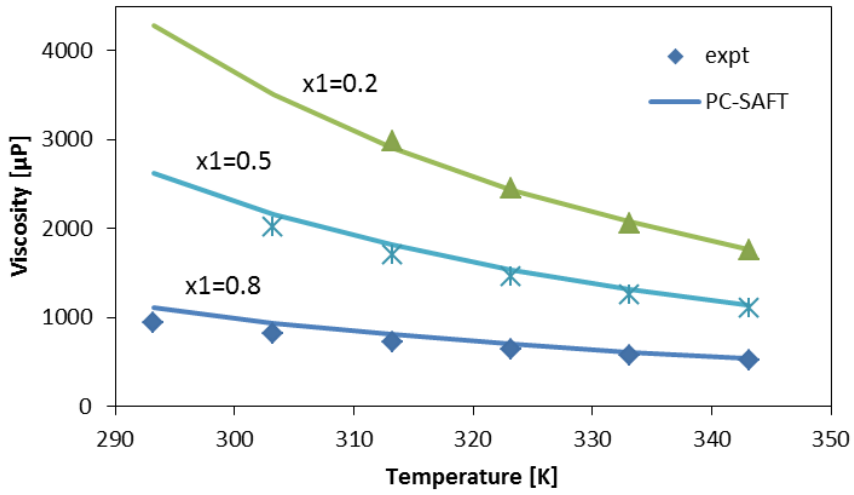

Figure 6–3. Viscosity isopleths (0.2, 0.5, and 0.8 mole fraction of nC_7) for the binary mixture nC_7 (1) - nC_{20} (2).

The accuracy of the model for mixtures was considered via modeling of the binary n-heptane – n-eicosane (nC_7 – nC_{20}) mixture. Experimental data from Queimada et al. [268] were used to access model accuracy. Figure 6–3 presents the three isopleths selected. The agreement with the experimental data is excellent, with AAD being less than 11%.

Validation of the cubic EoS based FT viscosity models was done by comparing model predictions to data reported by Quiñones-Cisneros et al. [96] for the mixture of methane – propane (see Figure 6–4). The validation used the SRK EoS with critical parameters obtained from the literature. Component specific friction theory parameters were taken from Quiñones-Cisneros et al. The parameter values are presented in Table 5–2 and Table 6–3.

Table 6–3. Parameters for SRK with FT from Quiñones-Cisneros et al. [96]

	a_1 [µP/bar]	a_2 [µP/bar]	b_1 [µP/bar]	b_2 [µP/bar]	c_2 [µP/bar^2]
methane	0.0954878	-0.0983074	-0.4247340	0.0598492	$1.34730 \cdot 10^{-5}$
propane	0.0404072	-0.2491910	-0.7454420	0.0144118	$1.53201 \cdot 10^{-5}$

Figure 6–4 indicates excellent agreement between model predictions and experimental data for a wide range of pressures.

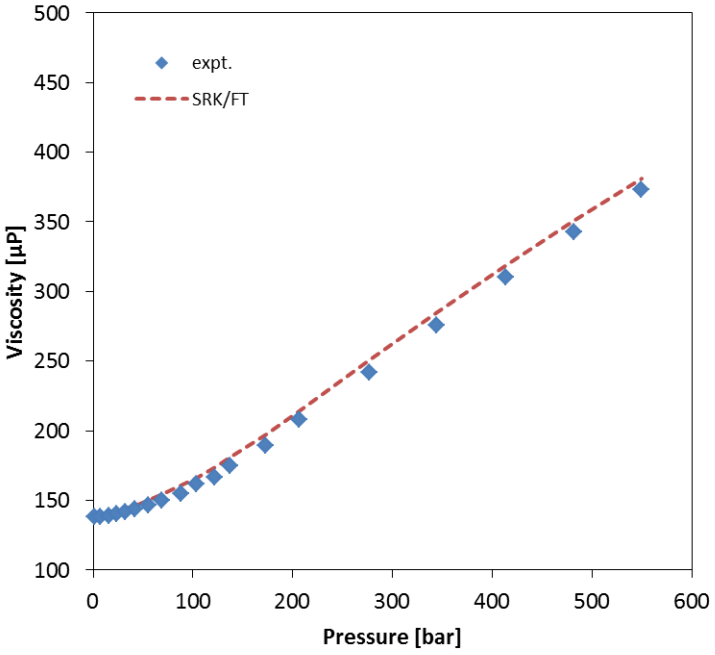

Figure 6–4. The viscosity of methane-propane (79.10 mole % methane) mixture at the isotherm 410.93 K.

6.1.b. Friction Theory Pure Component Parameters for PC-SAFT and tPC-PSAFT Based Viscosity Models

Today, there are no literature reported parameters of FT for the components of interest to this work, using PC-SAFT or tPC-PSAFT EoS. In order to obtain values for these parameters, the following procedure was followed:

PC-SAFT and tPC-PSAFT were used to calculate the values of the repulsive and attractive pressure contributions. The parameters used for this calculation are shown in

- Table 4–2 and Table 5–6 and are the same with the one reported in previous studies [142, 218].

- The pressure values calculated were used by the FT model in order to calculate the viscosity of the liquid phase. The critical properties of the components were taken from the literature [66] (see Table 5–2).

- PSO was used to fit the values of the five FT parameters on viscosity data from NIST.

Table 6–4 and Table 6–5 contain the regressed parameters for all the components for PC-SAFT and tPC-PSAFT based models, respectively. Table 6–6 and Table 6–7 contain the pressure and temperature ranges of data used for the regression, the error with respect to NIST data and the computation time needed for PC-SAFT and tPC-PSAFT regression. It should be noted that H_2O and H_2S are the only molecules from the list that have non-zero dipole moment and κ association parameter for the F_c factor, according to Reid et al. [66] Thus, they were modeled with and without account for polarity in the empirical factor, so as to investigate the effect of it. Also, since tPC-PSAFT reduces to PC-SAFT for non-polar molecules, only CO_2 (quadrupolar) and H_2O (dipolar) were modeled with tPC-PSAFT.

Table 6–4. Regressed FT parameters for use with PC-SAFT

Component	a_1 [μP/bar]	a_2 [μP/bar]	b_1 [μP/bar]	b_2 [μP/bar]	c_2 [μP/bar^2]
CH_4	-0.6766404	0.6033063	-0.7285307	0.7739417	$2.6487315 \cdot 10^{-5}$
H_2O	1.2545321	2.6095736	0.7773817	1.7814870	$-5.5614118 \cdot 10^{-6}$
N_2	-4.0448559	-3.2140339	-3.1808353	-1.2950454	$1.8456631 \cdot 10^{-4}$
O_2	-3.9732470	-2.5014399	-3.1873003	-0.7553231	$1.1865940 \cdot 10^{-4}$
H_2S	-0.2738228	-0.0482358	-0.4218731	0.1720901	$6.4853264 \cdot 10^{-6}$
CO_2	-2.3462441	-2.1648157	-2.0007769	-1.1615755	$2.3103741 \cdot 10^{-5}$

Table 6–5. Regressed FT parameters for use with tPC-PSAFT

Component	a_1 [μP/bar]	a_2 [μP/bar]	b_1 [μP/bar]	b_2 [μP/bar]	c_2 [μP/bar^2]
H_2O	-1.5058787	-1.7914577	-1.1704285	-1.1514768	$3.7225960 \cdot 10^{-6}$
CO_2	-1.4707083	-2.2150631	-1.2277122	-1.2431046	$2.5466213 \cdot 10^{-5}$

Table 6–6. Conditions ranges and accuracy of PC-SAFT-based viscosity model

Component	points for regression (liquid)	T [K]	P [MPa]	viscosity % AAD compared to NIST data		CPU* time for regression [s] (PSO)
				liquid	vapor	
CH_4	6	180-186	4-12	$1.40 \cdot 10^{-3}$	3.22	6.88
H_2O	168	275-640	2-20	4.75	21.17	12.82
N_2	18	80-120	2-12	0.63	2.81	7.21
O_2	25	80-150	2-12	0.77	2.56	8.05
H_2S	87	190-370	2-20	1.28	5.87	10.70
CO_2	45	220-300	2-20	0.43	4.14	8.60

* All calculations were performed using an Intel® Core™ i7 CPU M620 @ 2.67 GHz

By looking at Table 6–6, it can be seen that the errors for liquid viscosity, which is the property that the parameters are fitted to, exhibits very reasonable values; less than 3% AAD. It is interesting to note also the very low error that CH_4 exhibits. This is most probably due to the fact that the temperature range that CH_4 is liquid is very small.

Supercritical phase was not included in the regression of the parameters; nevertheless it can be accurately reproduced by the model.

For the vapor phase, the errors are higher and close to the inherit error of the underlying Chung's equation for viscosity. The EoS model introduced in this work has small effect on the final result at the low pressure limit.

Table 6–6 and Table 6–7 show that PC-SAFT and tPC-PSAFT behave similarly for CO_2 and H_2O, with tPC-PSAFT giving a little higher error for the liquid phase, but predicting the vapor phase more accurately.

For the polar molecules, when PC-SAFT is used, the error depends highly on whether the polar or the non-polar expression of the empirical factor F_c is implemented. Also, results from tPC-PSAFT seem to be rather indifferent of the empirical factor model used. This can lead to the conclusion that, if the polar interactions are accounted for explicitly in the EoS, and thus in the dense state correction of the friction theory, there is no need to account for them again in the dilute gas limit.

Table 6–7. Conditions ranges and accuracy for tPC-PSAFT case

Component	points for regression (liquid)	T [K]	P [MPa]	viscosity % AAD compared to NIST data		CPU time for regression [s] (PSO)
				Liquid	vapor	
H_2O	168	275-640	2-20	5.29	11.38	18.41
CO_2	45	220-300	2-20	0.62	1.50	12.26

In Figure 6–5, it can be seen that the model can predict the viscosity of the supercritical phase without inclusion of supercritical data in the regression process.

Water, for the conditions range considered in this work is either in the liquid or in the vapor phase, but is not supercritical. In Figure 6–6, the phase change can be detected by locating the discontinuity between the predictions for the liquid and the vapor viscosity.

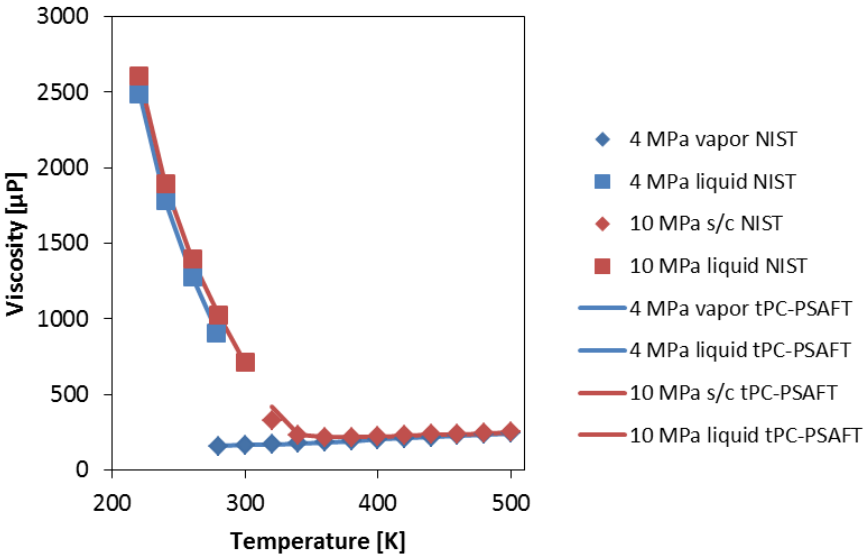

Figure 6–5. Viscosity of pure CO_2 for the isobars of 4 MPa (subcritical) and 10 MPa (supercritical).

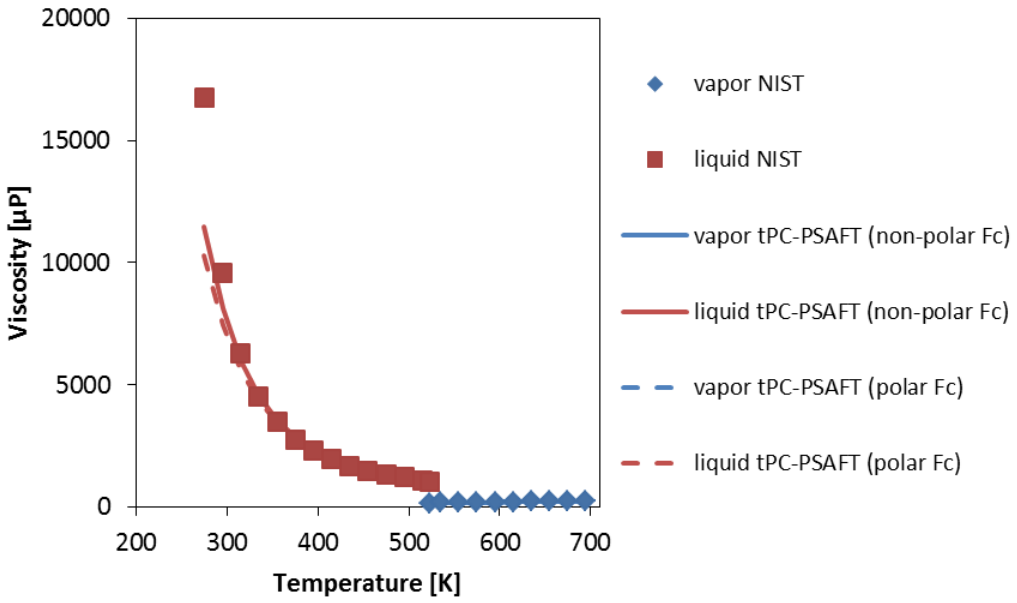

Figure 6–6. Viscosity of pure H_2O for the isobars of 4 MPa (subcritical) with and without account for polarity in the empirical factor.

6.1.c. Friction Theory Pure Component Parameters for the Cubic EoS Based Viscosity Models

Following the procedure described above with cubic Eos (including the Yokozeki EoS [269]) instead of PC-SAFT and tPC-SAFT, FT model parameters were estimated by regressing experimental viscosity data for pure CO_2. Table 6–8 to Table 6–13 show the parameter values and the error compared to the NIST data for different EoS.

Table 6–8. Regressed FT parameters for Pure CO_2

Model	a_1 [µP/bar]	a_2 [µP/bar]	b_1 [µP/bar]	b_2 [µP/bar]	c_2 [µP/bar^2]	% AAD
RK	0.5259166	0.7877899	-0.3734228	0.2482251	-0.0000148	0.51
SRK	1.1264383	0.6296456	0.3112664	-0.0432586	-0.0000223	0.29
PR	1.4846943	0.8079415	0.7647865	-0.0110141	-0.0000277	0.36
PR/G	1.4781077	0.8332508	0.7535354	0.0088935	-0.0000281	0.35
Yokozeki	0.2712355	0.9787733	-0.6542732	0.8064210	-0.0000059	0.52
PC-SAFT	-2.3462441	-2.1648157	-2.0007769	-1.1615755	$2.3103741 \cdot 10^{-5}$	0.43
tPC-PSAFT	-1.4707083	-2.2150631	-1.2277122	-1.2431046	$2.5466213 \cdot 10^{-5}$	0.62

Table 6–9. Regressed FT parameters for Pure CH_4

Model	a_1 [μP/bar]	a_2 [μP/bar]	b_1 [μP/bar]	b_2 [μP/bar]	c_2 [μP/bar^2]	% AAD
RK	1.283537619	0.927985	0.858294937	-0.865678338	$-5.65374\cdot10^{-5}$	$8.67\cdot10^{-3}$
SRK	1.461625401	-0.138352	0.772174838	0.264245342	$-5.93232\cdot10^{-5}$	$8.64\cdot10^{-3}$
PR	1.183733278	1.067459	0.597084008	1.249648652	$-4.41826\cdot10^{-5}$	$9.59\cdot10^{-3}$
PR/G	1.286883915	0.04742	0.500316153	1.939819575	$-4.34523\cdot10^{-5}$	$9.64\cdot10^{-3}$
PC-SAFT tPC-PSAFT	-0.6766404	0.6033063	-0.7285307	0.7739417	$2.6487315\cdot10^{-5}$	$1.40\cdot10^{-3}$

Table 6–10. Regressed FT parameters for Pure O_2

Model	a_1 [μP/bar]	a_2 [μP/bar]	b_1 [μP/bar]	b_2 [μP/bar]	c_2 [μP/bar^2]	% AAD
RK	-0.13525908	-1.240408	-1.000995	-0.499172273	$5.06998\cdot10^{-5}$	2.07
SRK	-0.51855375	-1.751909	-1.336023546	-0.798349358	$7.68797\cdot10^{-5}$	2.28
PR	-0.48311911	-1.745845	-1.186958813	-0.821956671	$6.23334\cdot10^{-5}$	2.41
PR/G	-0.13525908	-1.240408	-1.000995	-0.499172273	$5.06998\cdot10^{-5}$	2.07
PC-SAFT tPC-PSAFT	-3.9732470	-2.5014399	-3.1873003	-0.7553231	$1.1865940\cdot10^{-4}$	0.77

Table 6–11. Regressed FT parameters for Pure N_2

Model	a_1 [μP/bar]	a_2 [μP/bar]	b_1 [μP/bar]	b_2 [μP/bar]	c_2 [μP/bar^2]	% AAD
RK	-0.34362333	-0.660244	-1.27074595	-0.093068401	$7.32792\cdot10^{-5}$	0.68
SRK	-0.84841972	-1.405973	-1.711523609	-0.535851595	0.000123635	0.97
PR	-0.97421735	-1.609931	-1.707982283	-0.650107207	0.000111265	1.20
PR/G	-0.91729329	-1.631011	-1.650942967	-0.686784342	0.000109405	1.21
PC-SAFT tPC-PSAFT	-4.0448559	-3.2140339	-3.1808353	-1.2950454	$1.8456631\cdot10^{-4}$	0.63

Table 6–12. Regressed FT parameters for Pure H_2S

Model	a_1 [μP/bar]	a_2 [μP/bar]	b_1 [μP/bar]	b_2 [μP/bar]	c_2 [μP/bar^2]	% AAD
RK	0.787127344	0.937657	0.071452369	0.617737778	$-1.65707\cdot10^{-5}$	3.35
SRK	1.012504615	1.042997	0.311824826	0.609954493	$-2.12331\cdot10^{-5}$	3.18
PR	0.849472481	0.711237	0.258708261	0.452054854	$-1.10714\cdot10^{-5}$	2.65
PR/G	0.837773717	0.704878	0.246742899	0.451667869	$-1.08532\cdot10^{-5}$	2.66
PC-SAFT tPC-PSAFT	-0.2738228	-0.0482358	-0.4218731	0.1720901	$6.4853264\cdot10^{-6}$	1.28

Table 6–13. Regressed FT parameters for Pure H_2O

Model	a_1 [μP/bar]	a_2 [μP/bar]	b_1 [μP/bar]	b_2 [μP/bar]	c_2 [μP/bar^2]	% AAD
RK	0.754153106	-1.44545	0.600600492	-1.114158543	$6.81189\cdot10^{-6}$	9.90
SRK	0.562489036	-1.355196	0.421316541	-0.985377222	$5.76979\cdot10^{-6}$	6.17
PR	0.640987902	-1.309765	0.518511837	-0.985871723	$4.16267\cdot10^{-6}$	6.16
PR/G	0.655845345	-1.270455	0.531077943	-0.96506742	$3.91747\cdot10^{-6}$	6.09
PC-SAFT	1.2545321	2.6095736	0.7773817	1.7814870	$-5.5614118\cdot10^{-6}$	4.75
tPC-PSAFT	-1.5058787	-1.7914577	-1.1704285	-1.1514768	$3.7225960\cdot10^{-6}$	5.29

6.1.d. Comparison for Pure CO_2

In this part, two different approaches of modeling the viscosity of pure CO_2, using PR and PC-SAFT EoS, are compared. Calculations were carried out with Vesovic et al. [93] model and Friction Theory (FT) [96]. In Figure 6–7 the viscosity of CO_2 along two isobars, one subcritical and one supercritical, is presented.

The two models in combination with PC-SAFT are in very good agreement with the experimental data from NIST. Vesovic et al. model produces accurate predictions of viscosity with both PR and PC-SAFT. PR with FT shows increasing inaccuracy with increasing pressure, especially at the supercritical regime, leading to the conclusion that PR cannot predict the viscosity as accurately as PC-SAFT, with the same set of fitting data.

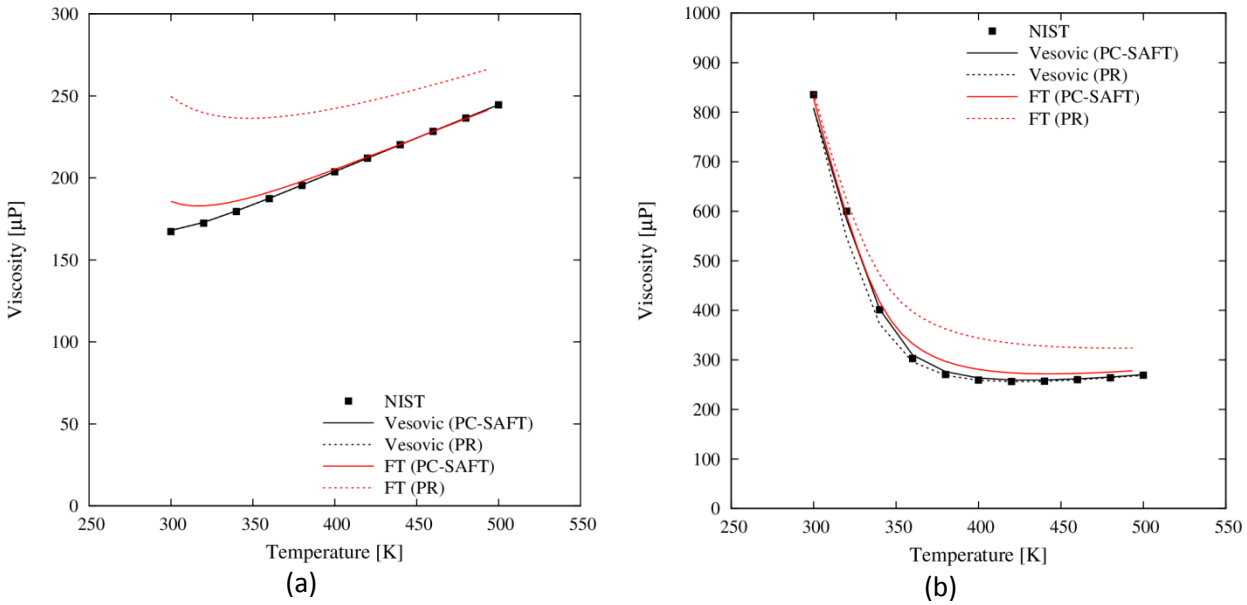

Figure 6–7. Viscosity of pure CO_2. Experimental data (NIST database) and predictions from PR and PC-SAFT EoS, using Vesovic's model and Friction Theory at (a) 5 MPa and (b) 15 MPa.

6.1.e. Extension to CO_2 Mixtures

Experimental data of viscosity for CO_2 mixtures with components of interest to CCS are scarce in the literature. Experimental data at high pressures are found only for selected systems [270] and the majority of the data found are measured at atmospheric pressure.

This limitation makes model validation at high pressures very difficult. FT consists of a dilute gas limit term (low pressure) and a dense state correction term (elevated pressure effect). At low pressures, the contribution of the second term is not significant and it cannot easily be assessed using only low pressure data.

Despite those limitations, model development was successful and predictions for binary and ternary mixtures of CO_2 are shown in the following figures.

$CO_2 - CH_4$

Various cubic EoS, PC-SAFT and its polar version tPC-PSAFT were applied to the binary mixture of CO_2 – CH_4 at the temperatures of 293.15 K and 303.15 K. Pressures between of ~0 – 2.5 MPa were considered. The repulsive and attractive terms of the pressure were used in FT as described previously. In Figure 6–8, experimental data [271] and calculations from the various EoS are shown.

Figure 6–8 provides some remarkable results: All cubic EoS predict a much steeper change in viscosity with pressure compared to experimental data, while the non-cubic EoS predict the correct pressure effect but they are systematically lower than the experimental values.

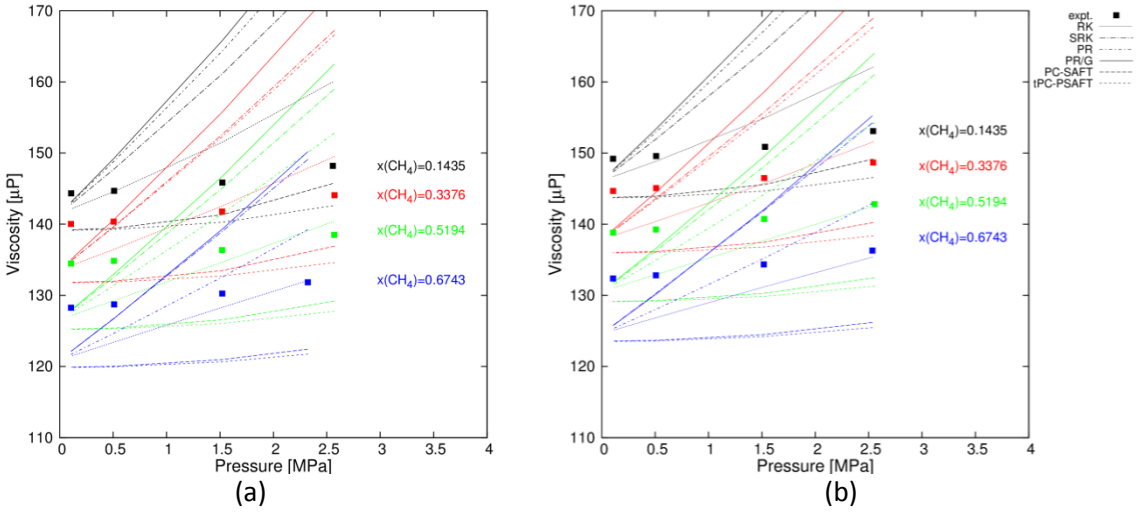

Figure 6–8. Viscosity of the CO_2 – CH_4 mixture at 293.15 K (a) and 303.15 K (b). Experimental data from [271].

$CO_2 - O_2$

Another important binary mixture of interest to CCS is the CO_2 – O_2. In this case, experimental viscosity data are only available at 1 atm.

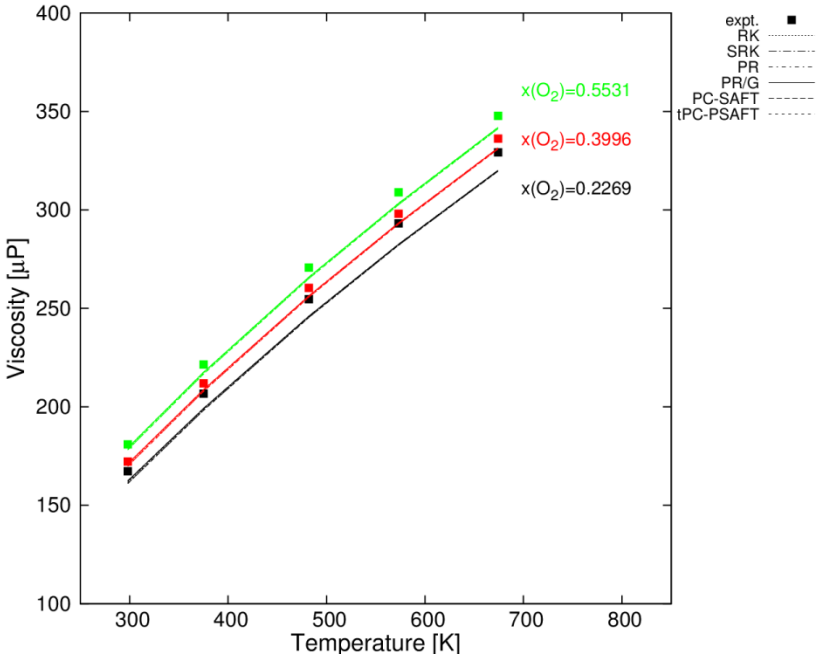

Figure 6–9. Viscosity of the $CO_2 - O_2$ mixture at 1 atm. Experimental data from [106].

The EoS effect is minimal and the dilute gas limit dominates the property value. All EoS predict very similar results at all compositions (see Figure 6–9).

$CO_2 - N_2$

The binary $CO_2 - N_2$ mixture is significant for this study, since mixtures of this type can be seen both inside and outside the pipeline during rupture. This system was studied using all EoS following the same approach with the previous systems. Here however, a modified mixing rule was introduced in order to address the problem of the systematic error described earlier.

Figure 6–10 illustrates the effect of EOS selection on FT viscosity model prediction. PC-SAFT and tPC-PSAFT are in excellent qualitative agreement with the experimental data and they capture the trend very well. Moreover, their quantitative performance is quite good, giving errors less than 1.5 % AAD. Note that, the cubic EoS fail to represent again the effect of pressure on viscosity.

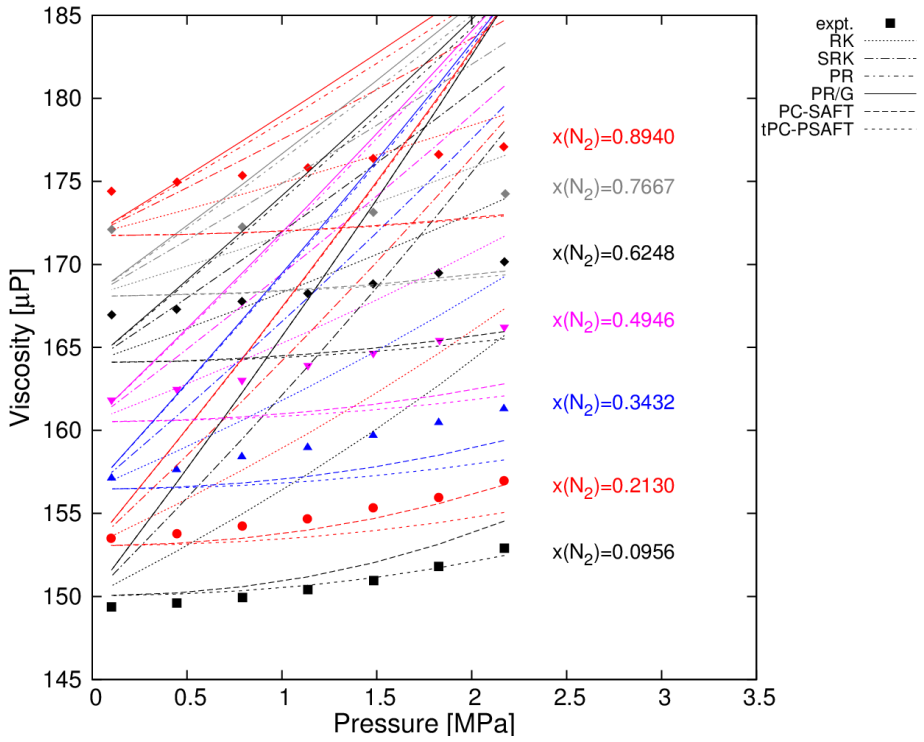

Figure 6–10. Viscosity of the CO_2 – N_2 mixture at 293.15 K . Experimental data from [101].

In order to improve model performance, a new mixing rule that carries an additional fitted binary parameter was considered. This parameter can be fitted to experimental viscosity data for binary systems, and enhances the accuracy of the method. The mixing rule used can be seen in the following equation:

$$\eta_{0,mix} = \sum_{i=1}^{nc}\sum_{j=1}^{nc} x_i x_j (1 - g_{ij}) ln\left(\sqrt{\eta_{0,i}\eta_{0,j}}\right) \tag{6.1}$$

This new mixing rule was applied to PC-SAFT only. Initially, with the original mixing rule, the AAD (over all the compositions and pressures studied) was 1.30 %. After fitting of the "g_{ij}" to the value of -0.0061, the AAD decreased to 0.68 %. Looking at the data in Figure 6–11, the agreement with the experimental data [102] improves dramatically.

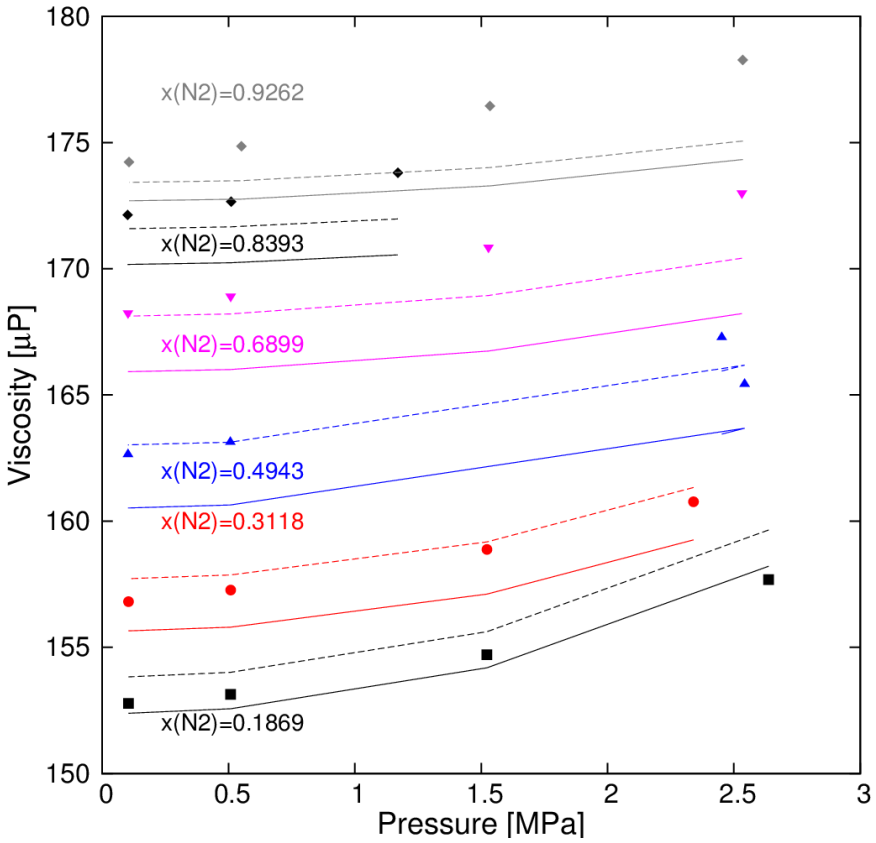

Figure 6–11. Viscosity of the CO_2 – N_2 mixture at 293.15 K . Effect of the newly introduced binary interaction parameter on the FT side, with the use of PC-SAFT. Dashed line: PC-SAFT with binary interaction parameter, solid line: PC-SAFT without binary interaction parameter. Experimental data from [102].

Summary of binary mixtures

To summarize the results of the several EoS used for modeling viscosity of binary mixtures, the % AAD was calculated against the experimental data and is tabulated in Table 6–14.

It appears that cubic EoS model all systems with similar accuracy, while PC-SAFT and tPC-PSAFT exhibit better results for CO_2-N_2, but worse for CO_2-CH_4.

If we compare the cubic EoS and the PC-SAFT/tPC-PSAFT based models, we observe that the errors exhibited are in the same order of magnitude. However, the error is of a different type. PC-SAFT/tPC-PSAFT models exhibit a systematic error but the cubic EoS models exhibit an error that increases with pressure.

Table 6–14. Average absolute deviation (% AAD) and maximum absolute deviation (% MAD) for the predictions of the binary mixtures viscosities based on Cubic EoS, PC-SAFT and tPC-SAFT.

	CO_2-CH_4		CO_2-O_2		CO_2 – N_2	
	% AAD	MAD%	% AAD	MAD%	% AAD	MAD%
RK	2.84	7.97	2.26	3.91	2.17	8.38
SRK	7.65	22.97	2.10	3.69	4.97	16.40
PR	4.69	22.59	2.04	3.60	6.63	21.40
PR/G	7.92	24.49	2.07	3.62	6.74	21.40
PC-SAFT	5.76	7.41	2.41	2.67	1.38	2.67
tPC-SAFT	6.20	8.07	2.41	2.80	1.47	2.80

Given that the model has been extensively tested and verified and that the conditions of the mixtures studied are in the vapor phase, it can be concluded that the dense phase correction produced by the cubic EoS is not suitable at low pressures as it is the case for the PC/SAFT/tPC-PSAFT model.

CO_2 – O_2 – N_2

Application of the proposed viscosity models to complex multi-component mixtures is important for improving the accuracy of hazard identification studies like the one considered in this project. Thus, ternary mixtures are modeled and the results are compared to experimental data. In all cases, experimental data are at ambient pressure.

The first mixture considered is the CO_2 - O_2 - N_2. Predictions using different EoS are compared to literature data [103] with the errors reported in Table 6–16. Details of the analysis of the results for all EoS can be found in Table 6–15. Overall, good agreement is obtained as indicated by the tabulation of Table 6–16.

Table 6–15. Experimental data [103] and EoS predictions for the viscosity of $CO_2 - O_2 - N_2$ mixture, in units of μP.

T (K)	x(O_2)	x(N_2)	x(CO_2)	expt	RK	SRK	PR	PR/G	PC-SAFT	tPC-PSAFT
297.45	0.0330	0.8830	0.0840	174.50	175.54	175.79	175.88	175.92	175.20	175.20
297.83	0.0900	0.8120	0.0980	175.50	176.77	177.02	177.11	177.14	176.41	176.41
295.93	0.1140	0.7960	0.0900	179.00	176.73	176.97	177.06	177.08	176.36	176.36
298.45	0.1180	0.7360	0.1460	176.00	176.40	176.65	176.76	176.78	176.01	176.01
297.80	0.2030	0.5000	0.2970	174.00	173.92	174.22	174.37	174.37	173.47	173.47
297.80	0.2130	0.2800	0.5070	168.00	168.28	168.66	168.87	168.86	167.77	167.77
296.94	0.2300	0.6800	0.0900	180.50	180.22	180.44	180.52	180.53	179.81	179.81
297.45	0.0800	0.8580	0.0620	177.80	177.39	177.62	177.70	177.73	177.03	177.03
297.85	0.1690	0.7030	0.1280	176.50	177.95	178.19	178.29	178.30	177.55	177.55
297.45	0.2680	0.5200	0.2120	176.50	177.86	178.12	178.24	178.24	177.41	177.41
297.30	0.3340	0.4000	0.2660	176.50	177.91	178.18	178.32	178.30	177.43	177.43

Table 6–16. % AAD and % MAD (Maximum Absolute Deviation) for viscosity prediction of CO_2 - O_2 - N_2 mixture with different EoS and FT at 1 bar.

	CO_2-O_2-N_2	
	% AAD	MAD%
RK	0.53	1.27
SRK	0.60	1.13
PR	0.64	1.09
PR/G	0.64	1.07
PC-SAFT	0.48	1.48
tPC-SAFT	0.48	1.48

6.2. Diffusion Coefficient

The self-diffusion coefficient of pure CO_2 over a range of temperature and pressure was studied using two models, [181] and [183], combined with three EoS, PR, SRK, PC-SAFT. As shown in Figure 6–12, the best agreement with the experimental data is achieved by PC-SAFT in combination with Yu and Gao model. The two diffusion coefficient models provide very similar predictions, unlike the three EoS that

show distinct differences, especially at high pressures. PC-SAFT exhibits the lowest error while SRK over-predicts, and PR under-predicts the experimental data.

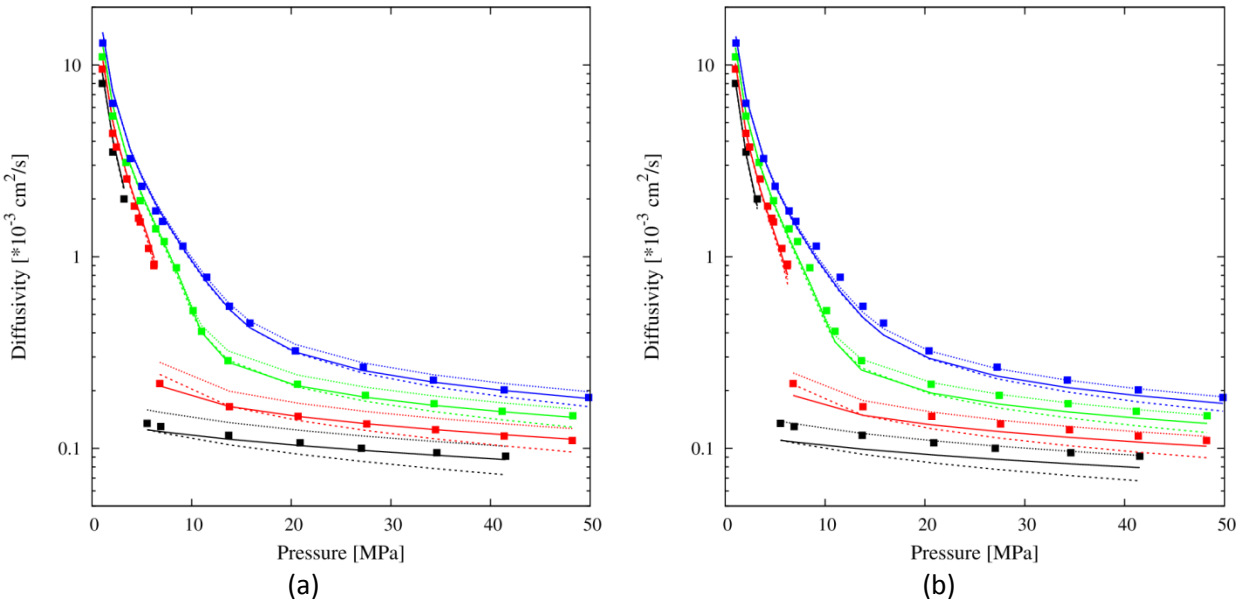

Figure 6–12. Self-diffusion coefficient of pure CO_2, calculated by Yu and Gao (a), and Reis et al. models. Solid line: PC-SAFT, dashed line: PR, dotted line: SRK. Experimental data (points) from [272].

6.3. Thermal Conductivity

The calculations were carried out in the temperature range of 220-500K and pressure range 0-20MPa. The results are very encouraging, and it is shown that both SAFT and PC-SAFT can predict accurately the thermal conductivity of pure CO_2 if they are coupled with Vesovic's model.

Figure 6–13 shows the thermal conductivity curve and the proximity to the reference data acquired from NIST Webbook [186], for three isobars of 2, 8, and 15 MPa, so as to cover both subcritical and supercritical regimes.

The two EoS work very well with this model, giving high accuracy results. The error (AAD) is less than 5% for the range studied in this work.

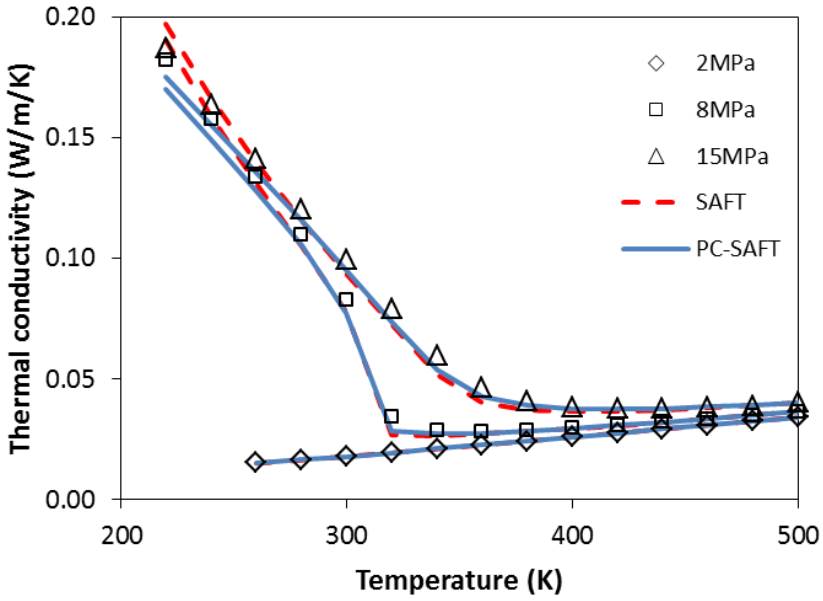

Figure 6–13: Thermal conductivity of pure CO_2 at 2, 8, and 15 MPa

For the rest of the calculations, Table 6–17 collects all the errors in % AAD for the entire pressure range that was investigated.

Table 6–17. Errors in CO_2 thermal conductivity calculations at pressures 0-20 MPa

	% AAD	
P (MPa)	SAFT	PC-SAFT
0	0.08	0.08
1	0.21	0.19
2	0.49	0.43
5	1.75	1.37
8	3.76	3.57
10	4.86	4.37
12	4.78	4.04
15	4.83	3.88
20	4.67	3.43

Figure 6–14 compares results obtained from the underlying model against data taken from the NIST web site for pure CO_2. The model predictions have been obtained using the Span and Wagner EoS for the prediction of pressure-density relationship. Two

isotherms below the critical point have been considered and a wide range of pressures is presented. Excellent agreement between model predictions and NIST data is obtained.

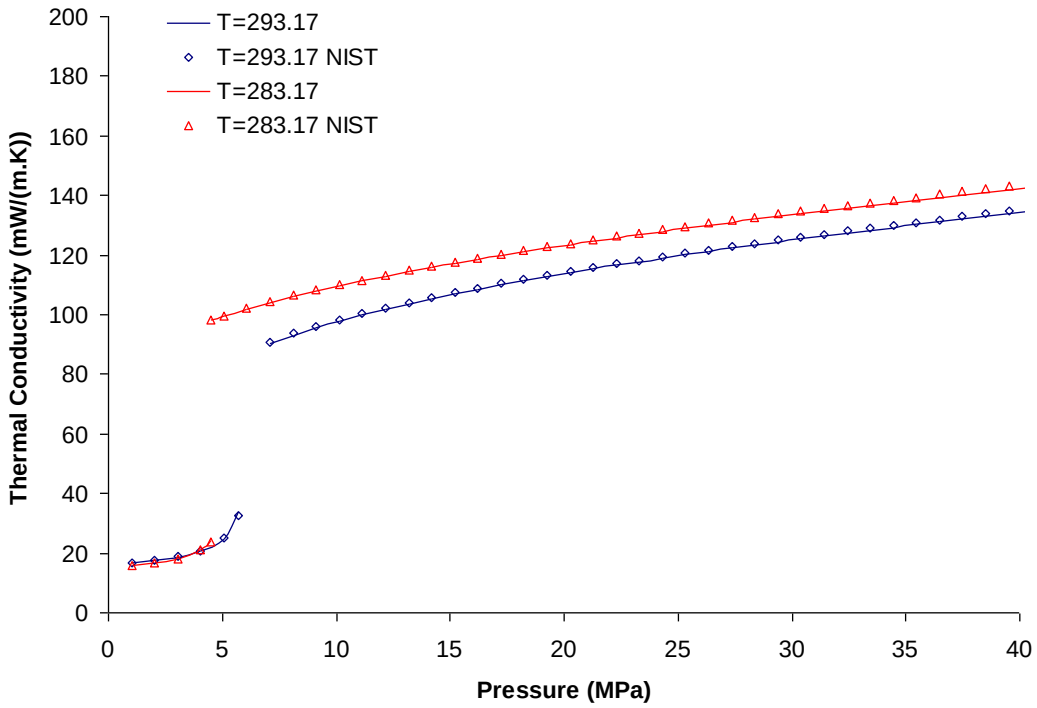

Figure 6–14. Thermal conductivity of pure CO_2 as a function of pressure for two sub-critical isotherms. The continuous lines represent predictions using Eq. (3.78) with Span and Wagner EoS. Symbols correspond to data obtained from the NIST Website.

7. Applications

7.1. Benchmarking

When it comes to applying certain thermodynamic models to broader purpose fluid simulators, the performance with respect to CPU time is a very significant issue. For this reason, a certain set of calculations were performed in order to compare SAFT, PC-SAFT, and PR. The benchmarking calculations include VLE and single phase properties, for a wide range of conditions and for both pure components and mixtures, in order to cover the most important and frequent calculations in a fluid simulator.

The assumptions and the environment under which the calculations were performed are defined by the following statements:

1. CPU times are all in seconds.
2. Input-Output time is not included.
3. Phase stability algorithms are implemented only in the case of Peng-Robinson EoS.
4. The single phase calculations were performed for the 608 points that the cubic EoS benchmarking was done for.
5. Phase equilibria calculations were performed over 1000 points, making sure that there is convergence for all of them.
6. Single phase properties include: molar volume, density, internal energy, Helmholtz energy, Gibbs free energy, enthalpy, Entropy, isothermal compressibility, thermal expansion coefficient, Cp, Cv, Joule-Thomson coefficient, speed of sound, adiabatic bulk modulus.
7. Calculations were performed on an Intel Core i7 M620 @ 2.67GHz.

The results of the benchmarking tests are summarized in the tables below:

Table 7–1. Benchmarking of SAFT, PC-SAFT and PR EoS, for several types of calculations.

	System	SAFT	PC-SAFT	Peng-Robinson	Calculation
		CPU time (sec)			
Single Phase Properties	Pure CO_2	0.2496	0.2612	-	
VLE	Pure CO_2	0.2652	0.2340	0.1402	Bubble Point
VLE (non-associating)	CO_2-CH_4	0.8424	0.5921	0.0391	TP-flash
VLE (associating)	CO_2-H_2O	5.2572	7.7317	0.0402	TP-flash

SAFT and PC-SAFT are substantially slower compared to Peng-Robinson and other cubic EoS only for the case of associating fluids.

Table 7–2. Calculation of pure CO_2 density.

T (K)	Pressure Range (MPa)	# points	SAFT	PC-SAFT	Peng-Robinson
280	0-12	2000	0.169	0.138	0.023
290	0-12	2000	0.172	0.141	0.024
320	0-12	2000	0.168	0.139	0.025

Generally SAFT and PC-SAFT have greater demands of CPU time, when compared to PR, and this is mainly due to the density solver. In the case of SAFT and PC-SAFT it is an advanced iterative scheme [273], while in the case of cubic EoS, the density roots are determined by an analytical solver.

The benchmarking would be more valuable if it was done as a cost-benefit analysis in the context of a flow simulator. In this case, the overhead in time demanded, can be acceptable, reasoned by the gain in accuracy of the results of the flow simulator.

Moreover, there are sophisticated techniques, such as look-up tables, which can be used in order to combine the use of highly accurate thermophysical properties predicted by a model like SAFT or PC-SAFT, with the benefit of low CPU cost during the execution of the flow simulator.

7.2. Modeling of CO_2 Pipeline Rupture

This PhD thesis was completed in the framework of the CO2PipeHaz project, which had as a main objective, the quantitative assessment of the hazards of CO_2 released following the failure of pressurized pipelines. Central to this is the determination of the highly transient outflow parameters including the discharge rate, pressure, temperature and fluid phase at the rupture plane in the event of pipeline failure. Such data serves as the input for predicting the subsequent atmospheric dispersion of the escaping CO_2, and hence, the basis for determining the minimum safe distances to populated areas.

The modeling of outflow following pipeline failure is especially challenging given the large number of complex and often interacting process governing the discharge process. In particular, during the transportation of CO_2 at high pressure, the near-isentropic expansion resulting from failure induces two-phase occurrence. Hence, the ability to accurately model the CO_2 phase equilibria is essential to the correct prediction of the discharge rate characteristics.

One of the project partners, University College London, has developed a specialized computational code for heterogeneous pipeline flow simulations [274-277].

An example which illustrates this integration will be presented here. The thermodynamic property predictions were added to the Homogeneous Relaxation Model [278, 279] which simulates transient pipeline depressurization. The "integrated" model is validated against experimental data and used to assess the effect of EoS model on the overall accuracy of small-scale outflow simulations. Results of this work showed that, at the selected conditions, the choice of EoS significantly affects outflow predictions such as temperature, discharge rate and pressure. A thorough study on the effect of thermodynamic model selection at different outflow conditions is currently underway.

Figure 7–1 shows the measured variation of pressure with time at the closed end of the pipeline following decompression initiation. Also shown are the predictions obtained using PC-SAFT and SRK EoS respectively. All predictions are in reasonable agreement with the experimental data; the pressure history predicted by the SRK is almost identical to that of the PC-SAFT model.

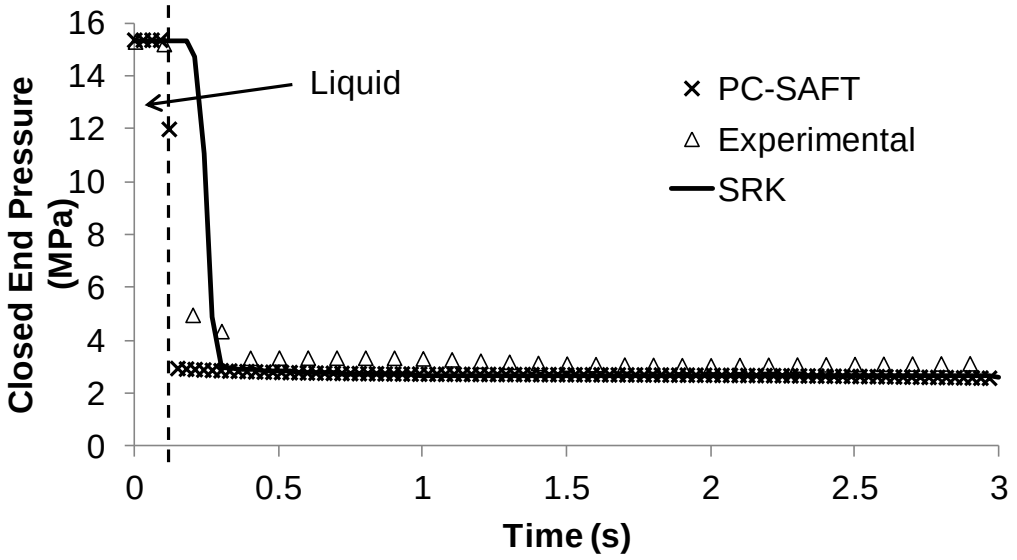

Figure 7–1. Variation of pressure with time at the closed end following the Full Bore Rupture of a pressurised pipeline using various EoS

The discharge rate predicted by the PC-SAFT model (Figure 7–2) shows an instantaneous increase to ca. 800 kg s^{-1} as the decompression begins, before steadily declining to ca. 600 kg s^{-1} throughout the course of the simulation. In comparison, the predictions of SRK show similar profiles; however the initial maximum discharge rates in either case are ca. 1000 kg s^{-1} and 250 kg s^{-1} respectively. The large difference in the SRK predictions compared to the other EoS is due to the significantly lower speed of sound, resulting in a slower depressurization allowing "vaporization" to occur more rapidly and thus a lower mass release rate.

The example shows that the thermodynamic model selection can greatly affect the results of pipeline simulations. In particular, it was found that the discharge rate, the parameter of most importance in this study, was highly sensitive with a variation of ca. 65 % possible in the results.

Table 7–3. Pipeline characteristics and initial conditions for gas phase release test. Experiments were conducted in INERIS, France.

Input Parameter	Value
Number of Components	1
Feed Composition	CO_2 - 100%
Feed Inlet Temperature (K)	293.15
Feed Inlet Pressure (bar)	39
Ambient Temperature (K)	283.15
Ambient Pressure (bar)	1.01
Pipeline Length (m)	37
Pipeline Internal Diameter (mm)	40
Pipeline Roughness (mm)	0.05
Failure Mode	Full Bore Rupture

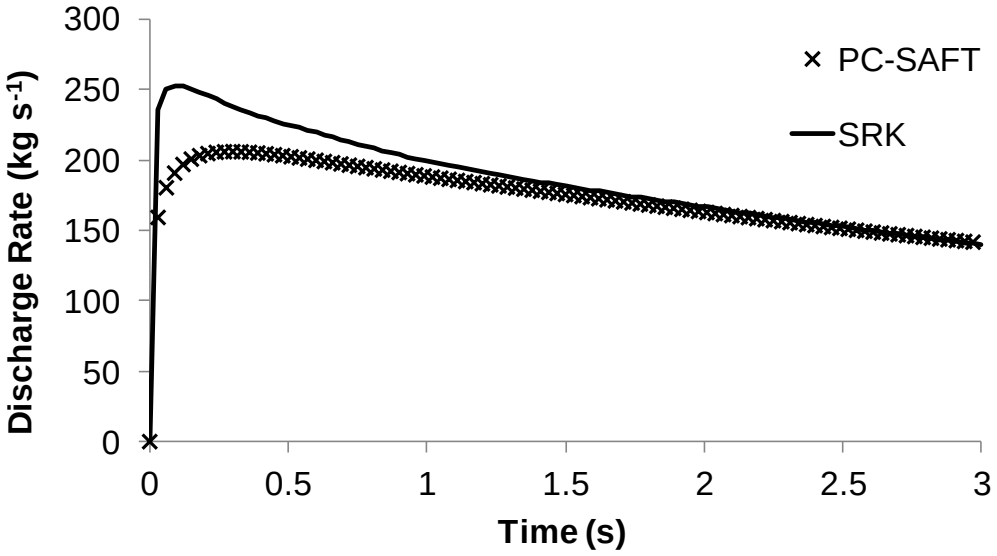

Figure 7–2. Variation of release rate with time following the Full Bore Rupture of a pressurised pipeline using various EoS

Unfortunately, given the scarcity of experimental data, it is not possible to definitively state which of the predicted discharge profiles is correct; however, the accuracy of the PC-SAFT EoS relative to the others tested here gives greater confidence in the predictions obtained with it.

8. Conclusions

The selection of a thermodynamic model is of crucial importance for the design and hazard assessment of Carbon Capture and Storage processes. Factors to be taken into account are the accuracy, the computational overhead and the predictive capabilities of the model.

Vapor – Liquid Equilibria of binary mixtures containing CO_2 is a problem that can be sufficiently solved by fitting binary interaction parameters to the conditions range that is of interest to CCS. Both cubic EoS and the SAFT-based ones can perform very satisfactorily in VLE correlation. Only exception is the RK, which is expected to be worse, due to the fact that it is less advanced than the others. Also, from the comparison of PR and PR/G, it seems that the differences in the account for temperature dependence, do not affect the result for mixtures, because the fitted binary parameter flattens out all the differences. In this work, binary interaction parameters for several mixtures related to CCS were optimized with the use of reliable experimental data from the literature, leading to a ready to use parameter table.

One interesting observation regarding the binary systems phase envelopes is that most of the impurities shift the envelope to higher pressures, with the exception of H_2S and SO_2. H_2S creates a very narrow phase envelope which almost overlaps with the pure CO_2 VLE curve, while SO_2 is the only component which shifts the binary phase envelope to lower pressure than the pure CO_2.

Especially for the system of CO_2 with water, it becomes apparent that the molecular interactions between the unlike species are the ones that drive the thermodynamic behavior. Thus, the cross-association interactions between CO_2 and water can improve substantially the results. Moreover, there are indications that the quadrupolar nature of CO_2 has to be taken into account in the model. Last, the solution for such a complex system might be the fitting of two different sets of parameters, one for the CO_2-rich side, and one for the CO_2-lean regime.

More complex systems, containing three or more components do not only depend on a good set of binary interaction parameters, but they can be more efficiently described by EoS with richer physical content such as PC-SAFT. This can be attributed to the fact that by increasing the number of components, the intermolecular interactions get more complex. PR and SRK are not dramatically worse than PC-SAFT, making the choice dependable on the trade-off of computational cost to accuracy.

The study of phase equilibria of CO_2-containing mixtures was extended to the Solid-Liquid Equilibria, assuming that the solid phase consists of pure CO_2. Although there is no availability of experimental data for SLE of CO_2 with components relevant to CCS, the implementation of the model was validated successfully against data of CO_2 solubility in liquid light hydrocarbons. Such a model can be extended to mixtures of interest to CCS, as soon as experimental data is available.

Derivative properties are definitely a key aspect for the modeling of depressurization processes, to the extent that they can be assumed as throttling, isenthalpic, processes. Speed of sound and Joule-Thomson inversion curve will give insight to the pressure wave propagation and the phase transitions that the stream will follow. Since these properties carry a significant amount of physical information, it is expected that EoS based on a more solid theoretical background, such as the SAFT family EoS investigated in this work, can give better results for these properties. Cubic EoS in general are much less accurate in predicting the derivative properties, while the fact that their parameters are the critical parameters of the pure components, makes it difficult to decide whether a reparameterization would be the solution. A significant drawback is the lack of experimental data for multicomponent systems of interest to CCS.

Transport properties, and especially viscosity, are essential to the flow simulators. Thus, accurate property models can improve the quality of flow simulators' results. Methods such as the Friction Theory can be an excellent tool for the prediction of viscosity through an EoS. Significant workload of parameter optimization is required though, since a component-specific parameter set is needed for every EoS. In this work, parameter tables for the components of interest were produced and validated against

available data. Due to the nature of the method (it consists of two terms, one for the dilute gas limit, and a second for the pressure dependence) high pressure data for multicomponent systems are really necessary for the further validation of the model. Nevertheless, for the available experimental viscosity data of CO_2 mixtures, the combination of PC-SAFT with Friction Theory, and the fitted parameter sets, gives results of sufficient accuracy. Apart from Friction Theory, component-specific methods, such as the method of Vesovic et al., were implemented and validated, giving a wider range of models to be selected for viscosity modeling. Thermal conductivity and self-diffusion coefficient were also studied in this work, by linking the EoS to property specific models. The results are very encouraging for the use of such combined methods for the prediction of these properties in order to be used for CCS applications.

The optimization of the parameters involved in models such as the Friction Theory, is considered as a multi-variable, and multi-objective optimization procedure. For overcoming this problem, a meta-heuristic method, namely Particle Swarm Optimization, was successfully implemented. This serves as an example of multi-disciplinary approach of problems, since a method initially developed for electrical engineering purposes (PSO) is used for the solution of chemical thermodynamics problems.

As far as it concerns the connection of the thermodynamic models of this work with flow simulators, it can be drawn as a conclusion that the selection of EoS can have a substantial effect on the final result. Unfortunately, the lack of experimental data for the more complex properties makes it difficult to fully validate the conclusion that comes from the already measured properties.

Finally, it was shown that, among the assessed EoS, SAFT family EoS, and especially PC-SAFT, can be in very good agreement with the experimental data for a wide range of properties and conditions, regarding CO_2 mixtures. This leads to the conclusion that it can serve as a good and reliable model for the design of CO_2 transport pipelines for CCS applications.

9. Further Work

Every question that is answered gives birth to more questions. This applies to this work too, giving a very attractive list of topics to be studied as follow-up to this thesis.

The collaboration with research groups that specialize in experimental measurements will give the opportunity of obtaining the data that are needed to further validate the findings of this work. As previously mentioned in this work, there are several gaps of experimental data, which by the time these are measured, more insight will be acquired for the nature of the mixtures, as well as for the model's accuracy.

Regarding the phase equilibria of binary systems, since all impurities but SO_2 shift the envelope to higher pressures, it would be interesting to investigate the combined effect of two impurities with opposite effects, such as SO_2 and N_2. Therefore, the ternary system CO_2-SO_2-N_2 is one of the suggestions for measuring its phase envelope. If a beneficial synergistic effect is proven by the experiments, it might act as the basis of the development of a new method for controlling the phase behavior of the CO_2 stream in the pipelines.

By having more reliable data on multicomponent systems, and more complex properties (i.e. Joule-Thomson inversion curve, speed of sound, diffusion coefficient, viscosity), the parameters of the models can be tuned better, or even lead to correlations that might be used as a quick first approach to any design problem. Since the EoS studied in this work have been already linked to the meta-heuristic optimization method of PSO, it would be useful to study how the parameters are influenced when the objective functions are more than one, and include derivative, or even transport, properties. This may lead to an engineering model with adaptive approach, where the parameters will change in a physically meaningful range of values, in order to predict different properties with equally high accuracy.

Some very interesting systems, such as the CO_2-water-brine can be a good test of how these models behave with systems that contain electrolytic interactions, and also an excellent motivation to develop further the models, and the thermodynamic simulator,

with theories for electrolytic interactions. A versatile model that can capture several types of interactions depending on the system that it deals with, can be a great tool for the industry, and process design.

High pressures, supercritical conditions, and low temperatures are admittedly the regimes that the models require to be most accurate, but also the lack of experimental data is significant. It is believed that as the research on this topic continues, the community will be spontaneously lead to perform experiments on those regimes. These measurements can prove crucial for the improvement of the viscosity models for mixtures, as well as the phase equilibria where solid phases are present. The pressure effect terms can be parameterized better, so that the models will cover wider conditions range with greater confidence.

Elevated pressures and temperatures usually are linked to the part of storage in CCS. It is reported in the literature that there is the possibility of chemical reactions occurrence upon the injection of the CO_2 stream in the underground cavities. Hence, a useful extension of the model would be the addition of a module that can calculate quantities that are related to reactions.

Another related research trend is the thermodynamic modeling of hydrates. This topic gains popularity because of the vast quantities of methane that are proven to exist worldwide in the form of hydrates. Techniques of exchanging methane with CO_2 as guest molecules in the clathrates will need thermodynamic models for both the pipeline transport and the storage parts. It will be interesting to investigate if models like the ones discussed in this work, can be suitably modified in order to account also for hydrates formation.

Of cornerstone importance is the continuous decrease of the computational cost that is added on a flow simulator, when higher order EoS are used. For this purpose, efficient algorithms of predicting whether a given system will be in the single phase or in phase equilibria have to be developed. This way, the calls of the most time-consuming parts of the thermodynamic models (flasher and density root finders) can be minimized. This can be also assisted by the measurement of more experimental data, which will make possible the derivation of system-specific correlations that will define the "surface

boundary" of phase equilibria, so that the algorithm will be quicker in identifying whether the flasher needs to be called or not. Another thought is that smart systems of look-up tables can be the interface between a very advanced thermodynamic model and a flow simulator with the need for efficient use of the computational resources.

Moreover, again in the framework of a wider multi-disciplinary project, it would be interesting to find out what would be the impact of the selection of different thermodynamic models to the final techno-economic and hazard assessments of CO_2 pipeline networks. The thermodynamic model selection should be a key part of techno-economic studies, both because it can affect the conditions, and thus the compression cost, or the material selection, but also it adds to the cost of the simulations in the stage of project design.

Appendix

Peng-Robinson EoS

The EoS used is the Peng-Robinson in its original form, as it was developed by Peng and Robinson [45] in 1976.

The pressure explicit expression of PR EoS is:

$$P = \frac{RT}{v-b} - \frac{\alpha(T)}{v(v+b)+b(v-b)} \tag{A.1}$$

where the first term describes the part of pressure due to the repulsive interactions according to van der Waals hard sphere equation, while the second term is the expression of the attractive interactions effect on pressure.

In order for this equation to be written as a cubic equation, it has to be solved for the compressibility factor, Z, as follows:

$$Z^3 - (1-B)Z^2 + (A - 3B^2 - 2B)Z - (AB - B^2 - B^3) = 0 \tag{A.2}$$

where:

$$Z = \frac{Pv}{RT} \tag{A.3}$$

$$A = \frac{aP}{(RT)^2} \tag{A.4}$$

$$B = \frac{bP}{RT} \tag{A.5}$$

The function $\alpha(T)$ can be given as the product of two parameters, one depending only on the critical temperature of the component, and the second depending on the temperature of the system, which can be taken into account as a reduced quantity, and the acentric factor, which is a measure of the deviation that the molecule exhibits from the spherical shape.

More specifically, it can be given as in Eq. (A.6):

$$\alpha(T) = a(T_c) \cdot \alpha(T_r, \omega) \tag{A.6}$$

Subsequently, there is one universal expression for the $\alpha(T_c)$:

$$\alpha(T_c) = 0.45724 \frac{(RT_c)^2}{P_c} \tag{A.7}$$

and a second for the parameter b:

$$b = 0.07780 \frac{RT_c}{P_c} \tag{A.8}$$

which both result from applying Eq. (A.1) at the critical point.

The function $\alpha(T_r, \omega)$ has been one of the most modified terms of PR EoS in these years of research, and for this study two expressions are used. The first is the original Soave-type expression, as reported by Peng and Robinson:

$$\alpha(T_r, \omega) = [1 + \kappa(1 - T_r^{0.5})]^2 \tag{A.9}$$

where:

$$\kappa = 0.37464 + 1.54226\omega - 0.26992\omega^2 \tag{A.10}$$

One more modern and more complex function for $\alpha(T_r, \omega)$ was developed by Gasem et al. [158] in 2001. This function follows an exponential trend, and it exhibits

appropriate temperature-limiting behavior. Comparisons with other $\alpha(T_r, \omega)$ functions, in the original paper of Gasem et al., show consistently lower error for the prediction of pure hydrocarbons' vapor pressure.

$$\alpha(T) = exp[(2 + 0.836T_r)(1 - T_r^{\kappa})] \tag{A.11}$$

$$\kappa = 0.134 + 0.508\omega - 0.0467\omega^2 \tag{A.12}$$

Mixing Rules

When extending to mixtures, the parameters α and b are subject to mixing rules. Again, there have been reported a few mixing rules sets in the literature [280], but the most established one, the simplest and most common are:

$$\alpha = \sum_i \sum_j x_i x_j \alpha_{ij} \tag{A.13}$$

$$b = \sum_i x_i b_i \tag{A.14}$$

with:

$$\alpha_{ij} = \left(1 - k_{ij}\right)\left(\alpha_i \alpha_j\right)^{0.5} \tag{A.15}$$

In Eq. (A.15), a new parameter is introduced, the binary interaction parameter, k_{ij}. This parameter is of semi-empirical nature, and its value is a result of fitting to experimental data.

Cubic Equation Root Finding

A simple method [281] for analytical root finding of cubic equations was programmed in an individual subroutine. Note that the symbols chosen for this part are independent of the rest of the report.

Suppose that the roots of Eq. (A.16) are needed to be found:

$$ax^3 + bx^2 + cx + d = 0 \tag{A.16}$$

where a, b, c and d are coefficients for the polyonym, while x is the variable.

The calculations that take place in that subroutine are described below:

$$F = \frac{3\frac{c}{a} - \frac{b^2}{a^2}}{3} \tag{A.17}$$

$$G = \frac{2\frac{b^3}{a^3} - 9\frac{bc}{a^2} + 27\frac{d}{a}}{27} \tag{A.18}$$

$$H = \frac{G^2}{4} + \frac{F^3}{27} \tag{A.19}$$

If $H < 0$, there are three different real roots can be found with the use of the following equations:

$$I = \left(\frac{G^2}{4} - H\right)^{1/2} \tag{A.20}$$

$$J = (I)^{1/3} \tag{A.21}$$

$$K = arccos\left(-\frac{G}{2I}\right) \tag{A.22}$$

$$L = -J \tag{A.23}$$

$$M = cos\left(\frac{K}{3}\right) \tag{A.24}$$

$$N = \sqrt{3} \cdot sin\left(\frac{K}{3}\right) \tag{A.25}$$

$$P = -\frac{b}{3a} \tag{A.26}$$

$$x_1 = 2J \cdot M + P \tag{A.27}$$

$$x_2 = L(M + N) + P \tag{A.28}$$

$$x_3 = L(M - N) + P \tag{A.29}$$

If $H > 0$, there is only one real root, and two imaginary, the real root is found by:

$$R = -\frac{G}{2} + \sqrt{H} \tag{A.30}$$

$$S = R^{1/3} \tag{A.31}$$

$$T = -\frac{G}{2} - \sqrt{H} \tag{A.32}$$

$$U = T^{1/3} \tag{A.33}$$

$$x_1 = (S + U) - \left(\frac{b}{3a}\right) \tag{A.34}$$

If $F = 0$ and $H = 0$, then all roots are real and equal with each other:

$$x_1 = x_2 = x_3 = -\left(\frac{d}{a}\right)^{1/3} \tag{A.35}$$

Studied Properties

Throughout this project, several properties have been studied and modeled for the systems of interest, for a wide range of conditions (T, P). These properties span from volumetric, residual, and derivative thermodynamic, to transport properties. Analytical equations, directly derived from PR EoS, are used to model these properties, when possible.

Especially for transport properties, specific models from the literature are combined with the PR EoS and the developed code in order to give high quality results.

The studied properties are listed in this section of the report, along with the equations that were used to calculate them.

Volumetric Properties

Density of pure components or mixtures is calculated straightforwardly after the analytical solution of the cubic EoS. The compressibility factor roots are converted to volumes and then to densities according to the following equation:

$$\rho = \frac{1}{V} = \frac{P}{ZRT} \tag{A.36}$$

Residual Properties

The residual properties that are calculated in the delivered software are presented below, along with the expressions used.

Internal Energy

$$U^{res} = \frac{T\frac{da}{dT} - a}{2\sqrt{2}b} ln\left[\frac{Z + \left(1+\sqrt{2}\right)B}{Z + \left(1-\sqrt{2}\right)B}\right] \tag{A.37}$$

Enthalpy

$$H^{res} = U^{res} + (Z-1)RT \tag{A.38}$$

where U^{res} has been evaluated before, with the use of Eq. (A.37).

Entropy

$$S^{res} = Rln[Z-B] + \frac{\frac{da}{dT}}{2\sqrt{2}b} ln\left[\frac{Z+\left(1+\sqrt{2}\right)B}{Z+\left(1-\sqrt{2}\right)B}\right] \tag{A.39}$$

Helmholtz Free Energy

$$F^{res} = U^{res} - T \cdot S^{res} \tag{A.40}$$

where U^{res} and S^{res} have been evaluated before, with the use of Eq. (A.37) and Eq. (A.39).

Gibbs Free Energy

$$G^{res} = F^{res} + Z - 1 \tag{A.41}$$

For the evaluation of the above quantities, an expression is needed for $\frac{da}{dT}$ which comes from differentiating the expression for a with respect to temperature:

$$a' = \frac{da}{dT} = \frac{1}{2}\sum_i \sum_j x_i x_j \left(1-k_{ij}\right)\left[a_i' \sqrt{\frac{a_j}{a_i}} + a_j' \sqrt{\frac{a_i}{a_j}}\right] \tag{A.42}$$

where

$$a_i' = \frac{da_i}{dT} = \frac{-\kappa_i a_i}{\left[1+\kappa_i\left(1-\sqrt{\frac{T}{T_{ci}}}\right)\right]\sqrt{TT_{ci}}} \tag{A.43}$$

for the a expression of Peng and Robinson (Eq. (A.9)), and:

$$a_i' = \frac{da_i}{dT} = \frac{a[0.836(1 - T_r^m) - m(2 + 0.836T_r)T_r^{m-1}]}{T_c} \tag{A.44}$$

for the temperature dependent function reported by Gasem et al.

Heat of Vaporization

As heat of vaporization, is defined the amount of heat that is required to convert a unit of mass of a system from liquid to vapor phase, without a change in temperature.

$$\Delta H_{vap} = H_{vapor}^{res} - H_{liquid}^{res} \tag{A.45}$$

Thus, this quantity can be immediately calculated after the evaluation of residual enthalpies of the saturated liquid and vapor phases at equilibrium.

Derivative Properties

Other derivative properties that are calculated in the code include the heat capacities (isobaric and isochoric), speed of sound, Joule-Thomson coefficient, isothermal compressibility coefficient, and thermal expansion coefficient.

More specifically:

Isochoric Heat Capacity

$$C_v^{res} = \left(\frac{\partial U^{res}}{\partial T}\right)_v = \frac{T\frac{d^2a}{dT^2}}{2\sqrt{2}b} ln\left[\frac{Z + \left(1 + \sqrt{2}\right)B}{Z + \left(1 - \sqrt{2}\right)B}\right] \tag{A.46}$$

where the second derivative of a with respect to temperature is given by the expression:

$$a'' = \frac{d^2a}{dT^2} = \frac{1}{2}\sum_i\sum_j x_i x_j\left(1 - k_{ij}\right)\left[\frac{a_i' a_j'}{\sqrt{a_i a_j}} + a_i''\sqrt{\frac{a_j}{a_i}} + a_j''\sqrt{\frac{a_i}{a_j}} - \frac{1}{2}\left(a_i'^2\sqrt{\frac{a_j}{a_i^3}} + a_j'^2\sqrt{\frac{a_i}{a_j^3}}\right)\right] \tag{A.47}$$

The expression for the calculation of a_i'', for the case of Peng-Robinson $a(T)$ function is:

$$a_i'' = \frac{d^2 a_i}{dT^2} = \frac{a_{ci}\kappa_i\sqrt{\frac{T_{ci}}{T}}(1+\kappa_i)}{2TT_{ci}} \tag{A.48}$$

while for the $a(T)$ function of Gasem is:

$$\begin{aligned} a_i'' = \frac{d^2 a_i}{dT^2} = \frac{a}{T_c^2}\big[&[0.836(1-T_r^{\kappa}) - \kappa(2+0.836T_r)T_r^{\kappa-1}] \\ &+ [-2\cdot 0.836\kappa T_r^{\kappa-1} - \kappa(\kappa-1)(2+0.836T_r)T_r^{\kappa-2}]\big] \end{aligned} \tag{A.49}$$

Isobaric Heat Capacity

The isobaric heat capacity expression is more complex and it makes use of the previously calculated C_v^{res} as well the partial derivatives of pressure and volume with respect to temperature.

$$C_p^{res} = C_v^{res} + T\left(\frac{\partial P}{\partial T}\right)_v \left(\frac{\partial v}{\partial T}\right)_p - R \tag{A.50}$$

The auxiliary partial derivatives are evaluated with the use of the following equations:

$$\left(\frac{\partial P}{\partial T}\right)_v = \frac{R}{v-b} - \frac{a'}{v(v+b)+b(v-b)} \tag{A.51}$$

$$\left(\frac{\partial v}{\partial T}\right)_p = \frac{R}{P}\left[T\left(\frac{\partial Z}{\partial T}\right)_p + Z\right] \tag{A.1}$$

Here another auxiliary derivative is needed, the partial derivative of compressibility factor with respect to temperature under constant pressure, which is calculated by the expression:

$$\left(\frac{\partial Z}{\partial T}\right)_p = \frac{\left(\frac{\partial A}{\partial T}\right)_p (B - Z) + \left(\frac{\partial B}{\partial T}\right)_p [-Z^2 + (6BZ + 2Z) - 3B^2 - 2B + A]}{3Z^2 - 2(1 - B)Z + A - 2B - 3B^2} \quad \text{(A.52)}$$

with

$$\left(\frac{\partial A}{\partial T}\right)_p = \frac{P}{(RT)^2}\left(a' - 2\frac{a}{T}\right) \quad \text{(A.53)}$$

$$\left(\frac{\partial B}{\partial T}\right)_p = -\frac{bP}{RT^2} \quad \text{(A.54)}$$

Speed of Sound

The definition of thermodynamic speed of sound (or fluid sonic velocity) is:

$$w = \sqrt{\left(\frac{\partial P}{\partial \rho}\right)_S} \quad \text{(A.55)}$$

However, the calculation of this quantity can be done with a simpler working equation that is derived from the previous:

$$w = v\sqrt{-\frac{C_p}{C_v}\left(\frac{\partial P}{\partial v}\right)_T} \quad \text{(A.56)}$$

Noteworthy is the fact that the dimensional analysis of this equation gives $\left[\frac{volume \cdot pressure}{mole}\right]^{0.5}$, so it needs manipulation in order to give the result in the practically meaningful dimensions of $\left[\frac{length}{time}\right]$.

Joule-Thomson Coefficient

The Joule-Thomson coefficient is given by its definition as

$$JT = \left(\frac{\partial T}{\partial P}\right)_H \tag{A.57}$$

but it is calculated by the working equation:

$$JT = \frac{1}{C_p}\left(T\left(\frac{\partial v}{\partial T}\right)_P - v\right) \tag{A.58}$$

Isothermal Compressibility Coefficient

The isothermal compressibility coefficient can be easily calculated by its definition, which is the following expression:

$$B_{IC} = -\frac{1}{v}\left(\frac{\partial v}{\partial P}\right)_T \tag{A.59}$$

Subsequently, the evaluation of the isothermal bulk modulus is straightforward, by definition:

$$K_T = -\frac{1}{B_{IC}} \tag{A.60}$$

The partial derivative of volume with respect to pressure under constant temperature is evaluated by the equation:

$$\left(\frac{\partial v}{\partial P}\right)_T = \left[\left(\frac{\partial P}{\partial v}\right)_T\right]^{-1} = \left[-\frac{RT}{(v-b)^2} + \frac{2a(v+b)}{[v(v+b)+b(v-b)]^2}\right]^{-1} \quad \text{(A.61)}$$

Thermal Expansion Coefficient

The coefficient of thermal expansion describes how the size of system changes with a change in temperature. The evaluation of this quantity is performed with the use of the following equation which is also the definition of it.

$$\alpha_v = \frac{1}{v}\left(\frac{\partial v}{\partial T}\right)_P \quad \text{(A.62)}$$

References

1. Pohanish, P. R.; Greene, S. A., *Hazardous Materials Handbook*. Van Nostrand Reinhold: 1996; Vol. Carbon Dioxide.
2. Mahgerefteh, H.; Fairweather, M.; Falle, S.; Melheim, J.; Ichard, M.; Storvik, I.; Taraldset, O. J.; Skjold, T.; Economu, I.; Tsangaris, D., CO2PIPEHAZ: Quantitative Hazard Assessment for Next Generation CO_2 Pipelines. In *Hazards XXII – Process Safety and Environmental Protection*, Liverpool, UK, 2011.
3. Krajick, K.; Gubb, L., Defusing Africa's killer lakes. *Smithsonian* **2003**, *34*, 46-55.
4. Barrie, J.; Brown, K.; Hatcher, P. R.; Schellhase, H. U., Carbon dioxide pipelines: a preliminary review of design and risk. In *Greenhouse Gas Control Technologies 7*, Elsevier: Canada, 2004; Vol. 7.
5. Mahgerefteh, H.; Atti, O., Modeling low-temperature–induced failure of pressurized pipelines. *AIChE J.* **2006**, *52*, 1248-1256.
6. CO2PipeHaz: Quantitative Failure Consequence Hazard Assessment for Next Generation CO2 Pipelines: The Missing Link. http://www.co2pipehaz.eu/
7. Rubin, E.; de Coninck, H., IPCC special report on carbon dioxide capture and storage. *UK: Cambridge University Press. TNO (2004): Cost Curves for CO2 Storage, Part* **2005**, *2*.
8. Olivier, J. G. J.; Janssens-Maenhout, G.; Peters, J. A. H. W. *Trends in global CO_2 emissions - 2012 Report*; PBL Netherlands Environmental Assessment Agency: 2012.
9. United Nations *National greenhouse gas inventory data for the period 1990–2010*; United Nations: Framework Convention on Climate Change: 2012.
10. Lashof, D. A.; Ahuja, D. R., Relative contributions of greenhouse gas emissions to global warming. *Nature* **1990**, *344*, 529-531.
11. Herzog, H. J., Scaling up carbon dioxide capture and storage: From megatons to gigatons. *Energ. Econ.* **2011**, *33*, 597-604.
12. Orr, J. F. M., CO2 capture and storage: are we ready? *Energ. Environ. Sci.* **2009**, *2*, 449-458.
13. Li, H.; Yan, J., Evaluating cubic equations of state for calculation of vapor-liquid equilibrium of CO_2 and CO_2-mixtures for CO_2 capture and storage processes. *Appl. Energy* **2009**, *86*, 826-836.
14. Steinberg, M., History of CO_2 greenhouse gas mitigation technologies. *Energ. Convers. Manage.* **1992**, *33*, 311-315.
15. ICCDR In *1st International Conference on Carbon Dioxide Removal*, 1st International Conference on Carbon Dioxide Removal, 1992; Energy Conversion and Management: 1992; pp 283–826.

16. Statoil Sleipner CCS. http://www.statoil.com/AnnualReport2008/en/Sustainability/Climate/Pages/5-3-2-3_SleipnerCCS.aspx (January 2013),
17. Statoil Snøhvit CCS. http://www.statoil.com/AnnualReport2008/en/Sustainability/Climate/Pages/5-3-2-4_Sn%C3%B8hvitCCS.aspx (January 2013),
18. Zero Emissions Platform EU CCS Demonstration Projects. http://www.zeroemissionsplatform.eu/projects/eu-projects.html (January 2013),
19. Anderson, S.; Newell, R., Prospects for carbon capture and storage technologies. *Annu. Rev. Environ. Resour.* **2004**, *29*, 109-142.
20. Steeneveldt, R.; Berger, B.; Torp, T. A., CO_2 Capture and Storage: Closing the Knowing–Doing Gap. *Chem. Eng. Res. Des.* **2006**, *84*, 739-763.
21. Gibbins, J.; Chalmers, H., Carbon capture and storage. *Energ. Policy* **2008**, *36*, 4317-4322.
22. Haszeldine, R. S., Carbon Capture and Storage: How Green Can Black Be? *Science* **2009**, *325*, 1647-1652.
23. Plasynski, S. I.; Litynski, J. T.; McIlvried, H. G.; Srivastava, R. D., Progress and New Developments in Carbon Capture and Storage. *Crit. Rev. Plant Sci.* **2009**, *28*, 123-138.
24. Scrase, J. I.; Watson, J., Strategies for the deployment of CCS technologies in the UK: a critical review. *Energy Procedia* **2009**, *1*, 4535-4542.
25. Gough, C., State of the art in carbon dioxide capture and storage in the UK: An experts' review. *Int. J. Greenh. Gas Con.* **2008**, *2*, 155-168.
26. Gough, C.; Mander, S.; Haszeldine, S., A roadmap for carbon capture and storage in the UK. *Int. J. Greenh. Gas Con.* **2010**, *4*, 1-12.
27. Riahi, K.; Rubin, E. S.; Schrattenholzer, L., Prospects for carbon capture and sequestration technologies assuming their technological learning. *Energy* **2004**, *29*, 1309-1318.
28. Abu-Khader, M. M., Recent Progress in CO_2 Capture/Sequestration: A Review. *Energ. Source. Part A* **2006**, *28*, 1261-1279.
29. Khoo, H. H.; Tan, R. B. H., Life Cycle Investigation of CO2 Recovery and Sequestration. *Environ. Sci. Technol.* **2006**, *40*, 4016-4024.
30. Davison, J., Performance and costs of power plants with capture and storage of CO2. *Energy* **2007**, *32*, 1163-1176.
31. Koornneef, J.; van Keulen, T.; Faaij, A.; Turkenburg, W., Life cycle assessment of a pulverized coal power plant with post-combustion capture, transport and storage of CO2. *Int. J. Greenh. Gas Con.* **2008**, *2*, 448-467.
32. Koornneef, J.; Spruijt, M.; Molag, M.; Ramírez, A.; Turkenburg, W.; Faaij, A., Quantitative risk assessment of CO2 transport by pipelines--A review of uncertainties and their impacts. *J. Hazard. Mater.* **2010**, *177*, 12-27.
33. Marx, J.; Schreiber, A.; Zapp, P.; Haines, M.; Hake, J. F.; Gale, J., Environmental evaluation of CCS using Life Cycle Assessment–A synthesis report. *Energy Procedia* **2011**, *4*, 2448-2456.

34. Svensson, R.; Odenberger, M.; Johnsson, F.; Strömberg, L., Transportation systems for CO2--application to carbon capture and storage. *Energ. Convers. Manage.* **2004**, *45*, 2343-2353.
35. Forbes, S. M.; Verma, P.; Curry, T. E.; Friedmann, S. J.; Wade, S. M., *CCS Guidelines: Guidelines for Carbon Dioxide Capture, Transport, and Storage*. World Resources Institute: Washington, DC, 2008.
36. Zhang, Z. X.; Wang, G. X.; Massarotto, P.; Rudolph, V., Optimization of pipeline transport for CO_2 sequestration. *Energ. Convers. Manage.* **2006**, *47*, 702-715.
37. Cosham, A.; Eiber, R., Fracture propagation in CO2 pipelines. *Journal of Pipeline Engineering* **2008**, *7*.
38. de Koeijer, G.; Borch, J. H.; Jakobsenb, J.; Drescher, M., Experiments and modeling of two-phase transient flow during CO2 pipeline depressurization. *Energy Procedia* **2009**, *1*, 1683-1689.
39. Mohitpour, M.; Golshan, H.; Murray, A., *Pipeline Design & Construction: A Practical Approach*. 3rd ed.; ASME Press: NewYork, 2007.
40. Li, H.; Yan, J., Impacts of equations of state (EOS) and impurities on the volume calculation of CO_2 mixtures in the applications of CO_2 capture and storage (CCS) processes. *Appl. Energy* **2009**, *86*, 2760-2770.
41. Lachet, V.; de Bruin, T.; Ungerer, P.; Coquelet, C.; Valtz, A.; Hasanov, V.; Lockwood, F.; Richon, D., Thermodynamic behavior of the CO2+SO2 mixture: Experimental and Monte Carlo simulation studies. *Energy Procedia* **2009**, *1*, 1641-1647.
42. Caubet, F., The liquifaction of gas mixtures. *Z. Kompr. Fluess. Gase* **1904**, *8*, 65.
43. Bluemcke, A., II. Ueber die Bestimmung der spezifischen Gewichte und Dampfspannungen einiger Gemische von schwefliger Saeure und Kohlensaeure. *Ann. Phys. Leipzig* **1888**, *34*, 10-21.
44. Redlich, O.; Kwong, J. N. S., On the Thermodynamics of Solutions. V. An Equation of State. Fugacities of Gaseous Solutions. *Chem. Rev.* **1949**, *44*, 233-244.
45. Peng, D.-Y.; Robinson, D. B., A New Two-Constant Equation of State. *Ind. Eng. Chem. Fund.* **1976**, *15*, 59-64.
46. Soave, G., Equilibrium constants from a modified Redlich-Kwong equation of state. *Chem. Eng. Sci.* **1972**, *27*, 1197-1203.
47. Span, R.; Wagner, W., A new equation of state for carbon dioxide covering the fluid region from the triple-point temperature to 1100 K at pressures up to 800 MPa. *J. Phys. Chem. Ref. Data* **1996**, *25*, 1509–1596.
48. Chapman, W. G.; Gubbins, K. E.; Jackson, G.; Radosz, M., SAFT: Equation-of-state solution model for associating fluids. *Fluid Phase Equilibr.* **1989**, *52*, 31-38.
49. Huang, S. H.; Radosz, M., Equation of state for small, large, polydisperse, and associating molecules. *Ind. Eng. Chem. Res.* **1990**, *29*, 2284-2294.

50. Gross, J.; Sadowski, G., Perturbed-Chain SAFT: An Equation of State Based on a Perturbation Theory for Chain Molecules. *Ind. Eng. Chem. Res.* **2001**, *40*, 1244-1260.
51. Economou, I. G., Statistical Associating Fluid Theory: A Successful Model for the Calculation of Thermodynamic and Phase Equilibrium Properties of Complex Fluid Mixtures. *Ind. Eng. Chem. Res.* **2001**, *41*, 953-962.
52. Müller, E. A.; Gubbins, K. E., Molecular-Based Equations of State for Associating Fluids: A Review of SAFT and Related Approaches. *Ind. Eng. Chem. Res.* **2001**, *40*, 2193-2211.
53. Gregorowicz, J.; O'Connell, J. P.; Peters, C. J., Some characteristics of pure fluid properties that challenge equation-of-state models. *Fluid Phase Equilibr.* **1996**, *116*, 94-101.
54. Kortekaas, W. G.; Peters, C. J.; de Swaan Arons, J., Joule-Thomson expansion of high-pressure-high-temperature gas condensates. *Fluid Phase Equilibr.* **1997**, *139*, 205-218.
55. Kroon, M. C.; Karakatsani, E. K.; Economou, I. G.; Witkamp, G.-J.; Peters, C. J., Modeling of the Carbon Dioxide Solubility in Imidazolium-Based Ionic Liquids with the tPC-PSAFT Equation of State. *J. Phys. Chem. B* **2006**, *110*, 9262-9269.
56. Karakatsani, E. K.; Economou, I. G.; Kroon, M. C.; Peters, C. J.; Witkamp, G.-J., tPC-PSAFT Modeling of Gas Solubility in Imidazolium-Based Ionic Liquids†. *J. Phys. Chem. C* **2007**, *111*, 15487-15492.
57. Breure, B.; Bottini, S. B.; Witkamp, G.-J.; Peters, C. J., Thermodynamic Modeling of the Phase Behavior of Binary Systems of Ionic Liquids and Carbon Dioxide with the Group Contribution Equation of State. *J. Phys. Chem. B* **2007**, *111*, 14265-14270.
58. Andreu, J. S.; Vega, L. F., Modeling the Solubility Behavior of CO2, H2, and Xe in [Cn-mim][Tf2N] Ionic Liquids. *J. Phys. Chem. B* **2008**, *112*, 15398-15406.
59. Vega, L. F.; Vilaseca, O.; Llovell, F.; Andreu, J. S., Modeling ionic liquids and the solubility of gases in them: Recent advances and perspectives. *Fluid Phase Equilibr.* **2010**, *294*, 15-30.
60. Zhang, X.; Zhang, X.; Dong, H.; Zhao, Z.; Zhang, S.; Huang, Y., Carbon capture with ionic liquids: overview and progress. *Energ. Environ. Sci.* **2012**, *5*, 6668-6681.
61. Page, S. C.; Williamson, A. G.; Mason, I. G., Carbon capture and storage: Fundamental thermodynamics and current technology. *Energ. Policy* **2009**, *37*, 3314-3324.
62. Nešić, S., Key issues related to modelling of internal corrosion of oil and gas pipelines – A review. *Corros. Sci.* **2007**, *49*, 4308-4338.
63. Nakamura, R.; Breedveld, G. J. F.; Prausnitz, J. M., Thermodynamic Properties of Gas Mixtures Containing Common Polar and Nonpolar Components. *Ind. Eng. Chem. Proc. DD* **1976**, *15*, 557-564.
64. Carnahan, N. F.; Starling, K. E., Intermolecular repulsions and the equation of state for fluids. *AIChE J.* **1972**, *18*, 1184-1189.

65. McCoy, S. T.; Rubin, E. S., An engineering-economic model of pipeline transport of CO_2 with application to carbon capture and storage. *Int. J. Greenh. Gas Con.* **2008**, *2*, 219-229.
66. Reid, R. C.; Prausnitz, J. M.; Poling, B. E., *The Properties of Gases and Liquids*. 4th Edition ed.; McGraw-Hill: New York, 1987.
67. Frey, K.; Modell, M.; Tester, J. W., Density-and-temperature-dependent volume translation for the SRK EOS: 2. Mixtures. *Fluid Phase Equilibr.* **2013**, *343*, 13-23.
68. Carroll, J. J., Phase Equilibria Relevant to Acid Gas Injection, Part 1-Non-Aqueous Phase Behaviour. *J. Can. Pet. Technol.* **2002**, *41*, 25-31.
69. Li, H.; Jakobsen, J. P.; Wilhelmsen, Ø.; Yan, J., PVTxy properties of CO_2 mixtures relevant for CO_2 capture, transport and storage: Review of available experimental data and theoretical models. *Appl. Energy* **2011**, *88*, 3567-3579.
70. Yu, J.-M.; Lu, B. C. Y.; Iwai, Y., Simultaneous calculations of VLE and saturated liquid and vapor volumes by means of a 3P1T cubic EOS. *Fluid Phase Equilibr.* **1987**, *37*, 207-222.
71. Austegard, A.; Solbraa, E.; De Koeijer, G.; Mølnvik, M. J., Thermodynamic Models for Calculating Mutual Solubilities in H_2O–CO_2–CH_4 Mixtures. *Chem. Eng. Res. Des.* **2006**, *84*, 781-794.
72. Munkejord, S. T.; Jakobsen, J. P.; Austegard, A.; Mølnvik, M. J., Thermo- and fluid-dynamical modelling of two-phase multi-component carbon dioxide mixtures. *Int. J. Greenh. Gas Con.* **2010**, *4*, 589-596.
73. Hendriks, E.; Kontogeorgis, G. M.; Dohrn, R.; de Hemptinne, J.-C.; Economou, I. G.; Žilnik, L. F.; Vesovic, V., Industrial Requirements for Thermodynamics and Transport Properties. *Ind. Eng. Chem. Res.* **2010**, *49*, 11131-11141.
74. Llovell, F.; Vega, L. F., Prediction of Thermodynamic Derivative Properties of Pure Fluids through the Soft-SAFT Equation of State. *J. Phys. Chem. B* **2006**, *110*, 11427-11437.
75. Lafitte, T.; Bessieres, D.; Pineiro, M. M.; Daridon, J.-L., Simultaneous estimation of phase behavior and second-derivative properties using the statistical associating fluid theory with variable range approach. *J. Chem. Phys.* **2006**, *124*, 024509(1-16).
76. Llovell, F.; Vega, L. F., Global Fluid Phase Equilibria and Critical Phenomena of Selected Mixtures Using the Crossover Soft-SAFT Equation. *J. Phys. Chem. B* **2005**, *110*, 1350-1362.
77. Llovell, F.; Peters, C. J.; Vega, L. F., Second-order thermodynamic derivative properties of selected mixtures by the soft-SAFT equation of state. *Fluid Phase Equilibr.* **2006**, *248*, 115-122.
78. Llovell, F.; Vega, L. F., Phase equilibria, critical behavior and derivative properties of selected n-alkane/n-alkane and n-alkane/1-alkanol mixtures by the crossover soft-SAFT equation of state. *J. Supercrit. Fluid.* **2007**, *41*, 204-216.
79. Sherwood, T. K., Velocity of Sound in Compressed Gases. *J. Chem. Eng. Data* **1962**, *7*, 47-50.

80. Medwin, H., Counting bubbles acoustically: a review. *Ultrasonics* **1977**, *15*, 7-13.
81. Whiting, W. B.; Ackerberg, R. C., Prediction of acoustic velocities in nonideal gaseous mixtures. *AIChE J.* **1978**, *24*, 341-343.
82. Dean, E. A. *Atmospheric effects on the speed of sound*; Atmospheric Sciences Laboratory: 1979.
83. Zhang, J., Designing a cost-effective and reliable pipeline leak-detection system. *Pipes Pipelines Int.* **1997**, *42*, 20-26.
84. Liu, M.; Zang, S.; Zhou, D., Fast leak detection and location of gas pipelines based on an adaptive particle filter. *Int. J. Appl. Math. Comput. Sci.* **2005**, *15*, 541.
85. Stoianov, I.; Nachman, L.; Madden, S.; Tokmouline, T.; Csail, M. In *PIPENET: A Wireless Sensor Network for Pipeline Monitoring*, 6th International Symposium on Information Processing in Sensor Networks, 25-27 April 2007, 2007; 2007; pp 264-273.
86. Lund, H.; Flåtten, T.; Tollak Munkejord, S., Depressurization of carbon dioxide in pipelines–Models and methods. *Energy Procedia* **2011**, *4*, 2984-2991.
87. Alsiyabi, I.; Chapoy, A.; Tohidi, B., Effects of impurities on speed of sound and isothermal compressibility of CO_2-rich systems. In *3rd International Forum on the Transportation of CO_2 by Pipeline*, Gateshead, UK, 2012.
88. Mathias, P. M.; Copeman, T. W., Extension of the Peng-Robinson equation of state to complex mixtures: Evaluation of the various forms of the local composition concept. *Fluid Phase Equilibr.* **1983**, *13*, 91-108.
89. Polikhronidi, N. G.; Batyrova, R. G.; Abdulagatov, I. M.; Magee, J. W.; Stepanov, G. V., Isochoric heat capacity measurements for a CO_2 + n-decane mixture in the near-critical and supercritical regions. *J. Supercrit. Fluid* **2005**, *33*, 209-222.
90. Hanley, H. J. M., Prediction of the viscosity and thermal conductivity coefficients of mixtures. *Cryogenics* **1976**, *16*, 643-651.
91. Vesovic, V.; Wakeham, W. A., Prediction of the viscosity of fluid mixtures over wide ranges of temperature and pressure. *Chem. Eng. Sci.* **1989**, *44*, 2181-2189.
92. Vesovic, V.; Wakeham, W. A., The prediction of the viscosity of dense gas mixtures. *Int. J. Thermophys.* **1989**, *10*, 125-132.
93. Vesovic, V.; Wakeham, W. A.; Olchowy, G. A.; Sengers, J. V.; Watson, J. T. R.; Millat, J., The Transport Properties of Carbon Dioxide. *J. Phys. Chem. Ref. Data* **1990**, *19*, 763-808.
94. Homer, L.; Kayar, S. *Density, Heat Capacity, Viscosity, and Thermal Conductivity of Mixtures of CO_2, He, H_2, H_2O, N_2, and O_2*; Naval Medical Research Institute: 1994.
95. Fenghour, A.; Wakeham, W. A.; Vesovic, V., The Viscosity of Carbon Dioxide. *J. Phys. Chem. Ref. Data* **1998**, *27*, 31-44.
96. Quiñones-Cisneros, S. E.; Zéberg-Mikkelsen, C. K.; Stenby, E. H., The friction theory (f-theory) for viscosity modeling. *Fluid Phase Equilibr.* **2000**, *169*, 249-276.

97. Papari, M. M., Transport properties of carbon dioxide from an isotropic and effective pair potential energy. *Chem. Phys.* **2003**, *288*, 249-259.
98. Haghighi, B.; Djavanmardi, A. H.; Papari, M. M.; Najafi, M., Prediction of the Transport Properties of SF_6 with O_2, CO_2, CF_4, N_2 and CH_4 Mixtures at Low Density by the Inversion Method (Part II). *J. Chem. Theory Comput.* **2004**, *3*, 69-90.
99. Haghighi, B.; Djavanmardi, A. H.; Papari, M. M., Calculation of the Transport Properties of Gaseous Mixtures of CF_4 with O_2, N_2, CH_4 and CO_2 at Low Density Using Semi-Empirical Inversion Method. *Int. J. Comput. Method.* **2007**, *4*, 59-80.
100. Wilke, C. R., A Viscosity Equation for Gas Mixtures. *J. Chem. Phys.* **1950**, *18*, 517-519.
101. Kestin, J.; Leidenfrost, W., The effect of pressure on the viscosity of N_2-CO_2 mixtures. *Physica* **1959**, *25*, 525-536.
102. Kestin, J.; Kobayashi, Y.; Wood, R. T., The viscosity of four binary, gaseous mixtures at 20° and 30°C. *Physica* **1966**, *32*, 1065-1089.
103. Gururaja, G. J.; Tirunarayanan, M. A.; Ramachandran, A., Dynamic viscosity of gas mixtures. *J. Chem. Eng. Data* **1967**, *12*, 562-567.
104. Saxena, S. C.; Gambhir, R. S., The viscosity and translational thermal conductivity of gas mixtures. *Br. J. Appl. Phys.* **1963**, *14*, 436.
105. Kestin, J.; Ro, S. T.; Wakeham, W., An extended law of corresponding states for the equilibrium and transport properties of the noble gases. *Physica* **1972**, *58*, 165-211.
106. Kestin, J.; Khalifa, H. E.; Ro, S. T.; Wakeham, W. A., The viscosity and diffusion coefficients of eighteen binary gaseous systems. *Physica A* **1977**, *88*, 242-260.
107. Ely, J. F.; Hanley, H. J. M., Prediction of transport properties. 1. Viscosity of fluids and mixtures. *Ind. Eng. Chem. Fund.* **1981**, *20*, 323-332.
108. Ely, J. F.; Hanley, H. J. M., Prediction of transport properties. 2. Thermal conductivity of pure fluids and mixtures. *Ind. Eng. Chem. Fund.* **1983**, *22*, 90-97.
109. Posey, M. L.; Tapperson, K. G.; Rochelle, G. T., A simple model for prediction of acid gas solubilities in alkanolamines. *Gas Separation & Purification* **1996**, *10*, 181-186.
110. Gabrielsen, J.; Michelsen, M. L.; Stenby, E. H.; Kontogeorgis, G. M., A Model for Estimating CO2 Solubility in Aqueous Alkanolamines. *Ind. Eng. Chem. Res.* **2005**, *44*, 3348-3354.
111. Zhang, Y.; Chen, C.-C., Thermodynamic Modeling for CO2 Absorption in Aqueous MDEA Solution with Electrolyte NRTL Model. *Ind. Eng. Chem. Res.* **2010**, *50*, 163-175.
112. Austgen, D. M.; Rochelle, G. T.; Peng, X.; Chen, C. C., Model of vapor-liquid equilibria for aqueous acid gas-alkanolamine systems using the electrolyte-NRTL equation. *Ind. Eng. Chem. Res.* **1989**, *28*, 1060-1073.
113. Austgen, D. M.; Rochelle, G. T.; Chen, C. C., Model of vapor-liquid equilibria for aqueous acid gas-alkanolamine systems. 2. Representation of hydrogen sulfide

and carbon dioxide solubility in aqueous MDEA and carbon dioxide solubility in aqueous mixtures of MDEA with MEA or DEA. *Ind. Eng. Chem. Res.* **1991**, *30*, 543-555.
114. Posey, M. L.; Rochelle, G. T., A Thermodynamic Model of Methyldiethanolamine–CO2–H2S–Water. *Ind. Eng. Chem. Res.* **1997**, *36*, 3944-3953.
115. Giuffrida, A.; Bonalumi, D.; Lozza, G., Amine-based post-combustion CO2 capture in air-blown IGCC systems with cold and hot gas clean-up. *Appl. Energy* **2013**, *110*, 44-54.
116. Faramarzi, L.; Kontogeorgis, G. M.; Thomsen, K.; Stenby, E. H., Extended UNIQUAC model for thermodynamic modeling of CO2 absorption in aqueous alkanolamine solutions. *Fluid Phase Equilibr.* **2009**, *282*, 121-132.
117. Téllez-Arredondo, P.; Medeiros, M., Modeling CO_2 and H_2S solubilities in aqueous alkanolamine solutions via an extension of the Cubic-Two-State equation of state. *Fluid Phase Equilibr.* **2013**, *344*, 45-58.
118. Zoghi, A. T.; Feyzi, F.; Dehghani, M. R., Modeling CO2 Solubility in Aqueous N-methyldiethanolamine Solution by Electrolyte Modified Peng–Robinson Plus Association Equation of State. *Ind. Eng. Chem. Res.* **2012**, *51*, 9875-9885.
119. Nasrifar, K.; Tafazzol, A. H., Vapor–Liquid Equilibria of Acid Gas–Aqueous Ethanolamine Solutions Using the PC-SAFT Equation of State. *Ind. Eng. Chem. Res.* **2010**, *49*, 7620-7630.
120. Pahlavanzadeh, H.; Fakouri Baygi, S., Modeling CO2 solubility in Aqueous Methyldiethanolamine Solutions by Perturbed Chain-SAFT Equation of State. *J. Chem. Thermodyn.* **2013**, *59*, 214-221.
121. Rodriguez, J.; Mac Dowell, N.; Llovell, F.; Adjiman, C. S.; Jackson, G.; Galindo, A., Modelling the fluid phase behaviour of aqueous mixtures of multifunctional alkanolamines and carbon dioxide using transferable parameters with the SAFT-VR approach. *Mol. Phys.* **2012**, *110*, 1325-1348.
122. Farris, C. B., Unusual design factors for supercritical CO_2 pipelines. *Energy Prog.* **1983**, *3*, 150-158.
123. Skovholt, O., CO_2 transportation system. *Energ. Convers. Manage.* **1993**, *34*, 1095-1103.
124. Aursand, P.; Hammer, M.; Munkejord, S. T.; Wilhelmsen, Ø., Pipeline transport of CO_2 mixtures: Models for transient simulation. *Int. J. Greenh. Gas Con.* **2013**, *15*, 174-185.
125. Kunz, O.; Groupe Européen de Recherches Gazières, *The GERG-2004 wide-range equation of state for natural gases and other mixtures*. VDI Verlag: 2007.
126. Kunz, O.; Wagner, W., The GERG-2008 Wide-Range Equation of State for Natural Gases and Other Mixtures: An Expansion of GERG-2004. *J. Chem. Eng. Data* **2012**, *57*, 3032-3091.
127. Lemmon, E. W.; Huber, M. L.; McLinden, M. O., NIST reference fluid thermodynamic and transport properties-REFPROP. *Physical and Chemical Properties Division, National Institute of Standards and Technology, Boulder, Colorado* **2007**, *80305*.

128. Marchetti, C., On geoengineering and the CO₂ problem. *Climatic Change* **1977**, *1*, 59-68.
129. Holt, T.; Jensen, J. I.; Lindeberg, E., Underground storage of CO2 in aquifers and oil reservoirs. *Energ. Convers. Manage.* **1995**, *36*, 535-538.
130. Wallace, C. B., Drying supercritical CO2 demands care. *Oil Gas J.* **1985**, *83*, 98-99.
131. Ormiston, R. M.; Luce, M. C., Surface Processing of Carbon Dioxide in EOR Projects. *J. Petrol. Technol.* **1986**, *38*, 823-828.
132. Nguyen, D. N. In *Carbon Dioxide Geological Sequestration: Technical and Economic Reviews*, SPE/EPA/DOE Exploration and Production Environmental Conference, San Antonio, Texas, 2003; Society of Petroleum Engineers: San Antonio, Texas, 2003.
133. Koide, H.; Takahashi, M.; Shindo, Y.; Tazaki, Y.; Iijima, M.; Ito, K.; Kimura, N.; Omata, K., Hydrate formation in sediments in the sub-seabed disposal of CO2. *Energy* **1997**, *22*, 279-283.
134. Tsivintzelis, I.; Kontogeorgis, G. M.; Michelsen, M. L.; Stenby, E. H., Modeling phase equilibria for acid gas mixtures using the CPA equation of state. Part II: Binary mixtures with CO_2. *Fluid Phase Equilibr.* **2011**, *306*, 38-56.
135. Pappa, G. D.; Perakis, C.; Tsimpanogiannis, I. N.; Voutsas, E. C., Thermodynamic modeling of the vapor-liquid equilibrium of the CO_2/H_2O mixture. *Fluid Phase Equilibr.* **2009**, *284*, 56-63.
136. Perakis, C.; Voutsas, E.; Magoulas, K.; Tassios, D., Thermodynamic modeling of the vapor–liquid equilibrium of the water/ethanol/CO_2 system. *Fluid Phase Equilibr.* **2006**, *243*, 142-150.
137. Perakis, C. A.; Voutsas, E. C.; Magoulas, K. G.; Tassios, D. P., Thermodynamic Modeling of the Water + Acetic Acid + CO_2 System: The Importance of the Number of Association Sites of Water and of the Nonassociation Contribution for the CPA and SAFT-Type Models. *Ind. Eng. Chem. Res.* **2007**, *46*, 932-938.
138. Ji, X.; Tan, S. P.; Adidharma, H.; Radosz, M., SAFT1-RPM Approximation Extended to Phase Equilibria and Densities of CO_2–H_2O and CO_2–H_2O–NaCl Systems. *Ind. Eng. Chem. Res.* **2005**, *44*, 8419-8427.
139. Karakatsani, E. K.; Economou, I. G.; Kroon, M. C.; Bermejo, M. D.; Peters, C. J.; Witkamp, G.-J., Equation of state modeling of the phase equilibria of ionic liquid mixtures at low and high pressure. *PCCP* **2008**, *10*, 6160-6168.
140. Tang, X.; Gross, J., Modeling the phase equilibria of hydrogen sulfide and carbon dioxide in mixture with hydrocarbons and water using the PCP-SAFT equation of state. *Fluid Phase Equilibr.* **2010**, *293*, 11-21.
141. Nguyen-Huynh, D.; de Hemptinne, J.-C.; Lugo, R.; Passarello, J.-P.; Tobaly, P., Modeling Liquid–Liquid and Liquid–Vapor Equilibria of Binary Systems Containing Water with an Alkane, an Aromatic Hydrocarbon, an Alcohol or a Gas (Methane, Ethane, CO_2 or H_2S), Using Group Contribution Polar Perturbed-Chain Statistical Associating Fluid Theory. *Ind. Eng. Chem. Res.* **2011**, *50*, 7467-7483.

142. Diamantonis, N. I.; Economou, I. G., Modeling the phase equilibria of a H_2O–CO_2 mixture with PC-SAFT and tPC-PSAFT equations of state. *Mol. Phys.* **2012**, *110*, 1205-1212.
143. Lee, B. I.; Kesler, M. G., A generalized thermodynamic correlation based on three-parameter corresponding states. *AlChE J.* **1975**, *21*, 510-527.
144. Duan, Z.; Møller, N.; Weare, J. H., An equation of state for the CH_4-CO_2-H_2O system: I. Pure systems from 0 to 1000°C and 0 to 8000 bar. *Geochim. Cosmochim. Ac.* **1992**, *56*, 2605-2617.
145. Duan, Z.; Møller, N.; Weare, J. H., An equation of state for the CH_4-CO_2-H_2O system: II. Mixtures from 50 to 1000°C and 0 to 1000 bar. *Geochim. Cosmochim. Ac.* **1992**, *56*, 2619-2631.
146. Duan, Z.; Sun, R., An improved model calculating CO_2 solubility in pure water and aqueous NaCl solutions from 273 to 533 K and from 0 to 2000 bar. *Chem. Geol.* **2003**, *193*, 257-271.
147. Pitzer, K. S., Thermodynamics of electrolytes. I. Theoretical basis and general equations. *J. Phys. Chem.* **1973**, *77*, 268-277.
148. Li, Y.-K.; Nghiem, L. X., Phase equilibria of oil, gas and water/brine mixtures from a cubic equation of state and Henry's law. *Can. J. Chem. Eng.* **1986**, *64*, 486-496.
149. Harvey, A. H.; Prausnitz, J. M., Thermodynamics of high-pressure aqueous systems containing gases and salts. *AlChE J.* **1989**, *35*, 635-644.
150. Zuo, Y.-X.; Guo, T.-M., Extension of the Patel-Teja equation of state to the prediction of the solubility of natural gas in formation water. *Chem. Eng. Sci.* **1991**, *46*, 3251-3258.
151. Dubessy, J.; Tarantola, A.; Sterpenich, J., Modelling of Liquid-Vapour Equilibria in the H_2O-CO_2-NaCl and H_2O-H_2S-NaCl Systems to 270°C. *Oil Gas Sci. Technol.* **2005**, *60*, 339-355.
152. Hassanzadeh, H.; Pooladi-Darvish, M.; Elsharkawy, A. M.; Keith, D. W.; Leonenko, Y., Predicting PVT data for CO_2–brine mixtures for black-oil simulation of CO_2 geological storage. *Int. J. Greenh. Gas Con.* **2008**, *2*, 65-77.
153. Spycher, N.; Pruess, K.; Ennis-King, J., CO_2-H_2O mixtures in the geological sequestration of CO_2. I. Assessment and calculation of mutual solubilities from 12 to 100°C and up to 600 bar. *Geochim. Cosmochim. Ac.* **2003**, *67*, 3015-3031.
154. Prausnitz, J. M.; Lichtenthaler, R. N.; De Azevedo, E. G., *Molecular Thermodynamics of Fluid Phase Equilibria*. 3rd ed.; Prentice Hall: 1999.
155. Economou, I. G., Cubic and Generalized van der Waals Equations of State. In *Experimental Thermodynamics Volume VIII: Applied Thermodynamics of Fluids*, Goodwin, A. R. H.; Sengers, J. V.; Peters, C. J., Eds. Royal Society of Chemistry: Cambridge, UK, 2010.
156. Valderrama, J. O., The State of the Cubic Equations of State. *Ind. Eng. Chem. Res.* **2003**, *42*, 1603-1618.
157. Daridon, J. L.; Saint-Guirons, H.; Courette, B.; Xans, P.; Leibovici, C., A generalized process for phase equilibrium calculation with cubic equations of state *Int. J. Thermophys.* **1993**, *14*, 1101-1108.

158. Gasem, K. A. M.; Gao, W.; Pan, Z.; Robinson Jr, R. L., A modified temperature dependence for the Peng–Robinson equation of state. *Fluid Phase Equilibr.* **2001**, *181*, 113-125.
159. Reid, R. C.; Leland, T. W., Pseudocritical constants. *AIChE J.* **1965**, *11*, 228-237.
160. Chapman, W. G.; Gubbins, K. E.; Jackson, G.; Radosz, M., New reference equation of state for associating liquids. *Ind. Eng. Chem. Res.* **1990**, *29*, 1709-1721.
161. Huang, S. H.; Radosz, M., Equation of state for small, large, polydisperse, and associating molecules: Extension to fluid mixtures. *Ind. Eng. Chem. Res.* **1991**, *30*, 1994-2005.
162. Gross, J.; Sadowski, G., Application of the Perturbed-Chain SAFT Equation of State to Associating Systems. *Ind. Eng. Chem. Res.* **2002**, *41*, 5510-5515.
163. Wertheim, M. S., Fluids with highly directional attractive forces. I. Statistical thermodynamics. *J. Stat. Phys.* **1984**, *35*, 19-34.
164. Wertheim, M. S., Fluids with highly directional attractive forces. II. Thermodynamic perturbation theory and integral equations. *J. Stat. Phys.* **1984**, *35*, 35-47.
165. Wertheim, M. S., Fluids with highly directional attractive forces. III. Multiple attraction sites. *J. Stat. Phys.* **1986**, *42*, 459-476.
166. Wertheim, M. S., Fluids with highly directional attractive forces. IV. Equilibrium polymerization. *J. Stat. Phys.* **1986**, *42*, 477-492.
167. Karakatsani, E. K.; Economou, I. G., Perturbed Chain-Statistical Associating Fluid Theory Extended to Dipolar and Quadrupolar Molecular Fluids. *J. Phys. Chem. B* **2006**, *110*, 9252-9261.
168. Chen, S. S.; Kreglewski, A., Applications of the Augmented van der Waals Theory of Fluids.: I. Pure Fluids. *Ber. Bunsenges. Phys. Chem.* **1977**, *81*, 1048-1052.
169. Larsen, B.; Rasaiah, J. C.; Stell, G., Thermodynamic perturbation theory for multipolar and ionic liquids. *Mol. Phys.* **1977**, *33*, 987-1027.
170. Michelsen, M.; Mollerup, J., Thermodynamic Models: Fundamentals and Computational Aspects. In Tie-Line Publications, Denmark: 2007.
171. Michelsen, M. L., The isothermal flash problem. Part I. Stability. *Fluid Phase Equilibr.* **1982**, *9*, 1-19.
172. Michelsen, M. L., The isothermal flash problem. Part II. Phase-split calculation. *Fluid Phase Equilibr.* **1982**, *9*, 21-40.
173. Michelsen, M. L., Multiphase isenthalpic and isentropic flash algorithms. *Fluid Phase Equilibr.* **1987**, *33*, 13-27.
174. Kennedy, J.; Eberhart, R. In *Particle swarm optimization*, Neural Networks, 1995. Proceedings., IEEE International Conference on, Nov/Dec 1995, 1995; 1995; pp 1942-1948 vol.4.
175. Chung, T. H.; Ajlan, M.; Lee, L. L.; Starling, K. E., Generalized multiparameter correlation for nonpolar and polar fluid transport properties. *Ind. Eng. Chem. Res.* **1988**, *27*, 671-679.

176. Neufeld, P. D.; Janzen, A. R.; Aziz, R. A., Empirical Equations to Calculate 16 of the Transport Collision Integrals Omega [sup (l,s)*] for the Lennard-Jones (12--6) Potential. *J. Chem. Phys.* **1972**, *57*, 1100-1102.
177. Tan, S. P.; Adidharma, H.; Towler, B. F.; Radosz, M., Friction Theory Coupled with Statistical Associating Fluid Theory for Estimating the Viscosity of n-Alkane Mixtures. *Ind. Eng. Chem. Res.* **2006**, *45*, 2116-2122.
178. Chapman, S.; Cowling, T. G., *The Mathematical Theory of Non-Uniform Gases*. Cambridge University Press: Cambridge, 1970.
179. Percus, J. K.; Yevick, G. J., Analysis of Classical Statistical Mechanics by Means of Collective Coordinates. *Physical Review* **1958**, *110*, 1-13.
180. Carnahan, N. F.; Starling, K. E., Thermodynamic Properties of a Rigid-Sphere Fluid. *J. Chem. Phys.* **1970**, *53*, 600-603.
181. Yu, Y.-X.; Gao, G.-H., Self-diffusion coefficient equation for polyatomic fluid. *Fluid Phase Equilibr.* **1999**, *166*, 111-124.
182. Reis, R. A.; Silva, F. C.; Nobrega, R.; Oliveira, J. V.; Tavares, F. W., Molecular dynamics simulation data of self-diffusion coefficient for Lennard-Jones chain fluids. *Fluid Phase Equilibr.* **2004**, *221*, 25-33.
183. Reis, R. A.; Nobrega, R.; Oliveira, J. V.; Tavares, F. W., Self- and mutual diffusion coefficient equation for pure fluids, liquid mixtures and polymeric solutions. *Chem. Eng. Sci.* **2005**, *60*, 4581-4592.
184. Thijsse, B. J.; T Hooft, G. W.; Coombe, D. A.; Knaap, H. F. P.; Beenakker, J. J. M., Some simplified expressions for the thermal conductivity in an external field. *Physica A* **1979**, *98*, 307-312.
185. Scalabrin, G.; Marchi, P.; Finezzo, F.; Span, R., A Reference Multiparameter Thermal Conductivity Equation for Carbon Dioxide with an Optimized Functional Form. *J. Phys. Chem. Ref. Data* **2006**, *35*, 1549-1575.
186. Lemmon, E. W.; Linden, M. O.; Friend, D. G., Thermophysical Properties of Fluid Systems. In *NIST Chemistry WebBook, NIST Standard Reference Database Number 69*, Linstrom, P. J.; Mallard, W. G., Eds. National Institute of Standards and Technology: Gaithersburg MD, 20899.
187. Lee, Y.; Shin, M. S.; Kim, H., Estimation of 2nd-order derivative thermodynamic properties using the crossover lattice equation of state. *J. Chem. Thermodyn.* **2008**, *40*, 1580-1587.
188. Shin, M. S.; Lee, Y.; Kim, H., Estimation of second-order derivative thermodynamic properties using the crossover cubic equation of state. *J. Chem. Thermodyn.* **2007**, *40*, 688-694.
189. Lowder, J. E.; Kennedy, L. A.; Sulzmann, K. G. P.; Penner, S. S., Spectroscopic studies of hydrogen bonding in H2S. *J. Quant. Spectrosc. Ra.* **1970**, *10*, 17-23.
190. Vrabec, J.; Kumar, A.; Hasse, H., Joule-Thomson inversion curves of mixtures by molecular simulation in comparison to advanced equations of state: Natural gas as an example. *Fluid Phase Equilibr.* **2007**, *258*, 34-40.
191. Diamantonis, N. I.; Boulougouris, G. C.; Mansoor, E.; Tsangaris, D. M.; Economou, I. G., Evaluation of Cubic, SAFT, and PC-SAFT Equations of State

for the Vapor–Liquid Equilibrium Modeling of CO_2 Mixtures with Other Gases. *Ind. Eng. Chem. Res.* **2013**, *52*, 3933-3942.
192. Reamer, H. H.; Olds, R. H.; Sage, B. H.; Lacey, W. N., Phase Equilibrium in Hydrocarbon Systems.Methane–Carbon Dioxide System in the Gaseous Region. *Ind. Eng. Chem.* **1944**, *36*, 88-90.
193. Donnelly, H. G.; Katz, D. L., Phase Equilibria in the Carbon Dioxide–Methane System. *Ind. Eng. Chem.* **1954**, *46*, 511-517.
194. Davalos, J.; Anderson, W. R.; Phelps, R. E.; Kidnay, A. J., Liquid-vapor equilibria at 250.00.deg.K for systems containing methane, ethane, and carbon dioxide. *J. Chem. Eng. Data* **1976**, *21*, 81-84.
195. Mraw, S. C.; Hwang, S.-C.; Kobayashi, R., Vapor-liquid equilibrium of the methane-carbon dioxide system at low temperatures. *J. Chem. Eng. Data* **1978**, *23*, 135-139.
196. Esper, G. J.; Bailey, D. M.; Holste, J. C.; Hall, K. R., Volumetric behavior of near-equimolar mixtures for CO2+CH4 and CO2+N2. *Fluid Phase Equilibr.* **1989**, *49*, 35-47.
197. Arai, Y.; G.-I., K.; Saito, S., The Experimental Determination Of The P-V-T-X Relations For The Carbon Dioxide-Nitrogen And The Carbon Dioxide-Methane Systems. *J. Chem. Eng. Jpn.* **1971**, *4*, 113-122.
198. Dorau, W.; Al-Wakeel, I. M.; Knapp, H., VLE data for CO2-CF2Cl2, N2-CO2, N2-CF2Cl2 and N2-CO2-CF2Cl. *Cryogenics* **1983**, *23*, 29-35.
199. Brown, T. S.; Niesen, V. G.; Sloan, E. D.; Kidnay, A. J., Vapor-liquid equilibria for the binary systems of nitrogen, carbon dioxide, and n-butane at temperatures from 220 to 344 K. *Fluid Phase Equilibr.* **1989**, *53*, 7-14.
200. Al-Sahhaf, T. A., Vapor—liquid equilibria for the ternary system N2 + CO2 + CH4 at 230 and 250 K. *Fluid Phase Equilibr.* **1990**, *55*, 159-172.
201. Al-Sahhaf, T. A.; Kidnay, A. J.; Sloan, E. D., Liquid + vapor equilibriums in the nitrogen + carbon dioxide + methane system. *Ind. Eng. Chem. Fund.* **1983**, *22*, 372-380.
202. Yorizane, M.; Yoshimura, S.; Masuoka, H.; Miyano, Y.; Kakimoto, Y., New procedure for vapor-liquid equilibria. Nitrogen + carbon dioxide, methane + Freon 22, and methane + Freon 12. *J. Chem. Eng. Data* **1985**, *30*, 174-176.
203. Krichevskii, I.; Khazanova, N.; Lesnevskaya, L.; Scandalova, L., Liquid-gas Equilibria in Nitrogen-Carbon Dioxide at High Pressures. *Khim. Promst.* **1962**, *3*, 169-171.
204. Fredenslund, A.; Sather, G. A., Gas-liquid equilibrium of the oxygen-carbon dioxide system. *J. Chem. Eng. Data* **1970**, *15*, 17-22.
205. Blümcke, A., Ueber die Bestimmung der specifischen Gewichte und Dampfspannungen einiger Gemische von schwefliger Säure und Kohlensäure. *Ann. Phys. Leipzig* **1888**, *270*, 10-21.
206. Sarashina, E.; Arai, Y.; Saito, S., The P–V–T–X relation for the carbon dioxide – system. *J. Chem. Eng. Jpn.* **1971**, *4*, 379–381.
207. Bierlein, J. A.; Kay, W. B., Phase-Equilibrium Properties of System Carbon Dioxide-Hydrogen Sulfide. *Ind. Eng. Chem.* **1953**, *45*, 618-624.

208. Dodge, B. F.; Dunbar, A. K., An Investigation Of The Coexisting Liquid And Vapor Phases Of Solutions Of Oxygen And Nitrogen. *J. Am. Chem. Soc.* **1927**, *49*, 591-610.
209. Muirbrook, N. K.; Prausnitz, J. M., Multicomponent vapor-liquid equilibria at high pressures: Part I. Experimental study of the nitrogen - oxygen - carbon dioxide system at 0°C. *AIChE J.* **1965**, *11*, 1092-1096.
210. Poling, B. E.; Prausnitz, J. M.; O'Connell, J. P., *The Properties of Gases and Liquids*. 5th ed.; McGraw Hill: Singapore, 2007.
211. Alfradique, M., F.; Castier, M., Calculation of Phase Equilibrium of Natural Gases with the Peng-Robinson and PC-SAFT Equations of State. *Oil Gas Sci. Technol.* **2007**, *62*, 707-714.
212. Desiraju, G. R.; Steiner, T., *The weak hydrogen bond in structural chemistry and biology*. Oxford University Press Inc.: New York, 1999.
213. Kraska, T.; Gubbins, K. E., Phase Equilibria Calculations with a Modified SAFT Equation of State. 1. Pure Alkanes, Alkanols, and Water. *Ind. Eng. Chem. Res.* **1996**, *35*, 4727-4737.
214. Wolbach, J. P.; Sandler, S. I., Using Molecular Orbital Calculations To Describe the Phase Behavior of Hydrogen-Bonding Fluids. *Ind. Eng. Chem. Res.* **1997**, *36*, 4041-4051.
215. McCabe, C.; Galindo, A.; Cummings, P. T., Anomalies in the Solubility of Alkanes in Near-Critical Water. *J. Phys. Chem. B* **2003**, *107*, 12307-12314.
216. von Solms, N.; Michelsen, M. L.; Passos, C. P.; Derawi, S. O.; Kontogeorgis, G. M., Investigating Models for Associating Fluids Using Spectroscopy. *Ind. Eng. Chem. Res.* **2006**, *45*, 5368-5374.
217. Clark, G. N. I.; Haslam, A. J.; Galindo, A.; Jackson, G., Developing optimal Wertheim-like models of water for use in Statistical Associating Fluid Theory (SAFT) and related approaches. *Mol. Phys.* **2006**, *104*, 3561 - 3581.
218. Diamantonis, N. I.; Economou, I. G., Evaluation of Statistical Associating Fluid Theory (SAFT) and Perturbed Chain-SAFT Equations of State for the Calculation of Thermodynamic Derivative Properties of Fluids Related to Carbon Capture and Sequestration. *Energ. Fuel.* **2011**, *25*, 3334-3343.
219. Karakatsani, E. K.; Economou, I. G., Phase equilibrium calculations for multi-component polar fluid mixtures with tPC-PSAFT. *Fluid Phase Equilibr.* **2007**, *261*, 265-271.
220. Jönsson, B.; Karlström, G.; Wennerström, H., Ab initio molecular orbital calculations on the water-carbon dioxide system: Molecular complexes. *Chem. Phys. Lett.* **1975**, *30*, 58-59.
221. Sadlej, J.; Mazurek, P., Ab initio calculations on the water-carbon dioxide system. *J. Mol. Struct. THEOCHEM* **1995**, *337*, 129-138.
222. Danten, Y.; Tassaing, T.; Besnard, M., Ab Initio Investigation of Vibrational Spectra of Water–(CO2)n Complexes (n = 1, 2). *J. Phys. Chem. A* **2005**, *109*, 3250-3256.

223. King, M. B.; Mubarak, A.; Kim, J. D.; Bott, T. R., The mutual solubilities of water with supercritical and liquid carbon dioxides. *J. Supercrit. Fluid* **1992**, *5*, 296-302.
224. Valtz, A.; Coquelet, C.; Richon, D., Vapor–Liquid Equilibrium Data for the Sulfur Dioxide (SO2) + Difluoromethane (R32) System at Temperatures from 288.07 to 403.16 K and at Pressures up to 7.31 MPa. *Int. J. Thermophys.* **2004**, *25*, 1695-1711.
225. Nakayama, T.; Sagara, H.; Arai, K.; Saito, S., High pressure liquid---liquid equilibria for the system of water, ethanol and 1,1-difluoroethane at 323.2 K. *Fluid Phase Equilibr.* **1987**, *38*, 109-127.
226. Wiebe, R., The Binary System Carbon Dioxide-Water under Pressure. *Chem. Rev.* **1941**, *29*, 475-481.
227. Mueller, G.; Bender, E.; Maurer, G., **1988**, *92*, 148-160.
228. Takenouchi, S.; Kennedy, G. C., The binary system H 2 O-CO 2 at high temperatures and pressures. *Am J Sci* **1964**, *262*, 1055-1074.
229. Bamberger, A.; Sieder, G.; Maurer, G., High-pressure (vapor+liquid) equilibrium in binary mixtures of (carbon dioxide+water or acetic acid) at temperatures from 313 to 353 K. *J. Supercrit. Fluid* **2000**, *17*, 97-110.
230. Valtz, A.; Chapoy, A.; Coquelet, C.; Paricaud, P.; Richon, D., Vapour-liquid equilibria in the carbon dioxide-water system, measurement and modelling from 278.2 to 318.2 K. *Fluid Phase Equilibr.* **2004**, *226*, 333-344.
231. Wiebe, R.; Gaddy, V. L., The Solubility of Carbon Dioxide in Water at Various Temperatures from 12 to 40° and at Pressures to 500 Atmospheres. Critical Phenomena*. *J. Am. Chem. Soc.* **1940**, *62*, 815-817.
232. Li, Z.; Dong, M.; Li, S.; Dai, L., Densities and Solubilities for Binary Systems of Carbon Dioxide + Water and Carbon Dioxide + Brine at 59 °C and Pressures to 29 MPa. *J. Chem. Eng. Data* **2004**, *49*, 1026-1031.
233. Seitz, J. C.; Blencoe, J. G., The CO_2-H_2O system. I. Experimental determination of volumetric properties at 400°C, 10–100 MPa. *Geochim. Cosmochim. Ac.* **1999**, *63*, 1559-1569.
234. Duan, Z.; Zhang, Z., Equation of state of the H_2O, CO_2, and H_2O–CO_2 systems up to 10 GPa and 2573.15 K: Molecular dynamics simulations with ab initio potential surface. *Geochim. Cosmochim. Ac.* **2006**, *70*, 2311-2324.
235. Knapp, H.; Doring, R.; Oellrich, L.; Plocker, U.; Prausnitz, J., *Vapor-liquid equilibria for mixtures of low boiling substances*. Dechema Frankfurt: 1982; Vol. 1.
236. Brown, T. S.; Kidnay, A. J.; Sloan, E. D., Vapor—liquid equilibria in the carbon dioxide-ethane system. *Fluid Phase Equilibr.* **1988**, *40*, 169-184.
237. Davalos, J.; Anderson, W. R.; Phelps, R. E.; Kidnay, A. J., Liquid-vapor equilibria at 250.00 K for systems containing methane, ethane, and carbon dioxide. *J. Chem. Eng. Data* **1976**, *21*, 81-84.
238. Fredenslund, A.; Mollerup, J., Measurement and prediction of equilibrium ratios for the C_2H_6+CO_2 system. *J. Chem. Soc., Faraday Trans. 1* **1974**, *70*, 1653-1660.

239. Hamam, S. E. M.; Lu, B. C. Y., Vapor-liquid equilibrium in the ethane-carbon dioxide system. *Can. J. Chem. Eng.* **1974**, *52*, 283-286.
240. Ohgaki, K.; Katayama, T., Isothermal vapor-liquid equilibrium data for the ethane-carbon dioxide system at high pressures. *Fluid Phase Equilibr.* **1977**, *1*, 27-32.
241. Niesen, V. G.; Rainwater, J. C., Critical locus, (vapor + liquid) equilibria, and coexisting densities of (carbon dioxide + propane) at temperatures from 311 K to 361 K. *J. Chem. Thermodyn.* **1990**, *22*, 777-795.
242. Nagahama, K.; Konishi, H.; Hoshino, D.; Hirata, M., Binary vapor-liquid equilibria of carbon dioxide-light hydrocarbons at low temperature. *J. Chem. Eng. Jpn.* **1974**, *7*, 323-328.
243. Pozo de Fernandez, M. E.; Zollweg, J. A.; Streett, W. B., Vapor-liquid equilibrium in the binary system carbon dioxide + n-butane. *J. Chem. Eng. Data* **1989**, *34*, 324-328.
244. Shibata, S. K.; Sandler, S. I., High-pressure vapor-liquid equilibria involving mixtures of nitrogen, carbon dioxide, and n-butane. *J. Chem. Eng. Data* **1989**, *34*, 291-298.
245. Leu, A. D.; Robinson, D. B., Equilibrium phase properties of the n-butane-carbon dioxide and isobutane-carbon dioxide binary systems. *J. Chem. Eng. Data* **1987**, *32*, 444-447.
246. Cheng, H.; Pozo de Fernandez, M. E.; Zollweg, J. A.; Streett, W. B., Vapor-liquid equilibrium in the system carbon dioxide + n-pentane from 252 to 458 K at pressures to 10 MPa. *J. Chem. Eng. Data* **1989**, *34*, 319-323.
247. Leu, A. D.; Robinson, D. B., Equilibrium phase properties of selected carbon dioxide binary systems: n-pentane-carbon dioxide and isopentane-carbon dioxide. *J. Chem. Eng. Data* **1987**, *32*, 447-450.
248. Besserer, G. J.; Robinson, D. B., Equilibrium-phase properties of n-pentane-carbon dioxide system. *J. Chem. Eng. Data* **1973**, *18*, 416-419.
249. Ohgaki, K.; Katayama, T., Isothermal vapor-liquid equilibrium data for binary systems containing carbon dioxide at high pressures: methanol-carbon dioxide, n-hexane-carbon dioxide, and benzene-carbon dioxide systems. *J. Chem. Eng. Data* **1976**, *21*, 53-55.
250. Li, Y.-H.; Dillard, K. H.; Robinson, R. L., Vapor-liquid phase equilibrium for carbon dioxide-n-hexane at 40, 80, and 120 °C. *J. Chem. Eng. Data* **1981**, *26*, 53-55.
251. Kalra, H.; Kubota, H.; Robinson, D. B.; Ng, H.-J., Equilibrium phase properties of the carbon dioxide-n-heptane system. *J. Chem. Eng. Data* **1978**, *23*, 317-321.
252. Weng, W. L.; Lee, M. J., Vapor-liquid equilibrium of the octane/carbon dioxide, octane/ethane, and octane/ethylene systems. *J. Chem. Eng. Data* **1992**, *37*, 213-215.
253. Inomata, H.; Tuchiya, K.; Arai, K.; Saito, S., Measurement of Vapor-Liquid Equilibria at Elevated Temperatures and Pressures Using a Flow Type Apparatus. *J. Chem. Eng. Jpn.* **1986**, *19*, 386-391.

254. Chou, G. F.; Forbert, R. R.; Prausnitz, J. M., High-pressure vapor-liquid equilibria for carbon dioxide/n-decane, carbon dioxide/tetralin, and carbon dioxide/n-decane/tetralin at 71.1 and 104.4 °C. *J. Chem. Eng. Data* **1990**, *35*, 26-29.
255. Reamer, H. H.; Sage, B. H., Phase Equilibria in Hydrocarbon Systems. Volumetric and Phase Behavior of the n-Decane-CO_2 System. *J. Chem. Eng. Data* **1963**, *8*, 508-513.
256. Sebastian, H. M.; Simnick, J. J.; Lin, H.-M.; Chao, K.-C., Vapor-liquid equilibrium in binary mixtures of carbon dioxide + n-decane and carbon dioxide + n-hexadecane. *J. Chem. Eng. Data* **1980**, *25*, 138-140.
257. Pan, C.; Radosz, M., Modeling of solid-liquid equilibria in naphthalene, normal-alkane and polyethylene solutions. *Fluid Phase Equilibr.* **1999**, *155*, 57-73.
258. Ting, P. D. Thermodynamic stability and phase behavior of asphaltenes in oil and of other highly asymmetric mixtures. RICE UNIVERSITY, 2003.
259. Jensen, R. H.; Kurata, F., Heterogeneous phase behavior of solid carbon dioxide in light hydrocarbons at cryogenic temperatures. *AIChE J.* **1971**, *17*, 357-364.
260. Hoerr, C. W.; Harwood, H. J., SOLUBILITIES OF HIGH MOLECULAR WEIGHT ALIPHATIC COMPOUNDS IN n-HEXANE. *J. Org. Chem.* **1951**, *16*, 779-791.
261. Jacoby, R. H., Phase Behavior of Heavy Oils with Application to Reservoir Recovery Processes. In *Heavy Crude Oil Recovery*, Okandan, E., Ed. Springer Netherlands: 1984; Vol. 76, pp 1-47.
262. Angus, S.; Armstrong, B.; deReuck, K. M., *Carbon Dioxide International Thermodynamic Tables of the Fluid State* Pergamon Press: 1976.
263. Jäger, A.; Span, R., Equation of State for Solid Carbon Dioxide Based on the Gibbs Free Energy. *J. Chem. Eng. Data* **2012**, *57*, 590-597.
264. Anwar, S.; Carroll, J. J., Properties of CO2 Relevant To Sequestration–Density. *Acid Gas Injection and Related Technologies*, 75-80.
265. Chickos, J. S.; Acree Jr, W. E., Enthalpies of sublimation of organic and organometallic compounds. 1910–2001. *J. Phys. Chem. Ref. Data* **2002**, *31*, 537.
266. Giauque, W.; Egan, C., Carbon dioxide. The heat capacity and vapor pressure of the solid. The heat of sublimation. Thermodynamic and spectroscopic values of the entropy. *J. Chem. Phys.* **1937**, *5*, 45-54.
267. Tan, S. P.; Adidharma, H.; Towler, B. F.; Radosz, M., Friction Theory and Free-Volume Theory Coupled with Statistical Associating Fluid Theory for Estimating the Viscosity of Pure n-Alkanes. *Ind. Eng. Chem. Res.* **2005**, *44*, 8409-8418.
268. Queimada, A. J.; Quiñones-Cisneros, S. E.; Marrucho, I. M.; Coutinho, J. A. P.; Stenby, E. H., Viscosity and Liquid Density of Asymmetric Hydrocarbon Mixtures. *Int. J. Thermophys.* **2003**, *24*, 1221-1239.
269. Yokozeki, A., *Analytical Equation of State for Solid-Liquid-Vapor Phases. International Journal of Thermophysics* **2003**, *24*.

270. Li, H.; Wilhelmsen, Ø.; Lv, Y.; Wang, W.; Yan, J., Viscosities, thermal conductivities and diffusion coefficients of CO2 mixtures: Review of experimental data and theoretical models. *Int. J. Greenh. Gas Con.* **2011**, *5*, 1119-1139.
271. Kestin, J.; Yata, J., Viscosity and Diffusion Coefficient of Six Binary Mixtures. *J. Chem. Phys.* **1968**, *49*, 4780-4791.
272. Etesse, P.; Zega, J. A.; Kobayashi, R., High pressure nuclear magnetic resonance measurement of spin-lattice relaxation and self-diffusion in carbon dioxide. *J. Chem. Phys.* **1992**, *97*, 2022-2029.
273. Topliss, R. J.; Dimitrelis, D.; Prausnitz, J. M., Computational aspects of a non-cubic equation of state for phase-equilibrium calculations. Effect of density-dependent mixing rules. *Comput. Chem. Eng.* **1988**, *12*, 483-489.
274. Mahgerefteh, H.; Brown, S.; Denton, G., Modelling the impact of stream impurities on ductile fractures in CO2 pipelines. *Chem. Eng. Sci.* **2012**, *74*, 200-210.
275. Mahgerefteh, H.; Denton, G.; Rykov, Y., A hybrid multiphase flow model. *AIChE J.* **2008**, *54*, 2261-2268.
276. Mahgerefteh, H.; Saha, P.; Economou, I., A study of the dynamic response of emergency shutdown valves following full bore rupture of gas pipelines. *Process safety and environmental protection* **1997**, *75*, 201-209.
277. Mahgerefteh, H.; Saha, P.; Economou, I. G., Fast numerical simulation for full bore rupture of pressurized pipelines. *AIChE J.* **1999**, *45*, 1191-1201.
278. Chen, J.; Richardson, S.; Saville, G., Modelling of two-phase blowdown from pipelines—I. A hyperbolic model based on variational principles. *Chem. Eng. Sci.* **1995**, *50*, 695-713.
279. Chen, J.; Richardson, S.; Saville, G., Modelling of two-phase blowdown from pipelines—II. A simplified numerical method for multi-component mixtures. *Chem. Eng. Sci.* **1995**, *50*, 2173-2187.
280. Kontogeorgis, G. M.; Folas, G. K., *Thermodynamic Models for Industrial Applications: From Classical and Advanced Mixing Rules to Association Theories*. Wiley: 2010.
281. 1728 Software Systems. http://www.1728.org/cubic2.htm (2011),